PONTIFICIA UNIVERSIDAD CATÓLICA DEL PERÚ

ESCUELA DE POSGRADO

OBSERVATION AND CONTROL OF A BALL ON A TILTING

TESIS PARA OPTAR EL GRADO ACADÉMICO DE MAGISTER EN INGENIERÍA DE CONTROL Y AUTOMATIZACIÓN

AUTOR

Dimel Arturo Contreras Martinez

ASESOR

Supervisor (PUCP): Dr. Javier Sotomayor Moriano
Supervisor (TU Ilmenau): M.Sc. Christoph Weise

Septiembre, 2017

Technische Universität Ilmenau

Fakultät für Informatik und Automatisierung

Master Thesis

OBSERVATION AND CONTROL OF A BALL ON A TILTING PLATE

To achieve the Degree of:

Master of Science (M.Sc.)

in Technische Kybernetik und Systemtheorie

Submitted by:	Dimel Arturo Contreras Martinez
Date and Place of Birth:	05/05/1992 Lima, Peru
Supervisor (TU Ilmenau):	M.Sc. Christoph Weise
Responsible Professor (TU Ilmenau):	Prof.Dr.-Ing. Johann Reger
Supervisor (PUCP):	Dr. Javier Sotomayor Moriano
Date and Place:	18/09/2017, Ilmenau

Declaration

I declare that the work is entirely my own and was produced with no assistance from third parties.

I certify that the work has not been submitted in the same or any similar form for assessment to any other examining body and all references, direct and indirect, are indicated as such and have been cited accordingly.

Ilmenau, September 18, 2017
Dimel Arturo Contreras Martinez

Abstract

The ball and plate system is a nonlinear MIMO system that has interesting characteristics which are also present in aerospace and industrial systems, such as: instability, subactuation, nonlinearities such as friction, backlash, and delays in the measurements.

In this work, the modeling of the system is based on the Lagrange approach. Then it is represented in the state-space form with plate accelerations as inputs to the system. These have a similar effect as applying torques. In addition, the use of an internal loop of the servo system is considered. From the obtained model, we proceed to carry out the analysis of controllability and observability resulting in that the system is globally weak observable and locally controllable in the operating range. Then, the Jacobi linearization is performed to use the linearized model in the design of linear controllers for stabilization.

On the other hand, analyzing the internal dynamics of the ball and plate system turns out to be a non-minimum phase system, which makes it difficult to design the tracking control using the exact model. This is the reason why we proceed to make approximations. Using the approximate model, nonlinear controllers are designed for tracking using different approaches as: feedback linearization for tracking with and without integral action, backstepping and sliding mode. In addition, linear and nonlinear observers are designed to provide full state information to the controller.

Simulation tests are performed comparing the different control and observation approaches. Moreover, the effect of the delay in the measurement is analyzed, where it is seen that the greater the frequency of the reference signal the more the error is increased. Then, adding the Smith predictor compensates the delay and reduces the tracking error.

Finally, tests performed with the real system. The system was successfully controlled for stabilization and tracking using the designed controllers. However, it is noticed that the effect of the friction, the spring oscillation and other non-modeled characteristics significantly affect the performance of the control.

Zusammenfassung

Das "Ball und Platte" System ist ein nichtlineares MIMO System, das interessante Eigenschaften aufweist die auch in der Luft und Raumfahrt und in industriellen Systemen vorgestellt werden, wie z.B.: Instabilität, Unteraktuierung, Effekte von Nichtlinearitäten wie Reibung, Spiel und besitzt Verzögerungen bei den Messungen.

In dieser Arbeit wird die Modellierung des auf dem Lagrange-Ansatz basierenden Systems durchgeführt und dann in der Zustandsraumdarstellung mit Plattenbeschleunigungen als Eingaben in das System dargestellt, die eine ähnliche Wirkung haben wie die Drehmomente. Darüber hinaus wird die Verwendung einer internen Schleife im Servosystem berücksichtigt. Mit dem erhaltenen Modell analysieren wir, die Steuerbarkeit und Beobachtbarkeit. Das System ist global schwach beobachtbar und lokal steuerbar im Betriebsbereich. Anschließend wird die Jacobi-Linearisierung durchgeführt, um das linearisierte Modell mit linearen Regelungen zu stabilisieren.

Die Analyse der internen Dynamik des "Ball und Platte" Systems erweist sich als ein nichtminimales Phasensystem, was es schwierig macht, eine Folgeregelung mit dem exakten Modell zu entwerfen. Aus diesem Grund entwerfen wir Näherungen. Mit dem Näherungsmodell werden nichtlineare Folgeregelungen mit unterschiedlichen Ansätzen konzipiert : Rückkopplungslinearisierung für die Verfolgung mit und ohne I-Anteil, backstepping und sliding mode. Darüber hinaus sind lineare und nichtlineare Beobachter so ausgelegt, dass sie der Regelung vollständige Zustandsinformationen zur Verfügung stellen.

Simulationen werden durchgeführt, um die verschiedenen Steuerung und Beobachtungsansätze zu vergleichen. Darüber hinaus wird die Wirkung der Verzögerung in der Messung analysiert, wobei dort zu sehen ist, dass die grössere Frequenz des Referenzsignals den Fehler erhöht. Der hinzugefügte "Smith predictor" kompensiert die Verzögerung und verringert den Verfolgungsfehler.

Bei Tests mit dem realen System, wurde das System zur Stabilisierung und Verfolgung mit den konstruierten Reglungen erfolgreich gesteuert. Es wurde jedoch festgestellt, dass die Wirkung der Reibung, die Oszillation der Feder und andere nicht modellierte Eigenschaften die Leistungsfähigkeit der Regelung signifikant beeinflusst.

Acknowledgment

Contents

List of Figures

List of Tables

List of Abbreviations

DOF	Degrees of freedom
SISO	Single Input, Single Output system
MIMO	Multiple Inputs, Multiple Outputs system
SISO	Single Input, Single Output system
MIMO	Multiple Inputs, Multiple Outputs system
LQR	Linear quadratic regulator
EKF	Extended Kalman filter
PID	Proportional integral derivative controller
SMC	Sliding mode controller
MPC	Model predictive controller
GAS	Global asymptotically stable
HOSM	High order sliding mode
HOSMC	High order sliding mode controller
HOSMO	High order sliding mode observer
LHP	Left half plane
RHP	Right half plane
ARE	Algebraic Riccati equation
RDE	Differential Riccati equation
AFL	Approximate feedback linearization
SP	Smith predictor

1 Introduction

The ball and plate system was firstly established in Rockwell laboratory of Czechoslovakia University in the mid-1990s. This system is a multivariable plant (MIMO), which is the extension of the ball and beam system. It has four degree of freedom consisting of a ball that can roll freely on a rigid plate operated by servomotors, in order to control the position of the ball [4].

The ball and plate system is widely used as a test bed for verifying the performance and effectiveness of new control algorithms [5]. It serves to visually demonstrate and reinforce the underlying principles of nonlinear dynamics and control theory, because of its inherent nonlinearity, instability and under actuation. The system is also influenced by nonlinearities like frictions, backlash effect, measurement time delay, parameters uncertainty and so on [6].

The stabilization control is to hold the ball at a desired position on the plate and trajectory tracking control demands the ball to follow a geometric path with associated timing law. Both tasks are challenging problems, especially when high tracking precision is desired. Since only feedback control based on linearized models are not suitable for tracking under higher tracking velocity, control design using nonlinear model and approaches is expected to be better [7].

1.1 State of the Art

Table 1.1 shows an overview about the hardware that is used in other ball and plate systems. The actuation is commonly realized by combinations of DC motors. Other implemented concepts use magnetic suspension actuators or stepper motors. The sensor system is realized either by cameras with machine vision or by touchscreen monitors. There are also works based on full setup commercial test-beds.

Most of the previous works use simplified models of the system, neglecting coupling terms. It is common to implement a cascaded structure for the controlled system, since the ball and plate system is under actuated with respect to the plate's angles and ball's position. An inner control loop is used for controlling the plate's angles and implemented commonly by a PID controller. In order to neglect the inner dynamics, the inner loop has to be very fast compared to the outer loop. The outer loop is used to control the ball's position. Many different concepts are implemented for the outer control loop. The used concepts are listed in Table 1.2 and can be divided into three general classes: Linear, nonlinear and knowledge based methods.

Table 1.1: List of used hardware in other projects.

Hardware	Used in
Actuation System	
DC Motors with Encoders	[8, 9, 10, 6]
Magnetic Suspension Actuators	[11]
Stepper Motors	[7]
Sensor System	
camera with machine vision	[9, 10, 7, 12, 5, 13, 4]
touchscreen sensor	[8, 11, 14, 15]
Commercial Test-beds	
Humusoft BP CE151	[16]
Googol Technology GPB2001	[17]

Table 1.2: List of control strategies applied in other projects.

Control Strategy	Used in
Linear Methods	
Lead Controller	[8]
Linear Quadratic Regulator (LQR)	[12, 9]
Model Predictive Control (MPC)	[16]
Nonlinear Methods	
Backstepping	[7, 11]
Flatness-based Linearization	[5, 13, 14]
Sliding-Mode Control (SMC)	[10, 6]
PD-Controller with Nonlinear Compensation	[4]
Knowledge Based Methods	
Fuzzy Sliding Mode Control	[18]
Neural Network Tuned PID	[17]

Linear methods in previous works are lead control, linear quadratic regulation and model predictive control. These control strategies are based on a decoupled, (simplified) linearized model.

The shown nonlinear methods are backstepping, flatness based input-output linearization, sliding mode control and a PD-controller with nonlinear compensation terms. These strategies are also based on simplified models, which are mainly provided to decouple the two axis of the system. Thus, the controlled systems are reduced to two ball and beam systems. The flatness-based concept requires the negligence of some terms, which increase the vector relative degree of the system.

In [13] two different flatness-based controllers are presented and compared with respect to robustness: An exact feedback linearization control law and an exact feedforward linearization control law. It is shown experimentally that the feedforward control law leads to a smoother tracking performance. Moreover, it is more robust against modeling errors and measurement noise than the feedback control [cf. 13].

Finally, there are some works that use knowledge based concepts for the regulation and tracking of the ball and plate system. These concepts are for instance a fuzzy sliding mode control and a PID controller, which is tuned by a radial basis function neural network.

Most of the shown concepts require full state information. Hence, a Luenberger or Kalman observer is used in many cases.

1.2 Objectives

This master thesis continues the work of previous projects [19, 3]. The concept of mechanism using belt-pulley will be changed to the transmition of movement using the cam-plate .

The main tasks in this work are:

- The modelling of the ball and plate system in work. Also analyze the controllability, observability of the system using the obtained model.

- The real time evaluation of the hardware, like the touch screen sensor and servomotors using dSpace real time system.

- Design the controller for regulation and tracking using different methods of nonlinear and linear controllers, and the comparison between them.

- Design the observer for the full feedback state controller, and compare some methods for obtain the best results (performance and robustness). Also will be designed a Smith predictor for compensate the dead-time of the touch screen sensor.

- Simulate the control system (controller , observer and predictor) using the exact nonlinear model in Simulink.

- Perform experimental test to verify the correct operation of the control system designed using the software and hardware provided by dSPACE for real time implementation

1.3 Limitation and Scope

The controlled system to design only will be the outer loop because the inner loop will be controlled by the servomotor controller. Also, for that reason only will be necessary to use the ball dynamic to design the control system because the plate dynamics will be controlled using the torques exerted by the servomotors. The servomotor are selected, such that the inner loop is fast enough.

1.4 Overview

The content presented in this thesis is organized as follows

Chapter 2 presents the most important concepts used in this thesis related to the analysis of the system and the design of the control system. Specifically, approximate and exact linearization, characteristics of the ball and plate system as the concepts of subactuated systems and non-minimal phase systems. In addition, the controller design process is presented using the linear approach, such as the pole placement and LQR, as well as nonlinear approaches: feedback linearization, backstepping and sliding mode. In the same way for the observer the design process is presented using linear approaches, such as the Luenberger observer and the Kalman filter; as well as nonlinear approaches, such as the nonlinear Luenberger observer and the extended Kalman filter. Finally, the compensation of the delay for the state estimation is presented.

Chapter 3 describes the ball and plate system implemented by the Control Engineering Group of TU Ilmenau. Specifically, the main characteristics and restrictions of the hardware components, such as the servo system, touch screen, encoders, dSPACE real-time system and the mechanism for motion transmission based on two cam-plate and a cardan joint are described in detail. It also presents the physical configuration of these components in order to have a better understanding of the operation of the system.

Chapter 4 presents the considerations taken for the mathematical modeling of the ball and plate system. This chapter also presents the calculation of the kinematics using matrices of coordinate transformation and the deduction of the dynamics equations using the Euler-Lagrange approach.

Chapter 5 presents the ball and plate system in its state-space and input affine representation, afterwards the analysis of observability and controllability is made through the rank condition of the matrices of observability and controllability, respectively. In addition, the Jacobi linearization of the system is performed to then analyze locally the stability in open loop. This linearization will then be used in later chapters to design the controller and linear observer for operation near to the equilibrium point.

Chapter 6 presents the design process of linear and nonlinear controllers. In the linear approach are considered the methods of pole placement and LQR. In the nonlinear approach the exact linearization of the system is analyzed through feedback linearization; however, the case of input-state is not possible, hence the case of input-output is studied but results a non-minimum phase system. Therefore, is difficult to use the exact model to design tracking controllers, mainly by the feedforward action, so proceed to take the approximation of the ball and plate system in its closest approximation with flat outputs. Then using the approximate model we proceed with

the controller design based on feedback linearization for tracking, the backstepping controller and finally the controller based on sliding mode.

Chapter 7 presents the design process of linear and nonlinear observers. In the linear approach the Luenberger observer and Kalman filter are considered. Also, in the nonlinear approach, the nonlinear Luenberger-like observer is used for the linear form of Brunovsky, calculated for the approximate model type flat, and then, through the observability matrix, the linear observer gain is converted to the nonlinear gain. The other nonlinear observer approach used is the extended Kalman filter which calculates the gain of the observer at each sampling time using the linearized system around the estimated mean of the states and the covariance matrices of the measurement noise and the disturbance input.

Chapter 8 simulations are shown and the performance of the different concepts is compared. It also shows the benefit of the inclusion of the Smith predictor to compensate the delay in the measurement of the ball's position.

Chapter 9 presents the experimental results of the most promising approach used for the design of the controller and observer for tracking control using different reference trajectories. In addition, the benefit of the inclusion of Smith predictor to compensate the delay in the measurement of the position of the ball is presented.

Chapter 10 concludes and summarizes the results of the present work as well as some useful recommendations. In addition, ideas are presented for possible future research work that could improve the results obtained.

2 Conceptual Framework

2.1 Linearization

The nonlinear system is represented using the following model:

$$\dot{\mathbf{x}} = f(\mathbf{x}, \mathbf{u})$$
$$\mathbf{y} = h(\mathbf{x}, \mathbf{u}),$$

(2.1)

where $\mathbf{x} \subset \mathbb{R}^n$, $\mathbf{u} \subset \mathbb{R}^p$ and $\mathbf{y} \subset \mathbb{R}^q$.

Jacobi Linearization around an Equilibrium Point [20]. A common source of linear system models is the approximation of a nonlinear system by a linear one. These approximations are aimed at studying the local behavior of a system, where the nonlinear effects are expected to be small.

To study local behavior of the system around the equilibrium point$(\mathbf{x}_e, \mathbf{u}_e)$, with $x - x_e$ and $u - u_e$ are both small, so that nonlinear perturbations around this equilibrium point can be ignored compared with the (lower-order) linear terms. These variables

$$\mathbf{z} = \mathbf{x} - \mathbf{x}_e, \quad \mathbf{v} = \mathbf{u} - \mathbf{u}_e, \quad \mathbf{w} = \mathbf{y} - h(\mathbf{x}_e, \mathbf{u}_e)$$

(2.2)

used are all close to zero when we are near the equilibrium point.

The Jacobi linearization of the nonlinear system is:

$$\dot{\mathbf{z}} = A\mathbf{z} + B\mathbf{v}, \quad \mathbf{w} = C\mathbf{z} + D\mathbf{v}$$

(2.3)

where

$$A = \frac{\partial f(\mathbf{x}, \mathbf{u})}{\partial \mathbf{x}}\bigg|_{\mathbf{x}_e, \mathbf{u}_e}, B = \frac{\partial f(\mathbf{x}, \mathbf{u})}{\partial \mathbf{u}}\bigg|_{\mathbf{x}_e, \mathbf{u}_e}, C = \frac{\partial h(\mathbf{x}, \mathbf{u})}{\partial \mathbf{x}}\bigg|_{\mathbf{x}_e, \mathbf{u}_e}, D = \frac{\partial h(\mathbf{x}, \mathbf{u})}{\partial \mathbf{u}}\bigg|_{\mathbf{x}_e, \mathbf{u}_e}.$$

(2.4)

The system 2.3 approximates the original system 2.1 when it's near the equilibrium point. If the linearization is asymptotically stable, then the equilibrium point x_e is locally asympotically stable for the nonlinear system.

Feedback Linearization. Feedback linearization is another type of linearization that uses feedback to convert the dynamics of a nonlinear system into those of a exact linear one [21].

More generally, we say that a system 2.1 is feedback linearizable if we can find a control law $u = \alpha(x, v)$ such that the resulting closed loop is input/output linear with input v and output y. We can also use the tools of linear system theory to analyze and design the control law for the linearized system, considering to apply the input transformation to obtain the actual input that will be applied to the system [21]. More details of this process are presented in 2.3.2.1.

2.2 Underactuated System

Underactuated multibody systems are system that have fewer control input than degrees of freedom . The concept of degrees of freedom is usually refereed to the generalized coordinates $\mathbf{q}$. Also is assumed than the number of inputs and outputs coincides [1].

In order to establish the nonlinear input-output normal form of an underactuated multibody systems the equation of motion (2.5a) with output (2.5b) is partitioned into two parts, actuated and unactuated part, presented in (2.6).

$$\mathbf{M}(\mathbf{q})\,\ddot{\mathbf{q}} + \mathbf{C}(\mathbf{q}, \dot{\mathbf{q}})\,\dot{\mathbf{q}} + \mathbf{G}(\mathbf{q}) = \mathbf{B}(\mathbf{q})\,\mathbf{u} \tag{2.5a}$$

$$\mathbf{y} = \mathbf{h}(\mathbf{q}) \tag{2.5b}$$

The actuated part is represented by the first row of (2.6) with input matrix $\mathbf{B}_a(\mathbf{q})$ nonsingular, and the unactuated part represented by the second row with input matrix $\mathbf{B}_u(\mathbf{q})$ singular or not full rank.

$$\begin{pmatrix} \mathbf{M}_{aa}(\mathbf{q}) & \mathbf{M}_{au}(\mathbf{q}) \\ \mathbf{M}_{au}^{\mathsf{T}}(\mathbf{q}) & \mathbf{M}_{uu}(\mathbf{q}) \end{pmatrix} \begin{pmatrix} \ddot{\mathbf{q}}_a \\ \ddot{\mathbf{q}}_u \end{pmatrix} + \begin{pmatrix} \mathbf{C}_{aa}(\mathbf{q}, \dot{\mathbf{q}}) & \mathbf{C}_{au}(\mathbf{q}, \dot{\mathbf{q}}) \\ \mathbf{C}_{ua}(\mathbf{q}, \dot{\mathbf{q}}) & \mathbf{C}_{uu}(\mathbf{q}, \dot{\mathbf{q}}) \end{pmatrix} \begin{pmatrix} \dot{\mathbf{q}}_a \\ \dot{\mathbf{q}}_u \end{pmatrix} + \begin{pmatrix} \mathbf{G}_a(\mathbf{q}) \\ \mathbf{G}_u(\mathbf{q}) \end{pmatrix} = \begin{pmatrix} \mathbf{B}_a(\mathbf{q}) \\ \mathbf{B}_u(\mathbf{q}) \end{pmatrix} \mathbf{u} \tag{2.6}$$

The actuated part has an independent input which directly acts on the generalized coordinates. The second part has not direct actuation input and thus is unactuated. The equation of motion simply reads as follows

$$\begin{pmatrix} \mathbf{M}_{aa}(\mathbf{q}) & \mathbf{M}_{au}(\mathbf{q}) \\ \mathbf{M}_{au}^{\mathsf{T}}(\mathbf{q}) & \mathbf{M}_{uu}(\mathbf{q}) \end{pmatrix} \begin{pmatrix} \ddot{\mathbf{q}}_a \\ \ddot{\mathbf{q}}_u \end{pmatrix} + \begin{pmatrix} \mathbf{C}_{aa}(\mathbf{q}, \dot{\mathbf{q}}) & \mathbf{C}_{au}(\mathbf{q}, \dot{\mathbf{q}}) \\ \mathbf{C}_{ua}(\mathbf{q}, \dot{\mathbf{q}}) & \mathbf{C}_{uu}(\mathbf{q}, \dot{\mathbf{q}}) \end{pmatrix} \begin{pmatrix} \dot{\mathbf{q}}_a \\ \dot{\mathbf{q}}_u \end{pmatrix} + \begin{pmatrix} \mathbf{G}_a(\mathbf{q}) \\ \mathbf{G}_u(\mathbf{q}) \end{pmatrix} = \begin{pmatrix} \mathbf{B}_a(\mathbf{q}) \\ \mathbf{0} \end{pmatrix} \mathbf{u} \tag{2.7}$$

While the control of fully actuated multibody systems is relatively straightforward and well established, the output trajectory tracking control problem of underactuated multibody systems

is much more complicated and not fully solved yet. The most obvious form of underactuation are multibody systems with passive joints [1].

Determination of the relative degree is useful for characterization of nonlinear systems. In general the determination of the relative degree requires a state-space representation and also the symbolic calculation of Lie derivatives [1] . Using the vector relative degree is possible to classify the underactuated multibody systems as is presented in Figure 2.1.
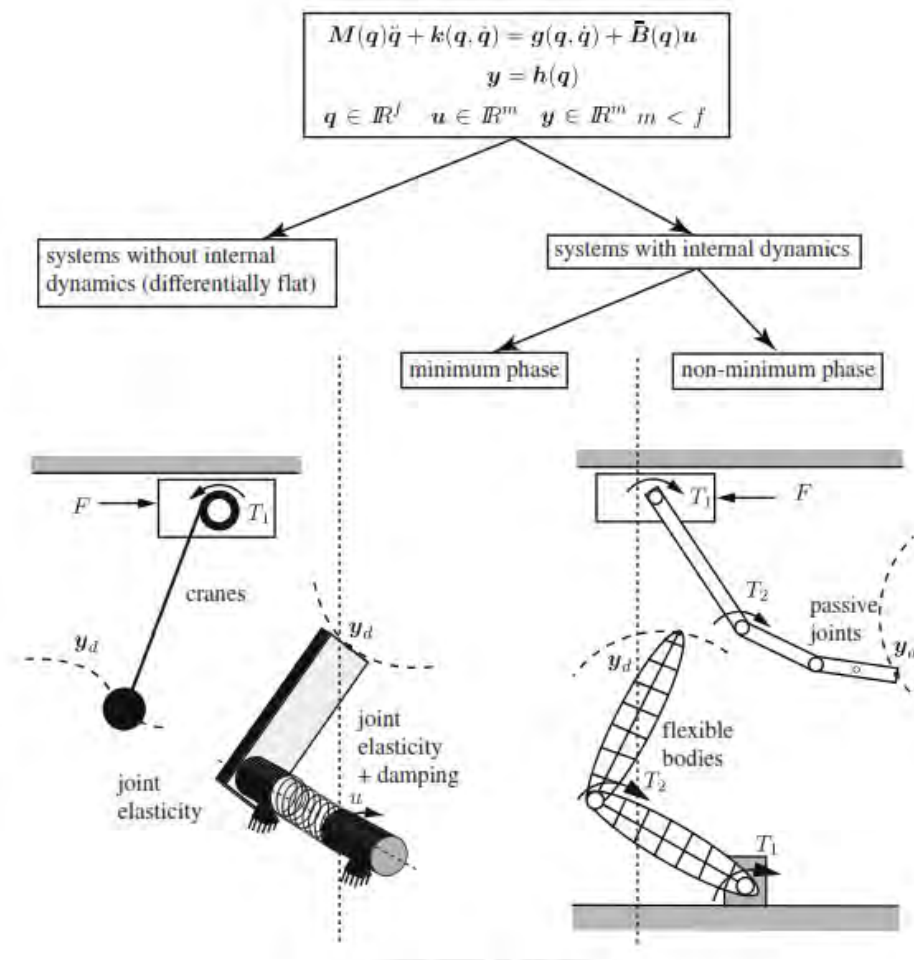
Figure 2.1: Classification of some underactuated multibody systems [1].

2.3 Full State-Feedback Controller

The controller full state feedback use information of all states to calculate the control action. The objective is that the designed control law has desirable closed-loop stability and performance.

2.3.1 Linear Controllers

For the case of linear (or linearized) system order n ($\mathbf{x} \subset \mathbb{R}^n$) represented by (2.8)

$$\dot{\mathbf{x}} = A\mathbf{x} + B\mathbf{u}$$
$$\mathbf{y} = C\mathbf{x}$$
(2.8)

The linear controller can be represented only as a state feedback gain. There are some alternatives to design the full-state feedback controller presented below [20].

Pole Placement. The eigenvalues of the closed loop system (2.9) can be assigned choosing the gain of the controller K in the complex plane.

$$\dot{\mathbf{x}} = (A - BK)\mathbf{x} + k_r r$$
$$\mathbf{y} = C\mathbf{x}$$
(2.9)

where r is the reference input and k_r the inverse of the DC gain of the closed loop system calculated as $k_r = -\left(C(A - BK)^{-1}B\right)^{-1}$. The useful equation to calculate in general the controller gain K in order to obtain the desired poles p_1, p_2, ... p_n is (2.10).

$$\det(sI - (A - BK)) = (s - p_1)(s - p_2)\ldots(s - p_n)$$
(2.10)

The desired poles represent the desired behavior of the closed loop system. Also is possible to calculate K converting first the system to the canonical controllable form.

Linear quadratic regulator (LQR). As an alternative to select the closed loop eigenvalue locations to accomplish a certain objective, the gains for a state feedback controller can instead be chosen by attempting to optimize a cost function. This can be particularly useful in order to balance the performance of the system with the magnitude of the inputs required to achieve that level of performance.

This controller solve the quadratic optimization problem: considering the linear system $\dot{\mathbf{x}} = A\mathbf{x} + B\mathbf{u}$, determine the gain K in $\mathbf{u} = -K\mathbf{x}$ that minimize the cost function [22] :

$$J = \int_0^\infty (\mathbf{x}^\mathsf{T} Q\mathbf{x} + \mathbf{u}^\mathsf{T} R\mathbf{u})\, dt,$$
(2.11)

where:
Q : weight matrix of the error states, positive definite or semi definite,
R : weight matrix of the control action , positive definite .

The control gain obtained is:

$$K_{lqr} = R^{-1}B^\mathsf{T}P \tag{2.12}$$

P is symmetric and positive definite matrix, that satisfy the Algebraic Riccati equation:

$$A^\mathsf{T}P + PA - PBR^{-1}B^\mathsf{T}P + Q = 0. \tag{2.13}$$

2.3.2 Nonlinear Controllers

2.3.2.1 Feedback Linearization

The central idea of the approach is to algebraically transform a nonlinear system dynamics into a (fully or partly) linear one, so that linear control techniques can be applied [21].

Input affine representation of nonlinear systems (2.14) can often be very useful to obtain a solution of a control problem.

$$
\begin{aligned}
\dot{\mathbf{x}} &= f(\mathbf{x}) + g(\mathbf{x})\mathbf{u}, && \mathbf{x} \subset \mathbb{R}^n, \mathbf{u} \subset \mathbb{R}^p \\
\mathbf{y} &= h(\mathbf{x}), && \mathbf{y} \subset \mathbb{R}^q
\end{aligned}
\tag{2.14}
$$

We consider to work with square systems, i.e. systems with the same number of inputs and outputs ($p = q$). The state vector $\mathbf{x}$ are local coordinates for the smooth n-dimensional manifold M_n. The vector fields $f(\mathbf{x})$, $g(\mathbf{x})$ are defined on the manifold M_n and are given in the local coordinates $\mathbf{x}$. For many necessary calculations it is sufficient to assume that the vector fields are sufficiently often differentiable. Both, the output function $h(\mathbf{x})$ and the input function $\mathbf{u}$ are smooth nonlinear functions [1].

Feedback linearization uses the geometric approach : the Lie algebra, the diffeomorphism, distribution and involutivity are concepts presented detail in [23].

Relative Degree. The relative degree is a system property, defined as the exactly number of derivatives of the output y which must be taken until of the inputs appear explicitly [1]. In the present work the notation of the relative degree will be r .

Input-State Linearization SISO case. Input state or full state linearization is a type of feedback linearization which can be applied to an input affine nonlinear systems as (2.14) with relative degree $r = n$ at some operation point [1].

A single-input nonlinear system in the form (2.14) with $f(\mathbf{x})$ and $g(\mathbf{x})$ smooth vector fields on $\mathbb{R}^n$, is said to be input-state linearizable if there exists a region Ω in $\mathbb{R}^n$, a diffeomorphism $T : \Omega \to \mathbb{R}^n$, and a nonlinear feedback control law

$$u = \alpha\left(\mathbf{x}\right) + \beta\left(\mathbf{x}\right)v, \tag{2.15}$$

such that the new state variables $\mathbf{z} = T(\mathbf{x})$ and new input v satisfy a linear time-invariant relation

$$\dot{\mathbf{z}} = A_z\mathbf{z} + B_z v \tag{2.16a}$$

where

$$A_z = \begin{pmatrix} 0 & 1 & 0 & \dots & 0 \\ 0 & 0 & 1 & \dots & 0 \\ \vdots & \vdots & \vdots & \vdots & \vdots \\ 0 & 0 & 0 & \dots & 1 \\ 0 & 0 & 0 & \dots & 0 \end{pmatrix}_{nxn} , \quad B_z = \begin{pmatrix} 0 \\ 0 \\ \vdots \\ 0 \\ 1 \end{pmatrix}_{nx1} . \tag{2.16b}$$

The new state $\mathbf{z}$ is called the linearizing state, and the control u is called the linearizing control law. Also the linear system (2.16) obtained after linearization is called Brunovsky form or Canonical Form [21].

The nonlinear system (2.14), with $f(\mathbf{x})$ and $g(\mathbf{x})$ being smooth vector fields, is input-state linearizable if, and only if, there exists a region Ω such that the following conditions hold [21]

- the vector fields $\left[g, ad_f g, \dots, ad_f^{n-1} g\right]$ are linearly independent in Ω.

- the distribution $\left[g, ad_f g, \dots, ad_f^{n-2} g\right]$ is involutive in Ω.

Input-Output Linearization SISO case. Input-output linearization is a type of feedback linearization for input affine nonlinear systems (2.14), where the given output $y = h(\mathbf{x})$ yields a relative degree $r < n$. In this case, it is not possible to apply input-state linearization, but it might be still possible to obtain by coordinate transformation and state feedback a subsystem with a linear behavior between the input and output. However, in this case there is no linear relationship between the input and all states of the transformed system and a nonlinear unobservable system remains called internal dynamics [1].

Using the new states **z** with the following notation :

$$
\mathbf{z} = \begin{pmatrix} z_1 \\ z_2 \\ \vdots \\ z_r \\ z_{r+1} \\ \vdots \\ z_n \end{pmatrix} = \begin{pmatrix} \xi_1 \\ \vdots \\ \xi_r \\ \eta_1 \\ \vdots \\ \eta_{n-r} \end{pmatrix} = \begin{pmatrix} \boldsymbol{\xi} \\ \boldsymbol{\eta} \end{pmatrix} \tag{2.17}
$$

and the state feedback law

$$
u = \frac{1}{\mathcal{L}_g \mathcal{L}_f^{r-1} h(\mathbf{x})} \left(-\mathcal{L}_f^r h(\mathbf{x}) + v \right) \tag{2.18}
$$

the system (2.14) is transformed to the Byrnes Isidori Normal Form (2.19) [23].

$$
\dot{\boldsymbol{\xi}} = A_z \boldsymbol{\xi} + B_z v \Leftrightarrow \begin{cases} \xi_1 &= y \\ \dot{\xi}_1 &= \xi_2 \\ &\vdots \\ \dot{\xi}_{r-1} &= \xi_r \\ \dot{\xi}_r &= v \end{cases} \tag{2.19a}
$$

$$
\dot{\boldsymbol{\eta}} = \mathbf{q}\left(\boldsymbol{\xi}, \boldsymbol{\eta}\right) \Leftrightarrow \begin{cases} \dot{\eta}_1 &= \tau_{r+1}\left(\boldsymbol{\xi}, \boldsymbol{\eta}\right) \\ &\vdots \\ \dot{\eta}_{n-r} &= \tau_n\left(\boldsymbol{\xi}, \boldsymbol{\eta}\right) \end{cases} \tag{2.19b}
$$

The new system is composed of two subsystems. The first subsystem is linear, has dimension r and represent a chain of integrators. The second subsystem is in general nonlinear of dimension $n - r$ and is called internal dynamics. The $n - r$ internal states are chosen according to

$$
\mathcal{L}_g \tau_j = 0 \ \text{ for } \ r + 1 \le j \le n, \tag{2.20}
$$

in order to obtain the internal dynamics in the form

$$
\dot{\boldsymbol{\eta}} = \mathbf{q}\left(\boldsymbol{\xi}, \boldsymbol{\eta}\right), \tag{2.21}
$$

otherwise the internal dynamics has the following form

$$
\dot{\boldsymbol{\eta}} = \mathbf{q}\left(\boldsymbol{\xi}, \boldsymbol{\eta}\right) + \mathbf{p}\left(\boldsymbol{\xi}, \boldsymbol{\eta}\right) \frac{1}{\mathcal{L}_g \mathcal{L}_f^{r-1} h(\mathbf{x})} \left(-\mathcal{L}_f^r h(\mathbf{x}) + v \right). \tag{2.22}
$$

The internal dynamics do not influenced the ζ states, and thus are observable. However, the internal dynamics are influenced by the ζ states and might influenced the new input v [1].

Similar to the input-state linearization approach one can use linear control methods. However, the control task is also influenced by the whole dynamics therefore the internal η states have to be bounded [1] .

Output Tracking Control SISO case. Output trajectory tracking deals with the problem of forcing the physical system to reproduce or follow a predefined desired reference output trajectory $y_d(t)$. In a perfect world, with precisely known initial conditions and model parameters and no external disturbances, this can be achieved by a pure feedforward control based on an exact inverse model of the physical system. However, since there are always disturbances or unknowns a control schema with additional feedback is required to compensate for these disturbances. This yields a so-called two degrees of freedom control structure, composed of a feedforward control and a feedback control. A trajectory generator provides a sufficiently smooth desired output trajectory. Moreover, the desired trajectory is at least r times differentiable [1].

In general, the design of the feedforward and feedback controller can be performed separately. There is a large number of techniques available for the design of the feedback part, such Jacobi linearization around the desired trajectory, resulting in a time-varying system [1]. A unified approach to design feedforward an feedback control based on feedback linearization for minimum phase nonlinear system is presented in (2.32).

The design of the feedforward controller is based on the model inversion. Model inversion, or dynamic inversion, means that for a given trajectory $y_d(t)$ the corresponding input $u_d(t)$ and the corresponding trajectories of the states $x_d(t)$ are computed as follows [1]

1. the input $u_d(t)$ and states $x_d(t)$ satisfy the differential equation of the system

$$\dot{x}_d = f\left(x_d\right) + g\left(x_d\right) u_d \tag{2.23}$$

2. the states $x_d(t)$ yields the desired output

$$h\left(x_d\right) = y_d \tag{2.24}$$

3. the states $x_d(t)$ satisfy the initial condition

$$x(t_0) = x_0 \tag{2.25}$$

Also the model inversion can be performed using the normal form (2.19). In order to perform the tracking control, the coordinates $\boldsymbol{\xi}$ must satisfy

$$
\begin{aligned}
\xi_1 &= y_d \\
\xi_2 &= \dot{y}_d \\
&\;\;\vdots \\
\xi_r &= y_d^{(r-1)}
\end{aligned}
\tag{2.26}
$$

with $\boldsymbol{\xi} = \boldsymbol{\xi}_d$.

Also, the rth derivative of the output has to satisfy

$$
y_d^{(r)} = \bar{\beta}\left(\boldsymbol{\xi}_d, \eta\right) + \bar{\alpha}\left(\boldsymbol{\xi}_d, \eta\right) u_d,
\tag{2.27}
$$

with the coefficient $\bar{\alpha}\left(z_o\right) \neq 0$, the feedforward control law for exact output tracking u_d is calculated as follows

$$
u_d = \frac{1}{\bar{\alpha}\left(z_o\right)}\left(-\bar{\beta}\left(\boldsymbol{\xi}_d, \eta\right) + y_d^{(r)}\right).
\tag{2.28}
$$

The η states appear unconstrained by the tracking problem and are the solution of the internal dynamics, which is driven by the $\boldsymbol{\xi}_d$ states, that must be stable in order to obtain a bounded feedforward control [1].

The simple pole-placement controller for stabilization (2.18) can be extended to asymptotic tracking control tasks of minimum phase nonlinear system with relative degree r [21]. Let

$$
\boldsymbol{\xi}_d = \begin{pmatrix} y_d & \dot{y}_d & \cdots & y_d^{(r-1)} \end{pmatrix}^{\mathsf{T}},
\tag{2.29}
$$

and define the tracking error vector by

$$
e(t) = \boldsymbol{\xi}(t) - \boldsymbol{\xi}_d(t)
\tag{2.30a}
$$

$$
\begin{pmatrix} e \\ \dot{e} \\ \vdots \\ e^{(r-1)} \end{pmatrix} = \begin{pmatrix} \xi_1 - y_d \\ \xi_2 - \dot{y}_d \\ \vdots \\ \xi_r - y_d^{(r-1)} \end{pmatrix},
\tag{2.30b}
$$

Choose constants p_i such that the polynomial (2.31) has all roots strictly in the left-half plane (LHP).

$$
P(s) = s^r + p_{r-1}s^{r-1} + \ldots p_1 s + p_0
\tag{2.31}
$$

Then, using the control law

$$u = \frac{1}{\mathcal{L}_g \mathcal{L}_f^{r-1} h(\mathbf{x})} \left(-\mathcal{L}_f^r h(\mathbf{x}) + y_d^{(r)} - p_{r-1} e^{(r-1)} - \ldots - p_0 e \right) \tag{2.32}$$

the whole state remains bounded and the tracking error $e(t)$ converges to zero [21].

Feedback Linearization MIMO case. The concepts used in the above sections for SISO systems can be extended to MIMO systems [23] .

Considering the MIMO square input affine system (2.14) in a better representation as follows

$$\dot{\mathbf{x}} = f(\mathbf{x}) + \sum_{i=1}^{p} g_i(\mathbf{x})\mathbf{u}_i$$
$$y_1 = h_1(\mathbf{x})$$
$$y_2 = h_2(\mathbf{x})$$
$$\vdots \tag{2.33}$$
$$y_p = h_p(\mathbf{x})$$

The relative degree of each output is calculated using the differentiation until the first time at least one of the p inputs appears explicitly, then is obtained

$$y_i^{(k)} = \mathcal{L}_f^k h_i(\mathbf{x}), \quad 0 \le k \le r_i - 1, \quad 0 \le i \le p \tag{2.34}$$

$$y_i^{(r_i)} = \mathcal{L}_f^{r_i} h_i(\mathbf{x}) + \sum_{j=1}^{p} \mathcal{L}_{g_j} \mathcal{L}_f^{r_i-1} h_i(\mathbf{x}) u_j \tag{2.35}$$

with $\sum_{j=1}^{p} \mathcal{L}_{g_j} \mathcal{L}_f^{r_i-1} h_i(\mathbf{x}) u_j \neq 0$ results the vector relative degree $r = \{r_1, r_2, \ldots, r_p\}$ and $r = r_1 + \ldots r_p$ is called the sum or total relative degree.

The rth derivative of each output can be summarized in the following vector representation

$$\begin{bmatrix} y_1^{(r_1)} \\ \vdots \\ y_p^{(r_p)} \end{bmatrix} = \begin{bmatrix} \mathcal{L}_f^{r_1} h_1(\mathbf{x}) \\ \vdots \\ \mathcal{L}_f^{r_p} h_p(\mathbf{x}) \end{bmatrix} + \begin{bmatrix} \mathcal{L}_{g_1} \mathcal{L}_f^{r_1-1} h_1(\mathbf{x}) & \ldots & \mathcal{L}_{g_p} \mathcal{L}_f^{r_1-1} h_1(\mathbf{x}) \\ \vdots & \ddots & \vdots \\ \mathcal{L}_{g_1} \mathcal{L}_f^{r_p-1} h_p(\mathbf{x}) & \ldots & \mathcal{L}_{g_p} \mathcal{L}_f^{r_p-1} h_p(\mathbf{x}) \end{bmatrix} \begin{pmatrix} u_1 \\ \vdots \\ u_p \end{pmatrix}. \tag{2.36}$$

Using the new variable v as input of the linearized system, then following equation is obtained:

$$v = b(\mathbf{x}) + A(\mathbf{x})\mathbf{u}. \tag{2.37}$$

The matrix $A(\mathbf{x})$ is called decoupling matrix and must be regular in order to have well defined vector relative degree r and therefore a **noninteracting control problem** [23].

The control law in original coordinates, called decoupling control law, is calculated as

$$\mathbf{u} = A^{-1}(\mathbf{x})\,(v - b(\mathbf{x})) \tag{2.38}$$

The new state vector using the state transformation as follows

$$z = T(\mathbf{x}) = \begin{bmatrix} \xi \\ \eta \end{bmatrix}, \tag{2.39}$$

convert the system (2.33) into the Byrnes Isidori Normal Form [23] presented below

$$\text{External dynamics} \begin{cases} \dot{\xi}_1^1 &= \xi_2^1 \\ \vdots \\ \dot{\xi}_{r_1}^1 &= b_1(\boldsymbol{\xi}, \boldsymbol{\eta}) + \sum_{j=1}^{p} a_{1j}(\boldsymbol{\xi}, \boldsymbol{\eta}) u_j \\ y_1 &= \xi_1^1 \\ \dot{\xi}_1^2 &= \xi_2^2 \\ \vdots \\ \dot{\xi}_{r_2}^2 &= b_2(\boldsymbol{\xi}, \boldsymbol{\eta}) + \sum_{j=1}^{p} a_{2j}(\boldsymbol{\xi}, \boldsymbol{\eta}) u_j \\ y_2 &= \xi_1^2 \\ \vdots \\ \dot{\xi}_1^p &= \xi_2^p \\ \vdots \\ \dot{\xi}_{r_p}^p &= b_p(\boldsymbol{\xi}, \boldsymbol{\eta}) + \sum_{j=1}^{p} a_{pj}(\boldsymbol{\xi}, \boldsymbol{\eta}) u_j \\ y_p &= \xi_1^p \end{cases} \tag{2.40}$$

$$\text{Internal dynamics} \left\{ \dot{\boldsymbol{\eta}} = q(\boldsymbol{\xi}, \boldsymbol{\eta}) + \sum_{j=1}^{p} p_j(\boldsymbol{\xi}, \boldsymbol{\eta}) u_j \right. \quad . \tag{2.41}$$

Also, if the distribution $\{g_1, \ldots, g_p\}$ is involutive and the vector fields $\tau_{r+1}(\mathbf{x})$ to $\tau_n(\mathbf{x})$ are chosen such that

$$\frac{\partial \tau_i(\mathbf{x})}{\partial \mathbf{x}} g(\mathbf{x}) = 0 \quad , \quad n - r \leq i \leq n \tag{2.42}$$

the internal dynamics can be expressed as

$$\dot{\boldsymbol{\eta}} = q(\boldsymbol{\xi}, \boldsymbol{\eta}), \quad \boldsymbol{\eta} \subset \mathbb{R}^{n-r}. \tag{2.43}$$

Finally the exact linearized system, sometimes reduced order, is as follows

$$\dot{\boldsymbol{\xi}} = A_z \boldsymbol{\xi} + B_z v, \quad \boldsymbol{\xi} \subset \mathbb{R}^r$$
$$y = C \boldsymbol{\xi},$$

(2.44)

where (A_z, B_z, C_z) is a Brunovsky form, i.e. controllable and observable.

2.3.2.2 Backstepping Control

The backstepping approach, a recursive Lyapunov-based scheme, was proposed in the beginning of 1990s. With this method, the construction of feedback control laws and Lyapunov functions is systematic, following a step-by-step algorithm [24]. In the last two decades, backstepping has gained immense popularity as a nonlinear control design algorithm providing an alternative to feedback linearization [25].

Backstepping can be used to relax the matching condition, which blocked the traditional Lyapunov-based design. A major advantage of backstepping is that it has the flexibility to avoid cancellations of useful nonlinearities and achieve regulation and tracking properties. The technique was comprehensively addressed by Krstic, Kanellakopoulos and Kokotovic [24].

Backstepping is suited for the class of **strict feedback systems** [24]. The idea of backstepping is to design a controller recursively by considering some of the state variables as **virtual controls** and designing for them intermediate control laws. Backstepping achieves the goals of stabilization and tracking. The proof of these properties is a direct consequence of the recursive procedure, because a Lyapunov function is constructed for the entire system [24].

Integrator Backstepping assumption. Consider the system

$$\dot{x}_1 = f(x_1) + g(x_1)u \ , \ f(0) = 0$$

(2.45)

where $x_1 \subset \mathbb{R}^{n_1}$ is the state and $u \subset \mathbb{R}$ is the control input. There exist a continuously differentiable feedback control law

$$u = \alpha(x_1), \ \alpha(0) = 0,$$

(2.46)

and a smooth, positive definite, radially unbounded function $V : \mathbb{R}^{n_1} \to \mathbb{R}$ such that

$$\frac{\partial V(x_1)}{\partial x_1} (f(x_1) + g(x_1)\alpha(x_1)) \leq -W(x_1) \leq 0, \ \forall x_1 \subset \mathbb{R}^{n_1},$$

(2.47)

where $W : \mathbb{R}^{n_1} \to \mathbb{R}$ is positive semidefinite. Under this assumption, the control (2.46) applied to the system (2.45), guarantees global boundedness of $x_1(t)$, and via the LaSalle Theorem, the

regulation of $W(\boldsymbol{x}_1(t))$:

$$\lim_{x \to \infty} W(\boldsymbol{x}_1(t)) = 0. \tag{2.48}$$

Clearly, if $W(\boldsymbol{x}_1)$ is positive definite, the control renders $\boldsymbol{x}_1 = \boldsymbol{0}$ the globally asymptotically stable equilibrium of (2.45) [26].

Integrator Chain Backstepping. Let the system satisfying the previous assumption with $\alpha(\boldsymbol{x}_1) = \alpha_0(\boldsymbol{x}_1)$ be augmented by a chain of k integrators such that u is replaced by x_2, the state of the last integrator in the chain :

$$
\begin{aligned}
\dot{\boldsymbol{x}}_1 &= f(\boldsymbol{x}_1) + g(\boldsymbol{x}_1) x_2 \\
\dot{x}_2 &= x_3 \\
&\vdots \\
\dot{x}_{k-1} &= x_k \\
\dot{x}_k &= u.
\end{aligned}
\tag{2.49}
$$

For this system, the procurement of integrator backstepping presented in [26] with $x_2, \ldots, x_k$ as virtual controls, results in the Lyapunov function

$$V_a(\boldsymbol{x}_1, x_2, \ldots, x_k) = V(\boldsymbol{x}_1) + \frac{1}{2} \sum_{i=1}^{k} (x_i - \alpha_{i-1}(\boldsymbol{x}_1, x_2, \ldots, x_{k-1}))^2. \tag{2.50}$$

Any choice of feedback control which renders $\dot{V}_a \leq -W_a(\boldsymbol{x}_1, x_2, \ldots, x_k) \leq 0$, with $W_a(\boldsymbol{x}_1, x_2, \ldots, x_k) = 0$ only if $W(\boldsymbol{x}_1) = 0$ and $\boldsymbol{x}_1 \neq \alpha_{i-1}(\boldsymbol{x}_1, x_2, \ldots, x_{k-1})$, $i = 1, \ldots, k$, guarantees that $(\boldsymbol{x}_1(t), x_2(t), \ldots, x_k(t))^T$ is globally bounded and converges to a largest invariant set. Furthermore, if $W(\boldsymbol{x}_1)$ is positive definite, that is $\boldsymbol{x}_1 = \boldsymbol{0}$ can be rendered globally asymptotically stable through $\boldsymbol{x}_1$ then (2.50) is a control Lyapunov function for (2.49) and the equilibrium $\boldsymbol{x}_1 = \boldsymbol{0}, x_2 = \ldots = x_k = 0$ can be rendered globally asymptotically stable through u [26].

2.3.2.3 Sliding Mode Control

Sliding mode control is a particular approach of robust control. In the formulation of practical control problems, there will be discrepancy between the actual plant and its mathematical model used for controller design. These discrepancies arise from unknown external disturbances, plant parameters, and unmodeled dynamics. Using sliding mode control is possible to the design control laws that provide the desired performance to the closed-loop system in the presence of the mentioned discrepancies [27].

The modeling inaccuracies can have strong adverse effects on nonlinear control systems. Sliding mode control is based on the remark that is much easier to control 1st order systems, be they nonlinear or uncertain, than it is to control general n^{th} order systems. High order systems can be replaced by 1st order problems. It is then easy to show that, for the transformed system, perfect performance can in principle be achieved in presence of arbitrary parameter inaccuracies. However, it is obtained at the price of extremely high control activity. This lead us to modify the control law, given the admissible control activity, is aimed at achieving an effective trade-off between tracking performance and parametric uncertainty [21].

Sliding Variable. The idea of sliding mode control is based on the introduction of a designed function σ named sliding variable. As soon as the properly designed sliding variable becomes equal to zero, it defines the sliding manifold or sliding surface. The proper design of the sliding variable yields suitable closed-loop system performance while the systems trajectories belong to the sliding surface [27].

Conventional Sliding Mode Control. Conventional sliding mode control is focus in the creation of sliding surfaces , or hyperplanes, which give appropriate close-loop dynamics when sliding motion is induced [27].

Consider a surface in the state space given by

$$\mathbb{S} = \{\mathbf{x} : \sigma(\mathbf{x}) = 0\}, \tag{2.51}$$

an ideal sliding mode is said to take place if the states $\mathbf{x}(t)$ evolve with time such that $\sigma(\mathbf{x}(t_r)) = 0$ for some finite $t_r \in \mathbb{R}^+$ and $\sigma(\mathbf{x}(t)) = 0$ for all $t > t_r$.

During a sliding mode, $\sigma(\mathbf{x}(t)) = 0$ for all $t > t_r$. Intuitively this dynamical collapse implies the motion of the system when confined to $\mathbb{S}$ will be of reduced dynamical order. If the control action $u = u(\mathbf{x})$ is discontinuous, the differential equation describing the resulting closed loop system is discontinuous respect to the state vector and therefore is now not applicable the classical theory of differential equations since Lipschitz assumptions are usually employed to guarantee the existence of unique solution. The solution concept proposed by Filippov for differential equations with discontinuities right-hand sides constructs a solution as the average of the solutions obtained from approaching the point of discontinuity from different directions [27].

The equivalent control u_{eq} is the control action necessary to maintain an ideal sliding motion on the sliding surface. The idea is to exploit the fact that in conventional sliding modes both $\sigma = \dot{\sigma} = 0$. The equivalent control depends on the disturbance which will be generally unknown [27].

The conventional sliding mode design approach requires the system requires the relative degree to be equal to one with respect to the sliding variable, it is very limited, and very often yields to high-frequency switching control action that leads to the so-called chattering effect. These intrinsic difficulties are mitigated by high-order sliding mode controllers (HOSM) [27].

Chattering Attenuation. In many practical control systems is important to avoid control chattering by providing continuous and smooth control signal but at the same time it is desirable to retain the robustness and insensitivity of the control system to bounded model uncertainties and external disturbances. Chattering elimination using **quasi-sliding mode** is a solution make the control function continuous and smooth is to approximate the discontinuous function $v(\sigma) = -\rho\,\text{sign}(\sigma)$ by some continuous/smooth function as **sigmoidal function** represented by

$$\text{sign}(\sigma) \approx \frac{\sigma}{|\sigma| + \varepsilon} \tag{2.52}$$

where ε is a small positive scalar. It can be observed that

$$\lim_{\varepsilon \to \infty} \frac{\sigma}{|\sigma| + \varepsilon} = \text{sign}(\sigma), \ \ \sigma \neq 0. \tag{2.53}$$

The value of ε should be selected to trade-off the requirement to maintain an ideal performance with that of a smooth control effort. The smooth control cannot provide finite-time convergence of the sliding variable σ to zero in the presence of external disturbance. Besides, the sliding variable and the state variables do not converge to zero at all, but instead converge to domains in a vicinity of the origin due the effect of the disturbances (if exist).

The price to pay for obtaining smooth control action is a loss of robustness and, as result, a loss of accuracy. However, the system's performance under the smooth control law is close to the system's performance under the discontinuous sliding mode control. Another method of chattering elimination is **asymptotic sliding mode**. This method design a sliding mode control in terms of the control function derivative ($v = \dot{u}$). In this case, the actual control, which is the integral of the high frequency switching function, is continuous. In this approach, the original variable σ converges to zero only asymptotically. This is the price to pay for chattering attenuation [27].

High Order Sliding Mode Control (HOSMC). The high-order sliding modes solve the problems of arbitrary relative degree r. The realization of the scheme requires to calculate or measure a number of successive time derivatives of the sliding variables. However, that problem is solved within a similar framework that use arbitrary-order exact robust differentiators. The higher order sliding mode controllers are able to drive to zero not only the sliding variable but also its $k-1$ successive derivatives (k^{th} order sliding mode)[27].

The two most well-known arbitrary order sliding mode controllers are the **nested sliding controllers** and the **quasi-continuous sliding controllers**. These controllers have the following form

$$u = -\alpha \Psi_{r-1,r} \left(\sigma, \dot{\sigma}, \dots, \sigma^{(r-1)} \right) \tag{2.54}$$

defined by recursive procedures and solve the general output regulation problem. The parameters of the controller can be chosen for each relative degree r [27].

The nested sliding mode controllers, used in the present thesis work, are defined by r-sliding controllers, based on a pseudo-nested structure of 1-sliding modes. The controllers are built by the following recursive procedure :

$$N_{i,r} = \left(|\sigma|^{q/r} + |\dot{\sigma}|^{q/(r-1)} + \dots + |\sigma^{(i-1)}|^{q/(r-i+1)} \right)^{1/q} \tag{2.55}$$

$$\Psi_{0,r} = \mathrm{sign}(\sigma), \quad \Psi_{i,r} = \mathrm{sign} \left(\sigma^{(i)} + \beta_i N_{i,r} \Psi_{i-r,r} \right), \tag{2.56}$$

with $q \in \mathbb{N}$, $q > 1$ and β_i are tuning parameters which define the convergence rate [27].

2.4 Non-Minimum Phase System

In general, a nonlinear system is non-minimum phase when it has unstable zero dynamics [21]. In order to understand the concept of the non-minimum phase property and its influence in the control design are presented the following definitions :

Internal Dynamics. Is the part of the system dynamics that result unobservable in the input-output linearization. The internal states can be chosen. If the internal dynamics is stable (bounded during tracking), the tracking control design can be solved. For linear systems are the internal dynamics result the zero dynamics [21].

Zero Dynamics. The zero-dynamics is an intrinsic feature of a nonlinear system which does not depend on the choice of control law or desired trajectories. Also, zero-dynamics is defined to be the internal dynamics of the system when the system output and its derivatives are kept at zero by the input. Examining the stability of zero-dynamics is much easier than examining the stability of internal dynamics because zero dynamics involves only internal states and has reduced form (while the internal dynamics is coupled to the external dynamics and desired trajectories) [21].

Minimum Phase System. The nonlinear system is said to be locally asymptotically (exponentially) minimum phase at $\mathbf{x}_0$ if the the equilibrium point $\boldsymbol{\eta} = 0$ is locally asymptotically (exponentially) stable.

It is important to note that the minimum phase property of a nonlinear system depends on the equilibrium point $\mathbf{x}_0$ of the undriven system under consideration. Thus, a nonlinear system may be minimum phase at some equilibrium points and be non-minimum phase at some others [28].

For linear systems, the stability of the zero-dynamics implies the global stability of the internal dynamics. However in nonlinear systems is different, local or even global asymptotic stability of the zero-dynamics is enough to guarantee the local asymptotic stability of the internal dynamics [21].

Dynamic Inversion. For non-minimum phase systems is applied stable inversion dynamics that requires the solution of a boundary value problem and yields a non-causal solution. However, stable inversion requires hyperbolic zero-dynamics i.e. that the zero-dynamics have no eigenvalues on the imaginary axis [1].

Trajectory Tracking for Non-minimum Phase Systems. For non-minimum phase systems perfect tracking and asymptotic tracking cannot be achieved. The inability of perfect tracking for a non-minimum phase system has its roots in its inherent tendency of undershooting in its step response. Thus the control design objective for non-minimum phase system should not be perfect tracking or asymptotic tracking. Instead we should be satisfied with bounded error tracking for desired trajectories of interest. For non-minimum phase systems perfect tracking of arbitrary trajectories requires infinite control effort [21].

The tracking control is a topic of active current research. There are some methods to solve the tracking problem for non-minimum phase systems presented below [21].

- Output redefinition so that the resulting zero-dynamics is stable. The new output should be practically the same that the original output in the operation range.

- Approximate zero-dynamics or approximate feedback linearization. Obtain flat outputs neglecting some terms that affect the full relative degree.

- Modification of the plant, i.e. addition of actuators and sensors, or modification of the construction of the plant.

Also, there are other methods presented in [28] for tracking with bounded state trajectories of non-minimum phase systems presented below:

- The Method of Devasia, Chen, and Paven

  This method has two steps, the first use numerical methods to solve the internal dynamics that represent non-causal solution for the feedforward part, and the second step stabilize the Jacobi linearized closed loop system.

- Byrnes Isidori Regulator This method use a exosystem to generate the reference trajectory and stabilize the tracking error using the Jacobi linearized closed loop system.

The previous methods are restricted usually to smooth trajectories and low frequencies, and depend of the neighborhood of the Jacobi linearization used for the stabilization. Also, for real time application, it result computational expensive.

2.5 Output Feedback and Observers

In most cases the complete state information is not available due to lack of sensors, thus is necessary to observe the other not measured states. Also, when the output measurement is corrupted by noise, it is useful to apply and observer which reduces the noise effects and acts as a filter. This case corresponds to the full-order observer. When the observability condition is fulfilled is possible to design an observer. Furthermore its is required that the estimation error converges quickly relative to the system's dynamics, so that it can be used for the controller.

2.5.1 Linear Observers

An observer is a linear dynamical system that takes the inputs and outputs of the system we are observing and produces an estimate of the system's state.
The general representation is as follows [20]

$$\dot{\hat{\mathbf{x}}} = A\hat{\mathbf{x}} + B\mathbf{u} + L(\mathbf{y} - C\hat{\mathbf{x}}) \tag{2.57}$$

This version will also works for unstable systems. The feedback from the measured output is provided by adding the term $L(y - C\hat{x})$. The dynamics of the estimation error is presented below

$$\dot{\tilde{\mathbf{x}}} = (A - LC)\tilde{\mathbf{x}} \tag{2.58}$$

The most used methods to calculate the observer gain are:

Pole placement (Luenberger). Is a generic observer with which the objective is to guarantee the stability of the estimation error and to fulfill design characteristics using the poles placement. The matrix L must be chosen in such a way that the matrix $A - LC$ has eigenvalues with negative real parts, such that the error $\tilde{x}$ will go to zero. The convergence rate is determined by an appropriate selection of the eigenvalues. The observer design problem is the dual of the state feedback design problem as follows:

$$A \leftrightarrow A^{\mathsf{T}}, \ B \leftrightarrow C^{\mathsf{T}}, \ K \leftrightarrow L^{\mathsf{T}} \tag{2.59}$$

The observer gain L is a matrix that tells how the estimation error is weighted and distributed among the states. The observer thus combines measurements with a dynamical model of the system [20].

Kalman Bucy Filter like Observer. Theoretically the Kalman filter is an estimator for the linear-quadratic problem, it is an interesting technique to estimate the instantaneous state of a linear dynamic system perturbed by white-noise measurements that is linearly related to the corrupted white noise state. The resulting estimator is statistically optimal with respect to any quadratic function of the estimation error [29].

The Kalman filter analyses a dynamic system's behavior with external disturbance and measurement noise. In general, the output is affected by noise measurement. In addition, the process dynamics are also affected by disturbances. By defining, a continuous-time process and measurement model is as follows:

$$\begin{aligned} \dot{\mathbf{x}} &= A\mathbf{x} + B\mathbf{u} + W\omega \\ \mathbf{y} &= C\mathbf{x} + \eta \end{aligned} \tag{2.60}$$

where w and v are zero-mean Gaussian noises (uncorrelated from each other). The following process and measurement covariance matrices hold namely :

$$E\{\eta(t)\eta^{\mathsf{T}}(s)\} = R\delta(t-s) \tag{2.61a}$$
$$E\{\eta(t)\omega^{\mathsf{T}}(s)\} = 0 \tag{2.61b}$$
$$E\{\omega(t)\omega^{\mathsf{T}}(s)\} = Q\delta(t-s) \tag{2.61c}$$

Using the general structure of the linear observer (2.57), in this approach L is the Kalman gain calculated as:

$$L = SC^{\mathsf{T}}R^{-1}, \tag{2.62}$$

where covariance matrix S, is the solution to a Riccati Differential Equation (RDE) or an Algebraic Riccati Equation (ARE). For the time invariant linear case, the ARE is

$$AS + SA^\mathsf{T} - SC^\mathsf{T}R^{-1}CS + WQW^\mathsf{T} = 0. \tag{2.63}$$

The dependent variable in the Riccati differential equation of the Kalman-Bucy filter is the covariance matrix of the estimation error, defined as the difference between the estimated state vector $\hat{x}$ and the true state vector **x**. The matrix S is the covariance matrix of the estimation error, with initial value chosen as:

$$S_0 = E\{[\mathbf{x}(t) - \mathbf{x}(\hat{t})][x(t) - \mathbf{x}(\hat{t})]^\mathsf{T}\} \text{ at } t \to \infty \tag{2.64}$$

The state error covariance S is a square and symmetric order n matrix, and must remain positive definite to retain filter stability. Diagonal elements of this matrix are variances of errors of the estimations for corresponding components of the state vector.

2.5.2 Nonlinear Observers

Extended Luenberger Observer. The gain of this Luenberger-like observer can be calculated straightforward. The nonlinear system to is considered fully linearized using exact linearization, then a linear observer can be used to calculate the nonlinear observer gain for the nonlinear system. The proof is presented in the work [30].

The representation of the linear observer using the Brunovsky form (2.16) with the Luenberger's structure is:

$$\begin{aligned}
\dot{\hat{\mathbf{z}}} &= A_z\hat{\mathbf{z}} + B_z\mathbf{v} + G(\mathbf{y} - \hat{\mathbf{y}}) \\
\hat{\mathbf{y}} &= C_z\hat{\mathbf{z}}
\end{aligned} \tag{2.65}$$

where G is the linear observer gain and is calculated using the pole placement or Kalman approach.

The linear observer (2.65) is converted to the nonlinear observer presented below

$$\dot{\hat{\mathbf{x}}} = \bar{f}(\hat{\mathbf{x}}) + \bar{g}(\hat{\mathbf{x}})\mathbf{u} + L(\hat{\mathbf{x}})(\mathbf{y} - h(\hat{\mathbf{x}})), \quad \hat{\mathbf{x}}(0) = \hat{\mathbf{x}}_0 \tag{2.66}$$

using the transformation of the observer gain trough the observability matrix as follows

$$L(\hat{\mathbf{x}}) = \bar{O}^{-1}(\hat{\mathbf{x}})G \tag{2.67}$$

where $\bar{O}(\hat{\mathbf{x}})$ is the observability matrix (2.68) of the system and is calculated as the Jacobian matrix obtained from nonlinear coordinate transformation [31].

$$\bar{O}(\hat{\mathbf{x}}) = \frac{d\mathbf{T}(\mathbf{x})}{d\hat{\mathbf{x}}} = \frac{d}{d\hat{\mathbf{x}}} \begin{pmatrix} h(\mathbf{x}) \\ \mathcal{L}_f h(\mathbf{x}) \\ \vdots \\ \mathcal{L}_f^{n-1} h(\mathbf{x}) \end{pmatrix} \tag{2.68}$$

Extended Kalman Filter (EKF). The extended Kalman filter is a local observer. This method is useful when is possible to model the process and measurement noise together with the nonlinear representation of the system :

$$\begin{aligned} \dot{\mathbf{x}} &= f(\mathbf{x}) + g(\mathbf{x})\mathbf{u} + W\omega \\ \mathbf{y} &= h(\mathbf{x}) + \eta \end{aligned} \tag{2.69}$$

where ω , η, W are identical referring to (7.6).

Using the extended kalman filter method is possible to calculate the observer gain with the approximate linearized system (around the mean of the states) and then replace it in the nonlinear observer structure (2.73) [32].

The linearized system around the mean of the states is represented by :

$$A = \frac{\partial f(\mathbf{x})}{\partial \mathbf{x}}\bigg|_{\mathbf{x}=\hat{\mathbf{x}}}, \quad B = g(\hat{\mathbf{x}}), \quad C = \frac{\partial h(\mathbf{x})}{\partial \mathbf{x}}\bigg|_{\mathbf{x}=\hat{\mathbf{x}}}. \tag{2.70}$$

The Kalman gain is calculated as follows

$$L = SC^\mathsf{T} R^{-1}, \tag{2.71}$$

being S be a solution of the following Riccati equation

$$AS + SA^\mathsf{T} - SC^\mathsf{T} R^{-1} CS + WQW^\mathsf{T} = 0. \tag{2.72}$$

Finally the EKF observer equation results in :

$$\dot{\hat{\mathbf{x}}} = f(\hat{\mathbf{x}}) + g(\hat{\mathbf{x}})\mathbf{u} + L(\mathbf{y} - h(\hat{\mathbf{x}})) \tag{2.73}$$

2.6 Delay compensation in the measurement

Dead time processes, also called process with delay, are common in industry and it has been shown that the controller design for systems exhibiting dead time is more difficult than for dead

time free systems. Dead times are mainly caused by information, energy or mass transportation phenomena, but they can also be caused by processing time or by the accumulation of time lags in a number of simple dynamic systems connected in series [2].

Furthermore there are two types of dead-time system: dead time in the actuators and dead time in the measurements, in this work is only analyzed dead time in the measurements because the problem is with the considerable dead time of the touch screen [2].

2.6.1 Smith Predictor

The Smith predictor uses the system model without delay and the value of the delay to predict the actual value of the delayed outputs. Using a perfect model of the system this approach gives a ideal solution [2].

There are some approaches to work with the Smith predictor, in discrete and continuous time, also work with the nonlinear or linear systems (linearized model in the case of nonlinear system).

The continuous representation of the Smith predictor for linear SISO systems with output delayed τ seconds is presented in Figure 2.2.
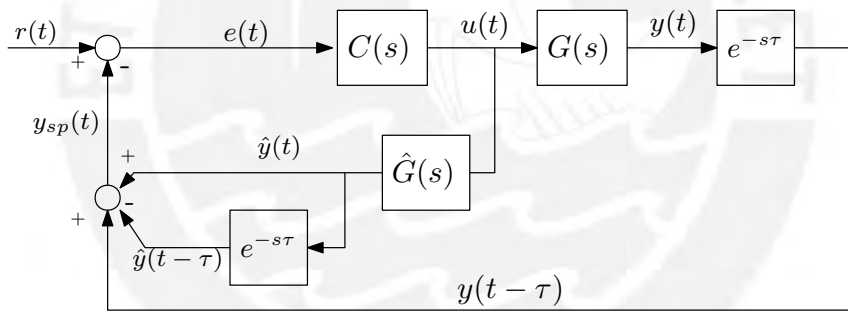
Figure 2.2: Continuous representation of the Smith predictor [2].

The predicted continuous output is given by

$$y_{sp}(t) = y(t - \tau) - \hat{y}(t - \tau) + \hat{y}(t); \tag{2.74a}$$

hence, the continuous control error is calculated with the following equation

$$e(t) = r(t) - y_{sp}(t) \tag{2.74b}$$

$$e(t) = r(t) - (y(t - \tau) - \hat{y}(t - \tau) + \hat{y}(t)). \tag{2.74c}$$

3 Physical Setup

This chapter describes features of the ball and plate system hardware developed by the Control Engineering Group of TU Ilmenau, in addition to the configuration it has. The details of the calculations and selection criteria of the components are detailed in [3].

The physical setup of the ball and plate system is shown in Figure 3.1. The principle of operation is based on the transmission of the movement from the servomotor to the screen using cam-plates and a cardan joint in the rotation center.

The main characteristics of the physical configuration of the system are [3]:

- It has a spring connected to the screen and a fixed point, so that it always keeps in contact the cam-plates and the support wheels connected to the screen.

- Because there is no fixed connection between the support wheels connected to the screen and the cam-plates, there is movement of the contact points when rotating simultaneously on both x and y axes (cf. Figure 3.1). Therefore, a compensation of the error caused by the movement of the contact points using experimentally calculated lookup tables is performed.

- The dimension of the screen is 39 cm x 70 cm. However, the operation range of displacement of the ball over the screen is considered from -0.25 m to 0.25 m in the $x-$ axis and from -0.15 m to 0.15 m in the $y-$ axis.

- The operation range of rotation in both axes allowed according to the physical configuration is from -10 to 10 degrees.

- The maximum angular acceleration of the screen is $|\ddot{\varphi}| = 7 \text{rad/s}^2$ in such a way that the ball does not lose contact with the surface of the screen, or said otherwise, that the ball does not jump to obtain a measurement without errors of the ball's position.
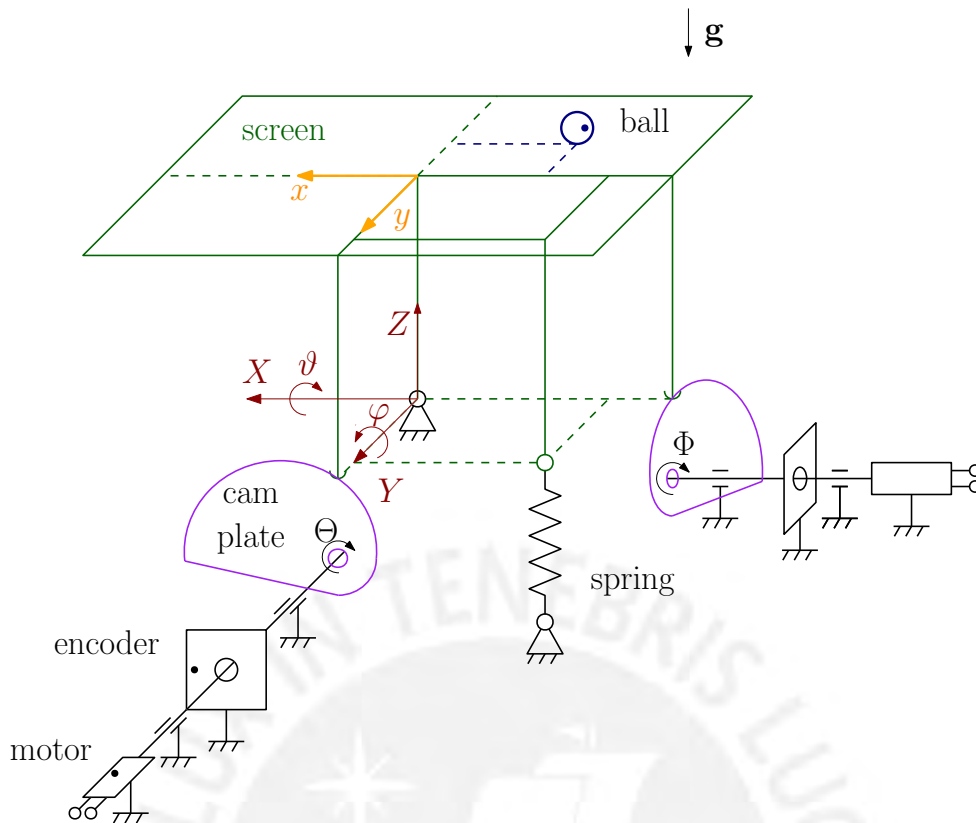
Figure 3.1: Physical configuration of the ball and plate system [3].

3.1 Implementation

3.1.1 Servo System

There are many types of servosystems, in this case is referred to the AC servosystem. Highly accurate AC servo systems consisting of compact, high-torque servo motors and a rich lineup of servo driver. They are ideal for applications where high precision movement is required, such as semiconductor manufacturing equipment, chip mounters, robots, and machine tools. The servo system uses feedback loops so that the difference between the response and command values will be as close as possible to zero. The servo system consists of three feedback loops : position loop, speed loop, and current loop [33].

The model of the servomotor used is the Cartridge DDR C041A (cf. Figure 3.2), and the servo driver AKD of the brand Kollmorgen. The specs of the servosystem are presented in Table 3.1 obtained from [34].

Table 3.1: Specs of the Kollmorgen Cartridge Servosystem.

Brand	Kollmorgen
Servomotor model	C041A-13-3305
Maximum speed	1750 RPM
Continuous torque	4.57 N-m
Continuous current	2.38 A
Peak torque	12.3 N-m
Frecuency	50 Hz
Servodriver model	ADK Servodriver

Figure 3.2: Servomotor Kollmorgen Cartridge DDR C041A.

3.1.2 Touch Screen

Lumio's patented technology is based on the highly efficient use of small amounts of infrared light, tiny cameras and advanced algorithms. The device controller supports USB (HID) and serial R232 communications, emulates legacy protocols and operates in a wide variety of operating systems [35].

The Lumio touch screen used is shown Figure 3.3a, it has a resolution of $4096x4096$ pixels and screen size of $0.395mx0.7m$. Also can operate in single-touch and multi-touch mode.

3.1.3 Encoders

The encoder used is C80E ROTAPULS incremental encoder with resolution 4096 pulses/rev. This encoder is hollow shaft and is presented in the Figure 3.3b.

(a) Lumio Crystal Touch Screen. (b) Incremental encoder C80E ROTAPULS.

Figure 3.3: Instrumentation sensors.

3.1.4 Real Time System - dSpace

The harware component used is DS1104 RD Controller Board and the software component Control Desk v5.1 both from dSpace GmbH.

The DS1104 RD Controller Board is a piece of hardware that upgrades your PC to a powerful development system for rapid control prototyping. The real-time hardware based on PowerPC technology and its set of I/O interfaces makes the board an ideal solution for developing controllers in various industrial field [36].

The simulations have been done in Matlab/Simulink and the implementation of the C-code generated is downloaded in the DS1104 RD Controller Board. Then for monitoring, saving data and run the program is used the dSpace Control Desk v 5.1 as a process interface.

3.1.5 Mechanics

The ball and plate system use the cam-plate mechanism for transmit the movement from the motors to the screen (cf. Figure 3.4). Also, a cardan-joint is used as center of rotation and a spring to maintain the contact between the wheels (attached to the screen) and the cam plates.

3.2 Implementation

The system implemented by the Control Engineering Group of TU Ilmenau, presented in Figure 3.5 , is used to validate the dynamical model and to perform the experimental tests of the control system designed in the present work.
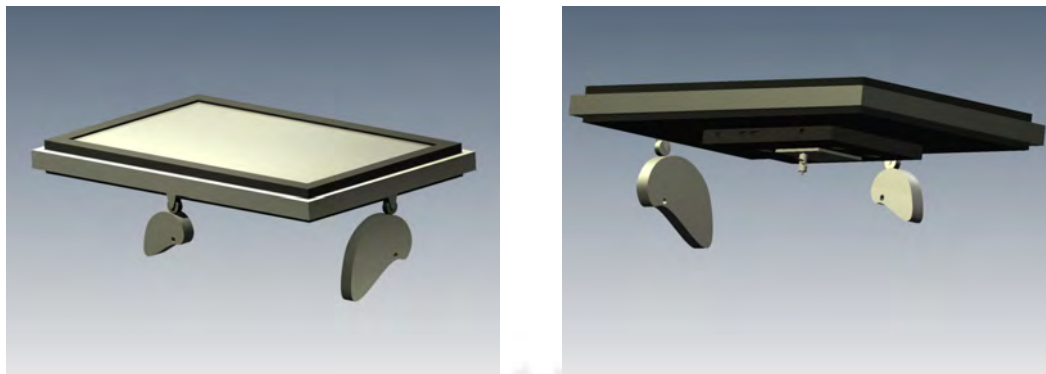
(a) Isometric view from top.

(b) Isometric view from bottom.

Figure 3.4: Mechanism of movement transmission using cam-plates.

Figure 3.5: Ball and plate system implemented by the Control Engineering Group of TU Ilmenau [3].

4 Modeling of the System

In order to obtain the equations of the ball and plate system, for purposes of system analysis and controller design , we proceed to calculate the kinematics and then the dynamic modeling using the Euler-Lagrange approach [37]. The tables of variables and parameters presented in appendix A is taken into account for the modeling process.

4.1 Considerations

In order to simplify the mathematical modeling, the following assumptions are used [8, 18]

- The ball never loses contact with the plate.

- There is no sliding between the ball and the plate.

- There is no rolling friction between the ball and the plate.

- The ball no spin about its vertical axis.

- The servomotors are considered to be sufficiently powerful. Moreover, the servo system has an inner control loop to compensate the effect of the displaced center of mass of the plate with respect to the geometric center (the distribution of mass in the screen is not uniform) and the effect of the spring on the dynamics of the plate (since its function is mainly to keep the monitor in contact with the cam plates but not to influence in the dynamics of the ball). In other words, the inner loop of the servosystem practically controls the plate's dynamics.

4.2 Physical Configuration

In order to express the position of the ball (center of mass) in the ball and plate system, two coordinates systems are used. The first coordinates system $OXYZ$ is fixed with center located in the cardan-joint and serves mainly for the calculation of the energy (kinetic and potential) of the ball because represent absolute coordinates. The second coordinate system $Oxyz$ is mobile, also with center located in the cardan-joint, important because it relates directly to the position reference for the tracking control.
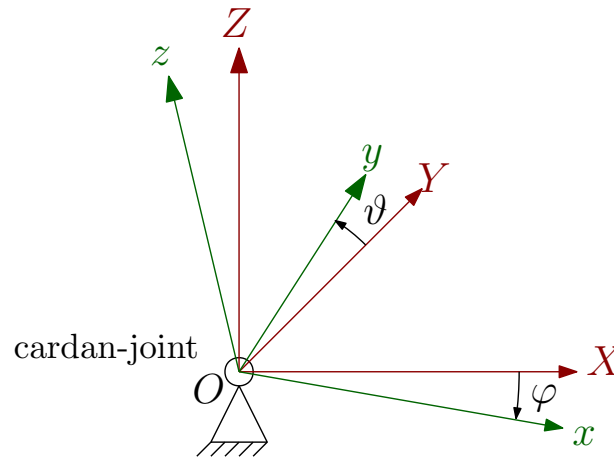
Figure 4.1: Fixed (red) and mobile (green) coordinate system.

The plane Oxy in Figure 4.1 is parallel to the surface of the screen (plate) as shown in Figure 3.1.

The ball's position vector and the ball's velocity vector in the space fixed coordinate system are defined as follows

$$\vec{r} = \begin{pmatrix} X \\ Y \\ Z \end{pmatrix}, \quad \dot{\vec{r}} = \begin{pmatrix} \dot{X} \\ \dot{Y} \\ \dot{Z} \end{pmatrix}, \tag{4.1}$$

also ball's position vector and the ball's velocity vector in the mobile coordinate system are defined as

$$\vec{r}' = \begin{pmatrix} x \\ y \\ z \end{pmatrix}, \quad \dot{\vec{r}}' = \begin{pmatrix} \dot{x} \\ \dot{y} \\ \dot{z} \end{pmatrix}. \tag{4.2}$$

The transformation between both coordinate systems is presented in the kinematic section (4.7).

4.3 Kinematics

The kinematics represent the relation between the space-fixed coordinates and plate-fixed coordinates. In this part is used the convention of positive angles in counterclockwise (CCW).

4.3.1 Rotational Matrix

Using the transformation matrices due rotation, the following coordinate transformations are considered to transform the ball's position from the mobile coordinates $Oxyz$ to the fixed coordinates $OXYZ$ presented in Figure 4.1 : first rotation around the X-axis (ϑ) (4.3) and then around the y-axis (φ) (4.4).

Rotation about the $X-$axis:

$$\mathbf{R}_x\left(\vartheta\right) = \begin{pmatrix} 1 & 0 & 0 \\ 0 & \cos(\vartheta) & -\sin(\vartheta) \\ 0 & \sin(\vartheta) & \cos(\vartheta) \end{pmatrix} \tag{4.3}$$

Rotation about the y-axis:

$$\mathbf{R}_y\left(\varphi\right) = \begin{pmatrix} \cos(\varphi) & 0 & \sin(\varphi) \\ 0 & 1 & 0 \\ -\sin(\varphi) & 0 & \cos(\varphi) \end{pmatrix} \tag{4.4}$$

The total transformation matrix is calculated as the product of the previous matrices.

$$\mathbf{R}_{xy}\left(\vartheta, \varphi\right) = \mathbf{R}_x\left(\vartheta\right) \mathbf{R}_y\left(\varphi\right) \tag{4.5a}$$

$$\mathbf{R}_{xy}\left(\vartheta, \varphi\right) = \begin{pmatrix} \cos(\varphi) & 0 & \sin(\varphi) \\ \sin(\vartheta)\sin(\varphi) & \cos(\vartheta) & -\sin(\vartheta)\cos(\varphi) \\ -\cos(\vartheta)\sin(\varphi) & \sin(\vartheta) & \cos(\vartheta)\cos(\varphi) \end{pmatrix} \tag{4.5b}$$

4.3.2 Transformation of Coordinates

The z-coordinate of the ball is constant

$$\tilde{d} = d_{cs} + r_b, \tag{4.6}$$

where d_{cs} is the distance between the cardan joint and the screen surface, and r_b the radius of the ball.

On the other hand, in order to obtain the ball's position in absolute coordinates the transformation from the mobile coordinates to the fixed coordinates is performed as follows

$$
\begin{pmatrix} X \\ Y \\ Z \end{pmatrix} = \mathbf{R}_{xy}\left(\vartheta, \varphi\right) \begin{pmatrix} x \\ y \\ \tilde{d} \end{pmatrix}.
$$
(4.7)

Therefore, ball's position in fixed coordinates results

$$
\vec{r} = \begin{pmatrix} X \\ Y \\ Z \end{pmatrix} = \begin{pmatrix} \cos(\varphi)x + \sin(\varphi)\tilde{d} \\ \sin(\vartheta)\sin(\varphi)x + \cos(\vartheta)y - \sin(\vartheta)\cos(\varphi)\tilde{d} \\ -\cos(\vartheta)\sin(\varphi)x + \sin(\vartheta)y + \cos(\vartheta)\cos(\varphi)\tilde{d} \end{pmatrix}.
$$
(4.8)

This result will be useful for calculating the energy of the ball.

4.4 Dynamic Modeling

In order to obtain the equations of motion of the ball and plate system, the Euler-Lagrange approach is used. The Euler-Lagrange approach will be used since it is easier for sub actuated systems, like the present one, than the Newton approach [37].

4.4.1 Lagrange Approach

Only the equations for the ball's dynamics will be deducted due to the assumption of the internal loop of the servosystem presented in 4.1.

4.4.1.1 Kinetics Energy

Using the methodology presented in [5] the kinetics are obtained as follows:

Angular Velocity of the Plate   The angular velocity of the plate in global coordinates is

$$
\vec{\omega}_{p} = \begin{pmatrix} \omega_{px} \\ \omega_{py} \\ \omega_{pz} \end{pmatrix}.
$$
(4.9)

Also, relation between the rotation matrix and the angular velocity of the plate is given by [37]

$$\mathbf{R}_{xy}\left(\vartheta, \varphi\right) \dot{\mathbf{R}}_{xy}^{\mathsf{T}}\left(\vartheta, \varphi\right) = \begin{pmatrix} 0 & -\omega_{pz} & \omega_{py} \\ \omega_{pz} & 0 & -\omega_{px} \\ -\omega_{py} & \omega_{px} & 0 \end{pmatrix}, \tag{4.10}$$

in such a way that after the multiplication of the matrices (4.5b) and comparing term by term, the determined angular velocity of the plate results

$$\vec{\omega}_{p} = \begin{pmatrix} \dot{\vartheta}\cos(\varphi) \\ \dot{\varphi} \\ \dot{\vartheta}\sin(\varphi) \end{pmatrix}. \tag{4.11}$$

Angular Velocity of the Ball   The relative angular velocity of the ball respect to the plate (considering rolling without twisting) is

$$\vec{\omega}_{b/p} = \begin{pmatrix} -\frac{\dot{y}}{r_b} \\ \frac{\dot{x}}{r_b} \\ 0 \end{pmatrix}. \tag{4.12}$$

Hence, the absolute angular velocity of the ball results

$$\vec{\omega}_{b} = \vec{\omega}_{p} + \vec{\omega}_{b/p} = \begin{pmatrix} \dot{\vartheta}\cos(\varphi) - \frac{\dot{y}}{r_b} \\ \dot{\varphi} + \frac{\dot{x}}{r_b} \\ \dot{\vartheta}\sin(\varphi) \end{pmatrix}. \tag{4.13}$$

Kinetic Energy of the Ball   Using the ball's position in absolute coordinates (4.8) and the absolute angular velocity of the ball (4.13), the kinetic energy of the ball is calculated as

$$T = \frac{1}{2}m_{b}\dot{\vec{r}} \cdot \dot{\vec{r}} + \frac{1}{2}J_{b}\vec{\omega}_{b} \cdot \vec{\omega}_{b} \tag{4.14a}$$

$$T = \frac{1}{2}m_{b}\left(\dot{X}^2 + \dot{Y}^2 + \dot{Z}^2\right) + \frac{1}{2}J_{b}\left[\left(\dot{\vartheta}\cos(\varphi) - \frac{\dot{y}}{r_b}\right)^2 + \left(\dot{\varphi} + \frac{\dot{x}}{r_b}\right)^2 + \left(\dot{\vartheta}\sin(\varphi)\right)^2\right], \tag{4.14b}$$

with J_b as the identical moment of inertia in x and y-axis and m_b as the mass of the ball.

4.4.1.2 Potential Energy

The potential energy of the ball is calculated as follows

$$V = m_b g Z. \tag{4.15}$$

Using the absolute coordinate Z of the ball from (4.8), the potential energy results:

$$V = m_b g \left(-\cos(\vartheta)\sin(\varphi)x + \sin(\vartheta)y + \cos(\vartheta)\cos(\varphi)\tilde{d} \right). \tag{4.16}$$

4.4.1.3 Lagrange Equations

As mentioned before, only the dynamical modeling of the ball is considered. The Lagrangian is calculated by

$$L = T - V. \tag{4.17}$$

The vector of generalized coordinates, that represents the degree of freedom of the system, for the ball and plate system is

$$q = \begin{pmatrix} x & y & \vartheta & \varphi \end{pmatrix}^{\mathsf{T}}. \tag{4.18}$$

Furthermore the Lagrange's equation is [cf. 37]

$$\frac{\mathrm{d}}{\mathrm{d}t}\left(\frac{\partial L}{\partial \dot{q}_i} \right) - \frac{\partial L}{\partial q_i} = Q_i, \tag{4.19}$$

with the generalized force Q_i.

Neglecting the viscous damping the overall system is conservative ($Q_1 = 0$, $Q_2 = 0$). Also, considering only the degree of freedom of the ball (x and y), the resulting equations are in x-axis

$$\ddot{x}\left(m_b + \frac{J_b}{r_b^2} \right) + \ddot{\varphi}\left(m_b\tilde{d} + \frac{J_b}{r_b} \right) - y\sin(\varphi)\ddot{\vartheta}m_b + \frac{1}{2}\sin(2\varphi)\dot{\vartheta}^2 m_b\tilde{d} - x\sin^2(\varphi)\dot{\vartheta}^2 m_b$$
$$- 2\dot{y}^2\sin(\varphi)\dot{\vartheta}m_b - \dot{\varphi}^2 x m_b - m_b g\cos(\vartheta)\sin(\varphi) = 0, \tag{4.20}$$

and in y-axis

$$\ddot{y}\left(m_b + \frac{J_b}{r_b^2} \right) + \ddot{\vartheta}\left(\sin(\varphi)x m_b - \cos(\varphi)\tilde{d}m_b - \frac{J_b}{r_b}\cos(\varphi) \right) + \frac{J_b}{r_b}\dot{\varphi}\sin(\varphi)\dot{\vartheta}$$
$$+ 2\sin(\varphi)\dot{\vartheta}\dot{\varphi}\tilde{d}m_b + 2\dot{\varphi}x\cos(\varphi)\dot{\vartheta}m_b + 2\sin(\varphi)\dot{x}\dot{\vartheta}m_b - y\dot{\vartheta}^2 m_b + m_b g\sin(\vartheta) = 0 \tag{4.21}$$

5 Analysis of the System

The rewriting of the equations obtained in the modelling into state-space representation allows the analysis regarding observability and controllability. This process allows to obtain a model in the most compact representation (input affine state-space model) to later design the controller and observer in the operating range, knowing beforehand if the system is controllable and observable in said operating range.

5.1 Model of Ball and Plate Dynamics

New constants are used to reduce the length of the equations (4.20) and (4.21)

$$\bar{c}_1 = \frac{mr^2}{mr^2 + J}, \quad \bar{c}_2 = \frac{\tilde{d}mr^2 + Jr}{mr^2 + J}, \quad \bar{c}_3 = \frac{J + 2\tilde{d}mr}{mr}, \quad \bar{c}_4 = \frac{J + \tilde{d}mr}{mr} \tag{5.1}$$

The following equations are obtained after replacing the new constants

$$\ddot{x} = \bar{c}_1 \Big(-\frac{\tilde{d}}{2}\sin(2\varphi)\dot{\vartheta}^2 + x\sin^2(\varphi)\dot{\vartheta}^2 + 2\dot{y}\sin(\varphi)\dot{\vartheta} + \dot{\varphi}^2 x$$
$$+ g\cos(\vartheta)\sin(\varphi) - \frac{\bar{c}_2}{\bar{c}_1}\ddot{\varphi} + y\sin(\varphi)\ddot{\vartheta} \Big), \quad \text{(5.2a)}$$

$$\ddot{y} = \bar{c}_1 \Big(-\bar{c}_3\dot{\varphi}\dot{\vartheta}\sin(\varphi) - 2\dot{\varphi}x\cos(\varphi)\dot{\vartheta} - 2\sin(\varphi)\dot{x}\dot{\vartheta} + y\dot{\vartheta}^2 - g\sin(\vartheta)$$
$$+ \big(-x\sin(\varphi) + \bar{c}_4\cos(\varphi)\big)\ddot{\vartheta} \Big). \quad \text{(5.2b)}$$

The measured outputs of the system considering the available hardware, i.e. the touch screen and the two encoders, are

$$h(\mathbf{x}) = \begin{pmatrix} x & \varphi & y & \vartheta \end{pmatrix}^\mathsf{T}. \tag{5.3}$$

Note that the considered output for the trajectory tracking control is reduced to the ball's position.

State Space Model   Using the equations (5.2a) and (5.2b) obtains the following form of the system

$$\dot{\mathbf{x}} = F(\mathbf{x}, \mathbf{u})$$
$$\mathbf{y} = h(\mathbf{x}).$$

(5.4)

This leads to the state vector

$$\mathbf{x} = \begin{pmatrix} x_1 & x_2 & x_3 & x_4 & x_5 & x_6 & x_7 & x_8 \end{pmatrix}^{\mathsf{T}} = \begin{pmatrix} x & \dot{x} & \varphi & \dot{\varphi} & y & \dot{y} & \vartheta & \dot{\vartheta} \end{pmatrix}^{\mathsf{T}},$$

(5.5)

with

$$F(\mathbf{x}, \mathbf{u}) = \begin{pmatrix} x_2 \\ \bar{c}_1\big(-\frac{\bar{d}}{2}\sin(2x_3)x_8^2 + x_1\sin^2(x_3)x_8^2 + 2x_6\sin(x_3)x_8 + x_4^2 x_1 + \\ g\cos(x_7)\sin(x_3) - \frac{\bar{c}_2}{\bar{c}_1}u_1 + x_5\sin(x_3)u_2 \big) \\ x_4 \\ u_1 \\ x_6 \\ \bar{c}_1\{ -\bar{c}_3 x_4 x_8\sin(x_3) - 2x_4 x_1\cos(x_3)x_8 - 2\sin(x_3)x_2 x_8 + x_5 x_8^2 - \\ g\sin(x_7) + (-x_1\sin(x_3) + \bar{c}_4\cos(x_3))u_2 \} \\ x_8 \\ u_2 \end{pmatrix},$$

(5.6)

and the measured outputs of the system

$$h(\mathbf{x}) = \begin{pmatrix} x_1 & x_3 & x_5 & x_7 \end{pmatrix}^{\mathsf{T}}.$$

(5.7)

In order to obtain the system in the input-affine form, we use $\ddot{\vartheta}$ and $\ddot{\varphi}$ as inputs:

$$\mathbf{u} = \begin{pmatrix} u_1 & u_2 \end{pmatrix}^{\mathsf{T}} = \begin{pmatrix} \ddot{\varphi} & \ddot{\vartheta} \end{pmatrix}^{\mathsf{T}}$$

(5.8)

Therefore, the resulting input-affine system is

$$\dot{\mathbf{x}} = f(\mathbf{x}) + g(\mathbf{x})\mathbf{u}$$
$$\mathbf{y} = h(\mathbf{x}),$$

(5.9a)

where

$$f(\mathbf{x}) = \begin{pmatrix} x_2 \\ \bar{c}_1 \left(-\frac{\bar{d}}{2} x_8^2 \sin(2x_3) + x_1 x_8^2 \sin^2(x_3) + 2x_6 x_8 \sin(x_3) + x_1 x_4^2 + g\sin(x_3)\cos(x_7) \right) \\ x_4 \\ 0 \\ x_6 \\ \bar{c}_1 \left(-\bar{c}_3 x_4 x_8 \sin(x_3) - 2x_1 x_4 x_8 \cos(x_3) - 2x_2 x_8 \sin(x_3) + x_5 x_8^2 - g\sin(x_7) \right) \\ x_8 \\ 0 \end{pmatrix},$$

(5.9b)

and

$$g(\mathbf{x}) = \begin{pmatrix} 0 & 0 \\ -\bar{c}_2 & \bar{c}_1 x_5 \sin(x_3) \\ 0 & 0 \\ 1 & 0 \\ 0 & 0 \\ 0 & -\bar{c}_1 x_1 \sin(x_3) + \bar{c}_2 \cos(x_3) \\ 0 & 0 \\ 0 & 1 \end{pmatrix}.$$

(5.9c)

The highlighted blue terms represent the coupling terms between the two ball and beam subsystems (reference model presented in [38]) that conform the ball and plate system. It is also useful as a simple way to validate the model.

5.2 Observability

A system is observable if and only if the system state can be found by observing the input and output over a period of time from $\mathbf{x}(t)$ to $\mathbf{x}(t+h)$. Also, the observability condition is necessary to see what is going on inside the system under observation, and must be addressed before designing the observer [20].

The observability analysis is useful because it will determine if a set of sensors is sufficient for controlling a system [20].

5.2.1 Observability for MIMO Nonlinear System

For the analysis of observability, a system in the general nonlinear form is considered:

$$\dot{\mathbf{x}} = F(\mathbf{x}, \mathbf{u})$$
$$\mathbf{y} = h(\mathbf{x})$$

(5.10)

In order to determine the observability the following definitions are presented [cf. 39]:

Indistinguishability. A pair of initial states $(\mathbf{x}_0^1, \mathbf{x}_0^2)$ of the system are called indistinguishable, if:

$$\forall \mathbf{u} \in U, \forall t \geq 0 : h(\varphi(t; \mathbf{x}_0^1, \mathbf{u})) = h(\varphi(t; \mathbf{x}_0^2, \mathbf{u})).$$

(5.11)

Indistinguishability is so an equivalence relation on $\mathbf{x}$.

Observability. The system is called observable (relative to $\mathbf{x}_0$) if it does not admit any indistinguishable pair. This definition is very general and without any practical relevance, therefore the concept of weak observability is presented.

Weak Observability. The system is called weak observable (relative to $\mathbf{x}_0$) when a neighborhood S for any $\mathbf{x}$ exists in which there is no indistinguishable state from $\mathbf{x}$ in S. This definition does not prevent cases where the trajectories have to go far from S before one can distinguish between two different states of S. Therefore, the concept of local weak observability is presented.

Local Weak Observability. The system is called local weakly observable (with respect to $\mathbf{x}_0$), if a neighborhood S for all $\mathbf{x}$ exists, such that in each neighborhood V of $\mathbf{x}$ where is $V \subseteq S$, there is no indistinguishable state from $\mathbf{x}$ in V if in the time intervals considered the trajectories remain in V. This definition opens the way to using a geometric approach, and thereby the rank conditions.

Observability Map. In the case of smooth systems a possibility to check the observability is the differentiation of the ouput. This lead to define the observability map. In general the

observability map is defined as

$$o_k(\mathbf{x}) := \begin{pmatrix} h(\mathbf{x}) \\ \mathcal{L}_F h(\mathbf{x}) \\ \mathcal{L}_F^2 h(\mathbf{x}) \\ \vdots \\ \mathcal{L}_F^{k-1} h(\mathbf{x}) \end{pmatrix}, \quad \text{where} \quad h(\mathbf{x}) = \begin{pmatrix} h_1 \\ h_2 \\ \vdots \\ h_q \end{pmatrix}. \tag{5.12}$$

The expression $o_k(\mathbf{x})$ represent the observability map with order k. There are two types of observability [39]:

- Partial Observability: When $k < n$, means that only a part of states are observable (or necessary for the controller design).

- Full Observability: When $k = n$, means that all states can be observed. This case implies the existence of the "normal observable form".

It is also possible to reduce the length of the observability map when the system is full relative degree and the relative degree of each output is known, using the following vector

$$o_n(\mathbf{x}) = \begin{pmatrix} y_1 \\ \dot{y}_1 \\ \vdots \\ y_1^{(n_1-1)} \\ y_2 \\ \vdots \\ y_2^{(n_2-1)} \\ \vdots \\ y_q^{(n_q-1)} \end{pmatrix} = \begin{pmatrix} h_1 \\ \mathcal{L}_F h_1 \\ \vdots \\ \mathcal{L}_F^{(n_1-1)} h_1 \\ h_2 \\ \vdots \\ \mathcal{L}_F^{(n_2-1)} h_2 \\ \vdots \\ \mathcal{L}_F^{(n_q-1)} h_q \end{pmatrix}, \tag{5.13}$$

where the following relations must be satisfied (for detailed explanation see [40]):

$$\sum_{i=1}^{q} n_i = n, \quad \nu - 1 = \max_{i=1:q}\{n_i - 1\}, \quad \mathbf{u}^{[\nu-1]} \in D_u^\nu.$$

The previous representation of the observability map is only a simplification reducing the redundant terms. However, through the symbolic calculation (i. e. using Maple) it is possible to generalize the calculus by using the representation (5.12).

Observability Matrix. The observability matrix at the point $\mathbf{x} = \mathbf{x}_0$ is defined as

$$O_k(\mathbf{x}_o) := \left. \frac{\partial o_k(\mathbf{x})}{\partial \mathbf{x}} \right|_{\mathbf{x}=\mathbf{x}_o}. \tag{5.14}$$

The value of $\mathbf{x}_0$ represent any specific initial state of the system. The system is locally observable if the Jacobian $O_k(\mathbf{x}_o)$ has rank n, i.e. when the the rank condition is satisfied as follows:

$$\text{rank}(O_k(\mathbf{x}_0)) = n \tag{5.15}$$

The system is weak locally observable at $\mathbf{x}_0$, when the rank condition is fulfilled. However, when the rank condition is fulfilled for all $\mathbf{x}_0$, the system is weak globally observable.

5.2.2 Observability of the Ball and Plate System

The available outputs of the system are the ball's position and the plate's angles:

$$h(\mathbf{x}) = \begin{pmatrix} y_1 \\ y_2 \\ y_3 \\ y_4 \end{pmatrix} = \begin{pmatrix} x_1 \\ x_3 \\ x_5 \\ x_7 \end{pmatrix} \tag{5.16}$$

Observability map Building the observability map using (5.12) provides

$$o_n(\mathbf{x}) = \begin{pmatrix} y_1 \\ \vdots \\ y_4 \\ \dot{y}_1 \\ \vdots \\ \dot{y}_4 \\ \vdots \\ y_1^{(7)} \\ \vdots \\ y_4^{(7)} \end{pmatrix} = \begin{pmatrix} h(\mathbf{x}) \\ \mathcal{L}_F h(\mathbf{x}) \\ \mathcal{L}_F^2 h(\mathbf{x}) \\ \vdots \\ \mathcal{L}_F^7 h(\mathbf{x}) \end{pmatrix} = \begin{pmatrix} o_1(\mathbf{x}) \\ o_2(\mathbf{x}) \\ o_3(\mathbf{x}) \\ \vdots \\ o_8(\mathbf{x}) \end{pmatrix}. \tag{5.17}$$

The normal observer form is considered using $k = n$. The required Lie derivatives are calculated as follows:

$$o_1(\mathbf{x}) = h(\mathbf{x}) = \begin{pmatrix} x_1 & x_3 & x_5 & x_7 \end{pmatrix}^{\mathsf{T}} \tag{5.18a}$$

$$o_2(\mathbf{x}) = \mathcal{L}_F h(\mathbf{x}) = \frac{\partial o_1(\mathbf{x})}{\partial \mathbf{x}} F(\mathbf{x}, \mathbf{u}) = \begin{pmatrix} x_2 & x_4 & x_6 & x_8 \end{pmatrix}^{\mathsf{T}} \tag{5.18b}$$

$$o_3(\mathbf{x}) = \mathcal{L}_F^2 h(\mathbf{x}) = \frac{\partial o_2(\mathbf{x})}{\partial \mathbf{x}} F(\mathbf{x}, \mathbf{u}) \tag{5.18c}$$

$$\vdots \tag{5.18d}$$

$$o_8(\mathbf{x}) = \mathcal{L}_F^7 h(\mathbf{x}) = \frac{\partial o_7(\mathbf{x})}{\partial \mathbf{x}} F(\mathbf{x}, \mathbf{u}) \tag{5.18e}$$

Observability Matrix. Considering $k = n$ the observability matrix at $\mathbf{x} = \mathbf{x}_0$ is obtained by evaluating

$$O_n(\mathbf{x}_0) = \frac{\partial o_n(\mathbf{x})}{\partial \mathbf{x}} \Big|_{\mathbf{x}=\mathbf{x}_0}. \tag{5.19}$$

The resulting observability matrix using symbolic calculation is:

$$O_n(\mathbf{x}_o) = \begin{pmatrix}
1 & 0 & 0 & 0 & 0 & 0 & 0 & 0 \\
0 & 0 & 1 & 0 & 0 & 0 & 0 & 0 \\
0 & 0 & 0 & 0 & 1 & 0 & 0 & 0 \\
0 & 0 & 0 & 0 & 0 & 0 & 1 & 0 \\
0 & 1 & 0 & 0 & 0 & 0 & 0 & 0 \\
0 & 0 & 0 & 1 & 0 & 0 & 0 & 0 \\
0 & 0 & 0 & 0 & 0 & 1 & 0 & 0 \\
0 & 0 & 0 & 0 & 0 & 0 & 0 & 1 \\
* & * & * & * & * & * & * & * \\
\vdots & \vdots & \vdots & \vdots & \vdots & \vdots & \vdots & \vdots \\
* & * & * & * & * & * & * & *
\end{pmatrix}_{32x8}
\Rightarrow
\tilde{O}_n(\mathbf{x}_o) = \begin{pmatrix}
1 & 0 & 0 & 0 & 0 & 0 & 0 & 0 \\
0 & 1 & 0 & 0 & 0 & 0 & 0 & 0 \\
0 & 0 & 1 & 0 & 0 & 0 & 0 & 0 \\
0 & 0 & 0 & 1 & 0 & 0 & 0 & 0 \\
0 & 0 & 0 & 0 & 1 & 0 & 0 & 0 \\
0 & 0 & 0 & 0 & 0 & 1 & 0 & 0 \\
0 & 0 & 0 & 0 & 0 & 0 & 1 & 0 \\
0 & 0 & 0 & 0 & 0 & 0 & 0 & 1 \\
* & * & * & * & * & * & * & * \\
\vdots & \vdots & \vdots & \vdots & \vdots & \vdots & \vdots & \vdots \\
* & * & * & * & * & * & * & *
\end{pmatrix}_{32x8}$$

$$\tag{5.20}$$

Rank Condition of the Observability Matrix. The elements $*$ in the observability matrix obtained in (5.20) represent general terms that do not affect the rank of the matrix. After ordering the columns of the observability matrix it is obvious that there exist eight linearly independent columns. Hence, the rank is

$$\text{rank}(O_n(\mathbf{x}_o)) = 8 = n. \tag{5.21}$$

The rank is kept constant independent of the states $\mathbf{x}$ and inputs (universal inputs [39]). Therefore, global observability is shown for the ball and plate system.

5.3 Controllability

Controllability is a key issue that must be addressed before we start to design a control system. The analysis of controllability for MIMO nonlinear system is analogous to the SISO nonlinear case, detailed also in [32]. Furthermore, in the same way as the observability analysis, the controllability analysis is based on the geometric approach.

5.3.1 Controllability for MIMO Nonlinear Input Affine System

The nonlinear system in the input-affine representation is as follows

$$\dot{\mathbf{x}} = f(\mathbf{x}) + g(\mathbf{x})\mathbf{u}, \tag{5.22}$$

with $\mathbf{x} \in M \subset \mathbb{R}^n$, $u \in U \subset \mathbb{R}^p$.

In order to present the mean of controllability, the following definitions are useful:

Reachable Set from $\mathbf{x}_0$.   Let $R(\mathbf{x}_0, T) \subset \mathbb{R}^n$, with $T = [t_0, t_f]$, to be the subset of all states accessible from state $\mathbf{x}_0$ and through the admissible input, in time T with the trajectories being confined to a neighborhood V of $\mathbf{x}_0$ [28].

Locally Accessible.   The system is locally accessible if given any $\mathbf{x}_0 \in M$, the reachable set contains a nonempty open set of M for all neighborhood of V and all $T > 0$ [41].

Locally Strongly Accessible.   The system is locally accessible if given any $\mathbf{x}_0 \in M$ then for any neighborhood V of $\mathbf{x}_0$, the reachable set contains a nonempty open set for any $T > 0$ sufficiently small [41].

Controllable System.   The system is controllable if there exists an admissible input vector $u(t)$ such that the system state $\mathbf{x}(t)$ can travel from an initial point $\mathbf{x}(t_0)$ to $\mathbf{x}(t_f)$ within a finite time interval T [28].

The definitions presented above help to understand the concept of controllability. However, for the practical calculation whether the system is controllable or not, exist the geometric approach that use the Lie's algebra presented in [23]. First the controllability matrix has to be computed and then its rank is evaluated.

Controllability Matrix.   The matrix g($\mathbf{x}$) is decomposed into parts related to each input independently.

$$\dot{\mathbf{x}} = f(\mathbf{x}) + \sum_{i=1}^{p} g_i(\mathbf{x})u_i \tag{5.23}$$

The controllability matrix for the MIMO system is defined as follows:

$$Q(\mathbf{x}_0) := \begin{pmatrix} g_1 & \cdots & g_p & \mathrm{ad}_f g_1 & \cdots & \mathrm{ad}_f g_p & \cdots & \mathrm{ad}_f^{n-1} g_1 & \cdots & \mathrm{ad}_f^{n-1} g_p \end{pmatrix}, \tag{5.24}$$

 where the terms g_i and f represent $g_i(\mathbf{x})$ and $f(\mathbf{x})$ respectively, and are used in order to reduce the size of expressions [23, 42].

Rank Condition of the Controllability Matrix.   Evaluating the rank condition at any initial condition state $\mathbf{x}_0$:

$$\mathrm{rank}(Q(\mathbf{x}_0)) = n. \tag{5.25}$$

When the rank condition is fulfilled, then the system is locally controllable at $\mathbf{x}_0$. Also, when the rank condition is fulfilled for any $\mathbf{x}_0$, the system is globally controllable.

5.3.2 Controllability of the Ball and Plate System

The state-space equation of the system is represented as follows :

$$\dot{\mathbf{x}} = f(\mathbf{x}) + g_1(\mathbf{x})u_1 + g_2(\mathbf{x})u_2 \ , \tag{5.26a}$$

where:

$$
g_1(\mathbf{x}) = \begin{pmatrix} 0 \\ -\bar{c}_2 \\ 0 \\ 1 \\ 0 \\ 0 \\ 0 \\ 0 \end{pmatrix}, \qquad g_2(\mathbf{x}) = \begin{pmatrix} 0 \\ \bar{c}_1 x_5 \sin(x_3) \\ 0 \\ 0 \\ 0 \\ -\bar{c}_1 x_1 \sin(x_3) + \bar{c}_2 \cos(x_3) \\ 0 \\ 1 \end{pmatrix}. \tag{5.26b}
$$

Controllability Matrix   The controllability matrix (5.24) for $n = 8$ and $p = 2$ is:

$$
Q(\mathbf{x}) = \begin{pmatrix} g_1 & g_2 & \mathrm{ad}_f g_1 & \mathrm{ad}_f g_2 & \cdots & \mathrm{ad}_f^7 g_1 & \mathrm{ad}_f^7 g_2 \end{pmatrix}, \tag{5.27a}
$$

and can be represented in the following form:

$$
Q(\mathbf{x}) = \begin{pmatrix} Q_{11} & Q_{21} & Q_{12} & Q_{22} & \cdots & Q_{18} & Q_{28} \end{pmatrix}. \tag{5.27b}
$$

The Lie Brackets for the inputs u_1 and u_2 are calculated as follows:

$$
Q_{i1} = g_i \tag{5.28a}
$$

$$
Q_{i2} = \mathrm{ad}_f g_i = \frac{\partial g_i}{\partial \mathbf{x}} f - \frac{\partial f}{\partial \mathbf{x}} g_i \tag{5.28b}
$$

$$
Q_{i3} = \mathrm{ad}_f^2 g_i = \frac{\partial Q_{i2}}{\partial \mathbf{x}} f - \frac{\partial f}{\partial \mathbf{x}} Q_{i2} \tag{5.28c}
$$

$$
Q_{i4} = \mathrm{ad}_f^3 g_i = \frac{\partial Q_{i3}}{\partial \mathbf{x}} f - \frac{\partial f}{\partial \mathbf{x}} Q_{i3} \tag{5.28d}
$$

$$
\vdots \tag{5.28e}
$$

$$
Q_{i8} = \mathrm{ad}_f^7 g_i = \frac{\partial Q_{i7}}{\partial \mathbf{x}} f - \frac{\partial f}{\partial \mathbf{x}} Q_{i7} \tag{5.28f}
$$

$$
i = 1, 2
$$

Therefore controllability matrix $Q(\mathbf{x})$ is obtained and performing row swapping, in order to calculate the matrix rank, we obtain the matrix $\tilde{Q}(\mathbf{x})$ as follows:

$$
\tilde{Q}(\mathbf{x}) = \begin{pmatrix}
1 & 0 & 0 & 0 & 0 & 0 & 0 & 0 & \cdots & 0 \\
0 & 1 & 0 & 0 & 0 & 0 & 0 & 0 & \cdots & 0 \\
0 & 0 & -1 & 0 & 0 & 0 & 0 & 0 & \cdots & 0 \\
0 & 0 & 0 & -1 & 0 & 0 & 0 & 0 & \cdots & 0 \\
-\bar{c}_2 & * & * & * & * & * & * & * & \cdots & * \\
0 & \diamondsuit & * & * & * & \square & * & * & \cdots & * \\
0 & 0 & * & \bar{c}_2 & * & * & * & * & \cdots & * \\
0 & 0 & 0 & \diamondsuit & * & * & * & \square & \cdots & *
\end{pmatrix}_{8x16}
\tag{5.29}
$$

The elements $*$ of the controllability matrix represent the non constant terms, depending on the states of the system. These terms are quite extensive; therefore, not shown and only analyzed.

Rank Condition. Evaluating the rank locally at $\mathbf{x}_0$, the following cases are obtained:

- When $x_3 \equiv 0 \wedge x_4 \equiv 0 \wedge x_7 \equiv \frac{\pi}{2} \wedge x_8 \equiv 0 \Rightarrow \text{rank}(Q(\mathbf{x}_0)) = 4 \; (* = 0, \square = 0, \diamondsuit \neq 0)$.
  It represent the physical condition $\varphi = 0$, $\dot{\varphi} = 0$, $\vartheta = \frac{\pi}{2}$, which is impossible to occur because the designed ball and plate system have restriction in the plate angles from $-10°$ to $10°$.

- When $x_3 \equiv \frac{\pi}{2} \wedge x_4 \equiv 0 \wedge x_8 \equiv 0 \Rightarrow \text{rank}(Q(\mathbf{x}_0)) = 6 \; (* = 0, \square \neq 0, \diamondsuit = 0)$.
  It represent the physical condition $\varphi = \frac{\pi}{2}$, $\dot{\varphi} = 0$. In the same way as the previous case, this state is impossible to occur due to the designed physical configuration.

- In all other cases: $\text{rank}(Q(\mathbf{x}_0)) = 8 = n$.

The ball and plate system is locally controllable for the operation range, and therefore it is possible to influence the dynamics of all modes of the system with a controller.

5.4 Linearization

The system in the input affine form (5.9a) is used in this process. In order to use linear controller design techniques, linearization of the system will be performed since linear control techniques are easier to apply and assign performance.

5.4.1 Jacobi Linerization around the Equilibrium Point

The linearization is done around the equilibrium point, and the process explained in 2.1 is performed.

Calculation of the equilibrium point x_e. The equilibrium point is calculated zeroing the derivative of the states as follows

$$\dot{x} = 0 \Rightarrow f(x_e) + g(x_e)u_e = 0 \tag{5.30}$$

The states vector and input in the equilibrium are

$$\mathbf{x}_e = \begin{pmatrix} x_{1e} & x_{2e} & x_{3e} & x_{4e} & x_{5e} & x_{6e} & x_{7e} & x_{8e} \end{pmatrix}^\mathsf{T} \tag{5.31a}$$

$$\mathbf{u}_e = \begin{pmatrix} u_{1e} & u_{2e} \end{pmatrix}^\mathsf{T}. \tag{5.31b}$$

Using the equations (5.9b) and (5.9c) , the following equations are obtained

$$x_{2e} = 0 \tag{5.32a}$$

$$\bar{c}_1 \left(g \cos(x_{7e}) \sin(x_{3e}) \right) = 0 \tag{5.32b}$$

$$x_{4e} = 0 \tag{5.32c}$$

$$u_{1e} = 0 \tag{5.32d}$$

$$x_{6e} = 0 \tag{5.32e}$$

$$\bar{c}_1 \left(-g \sin(x_{7e}) \right) = 0 \tag{5.32f}$$

$$x_{8e} = 0 \tag{5.32g}$$

$$u_{2e} = 0 \tag{5.32h}$$

From (5.32b) and (5.32f) , the value of x_{3e} and x_{7e} result

$$x_{3e} = k\pi \quad , \quad k \in \mathbb{Z} \tag{5.33a}$$

$$x_{7e} = k\pi \tag{5.33b}$$

In the operation range is considered $k = 0$. Hence , the resulting equilibrium point is

$$\mathbf{x}_e = \begin{pmatrix} x_{1e} & 0 & 0 & 0 & x_{5e} & 0 & 0 & 0 \end{pmatrix}^\mathsf{T} \tag{5.34a}$$

$$\mathbf{u}_e = \begin{pmatrix} 0 & 0 \end{pmatrix}^\mathsf{T}. \tag{5.34b}$$

The obtained equilibrium point is interpreted as infinite equilibrium points corresponding to static positions of the ball on the plate in horizontal position.

Calculation of the linear matrices. Using the system in the input-affine form (5.9a), the matrices of the linearized system around the equilibrium point are calculated by the Jacobian method. First the dynamics matrix results

$$A = \frac{\partial f(\mathbf{x})}{\partial \mathbf{x}}\bigg|_{\mathbf{x}=\mathbf{x}_e} = \begin{pmatrix} 0 & 1 & 0 & 0 & 0 & 0 & 0 & 0 \\ 0 & 0 & \bar{c}_1 g & 0 & 0 & 0 & 0 & 0 \\ 0 & 0 & 0 & 1 & 0 & 0 & 0 & 0 \\ 0 & 0 & 0 & 0 & 0 & 0 & 0 & 0 \\ 0 & 0 & 0 & 0 & 0 & 1 & 0 & 0 \\ 0 & 0 & 0 & 0 & 0 & 0 & -\bar{c}_1 g & 0 \\ 0 & 0 & 0 & 0 & 0 & 0 & 0 & 1 \\ 0 & 0 & 0 & 0 & 0 & 0 & 0 & 0 \end{pmatrix}, \tag{5.35a}$$

the control matrix results

$$B = g(\mathbf{x}_e) = \begin{pmatrix} 0 & -\bar{c}_2 & 0 & 1 & 0 & 0 & 0 & 0 \\ 0 & 0 & 0 & 0 & 0 & -\bar{c}_2 & 0 & 1 \end{pmatrix}^{\mathsf{T}}, \tag{5.35b}$$

and the output matrix results

$$C = \frac{\partial h(\mathbf{x})}{\partial \mathbf{x}}\bigg|_{\mathbf{x}=\mathbf{x}_e} = \begin{pmatrix} 1 & 0 & 0 & 0 & 0 & 0 & 0 & 0 \\ 0 & 0 & 1 & 0 & 0 & 0 & 0 & 0 \\ 0 & 0 & 0 & 0 & 1 & 0 & 0 & 0 \\ 0 & 0 & 0 & 0 & 0 & 0 & 1 & 0 \end{pmatrix} \tag{5.35c}$$

The locally linearized system have the following form

$$\begin{aligned} \Delta\dot{\mathbf{x}} &= A\Delta\mathbf{x} + B\Delta u \\ \mathbf{y} &= C\mathbf{x} \end{aligned}, \tag{5.36}$$

where $\Delta\mathbf{x} = \mathbf{x} - \mathbf{x}_e$ and $\Delta\mathbf{u} = \mathbf{u} - \mathbf{u}_e$.

It is appreciated that the system obtained (5.36) represents the union of two decoupled linear systems.

6 Controller Design

The controllers to design are based on the Jacobi linearized model (5.36) and on the nonlinear model (5.9a) of the ball and plate system. The controllers are categorized by the linear and nonlinear approaches. Also they will be tested for regulation and tracking control. In this chapter is considered the full state feedback, then in the section 7 will be designed the correspondent observer.

6.1 Linear Controller Design

Considering the structure of the linearized system:

$$\dot{\mathbf{x}} = A\mathbf{x} + B\mathbf{u}$$
$$y = \mathbf{x} \tag{6.1}$$

The control action is calculated from the error and a control gain K as follows:

$$\mathbf{e} = \mathbf{x}^* - \mathbf{x} \tag{6.2a}$$
$$\mathbf{u} = K\mathbf{e}, \tag{6.2b}$$

where $\mathbf{x}^*$ is the reference state and $\mathbf{e}$ is the control error. Therefore the closed loop system has the following form:

$$\dot{\mathbf{x}} = A\mathbf{x} + BK(\mathbf{x}^* - \mathbf{x}) \tag{6.3a}$$
$$\dot{\mathbf{x}} = (A - BK)\mathbf{x} + BK\mathbf{x}^*, \tag{6.3b}$$

where K must guarantee stability, i.e. that $A - BK$ be Hurwitz. In order to design the linear controller, the design process explained in (2.3.1) is followed below.

6.1.1 Pole Placement

There are criteria for the first and second order systems to calculate the closed-loop poles that represent a desired performance, i.e. characteristics such as settling time, overshoot, rise time, etc. However, for high order systems, as the ball and plate, one is taken into account choose the

poles to ensure stable response without overshoot; therefore, pure real LHP poles are chosen. Also, poles closest to the imaginary axis are considered as dominant poles because determine the duration of the transient state.

On the other hand, it is important to verify that the required control effort and the states of the closed-loop system are within the physical and / or considered constraints (see section 3). In general, the further you move the LHP poles respect to the imaginary axis, the more control effort it takes.

As was explained in 5.4, the system (5.36) represent two decoupled linear subsystems; therefore, the controller gain K has the following form

$$K = \begin{pmatrix} K_{11} & K_{12} & K_{13} & K_{14} & 0 & 0 & 0 & 0 \\ 0 & 0 & 0 & 0 & K_{21} & K_{22} & K_{23} & K_{24} \end{pmatrix}. \tag{6.4}$$

Considering the following desired closed-loop poles

$$s_{desired} = \{s_1, s_2, s_3, s_4, s_5, s_6, s_7, s_8\}, \tag{6.5}$$

where the poles for the first linear subsystem, i.e. s_1, s_2, s_3, s_4, can be used in the second linear subsystem. Also the equation (2.10) is used to relate the characteristic polynomial of the system (5.36) to the desired characteristic polynomial as follows

$$\det(sI - (A - BK)) = (s - s_1)(s - s_2)\ldots(s - s_8), \tag{6.6}$$

obtaining

$$s^4 + (-\bar{c}_2 K_{12} + K_{14}) s^3 + (-\bar{c}_2 K_{11} + K_{13}) s^2 + \bar{c}_1 g K_{12} s + \bar{c}_1 g K_{11} = (s - s_1)(s - s_2)(s - s_3)(s - s_4) \tag{6.7a}$$

$$s^4 + (\bar{c}_2 K_{22} + K_{24}) s^3 + (\bar{c}_2 K_{21} + K_{23}) s^2 - \bar{c}_1 g K_{22} s - \bar{c}_1 g K_{21} = (s - s_5)(s - s_6)(s - s_7)(s - s_8) \tag{6.7b}$$

where there are eight unknown values and eight equations; therefore, K can be solved. For practical purposes, the controller gain K is calculated using the command $place(A, B, s_{desired})$ in Matlab.

Finally the control action results

$$\mathbf{u} = K(\mathbf{x}^* - \mathbf{x}), \tag{6.8}$$

where the reference state $\mathbf{x}^*$ for stabilization tasks to constant references is

$$\mathbf{x}^* = \begin{pmatrix} x_1^* & 0 & 0 & 0 & x_5^* & 0 & 0 & 0 \end{pmatrix}^\top, \tag{6.9a}$$

and for control of variant references as smooth functions or pseudo-tracking, since this type of control is only feedback for stabilization, could be improved using the following state reference

$$\mathbf{x}^* = \begin{pmatrix} x_1^* & \dot{x}_1^* & 0 & 0 & x_5^* & \dot{x}_5^* & 0 & 0 \end{pmatrix}^{\mathsf{T}}, \tag{6.9b}$$

that is deduced from the linearized model (5.36) as a approximation of the trajectory state generation.

6.1.2 LQR Controller

Using the procedure explained in 2.3.1, the cost function associated to the optimal control of the Jacobi linearized system (5.36) is

$$J = \int_0^\infty \left(\Delta \mathbf{x}^{\mathsf{T}} Q \Delta \mathbf{x} + \Delta \mathbf{u}^{\mathsf{T}} R \Delta \mathbf{u} \right) \mathrm{d}t, \tag{6.10}$$

where the matrices Q and R selected, after some tests, have the following form

$$Q = \rho \begin{pmatrix} 1 & 0 & 0 & 0 & 0 & 0 & 0 & 0 \\ 0 & \kappa & 0 & 0 & 0 & 0 & 0 & 0 \\ 0 & 0 & 1 & 0 & 0 & 0 & 0 & 0 \\ 0 & 0 & 0 & \kappa & 0 & 0 & 0 & 0 \\ 0 & 0 & 0 & 0 & 1 & 0 & 0 & 0 \\ 0 & 0 & 0 & 0 & 0 & \kappa & 0 & 0 \\ 0 & 0 & 0 & 0 & 0 & 0 & 1 & 0 \\ 0 & 0 & 0 & 0 & 0 & 0 & 0 & \kappa \end{pmatrix}, \quad R = \begin{pmatrix} 1 & 0 \\ 0 & 1 \end{pmatrix}, \tag{6.11}$$

with ρ and κ chosen according to the desired performance. The values $\rho = 300$ and $\kappa = 0.3$ give acceptable performance that will be presented in the simulation tests chapter.

The control gain is given by

$$K_{lqr} = R^{-1} B^{\mathsf{T}} P, \tag{6.12}$$

where the matrix P must satisfy the algebraic Riccati equation

$$A^{\mathsf{T}} P + PA - PBR^{-1}B^{\mathsf{T}}P + Q = 0, \tag{6.13}$$

and gives the control law of the form $\Delta\mathbf{u} = K_{lqr}\Delta\mathbf{x}$, which can then be used to derive the control law in terms of the original variables

$$\mathbf{u} = \mathbf{u}_e + \Delta\mathbf{u} = \mathbf{u}_e - K_{lqr}\Delta\mathbf{x} \tag{6.14a}$$

$$\mathbf{u} = -K_{lqr}\left(\mathbf{x} - \mathbf{x}^*\right), \tag{6.14b}$$

where the reference state is the same as that deduced in (6.9).

In practice the matrix P is calculated using the Matlab command $are(A, B, Q, R)$.

Finally, as results, the closed-loop response of the system to a step input of the desired position is shown in Figure. The response can be tuned by adjusting the weights Q and R.

The control diagram for simulation test of the linear controllers, pole placement and LQR controllers that use only feedback in the control action, applied to the nonlinear system (5.9a) is presented in Figure 6.1.
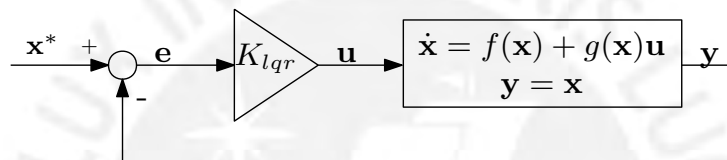
Figure 6.1: Linear controller applied to the nonlinear system.

6.2 Nonlinear Controller Design

6.2.1 Feedback Linearization

As was explained in the introduction (see section 1), the ball and plate system is a extension of the ball and beam system; therefore, some known characteristics of the ball and beam system are taken to be applied to the ball and plate system with the aim of facilitating the analysis and design of the control system. In this way, it is not possible to apply input-state linearization to the ball and plate system (5.9a) since it is not possible to apply input-state linearization to the ball and beam system because it does not satisfy the involutivity condition as is explained in [28].

Considering the nonlinear input affine model of the ball and plate system (5.9a), we proceed first to calculate the relative degree of each output and then analyze the internal dynamics in order to know if is possible to apply input-output linearization explained in 2.3.2.1.

Relative Degree of the System Calculating the relativ degree of each output:

$$y_1 = h_1(\mathbf{x}) = x_1$$
$$\dot{y}_1 = \mathcal{L}_f h_1(\mathbf{x}) = x_2 \tag{6.15a}$$
$$\ddot{y}_1 = \mathcal{L}_f^2 h_1(\mathbf{x}) + \mathcal{L}_{g_1}\mathcal{L}_f h_1(\mathbf{x})u_1 + \mathcal{L}_{g_2}\mathcal{L}_f h_1(\mathbf{x})u_2 = f_2(\mathbf{x}) - \bar{c}_2 u_1 + \bar{c}_1 x_5 \sin(x_3)u_2$$
$$y_2 = h_2(\mathbf{x}) = x_5$$
$$\dot{y}_2 = \mathcal{L}_f h_2(\mathbf{x}) = x_6$$
$$\ddot{y}_2 = \mathcal{L}_f^2 h_1(\mathbf{x}) + \mathcal{L}_{g_1}\mathcal{L}_f h_2(\mathbf{x})u_1 + \mathcal{L}_{g_2}\mathcal{L}_f h_2(\mathbf{x})u_2 = f_6(\mathbf{x}) + \bar{c}_1(-x_1\sin(x_3) + \bar{c}_4\cos(x_3))u_2$$
$$\tag{6.15b}$$

The vector relative degree obtained is

$$\mathbf{r} = \{r_1, r_2\} = \{2, 2\}, \tag{6.16}$$

but is necessary to verify if the vector relative degree is well defined using the decoupling matrix.

From (6.15), the following relationship is obtained

$$\begin{pmatrix} y_1^{(2)} \\ y_2^{(2)} \end{pmatrix} = \begin{pmatrix} \mathcal{L}_f^2 h_1(\mathbf{x}) \\ \mathcal{L}_f^2 h_2(\mathbf{x}) \end{pmatrix} + \begin{pmatrix} \mathcal{L}_{g_1}\mathcal{L}_f h_1(\mathbf{x}) & \mathcal{L}_{g_2}\mathcal{L}_f h_1(\mathbf{x}) \\ \mathcal{L}_{g_1}\mathcal{L}_f h_2(\mathbf{x}) & \mathcal{L}_{g_2}\mathcal{L}_f h_2(\mathbf{x}) \end{pmatrix} \begin{pmatrix} u_1 \\ u_2 \end{pmatrix} \tag{6.17}$$

and represent the change of input as follows

$$\begin{pmatrix} v_1 \\ v_2 \end{pmatrix} = B(\mathbf{x}) + A(\mathbf{x}) \begin{pmatrix} u_1 \\ u_2 \end{pmatrix}. \tag{6.18}$$

The matrix $A(\mathbf{x})$, called the decoupling matrix, is

$$A(\mathbf{x}) = \begin{pmatrix} -\bar{c}_2 & \bar{c}_1 x_5 \sin(x_3) \\ 0 & \bar{c}_1(-x_1\sin(x_3) + \bar{c}_4\cos(x_3)) \end{pmatrix} \tag{6.19}$$

and the matrix $B(\mathbf{x})$ obtained is

$$B(\mathbf{x}) = \begin{pmatrix} \bar{c}_1\left(-\frac{\bar{d}}{2}x_8^2\sin(2x_3) + x_1 x_8^2\sin^2(x_3) + 2x_6 x_8\sin(x_3) + x_1 x_4^2 + g\sin(x_3)\cos(x_7)\right) \\ \bar{c}_1\left(-\bar{c}_3 x_4 x_8\sin(x_3) - 2x_1 x_4 x_8\cos(x_3) - 2x_2 x_8\sin(x_3) + x_5 x_8^2 - g\sin(x_7)\right) \end{pmatrix} \tag{6.20}$$

The rank of $A(\mathbf{x})$ is 2, i.e. is invertible. Therefore, the vector relative degree (6.16) is well defined. Also, the sum relative degree is:

$$r = r_1 + r_2 = 4. \tag{6.21}$$

Therefore, there are $n - r = 4$ internal states.

Byrnes Isidori Normal Form The original system is transformed to the Byrnes Isidori normal form using the diffeomorphism

$$\mathbf{z} = \mathbf{T}(\mathbf{x}) = \begin{pmatrix} h_1(\mathbf{x}) \\ \mathcal{L}_f h_1(\mathbf{x}) \\ h_2(\mathbf{x}) \\ \mathcal{L}_f h_2(\mathbf{x}) \\ \tau_5(\mathbf{x}) \\ \tau_6(\mathbf{x}) \\ \tau_7(\mathbf{x}) \\ \tau_8(\mathbf{x}) \end{pmatrix} = \begin{pmatrix} \boldsymbol{\xi} \\ \boldsymbol{\eta} \end{pmatrix} = \begin{pmatrix} \xi_1^1 \\ \xi_2^1 \\ \xi_1^2 \\ \xi_2^2 \\ \eta_1 \\ \eta_2 \\ \eta_3 \\ \eta_4 \end{pmatrix}, \tag{6.22}$$

where $\boldsymbol{\xi}$ represent the external states and $\boldsymbol{\eta}$ the internal states. Also, $\mathbf{x} = \mathbf{T}^{-1}(\mathbf{z})$ and $\mathbf{T}(\mathbf{0}) = \mathbf{0}$.

External Dynamics The external dynamics is given by

$$\dot{\xi}_1^1 = \xi_2^1$$
$$\dot{\xi}_2^1 = v_1 \tag{6.23a}$$
$$y_1 = \xi_1^1$$

$$\dot{\xi}_1^2 = \xi_2^2$$
$$\dot{\xi}_2^2 = v_2 \tag{6.23b}$$
$$y_2 = \xi_1^2$$

which is presented in the form the Brunovsky as

$$\begin{pmatrix} \dot{\xi}_1^1 \\ \dot{\xi}_2^1 \\ \dot{\xi}_1^2 \\ \dot{\xi}_2^2 \end{pmatrix} = \begin{pmatrix} 0 & 1 & 0 & 0 \\ 0 & 0 & 0 & 0 \\ 0 & 0 & 0 & 1 \\ 0 & 0 & 0 & 0 \end{pmatrix} \begin{pmatrix} \xi_1^1 \\ \xi_2^1 \\ \xi_1^2 \\ \xi_2^2 \end{pmatrix} + \begin{pmatrix} 0 & 0 \\ 1 & 0 \\ 0 & 0 \\ 0 & 1 \end{pmatrix} \begin{pmatrix} v_1 \\ v_2 \end{pmatrix} \tag{6.24a}$$

$$\mathbf{y} = \begin{pmatrix} 1 & 0 & 0 & 0 \\ 0 & 0 & 1 & 0 \end{pmatrix} \begin{pmatrix} \xi_1^1 \\ \xi_2^1 \\ \xi_1^2 \\ \xi_2^2 \end{pmatrix} \tag{6.24b}$$

Internal Dynamics In order to get a representation of the internal dynamics without the direct influence of the inputs, the involutivity of the distribution $\{g_1, g_2\}$ is checked

$$[g_1, g_2] = \begin{bmatrix} 0 & 0 \\ -\bar{c}_2 & \bar{c}_1 x_5 \sin(x_3) \\ 0 & 0 \\ 1 & 0 \\ 0 & 0 \\ 0 & \bar{c}_1(-x_1 \sin(x_3) + \bar{c}_4 \cos(x_3)) \\ 0 & 0 \\ 0 & 1 \end{bmatrix} = \mathbf{0} \tag{6.25}$$

Therefore, according to (2.42) is possible to find $\tau_5(\mathbf{x}), \tau_6(\mathbf{x}), \tau_7(\mathbf{x}), \tau_8(\mathbf{x})$ in order to obtain the internal dynamics in the following form

$$\dot{\eta} = q(\xi, \eta), \quad q(\mathbf{0}, \mathbf{0}) = \mathbf{0}, \quad \eta \in \mathcal{R}^4. \tag{6.26}$$

The calculation of $\tau_5(x)$ to $\tau_8(x)$ according to (2.42), proceed as follows

$$\frac{\partial \tau_5(\mathbf{x})}{\partial \mathbf{x}} g(\mathbf{x}) = \frac{\partial \tau_6(\mathbf{x})}{\partial \mathbf{x}} g(\mathbf{x}) = \frac{\partial \tau_7(\mathbf{x})}{\partial \mathbf{x}} g(\mathbf{x}) = \frac{\partial \tau_8(\mathbf{x})}{\partial \mathbf{x}} g(\mathbf{x}) = \mathbf{0} \tag{6.27}$$

First is calculated $\tau_5(\mathbf{x})$:

$$\begin{bmatrix} \frac{\partial \tau_5(\mathbf{x})}{\partial x_1} & \cdots & \frac{\partial \tau_5(\mathbf{x})}{\partial x_8} \end{bmatrix} \begin{bmatrix} 0 & 0 \\ -\bar{c}_2 & \bar{c}_1 x_5 \sin(x_3) \\ 0 & 0 \\ 1 & 0 \\ 0 & 0 \\ 0 & \bar{c}_1(-x_1 \sin(x_3) + \bar{c}_4 \cos(x_3)) \\ 0 & 0 \\ 0 & 1 \end{bmatrix} = \mathbf{0}, \tag{6.28}$$

and the following relationships are obtained:

$$-\frac{\partial \tau_5(\mathbf{x})}{\partial x_2} \bar{c}_2 + \frac{\partial \tau_5(\mathbf{x})}{\partial x_4} = 0 \tag{6.29a}$$

$$\frac{\partial \tau_5(\mathbf{x})}{\partial x_2} \bar{c}_1 x_5 \sin(x_3) + \frac{\partial \tau_5(\mathbf{x})}{\partial x_6} \bar{c}_1(-x_1 \sin(x_3) + \bar{c}_4 \cos(x_3)) + \frac{\partial \tau_5(\mathbf{x})}{\partial x_8} = 0 \tag{6.29b}$$

Considering $\tau_5(\mathbf{x})$ dependent of the factors $\tau_5(\mathbf{x}) = \chi_1(x_2)\chi_2(x_4)\chi_3(x_6)\chi_4(x_8)$ and replacing it in (6.29), also considering $\tau_5(\mathbf{0}) = 0$, the value of $\tau_5(x)$ obtained is

$$\tau_5(\mathbf{x}) = k_3 e^{(k_1 x_2 - k_2 x_4 - \bar{c}_1 x_5 \sin(x_3) x_8)} - k_3 \tag{6.30}$$

In the same way, the expression for $\tau_6(\mathbf{x})$, $\tau_7(\mathbf{x})$, $\tau_8(\mathbf{x})$ are obtained and have the same form. In order to apply the feedback linearization method, is necessary to check the stability of the internal dynamics. In generally is difficult to determine the global stability because the internal dynamics may have a long terms. For that reason, it is possible to analyze the stability of the zero dynamics.

Zero Dynamics   The zero dynamics results from the zeroing of the outputs and their derivatives ($\boldsymbol{\xi} = \mathbf{0}$). The zero dynamics is obtained from:

$$\dot{\boldsymbol{\eta}} = \mathbf{q}(\mathbf{0}, \boldsymbol{\eta}), \quad \boldsymbol{\eta}(0) = \boldsymbol{\eta}_0 \tag{6.31}$$

If the zero dynamics is asymptotically stable, then the internal dynamics is locally asymptotically stable at $\boldsymbol{\xi} = \mathbf{0}$. Nevertheless, exist a theorem that said, the zero dynamics is independent of the internal states chosen but only depend of the output of the system (since it is an intrinsic property of the system) [1]. Also, it is not necessary to convert the system in the normal form to analyze the stability of the zero dynamics, is possible to calculate the unforced zero dynamics [21].
The internal states chosen are:

$$\boldsymbol{\eta} = \begin{bmatrix} \eta_1 & \eta_2 & \eta_3 & \eta_4 \end{bmatrix}^{\mathsf{T}} = \begin{bmatrix} x_3 & x_4 & x_7 & x_8 \end{bmatrix}^{\mathsf{T}} \tag{6.32}$$

then zeroing the outputs and its derivatives:

$$x_1 = 0, \quad x_2 = 0, \quad v_1 = 0 \tag{6.33a}$$
$$x_5 = 0, \quad x_6 = 0, \quad v_2 = 0 \tag{6.33b}$$

In the external dynamics, the inputs u_1^* and u_2^* needed to satisfy (6.33) are

$$\bar{c}_1 \left(-\frac{\tilde{d}}{2} x_8^2 \sin(2x_3) + g \sin(x_3) \cos(x_7) \right) - \bar{c}_2 u_1^* = 0 \tag{6.34a}$$
$$-\bar{c}_3 x_4 x_8 \sin(x_3) - g \sin(x_7) + \bar{c}_4 \cos(x_3) u_2^* = 0 \tag{6.34b}$$

hence the calculated inputs are

$$u_1^* = \frac{\bar{c}_1}{\bar{c}_2} \left(-\frac{\tilde{d}}{2} x_8^2 \sin(2x_3) + g \sin(x_3) \cos(x_7) \right) \tag{6.35a}$$

$$u_2^* = \frac{1}{\bar{c}_4 \cos(x_3)} \left(\bar{c}_3 x_4 x_8 \sin(x_3) + g \sin(x_7) \right) \tag{6.35b}$$

Replacing the inputs calculated into the equation of the internal states, the unforced zero dynamics obtained is

$$
\begin{aligned}
\dot{\eta}_1 &= \eta_2 \\
\dot{\eta}_2 &= \frac{\bar{c}_1}{\bar{c}_2} \left(-\frac{\tilde{d}}{2} x_8^2 \sin(2x_3) + g \sin(x_3) \cos(x_7) \right) \\
\dot{\eta}_3 &= \eta_4 \\
\dot{\eta}_4 &= \frac{1}{\bar{c}_4 \cos(x_3)} \left(\bar{c}_3 x_4 x_8 \sin(x_3) + g \sin(x_7) \right)
\end{aligned}
\tag{6.36}
$$

Furthermore is possible to simplify the analysis to local stability using the Lyapunov's indirect method [21], i.e. analyzing the stability of the Jacobi linearization of the zero dynamics around $\eta = 0$ as follows

$$\dot{\eta} = A_n \eta, \tag{6.37a}$$

with

$$A_n = \frac{\partial q(0, \eta)}{\partial \eta} |\eta = \eta_{eq} = 0. \tag{6.37b}$$

and the matrix A_n results

$$A_n = \begin{bmatrix} 0 & 1 & 0 & 0 \\ \frac{\bar{c}_1}{\bar{c}_2} & 0 & 0 & 0 \\ 0 & 0 & 0 & 1 \\ 0 & 0 & \frac{g}{\bar{c}_4} & 0 \end{bmatrix} \tag{6.38}$$

with the eigenvalues

$$\lambda = \{ \sqrt{\frac{g}{\bar{c}_4}}, -\sqrt{\frac{g}{\bar{c}_4}}, \sqrt{\frac{\bar{c}_1}{\bar{c}_2}g}, -\sqrt{\frac{\bar{c}_1}{\bar{c}_2}g} \}. \tag{6.39}$$

There are eigenvalues in the RHP, then the linearization of the zero dynamics is unstable and thus the internal zero dynamics is also unstable. Therefore, cannot be applied the input-output linearization using the nonlinear model (5.9a) according to [21].

Furthermore, tracking control cannot be done because it is not possible to perform the dynamic inversion [1]. From the methods explained in 2.4 for tracking control of non-minimum phase systems, the approximate feedback linearization will be used because it is a more practical alternative [28], and was selected after trying the other methods without getting good results; however, according to [21], perfect tracking cannot be achieved.

6.2.2 Approximate Feedback Linearization (AFL)

According to the approximate feedback linearization method explained in 2.4, the outputs of the approximate model to use must be flat outputs, i.e. a full relative degree system is needed. Therefore, it is initiated by eliminating some terms that affect the full relative degree of the outputs (see (6.15)), in the exact nonlinear model(5.9a), hence the coupling terms are removed and two decoupled ball and beam subsystems are obtained as follows [38]

$$
\begin{pmatrix} \dot{x}_1 \\ \dot{x}_2 \\ \dot{x}_3 \\ \dot{x}_4 \\ \dot{x}_5 \\ \dot{x}_6 \\ \dot{x}_7 \\ \dot{x}_8 \end{pmatrix} = \begin{pmatrix} x_2 \\ k_1 \sin(x_3) + k_2 x_1 x_4^2 \\ x_4 \\ 0 \\ x_6 \\ -k_1 \sin(x_7) + k_2 x_5 x_8^2 \\ x_8 \\ 0 \end{pmatrix} + \begin{pmatrix} 0 & 0 \\ -b & 0 \\ 0 & 0 \\ 1 & 0 \\ 0 & 0 \\ 0 & b \\ 0 & 0 \\ 0 & 1 \end{pmatrix} \begin{pmatrix} u_1 \\ u_2 \end{pmatrix}
\tag{6.40a}
$$

$$
\mathbf{y} = \begin{pmatrix} y_1 \\ y_2 \end{pmatrix} = \begin{pmatrix} x \\ y \end{pmatrix}
\tag{6.40b}
$$

where x and y are the ball's position in x-axis and y-axis respectively and

$$
k_1 = \frac{g m_b r_b^2}{m r_b^2 + J_b}, \quad k_2 = \frac{m_b r_b^2}{m r_b^2 + J_b}, \quad b = \frac{m_b \tilde{d} r_b^2 + J_b r_b}{m_b r^2 + J_b}.
\tag{6.41}
$$

However, the model (6.40) still does not have flat outputs. So, in order to obtain a flat model from the exact model (5.9a) of the ball and plate system, it is necessary to take into account the following assumptions

$$
| -\frac{\tilde{d}}{2} x_8^2 \sin(2x_3) + x_1 x_8^2 \sin^2(x_3) + 2 x_6 x_8 \sin(x_3) + x_1 x_4^2 | \ll |g \sin(x_3)|
\tag{6.42a}
$$

$$
| -\bar{c}_3 x_4 x_8 \sin(x_3) - 2 x_1 x_4 x_8 \cos(x_3) - 2 x_2 x_8 \sin(x_3) + x_5 x_8^2 | \ll |g \sin(x_7)|,
\tag{6.42b}
$$

where the terms $g \sin(x_3)$ and $g \sin(x_7)$ are considered main terms and the terms of the left are considered as neglected terms. This assumption is validated in the simulation test Figure 8.6.

Now, the relative degree of the approximate model to be used, is calculated as follows

$$
\begin{aligned}
y_1 &= x_1 \\
\dot{y}_1 &= x_2 \\
\ddot{y}_1 &= k_1 \sin(x_3) \\
y_1^{(3)} &= k_1 \cos(x_3)x_4 \\
y_1^{(4)} &= -k_1 \sin(x_3)x_4^2 + k_1 \cos(x_3)u_1
\end{aligned}
\tag{6.43a}
$$

$$
\begin{aligned}
y_2 &= x_5 \\
\dot{y}_2 &= x_6 \\
\ddot{y}_2 &= -k_1 \sin(x_7) \\
y_2^{(3)} &= -k_1 \cos(x_7)x_8 \\
y_2^{(4)} &= k_1 \sin(x_7)x_8^2 - k_1 \cos(x_7)u_2
\end{aligned}
\tag{6.43b}
$$

and results a vector relative degree $\mathbf{r} = \{r_1, r_2\} = \{4, 4\}$. Therefore, the approximate model to use in the control design processes is given by

$$
\begin{pmatrix} \dot{x}_1 \\ \dot{x}_2 \\ \dot{x}_3 \\ \dot{x}_4 \\ \dot{x}_5 \\ \dot{x}_6 \\ \dot{x}_7 \\ \dot{x}_8 \end{pmatrix} = \begin{pmatrix} x_2 \\ k_1 \sin(x_3) \\ x_4 \\ 0 \\ x_6 \\ -k_1 \sin(x_7) \\ x_8 \\ 0 \end{pmatrix} + \begin{pmatrix} 0 & 0 \\ 0 & 0 \\ 0 & 0 \\ 1 & 0 \\ 0 & 0 \\ 0 & 0 \\ 0 & 0 \\ 0 & 1 \end{pmatrix} \begin{pmatrix} u_1 \\ u_2 \end{pmatrix} = \bar{f}(\mathbf{x}) + \bar{g}(\mathbf{x})\mathbf{u}
\tag{6.44}
$$

$$
\mathbf{y} = \begin{pmatrix} y_1 \\ y_2 \end{pmatrix} = \begin{pmatrix} x \\ y \end{pmatrix},
$$

and it is considered that is composed of two subsystems, the first is formed by the dynamics of states x_1, x_2, x_3, x_4 and the second formed by the dynamics of states x_5, x_6, x_7, x_8 as follows

First subsystem

$$
\begin{pmatrix} \dot{x}_1 \\ \dot{x}_2 \\ \dot{x}_3 \\ \dot{x}_4 \end{pmatrix} = \begin{pmatrix} x_2 \\ k_1 \sin(x_3) \\ x_4 \\ 0 \end{pmatrix} + \begin{pmatrix} 0 \\ 0 \\ 0 \\ 1 \end{pmatrix} u_1
\tag{6.45a}
$$

$$
y_1 = x
$$

Second subsystem

$$
\begin{pmatrix} \dot{x}_5 \\ \dot{x}_6 \\ \dot{x}_7 \\ \dot{x}_8 \end{pmatrix} = \begin{pmatrix} x_6 \\ -k_1 \sin(x_7) \\ x_8 \\ 0 \end{pmatrix} + \begin{pmatrix} 0 \\ 0 \\ 0 \\ 1 \end{pmatrix} u_2
\tag{6.45b}
$$

$$
y_2 = y
$$

6.2.2.1 Feedforward Control

Using the approximate model (6.44), the state trajectory generated for the trajectory references $x^*(t)$ and $y^*(t)$, position references of the ball in x and y axes respectively, results

$$\mathbf{x}^* = \begin{pmatrix} x_1^* \\ x_2^* \\ x_3^* \\ x_4^* \\ x_5^* \\ x_6^* \\ x_7^* \\ x_8^* \end{pmatrix} = \begin{pmatrix} x^*(t) \\ \dot{x}^*(t) \\ \arcsin\left(\alpha_x(t)\right) \\ \beta_x(t) \\ y^*(t) \\ \dot{y}^*(t) \\ \arcsin\left(\alpha_y(t)\right) \\ \beta_y(t) \end{pmatrix} \tag{6.46a}$$

where

$$\alpha_x(t) = \frac{\ddot{x}^*(t)}{k_1}, \qquad \beta_x(t) = \frac{\ddot{x}^*(t)}{k_1 \cos(x_3)} \tag{6.46b}$$

$$\alpha_y(t) = -\frac{\ddot{y}^*(t)}{k_1}, \qquad \beta_y(t) = \frac{\ddot{y}^*(t)}{-k_1 \cos(x_7)}, \tag{6.46c}$$

with $\cos(x_3) \neq 0$ and $\cos(x_7) \neq 0$ for the considered operating range in section 3.

The calculation of the feedforward control action $\mathbf{u}_{ff}$ using the relationships from the state trajectory and the following system equations

$$u_1^* = \dot{x}_4^* \tag{6.47a}$$

$$u_2^* = \dot{x}_8^*, \tag{6.47b}$$

results

$$u_1^* = \frac{x^{*(4)}(t) + x_4^2 \ddot{x}^*(t)}{k_1 \cos(x_3)} \tag{6.47c}$$

$$u_2^* = \frac{y^{*(4)}(t) + x_8^2 \ddot{y}^*(t)}{-k_1 \cos(x_7)} \tag{6.47d}$$

$$\mathbf{u}_{ff} = \begin{pmatrix} u_1^* \\ u_2^* \end{pmatrix} \tag{6.47e}$$

This process is known as dynamic inversion because the control input is calculated from the desired output using the dynamics of the system.

The feedback control $\mathbf{u}_{fb}$ to be used may be any of the linear controllers designed in 6.1, such as pole placement or linear quadratic regulator (LQR), where the reference state as input to the feedback control is the state trajectory $\mathbf{x}^*$ calculated in (6.46a).

The total control action is computed as $\mathbf{u} = \mathbf{u}_{fb} + \mathbf{u}_{ff}$, and the control scheme is presented in Figure 6.2.
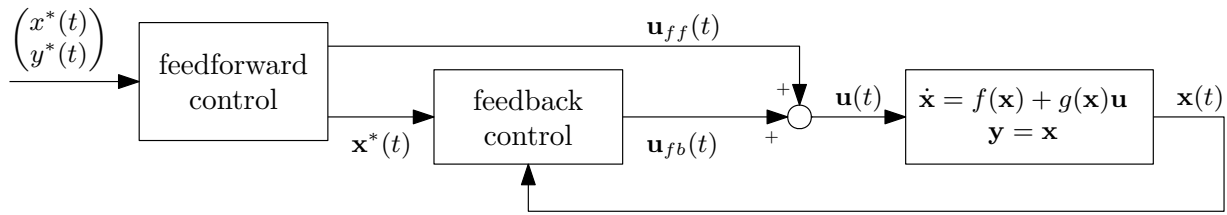
Figure 6.2: Scheme of the controlled system.

6.2.2.2 Tracking Control

The tracking control can be designed in a single expression joining the feedforward and feedback action using the approach of output tracking explained in 2.3.2.1, and developed below.

Using the last derivative of each output of the approximate model from (6.43)

$$y_1^{(4)} = -k_1 \sin(x_3)x_4^2 + k_1 \cos(x_3)u_1$$
$$v_1 = -k_1 \sin(x_3)x_4^2 + k_1 \cos(x_3)u_1 \tag{6.48a}$$

$$y_2^{(4)} = k_1 \sin(x_7)x_8^2 - k_1 \cos(x_7)u_2$$
$$v_2 = k_1 \sin(x_7)x_8^2 - k_1 \cos(x_7)u_2, \tag{6.48b}$$

the relationship of the input transformation is obtained as follows

$$\mathbf{v} = B(\mathbf{x}) + A(\mathbf{x})\mathbf{u} \tag{6.49a}$$

$$\begin{pmatrix} v_1 \\ v_2 \end{pmatrix} = \begin{pmatrix} -k_1 \sin(x_3)x_4^2 \\ k_1 \sin(x_7)x_8^2 \end{pmatrix} + \begin{pmatrix} k_1 \cos(x_3) & 0 \\ 0 & -k_1 \cos(x_7) \end{pmatrix} \begin{pmatrix} u_1 \\ u_2 \end{pmatrix}, \tag{6.49b}$$

and the inverse of the input transformation is given by

$$\mathbf{u} = \alpha(\mathbf{x}) + \beta(\mathbf{x})\mathbf{v} \tag{6.50a}$$

$$\begin{pmatrix} u_1 \\ u_2 \end{pmatrix} = \begin{pmatrix} \tan(x_3)x_4^2 \\ -\tan(x_7)x_8^2 \end{pmatrix} + \begin{pmatrix} \frac{1}{k_1} \sec(x_3) & 0 \\ 0 & -\frac{1}{k_1} \sec(x_7) \end{pmatrix} \begin{pmatrix} v_1 \\ v_2 \end{pmatrix}, \tag{6.50b}$$

where $\cos(x_3) \neq 0$ and $\cos(x_7) \neq 0$ for the operation range considered in section 3 .

Also, the states transformation is performed using the diffeomorphism $\mathbf{z} = T(\mathbf{x})$ as follows

$$\mathbf{z} = \begin{pmatrix} z_1 \\ z_2 \\ z_3 \\ z_4 \\ z_5 \\ z_6 \\ z_7 \\ z_8 \end{pmatrix} = \begin{pmatrix} y_1 \\ \dot{y}_1 \\ \ddot{y}_1 \\ y_1^{(3)} \\ y_2 \\ \dot{y}_2 \\ \ddot{y}_2 \\ y_2^{(3)} \end{pmatrix} = \begin{pmatrix} x_1 \\ x_2 \\ k_1 \sin(x_3) \\ k_1 \cos(x_3) x_4 \\ x_5 \\ x_6 \\ -k_1 \sin(x_7) \\ -k_1 \cos(x_7) x_8 \end{pmatrix} \tag{6.51}$$

Using the input transformation (6.49) and state transformation (6.51), the approximate model (6.44) is converted to a linear system in the Brunovsky form presented below.

$$\dot{\mathbf{z}} = \begin{pmatrix} 0 & 1 & 0 & 0 & 0 & 0 & 0 & 0 \\ 0 & 0 & 1 & 0 & 0 & 0 & 0 & 0 \\ 0 & 0 & 0 & 1 & 0 & 0 & 0 & 0 \\ 0 & 0 & 0 & 0 & 0 & 0 & 0 & 0 \\ 0 & 0 & 0 & 0 & 0 & 1 & 0 & 0 \\ 0 & 0 & 0 & 0 & 0 & 0 & 1 & 0 \\ 0 & 0 & 0 & 0 & 0 & 0 & 0 & 1 \\ 0 & 0 & 0 & 0 & 0 & 0 & 0 & 0 \end{pmatrix} \mathbf{z} + \begin{pmatrix} 0 & 0 \\ 0 & 0 \\ 0 & 0 \\ 1 & 0 \\ 0 & 0 \\ 0 & 0 \\ 0 & 0 \\ 0 & 1 \end{pmatrix} \mathbf{v} \tag{6.52}$$

$$\mathbf{y} = \begin{pmatrix} 1 & 0 & 0 & 0 & 0 & 0 & 0 & 0 \\ 0 & 0 & 0 & 0 & 1 & 0 & 0 & 0 \end{pmatrix} \mathbf{z}$$

The reference signals in z-coordinates, is denoted by $\mathbf{z}^*$. For example, for the case of tracking sinusoidal trajectories in each axis (x and y), $\mathbf{z}^*$ is given by

$$\mathbf{z}^* = \begin{pmatrix} y_1^*(t) \\ \dot{y}_1^*(t) \\ \ddot{y}_1^*(t) \\ y_1^{*(3)}(t) \\ y_2^*(t) \\ \dot{y}_2^*(t) \\ \ddot{y}_2^*(t) \\ y_2^{*(3)}(t) \end{pmatrix} = \begin{pmatrix} A \sin(\omega t) \\ A\omega \cos(\omega t) \\ -A\omega^2 \sin(\omega t) \\ -A\omega^3 \cos(\omega t) \\ A \sin(\omega t) \\ A\omega \cos(\omega t) \\ -A\omega^2 \sin(\omega t) \\ -A\omega^3 \cos(\omega t) \end{pmatrix} \tag{6.53a}$$

$$y_1^{(4)*} = A\omega^4 \sin(\omega t) \tag{6.53b}$$

$$y_2^{(4)*} = A\omega^4 \sin(\omega t). \tag{6.53c}$$

In addition, a circular trajectory with polynomial initialization for soft initialization (see appendix D), Lissajous curves, or any sufficiently differentiable function can be used as trajectory reference.

The error vector in z-coordinates, which consists of the tracking errors, e_1 and e_2, and its derivatives is

$$\mathbf{e} = \mathbf{z} - \mathbf{z}^* = \begin{pmatrix} e_1 \\ \dot{e}_1 \\ \ddot{e}_1 \\ e_1^{(3)} \\ e_2 \\ \dot{e}_2 \\ \ddot{e}_2 \\ e_2^{(3)} \end{pmatrix} = \begin{pmatrix} y_1 - y_1^*(t) \\ \dot{y}_1 - \dot{y}_1^*(t) \\ \ddot{y}_1 - \ddot{y}_1^*(t) \\ y_1^{(3)} - y_1^{*(3)}(t) \\ y_2 - y_2^*(t) \\ \dot{y}_2 - \dot{y}_2^*(t) \\ \ddot{y}_2 - \ddot{y}_2^*(t) \\ y_2^{(3)} - y_2^{*(3)}(t) \end{pmatrix}, \tag{6.54}$$

then the control action will be calculated using (2.32) . For the first subsystem (6.45a) is computed as follows

$$v_1 = y_1^{(4)} \tag{6.55a}$$

$$y_1^{(4)} = y_1^{*(4)} - \left(p_0 e_1 + p_1 \dot{e}_1 + p_2 \ddot{e}_1 + p_3 e_1^{(3)} \right) \tag{6.55b}$$

$$0 = e_1^{(4)} + p_3 e_1^{(3)} + p_2 \ddot{e}_1 + p_1 \dot{e}_1 + p_0 e_1. \tag{6.55c}$$

In order to stabilize asymptotically the error $\mathbf{e}$ to zero ($\mathbf{e} \to \mathbf{0}$) , the values of p_0 , p_1 , p_2 , p_3, are real values chosen so that the following characteristic polynomial of the error dynamics

$$\lambda^4 + p_3 \lambda^3 + p_2 \lambda^2 + p_1 \lambda + p_0, \tag{6.56}$$

be Hurwitz. It is also possible to use the desired poles of the error dynamics to create the polynomial (6.56).

Using the same procedure and characteristic polynomial for the second subsystem (6.45b), it results

$$v_2 = y_2^{(4)} \tag{6.57a}$$

$$y_2^{(4)} = y_2^{*(4)} - \left(p_0 e_2 + p_2 \dot{e}_2 + p_2 \ddot{e}_2 + p_3 e_2^{(3)} \right) \tag{6.57b}$$

$$0 = e_2^{(4)} + p_3 e_2^{(3)} + p_2 \ddot{e}_2 + p_1 \dot{e}_2 + p_0 e_2 \tag{6.57c}$$

Then the control action for the Brunovsky form is

$$v_1 = y_1^{*(4)} - \left(p_0 e_1 + p_1 \dot{e}_1 + p_2 \ddot{e}_1 + p_3 e_1^{(3)}\right) \tag{6.58a}$$

$$v_2 = y_2^{*(4)} - \left(p_0 e_2 + p_2 \dot{e}_2 + p_2 \ddot{e}_2 + p_3 e_2^{(3)}\right) \tag{6.58b}$$

Finally the control input to the original system (5.9a) using the inverse input transformation (6.50) is given by

$$u_1 = \frac{1}{k_1 \cos(x_3)} \left(k_1 \sin(x_3) x_4^2 + y_1^{*(4)} - \left(p_0 e_1 + p_1 \dot{e}_1 + p_2 \ddot{e}_1 + p_3 e_1^{(3)}\right)\right), \tag{6.59a}$$

$$u_2 = \frac{1}{-k_1 \cos(x_7)} \left(-k_1 \sin(x_7) x_8^2 + y_2^{*(4)} - \left(p_0 e_2 + p_2 \dot{e}_2 + p_2 \ddot{e}_2 + p_3 e_2^{(3)}\right)\right), \tag{6.59b}$$

and the control scheme of the tracking control approach developed is presented in Figure 6.3.
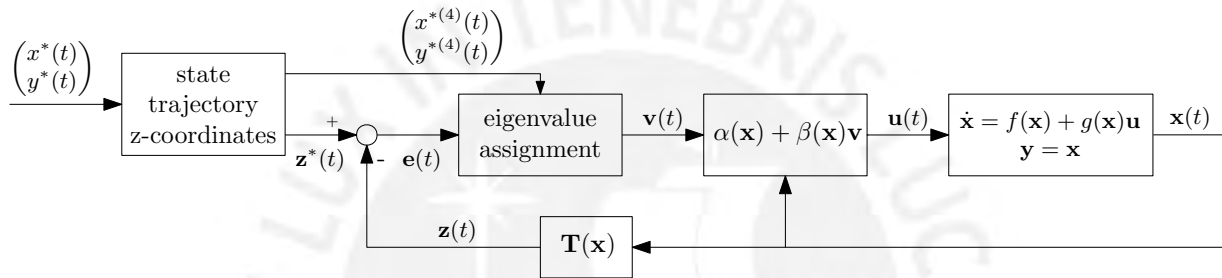
Figure 6.3: Scheme of tracking control using feedback linearization.

6.2.2.3 Tracking Control with Integral Action

Considering the case of presence of steady state error due disturbances or due to not use a exact model of the system in the control system design , integral action is added to the control action in order to provide zero steady-state error to the response [32, 20].

Therefore, the integral of the tracking error is included to the control law weighted by the integral gain p_I as follows

$$v_1 = y_1^{*(4)} - \left(p_0 e_1 + p_1 \dot{e}_1 + p_2 \ddot{e}_1 + p_3 e_1^{(3)}\right) - p_I \int_0^t e_1(\tau) d\tau \tag{6.60a}$$

$$v_2 = y_2^{*(4)} - \left(p_0 e_2 + p_2 \dot{e}_2 + p_2 \ddot{e}_2 + p_3 e_2^{(3)}\right) - p_I \int_0^t e_2(\tau) d\tau \tag{6.60b}$$

where p_0 , p_1 , p_2 , p_3 ,and p_I are real values chosen so that the following polynomial

$$\lambda^5 + p_3 \lambda^4 + p_2 \lambda^3 + p_1 \lambda^2 + p_0 \lambda + p_I \tag{6.61}$$

be Hurwitz.

Finally, the control input to the original system (5.9a) is calculated as follows

$$u_1 = \frac{1}{k_1 \cos(x_3)} \left(k_1 \sin(x_3) x_4^2 + y_1^{*(4)} - \left(p_0 e_1 + p_1 \dot{e}_1 + p_2 \ddot{e}_1 + p_3 e_1^{(3)} \right) - p_I \int\limits_0^t e_1(\tau) d\tau \right)$$

(6.62a)

$$u_2 = \frac{1}{-k_1 \cos(x_7)} \left(-k_1 \sin(x_7) x_8^2 + y_2^{*(4)} - \left(p_0 e_2 + p_2 \dot{e}_2 + p_2 \ddot{e}_2 + p_3 e_2^{(3)} \right) - p_I \int\limits_0^t e_2(\tau) d\tau \right)$$

(6.62b)

6.2.3 Backstepping Control

Using the approximate model (6.44), a system in the integrator chain form is obtained and the methodology explained in 2.3.2.2 can be applied. Moreover, it is possible to design the backstepping controller using the first subsystem (6.45a) in the integrator chain form as follows

$$\begin{aligned}
\dot{x}_1 &= x_2 \\
\dot{x}_2 &= k_1 \sin(x_3) \\
\dot{x}_3 &= x_4 \\
\dot{x}_4 &= u_1 \\
y_1 &= x_1.
\end{aligned}$$

(6.63)

The idea is to stabilize the tracking error $e_1 = x_1 - x_1^*$, which represents the trajectory tracking error of the ball on the x-axis, through four steps (the order and relative degree of the approximate model used) in which by means of virtual inputs the control action is calculated as shown below:

Step 1 The tracking error of the first output $y_1 = x_1$ and its derivative are

$$e_1 = x_1 - y_1^*$$

(6.64a)

$$\dot{e}_1 = x_2 - \dot{y}_1^*$$

(6.64b)

also using the Lyapunov function V_1 defined as

$$V_1(.) = \frac{1}{2} e_1^2 \geq 0,$$

(6.65)

and α_1 as artificial input to stabilize the error e_1 given by

$$\alpha_1 \to x_2 \tag{6.66a}$$

$$\alpha_1 = -c_1 e_1 + \dot{y}_1^* \ , \ \ c_1 > 0, \tag{6.66b}$$

then $e_1 \to 0$ since

$$\dot{e}_1 = -c_1 e_1. \tag{6.67}$$

By means of the virtual input α_1 (6.67), the derivative of the Lyapunov function V_1 results

$$\dot{V}_1(.) = e_1 \dot{e}_1 \tag{6.68a}$$

$$\dot{V}_1(.) = -c_1 e_1^2 \le 0, \tag{6.68b}$$

with V_1 radially unbounded and $V_1(0) = 0$, then e_1 is globally asymptotically stabilizable. Finally in this step, the error between the variable x_2 and the artificial input α_1 is

$$e_2 = x_2 - \alpha_1, \tag{6.69a}$$

and the derivative of the tracking error

$$\dot{e}_1 = -c_1 e_1 + e_2. \tag{6.69b}$$

Step 2   The error between the variable x_2 and the artificial input α_1 , and its derivative are

$$e_2 = x_2 - \alpha_1 \tag{6.70a}$$

$$\dot{e}_2 = \dot{x}_2 - \dot{\alpha}_1 \tag{6.70b}$$

$$\dot{e}_2 = k_1 \sin(x_3) + c_1 \dot{e}_1 - \ddot{y}_1^* \tag{6.70c}$$

$$\dot{e}_2 = k_1 \sin(x_3) - c_1^2 e_1 + c_1 e_2 - \ddot{y}_1^*, \tag{6.70d}$$

also using the Lyapunov function V_2 defined as

$$V_2(.) = \frac{1}{2} \left(e_1^2 + e_2^2 \right) \ge 0, \tag{6.71}$$

and α_2 as artificial input to stabilize the error e_2 as follows

$$\alpha_2 \to k_1 \sin(x_3). \tag{6.72}$$

Using the virtual input α_2 in calculation of the derivative of the Lyapunov function V_2 as follows

$$\dot{V}_2(.) = e_1\dot{e}_1 + e_2\dot{e}_2 \tag{6.73a}$$

$$\dot{V}_2(.) = e_1\left(e_2 - c_1e_1\right) + e_2\left(\alpha_2 - c_1^2 e_1 + c_1 e_2 - \ddot{y}_1^*\right) \tag{6.73b}$$

$$\dot{V}_2(.) = -c_1 e_1^2 + e_2\left(\alpha_2 + e_1 - c_1^2 e_1 + c_1 e_2 - \ddot{y}_1^*\right); \tag{6.73c}$$

and hence is convenient to select α_2 as

$$\alpha_2 = e_1\left(c_1^2 - 1\right) - e_2\left(c_1 + c_2\right) + \ddot{y}_1^* \ , \ \ c_2 > 0. \tag{6.74}$$

By means of the virtual input α_2 (6.74), the derivative of the Lyapunov function V_2 (6.73c) results

$$\dot{V}_2(.) = -c_1 e_1^2 - c_2 e_2^2 \le 0, \tag{6.75}$$

with V_2 radially unbounded and $V_2(\mathbf{0}) = 0$, then e_2 is globally asymptotically stabilizable. Finally in this step, the error between the variable $k_1 \sin(x_3)$ and the artificial input α_2 is

$$e_3 = k_1 \sin(x_3) - \alpha_2, \tag{6.76a}$$

and the derivative of the error e_2 results

$$\dot{e}_2 = -c_2 e_2 - e_1 + e_3. \tag{6.76b}$$

Step 3 The error between the variable $k_1 \sin(x_3)$ and the artificial input α_2 , and its derivative are

$$e_3 = k_1 \sin(x_3) - \alpha_2 \tag{6.77a}$$

$$\dot{e}_3 = k_1 \cos(x_3)x_4 - \dot{\alpha}_2 \tag{6.77b}$$

$$\dot{e}_3 = k_1 \cos(x_3)x_4 + \left(1 - c_1^2\right)\dot{e}_1 + (c_1 + c_2)\dot{e}_2 - y_1^{*(3)} \tag{6.77c}$$

$$\dot{e}_3 = k_1 \cos(x_3)x_4 + \left(1 - c_1^2\right)(e_2 - c_1 e_1) + (c_1 + c_2)(c_2 e_2 - e_1 + e_3) - y_1^{*(3)} \tag{6.77d}$$

$$\dot{e}_3 = k_1 \cos(x_3)x_4 + \left(-c_1 + c_1^3 - c_1 - c_2\right)e_1 + \left(1 - c_1^2 - c_1 c_2 - c_2^2\right)e_2 + (c_1 + c_2)e_3 - y_1^{*(3)}, \tag{6.77e}$$

also using the Lyapunov function V_3 defined as

$$V_3(.) = \frac{1}{2}\left(e_1^2 + e_2^2 + e_3^2\right) \ge 0, \tag{6.78}$$

and α_3 as artificial input to stabilize the error e_3 as follows

$$\alpha_3 \to x_4. \tag{6.79}$$

Using the virtual input α_3 in calculation of the derivative of the Lyapunov function V_3 as follows

$$\dot{V}_3(.) = e_1\dot{e}_1 + e_2\dot{e}_2 + e_3\dot{e}_3 \tag{6.80a}$$

$$\dot{V}_3(.) = e_1\left(e_2 - c_1 e_1\right) + e_2\left(-c_2 e_2 - e_1 + e_3\right) + e_3\dot{e}_3 \tag{6.80b}$$

$$\dot{V}_3(.) = -c_1 e_1^2 - c_2 e_2^2 + e_2 e_3 + e_3\dot{e}_3, \tag{6.80c}$$

also considering the indirect relationship

$$\dot{e}_3 \approx -e_2 - c_3 e_3 \ , \ \ c_3 > 0, \tag{6.81}$$

this implies

$$k_1 \cos(x_3)\alpha_3 + \left(-2c_1 + c_1^3 - c_2\right)e_1 + \left(2 - c_1^2 - c_1 c_2 - c_2^2\right)e_2 + (c_1 + c_2 + c_3)e_3 - y_1^{*(3)} = 0; \tag{6.82a}$$

and hence is convenient to select α_3 as

$$\alpha_3 = \frac{1}{k_1 \cos(x_3)}\left[\left(2c_1 - c_1^3 + c_2\right)e_1 + \left(c_1^2 + c_1 c_2 + c_2^2 - 2\right)e_2 - (c_1 + c_2 + c_3)e_3 + y_1^{*(3)}\right], \tag{6.82b}$$

where $\cos(x_3) \neq 0$ for the operation range considered in section 3 .

By means of the virtual input α_3 (6.82b), the derivative of the Lyapunov function V_3 (6.80c) results

$$\dot{V}_3(.) = -c_1 e_1^2 - c_2 e_2^2 - c_3 e_3^2 \leq 0, \tag{6.83}$$

with V_3 radially unbounded and $V_3(\mathbf{0}) = 0$, then e_3 is globally asymptotically stabilizable. Finally in this step, the error between the variable x_4 and the artificial input α_3 is

$$e_4 = x_4 - \alpha_3, \tag{6.84}$$

and the derivative of the error e_3 results

$$\dot{e}_3 = -c_3 e_3 - e_2 + k_1 \cos(x_3)e_4. \tag{6.85}$$

Step 4 The error between the variable x_4 and the artificial input α_3 , and its derivative are

$$e_4 = x_4 - \alpha_3 \tag{6.86a}$$

$$\dot{e}_4 = u_1 - \dot{\alpha}_3, \tag{6.86b}$$

also using the Lyapunov function V_4 defined as

$$V_4(.) = \frac{1}{2} \left(e_1^2 + e_2^2 + e_3^2 + e_4^2 \right) \geq 0 \tag{6.87}$$

Using the input u_1 in calculation of the derivative of the Lyapunov function V_4 as follows

$$\dot{V}_4(.) = e_1 \dot{e}_1 + e_2 \dot{e}_2 + e_3 \dot{e}_3 + e_4 \dot{e}_4 \tag{6.88a}$$

$$\dot{V}_4(.) = e_1 \left(e_2 - c_1 e_1 \right) + e_2 \left(-c_2 e_2 - e_1 + e_3 \right) + e_3 \left(-c_3 e_3 - e_2 + k_1 \cos(x_3)e_4 \right) + e_4 \left(u_1 - \dot{\alpha}_3 \right) \tag{6.88b}$$

$$\dot{V}_4(.) = -c_1 e_1^2 - c_2 e_2^2 - c_3 e_3^2 + e_4 \left(k_1 \cos(x_3)e_3 + u_1 - \dot{\alpha}_3 \right); \tag{6.88c}$$

and hence it is convenient to select u_1 as

$$u_1 = \dot{\alpha}_3 - k_1 \cos(x_3)e_3 - c_4 e_4 \ , \quad c_4 > 0, \tag{6.89}$$

with

$$\dot{\alpha}_3 = \frac{\sin(x_3)x_4}{k_1 \cos^2(x_3)} \left[\left(2c_1 - c_1^3 + c_2 \right) e_1 + \left(c_1^2 + c_1 c_2 + c_2^2 - 2 \right) e_2 - \left(c_1 + c_2 + c_3 \right) e_3 + y_1^{*(3)} \right] +$$

$$\frac{1}{k_1 \cos(x_3)} \left[\left(2c_1 - c_1^3 + c_2 \right) \dot{e}_1 + \left(c_1^2 + c_1 c_2 + c_2^2 - 2 \right) \dot{e}_2 - \left(c_1 + c_2 + c_3 \right) \dot{e}_3 + y_1^{*(4)} \right]. \tag{6.90}$$

By means of the input u_1 (6.89), the derivative of the Lyapunov function V_4 (6.88c) results

$$\dot{V}_4(.) = -c_1 e_1^2 - c_2 e_2^2 - c_3 e_3^2 - c_4 e_4^2 \leq 0, \tag{6.91}$$

with V_4 radially unbounded and $V_4(\mathbf{0}) = 0$, then e_4 is globally asymptotically stabilizable. Therefore e_1 , e_2 , e_3 , e_4 converge asymptotically to zero with the control law u_1.

On the other hand, for the second system (6.45b) the same procedure presented for the first subsystem is applied, and even the same positive constants c_1, c_2, c_3, c_4 can be considered because both have the same form. The idea is to stabilize the tracking error $e_5 = x_5 - x_5^*$, which represents the trajectory tracking error of the ball on the y-axis, obtaining the following equations

Step 1

$$e_5 = x_5 - y_2^* \tag{6.92a}$$

$$\alpha_5 = -c_1 e_5 + \dot{y}_2^* \tag{6.92b}$$

Step 2

$$e_6 = x_6 - \alpha_5 \tag{6.93a}$$

$$\alpha_6 = \left(c_1^2 - 1\right) e_5 - \left(c_1 + c_2\right) e_6 + \ddot{y}_2^* \tag{6.93b}$$

Step 3

$$e_7 = -k_1 \sin(x_7) - \alpha_6 \tag{6.94a}$$

$$\alpha_7 = -\frac{1}{k_1 \cos(x_7)} \left[\left(2c_1 - c_1^3 + c_2\right) e_5 + \left(c_1^2 + c_1 c_2 + c_2^2 - 2\right) e_6 - \left(c_1 + c_2 + c_3\right) e_7 + y_2^{*(3)} \right] \tag{6.94b}$$

where $\cos(x_7) \neq 0$ for the operation range considered in section 3 .

Step 4

$$e_8 = x_8 - \alpha_7 \tag{6.95a}$$

$$\dot{\alpha}_7 = -\frac{\sin(x_7) x_8}{k_1 \cos^2(x_7)} \left[\left(2c_1 - c_1^3 + c_2\right) e_5 + \left(c_1^2 + c_1 c_2 + c_2^2 - 2\right) e_6 - \left(c_1 + c_2 + c_3\right) e_7 + y_2^{*(3)} \right] +$$

$$- \frac{1}{k_1 \cos(x_7)} \left[\left(2c_1 - c_1^3 + c_2\right) \dot{e}_5 + \left(c_1^2 + c_1 c_2 + c_2^2 - 2\right) \dot{e}_6 - \left(c_1 + c_2 + c_3\right) \dot{e}_7 + y_2^{*(4)} \right] \tag{6.95b}$$

$$u_2 = \dot{\alpha}_7 + k_1 \cos(x_7) e_7 - c_4 e_8 \tag{6.95c}$$

6.2.4 Sliding Mode Control

Using the approximate model (6.44), a full relative degree system is obtained; hence the methodology explained for high order sliding mode (HOSM) 2.3.2.3 can be applied. Moreover,

it is possible to design the sliding mode controller using the first subsystem (6.45a)

$$
\begin{aligned}
\dot{x}_1 &= x_2 \\
\dot{x}_2 &= k_1 \sin(x_3) \\
\dot{x}_3 &= x_4 \\
\dot{x}_4 &= u_1 \\
y_1 &= x_1,
\end{aligned}
\tag{6.96}
$$

which is a high-order system with output relative degree $r = 4$ and therefore involves designing a HOSM controller class, as follows [27]:

First, defining the sliding variable and its derivatives

$$
\sigma_1 = x_1 - y_1^* \tag{6.97a}
$$
$$
\dot{\sigma}_1 = \dot{x}_1 - \dot{y}_1^* = x_2 - \dot{y}_1^* \tag{6.97b}
$$
$$
\ddot{\sigma}_1 = \ddot{x}_1 - \ddot{y}_1^* = k_1 \sin(x_3) - \ddot{y}_1^* \tag{6.97c}
$$
$$
\sigma_1^{(3)} = x_1^{(3)} - y_1^{*(3)} = k_1 \cos(x_3)x_4 - y_1^{*(3)}; \tag{6.97d}
$$

also, in the sliding surface is satisfied

$$
\sigma_1 = \dot{\sigma}_1 = \ddot{\sigma}_1 = \sigma_1^{(3)} = 0, \tag{6.98}
$$

where there is a discontinuity at 4-sliding mode (high frequency).

Then, according the methodology 2.3.2.3, using HOSM the **nested r-sliding mode controllers** are calculated as follows

$$
\Psi_{0,4} = \text{sign}(\sigma_1) \tag{6.99a}
$$
$$
\Psi_{1,4} = \text{sign}\left(\dot{\sigma}_1 + \beta_1 \left| \sigma_1 \right|^{3/4} \Psi_{0,4} \right) \tag{6.99b}
$$
$$
\Psi_{2,4} = \text{sign}\left(\ddot{\sigma}_1 + \beta_2 \left(\dot{\sigma}_1^4 + \left| \sigma_1 \right|^3 \right)^{1/6} \Psi_{1,4} \right) \tag{6.99c}
$$
$$
\Psi_{3,4} = \text{sign}\left(\sigma_1^{(3)} + \beta_3 \left(\ddot{\sigma}_1^6 + \dot{\sigma}_1^4 + \left| \sigma_1 \right|^3 \right)^{1/12} \Psi_{2,4} \right) \tag{6.99d}
$$

with α as design parameter and $\beta_1, \beta_2, \beta_3$ as controller gains to be tuned. Finally the control law for the whole first subsystem results

$$
u_1 = -\alpha \Psi_{3,4}. \tag{6.100}
$$

However, due to the signal function in the structure of the control law (6.100), it results non-smooth and high frequency signal that makes it impossible to use for real applications as is explained in 2.3.2.3. Therefore, in this case, the chattering evasion method using sigmoidal

function instead the signal function is used. The sigmoidal function is defined by (2.52) with ε chosen according to the trade-off between the robustness/accuracy of the control system and the smoothness of the control law resulting in the simulation and experimental tests. Finally the smooth control action using sigmoidal function results

$$\Psi_{0,4} = \text{sigmoid}(\sigma_1) \tag{6.101a}$$

$$\Psi_{1,4} = \text{sigmoid}\left(\dot{\sigma}_1 + \beta_1 \left|\sigma_1\right|^{3/4} \Psi_{0,4}\right) \tag{6.101b}$$

$$\Psi_{2,4} = \text{sigmoid}\left(\ddot{\sigma}_1 + \beta_2 \left(\dot{\sigma}_1^4 + \left|\sigma_1\right|^3\right)^{1/6} \Psi_{1,4}\right) \tag{6.101c}$$

$$\Psi_{3,4} = \text{sigmoid}\left(\sigma_1^{(3)} + \beta_3 \left(\ddot{\sigma}_1^6 + \dot{\sigma}_1^4 + \left|\sigma_1\right|^3\right)^{1/12} \Psi_{2,4}\right) \tag{6.101d}$$

$$u_1 = -\alpha\Psi_{3,4}. \tag{6.101e}$$

As was explained in 2.3.2.3, the smooth control cannot provide finite-time convergence of the sliding variable σ even for the approximate model (6.44). However, the control system's performance using smooth control action is expected to be close the performance using non-smooth control action.

On the other hand, it was explained in the begin of this approach, an approximate model (6.44) is used to be able to apply the HOSM method, hence it is expected that exact tracking for the approximate model will not lead to exact tracking for the exact system (5.9a). Therefore finding a trade-off between accuracy and a smooth control action is an acceptable decision.

In the same way, the control action for the second subsystem (6.45b) is calculated, using the same controller gains as for the first subsystem because they have the same form, and results

$$\Psi_{0,4} = \text{sigmoid}(\sigma_2) \tag{6.102a}$$

$$\Psi_{1,4} = \text{sigmoid}\left(\dot{\sigma}_2 + \beta_1 \left|\sigma_2\right|^{3/4} \Psi_{0,4}\right) \tag{6.102b}$$

$$\Psi_{2,4} = \text{sigmoid}\left(\ddot{\sigma}_2 + \beta_2 \left(\dot{\sigma}_2^4 + \left|\sigma_2\right|^3\right)^{1/6} \Psi_{1,4}\right) \tag{6.102c}$$

$$\Psi_{3,4} = \text{sigmoid}\left(\sigma_2^{(3)} + \beta_3 \left(\ddot{\sigma}_2^6 + \dot{\sigma}_2^4 + \left|\sigma_2\right|^3\right)^{1/12} \Psi_{2,4}\right) \tag{6.102d}$$

$$u_2 = -\alpha\Psi_{3,4}, \tag{6.102e}$$

with the sliding variable and its derivatives

$$\sigma_2 = x_5 - y_2^* \tag{6.103a}$$

$$\dot{\sigma}_2 = x_5 - \dot{y}_2^* \tag{6.103b}$$

$$\ddot{\sigma}_2 = -k_1 \sin(x_7) - \ddot{y}_2^* \tag{6.103c}$$

$$\sigma_2^{(3)} = -k_1 \cos(x_7)x_8 - y_2^{*(3)}. \tag{6.103d}$$

7 Observer Design and Delay Compensation

The observers to design are based on the Jacobi linearized model (5.36) and on the nonlinear model (5.9a) of the ball and plate system. The observers are categorized by the linear and nonlinear approaches, and are used to provide full state information to the controllers previously designed in section 6 .

7.1 Linear Observer Design

The structure of the linear observer has the following form:

$$\dot{\hat{\mathbf{x}}} = A\hat{\mathbf{x}} + B\mathbf{u} + L(y - C\hat{\mathbf{x}}), \;\; \hat{\mathbf{x}}_{(0)} = \hat{\mathbf{x}}_0$$
$$\mathbf{y} = C\hat{\mathbf{x}}$$

(7.1)

where $\hat{\mathbf{x}}$ are the estimated states, (A, B, C) the matrices of the Jabobi linearized system (5.36) and L the observer gain. The dynamics of the estimation error $\tilde{\mathbf{x}}$ is given by

$$\dot{\tilde{\mathbf{x}}} = (A - LC)\tilde{\mathbf{x}}$$

(7.2)

with L chosen such that $A - LC$ be Hurwitz, this implies that the estimation error converges asymptotically to zero.

The estimated states using the linear observer represent an approximation of the states near to the equilibrium point (5.34) .

7.1.1 Luenberger Observer

Luenberger observer use the pole placement method to design the observer, the observer gain L is calculated to make the observer dynamics (7.1) Λ times faster than the controlled system dynamics. For it, the real part of the observer poles must be Λ times the real part of the stable closed loop poles as follows

$$\text{Re}(\lambda\,(A - LC)) = \Lambda\,\text{Re}(\lambda\,(A - BK)),$$

(7.3)

with K the gain of the linear controller. Also, it is possible to calculate the linear observer gain from pure real poles $s_o = \{s_{o1}, s_{o2}, \ldots, s_{o8}\}$ in order to obtain the estimation error without overshoot (respect to zero) using the characteristic polynomial

$$\det(sI - (A - LC)) = (s - s_{o1})(s - s_{o2}) \ldots (s - s_{o8}) \tag{7.4a}$$

$$s_{oi} = \Lambda \operatorname{Re}(s_i), \quad i = 1, \ldots, 8 \tag{7.4b}$$

where s_i are the poles of the closed loop system. Then, the same procedure applied to the pole placement controller (6.6) is used.

Finally, the application diagram of the Luenberger observer in the closed loop system, using linear controller 6.1, is presented in Figure 7.1.
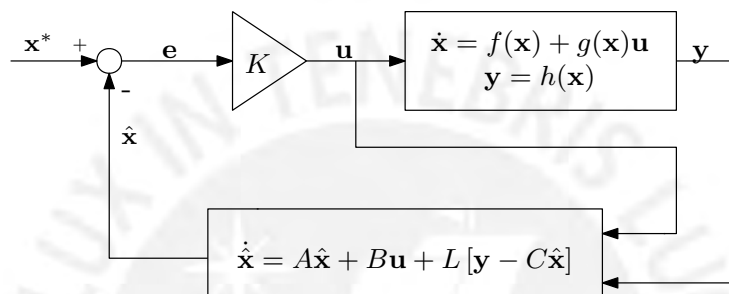

Figure 7.1: Diagram of application of the Luenberger observer in closed-loop system.

7.1.2 Kalman Bucy Filter

The Kalman Bucy filter consider the measurement noise and process disturbance to improve the pole placement observer as is explained in 2.5.1. Considering the the Jacobi linearized model (5.36) with the noises mentioned as follows

$$\dot{x} = Ax + B(\mathbf{u} + \boldsymbol{\omega}) = Ax + B\mathbf{u} + W\boldsymbol{\omega}$$
$$\mathbf{y} = Cx + \boldsymbol{\eta} \tag{7.5}$$

where $\boldsymbol{\eta}$ is the measurement noise vector zero-mean ($\bar{\boldsymbol{\eta}} = \mathbf{0}$) with covariance R, and $\boldsymbol{\omega}$ is the process disturbance vector with mean $\bar{\omega}$ covariance Q. Also, the disturbances matrix results $W = B$.

Following the procedure to design the Kalman Bucy filter explained in 2.5.1, first proceed with the calculation of the symmetric and positive definite matrices R and Q. The measurement noise vector is given by

$$\boldsymbol{\eta} = \begin{pmatrix} \eta_x & \eta_\phi & \eta_y & \eta_\theta \end{pmatrix}^\mathsf{T} \tag{7.6a}$$

with covariance matrix

$$R = E\{(\boldsymbol{\eta} - \bar{\boldsymbol{\eta}})\,(\boldsymbol{\eta} - \bar{\boldsymbol{\eta}})^\mathsf{T}\} = \begin{pmatrix} \sigma_{\eta_x}^2 & 0 & 0 & 0 \\ 0 & \sigma_{\eta_\phi}^2 & 0 & 0 \\ 0 & 0 & \sigma_{\eta_y}^2 & 0 \\ 0 & 0 & 0 & \sigma_{\eta_\theta}^2 \end{pmatrix}, \tag{7.6b}$$

where $\sigma_{\eta_x}^2$, $\sigma_{\eta_\phi}^2$, $\sigma_{\eta_y}^2$ and $\sigma_{\eta_\theta}^2$ are the variances of the measurement noises calculated from saved experimental data. Also, the process disturbance vector is given by

$$\boldsymbol{\omega} = \begin{pmatrix} \omega_1 & \omega_2 \end{pmatrix}^\mathsf{T} \tag{7.6c}$$

with covariance matrix

$$Q = E\{(\boldsymbol{\omega} - \bar{\boldsymbol{\omega}})\,(\boldsymbol{\omega} - \bar{\boldsymbol{\omega}})^\mathsf{T}\} = \begin{pmatrix} \sigma_{\omega_1}^2 & 0 \\ 0 & \sigma_{\omega_2}^2 \end{pmatrix}, \tag{7.6d}$$

where $\sigma_{\omega_1}^2$ and $\sigma_{\omega_2}^2$ are the variance of the process disturbances, also calculated from experimental data.

Using the covariance matrices calculated previously (7.6) and the matrices of the linearized model with noise and disturbance (7.5), the covariance matrix of the estimation error, S, is obtained by solving the following algebraic Riccati equation

$$AS + SA^\mathsf{T} - SC^\mathsf{T}R^{-1}CS + WQW^\mathsf{T} = 0; \tag{7.7}$$

finally, the Kalman gain is calculated as follows

$$L = SC^\mathsf{T}R^{-1}, \tag{7.8}$$

and is included in the linear observer with structure (7.1).

For practical purposes, the covariance matrix S is calculated using the command $are(A^\mathsf{T}, C^\mathsf{T}R^{-1}C, WQW^\mathsf{T})$ in Matlab.

The application diagram of the Kalman filter in the closed loop system, using the input affine representation of the plant (5.9a), is presented in Figure 7.2.
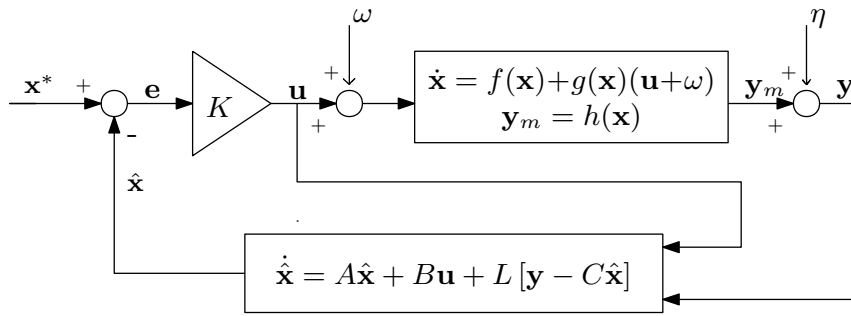
Figure 7.2: Diagram of application of the Kalman observer in closed-loop system.

7.2 Nonlinear Observer Design

The structure of the nonlinear observer, considering the nonlinear model of the system in the input-affine representation (5.9a), has the following form

$$\dot{\hat{\mathbf{x}}} = f(\hat{\mathbf{x}}) + g(\hat{\mathbf{x}})\mathbf{u} + L(\hat{\mathbf{x}})(\mathbf{y} - h(\hat{\mathbf{x}})), \tag{7.9}$$

with the time-variant observer gain L. Also, the observer gain is calculated from the linearized model around the estimated states, or from the approximate flat model (6.44) following the procedure explained in 2.5.2.

7.2.1 Nonlinear Luenberger-Like Observer

The nonlinear Luenberger-like observer considers the calculation of the observer gain L using the approximate model (6.44) in its linearized z-coordinates, and then convert the linear gain to the nonlinear coordinates using the Jacobian of the diffeomorphism as was explained in 2.5.2.

The representation of the linear observer for the approximate model in the Brunovsky form (6.52) using the Luenberger's structure is given by

$$\begin{aligned} \dot{\hat{Z}} &= A_z\hat{Z} + B_z\mathbf{v} + G(\mathbf{y} - \hat{\mathbf{y}}) \\ \hat{\mathbf{y}} &= C_z\hat{Z} \end{aligned}, \tag{7.10}$$

where G is the linear observer gain calculated using the pole placement method detailed in (7.1.1).

The linear observer (7.10) is converted to the nonlinear observer for the approximate model (6.44)

$$\dot{\hat{\mathbf{x}}} = \bar{f}(\hat{\mathbf{x}}) + \bar{g}(\hat{\mathbf{x}})\mathbf{u} + L(\hat{\mathbf{x}})\left(\mathbf{y} - h(\hat{\mathbf{x}})\right), \quad \hat{\mathbf{x}}(0) = \hat{\mathbf{x}}_0 \tag{7.11}$$

using the gain transformation through the Jacobian of the diffeomorphism (6.51)

$$
\bar{O}(\hat{\mathbf{x}}) = \frac{\mathrm{d}}{\mathrm{d}\hat{\mathbf{x}}} \begin{pmatrix} y_1(\hat{\mathbf{x}}) \\ \dot{y}_1(\hat{\mathbf{x}}) \\ \ddot{y}_1(\hat{\mathbf{x}}) \\ y_1^{(3)}(\hat{\mathbf{x}}) \\ y_2(\hat{\mathbf{x}}) \\ \dot{y}_2(\hat{\mathbf{x}}) \\ \ddot{y}_2(\hat{\mathbf{x}}) \\ y_2^{(3)}(\hat{\mathbf{x}}) \end{pmatrix} = \begin{pmatrix} 1 & 0 & 0 & 0 & 0 & 0 & 0 & 0 \\ 0 & 1 & 0 & 0 & 0 & 0 & 0 & 0 \\ 0 & 0 & k_1\cos(x_3) & 0 & 0 & 0 & 0 & 0 \\ 0 & 0 & -k_1\sin(x_3)x_4 & k_1\cos(x_3) & 0 & 0 & 0 & 0 \\ 0 & 0 & 0 & 0 & 1 & 0 & 0 & 0 \\ 0 & 0 & 0 & 0 & 0 & 1 & 0 & 0 \\ 0 & 0 & 0 & 0 & 0 & 0 & -k_1\cos(x_7) & 0 \\ 0 & 0 & 0 & 0 & 0 & 0 & k_1\sin(x_7)x_8 & -k_1\cos(x_7) \end{pmatrix},
$$

(7.12)

also called observability matrix, as follows

$$
L(\hat{\mathbf{x}}) = \bar{O}^{-1}(\hat{\mathbf{x}})G.
$$

(7.13)

Also, is important to note that in this method only the ball's position measurement is used; hence is possible to design another observer only for the angular velocities using the measured angles of the plate in order to reduce the noise in the estimated states.

7.2.2 Extended Kalman Filter (EKF)

The Extended Kalman filter consider the calculation of the observer gain using the Jacobi linearized model around the estimated states as was explained in 2.5.2.

The Jacobi linearized model around the estimated states, with noises and disturbances, is given by

$$
\begin{aligned}
\dot{\mathbf{x}} &= A_{\hat{\mathbf{x}}}\mathbf{x} + B_{\hat{\mathbf{x}}}\left(\mathbf{u} + \omega\right) = A_{\hat{\mathbf{x}}}\mathbf{x} + B_{\hat{\mathbf{x}}}\mathbf{u} + W_{\hat{\mathbf{x}}}\omega \\
\mathbf{y} &= C_{\hat{\mathbf{x}}}\mathbf{x} + \eta
\end{aligned}
$$

(7.14)

with the same measurement noise vector $\boldsymbol{\eta}$ and the process disturbance vector $\boldsymbol{\omega}$ as in (7.5). Also, the following time-variant matrices are computed, the state transition matrix is

$$A_{\hat{\mathbf{x}}} = \frac{\partial f(\mathbf{x})}{\partial \mathbf{x}}\bigg|_{\mathbf{x}=\hat{\mathbf{x}}} \tag{7.15a}$$

$$A_{\hat{\mathbf{x}}} = \begin{pmatrix} 0 & 1 & 0 & 0 & 0 & 0 & 0 & 0 \\ A_{21} & 0 & A_{23} & A_{24} & 0 & 2\bar{c}_1 \sin(\hat{x}_3)\hat{x}_8 & -\bar{c}_1 g \sin(\hat{x}_7) \sin(\hat{x}_3) & A_{28} \\ 0 & 0 & 0 & 1 & 0 & 0 & 0 & 0 \\ 0 & 0 & 0 & 0 & 0 & 0 & 0 & 0 \\ 0 & 0 & 0 & 0 & 0 & 1 & 0 & 0 \\ A_{61} & -2\bar{c}_1 \sin(\hat{x}_3)\hat{x}_8 & A_{63} & A_{64} & \bar{c}_1 \hat{x}_8^2 & 0 & -\bar{c}_1 g \cos(\hat{x}_7) & A_{68} \\ 0 & 0 & 0 & 0 & 0 & 0 & 0 & 1 \\ 0 & 0 & 0 & 0 & 0 & 0 & 0 & 0 \end{pmatrix}, \tag{7.15b}$$

where

$$A_{21} = \bar{c}_1 \left(\hat{x}_8^2 \sin^2(\hat{x}_3) + \hat{x}_4^2 \right) \tag{7.15c}$$

$$A_{24} = \bar{c}_1 \left(-\tilde{d}\hat{x}_8^2 \cos(2\hat{x}_3) + \hat{x}_1 \hat{x}_8^2 \sin(2\hat{x}_3) + 2\hat{x}_6 \hat{x}_8 \cos(\hat{x}_3) + g \cos(\hat{x}_7) \cos(\hat{x}_3) \right) \tag{7.15d}$$

$$A_{24} = 2\bar{c}_1 \hat{x}_1 \hat{x}_4 \tag{7.15e}$$

$$A_{28} = \bar{c}_1 \left(-\tilde{d}\hat{x}_8 \sin(2\hat{x}_3) + 2\hat{x}_1 \hat{x}_8 \sin^2(\hat{x}_3) + 2\hat{x}_6 \sin(\hat{x}_3) \right) \tag{7.15f}$$

$$A_{61} = -2\bar{c}_1 \hat{x}_4 \hat{x}_8 \cos(\hat{x}_3) \tag{7.15g}$$

$$A_{63} = \bar{c}_1 \left(-\bar{c}_3 \hat{x}_4 \hat{x}_8 \cos(\hat{x}_3) + 2\hat{x}_1 \hat{x}_4 \hat{x}_8 \sin(\hat{x}_3) - 2\hat{x}_2 \hat{x}_8 \cos(\hat{x}_3) \right) \tag{7.15h}$$

$$A_{64} = \bar{c}_1 \left(-\bar{c}_3 \hat{x}_8 \sin(\hat{x}_3) - 2\hat{x}_1 \hat{x}_8 \cos(\hat{x}_3) \right) \tag{7.15i}$$

$$A_{68} = \bar{c}_1 \left(-\bar{c}_3 \hat{x}_4 \sin(\hat{x}_3) - 2\hat{x}_1 \hat{x}_4 \cos(\hat{x}_3) - 2\hat{x}_2 \sin(\hat{x}_3) + 2\hat{x}_5 \hat{x}_8 \right), \tag{7.15j}$$

the input matrix is

$$B_{\hat{\mathbf{x}}} = g(\hat{\mathbf{x}}) \tag{7.15k}$$

$$B_{\hat{\mathbf{x}}} = \begin{pmatrix} 0 & 0 \\ -\bar{c}_2 & \bar{c}_1 \hat{x}_5 \sin(\hat{x}_3) \\ 0 & 0 \\ 1 & 0 \\ 0 & 0 \\ 0 & -\bar{c}_1 \hat{x}_1 \sin(\hat{x}_3) + \bar{c}_2 \cos(\hat{x}_3) \\ 0 & 0 \\ 0 & 1 \end{pmatrix}, \tag{7.15l}$$

and the output matrix $C_{\hat{x}}$ is constant and equal to C, see (5.36). Moreover, the disturbances matrix, now time-variant, results

$$W_{\hat{x}} = B_{\hat{x}}. \tag{7.15m}$$

Using the covariance matrices calculated previously (7.6) and the matrices of the linearized model about the estimated states (7.15), with noise and disturbance, the time variant covariance matrix of the estimation error, S, is obtained by solving continuously the following Riccati equation

$$A_{\hat{x}}S + SA_{\hat{x}}^{\mathsf{T}} - SC^{\mathsf{T}}R^{-1}CS + W_{\hat{x}}QW_{\hat{x}}^{\mathsf{T}} = 0; \tag{7.16}$$

finally, the time-variant Kalman gain must be calculated in real time as follows

$$L(\hat{x}) = SC^{\mathsf{T}}R^{-1}, \tag{7.17}$$

and is included in the linear observer with structure (7.9).

The application diagram of the EKF in the closed loop system, using the input affine representation of the plant (5.9a), is presented in Figure 7.3.
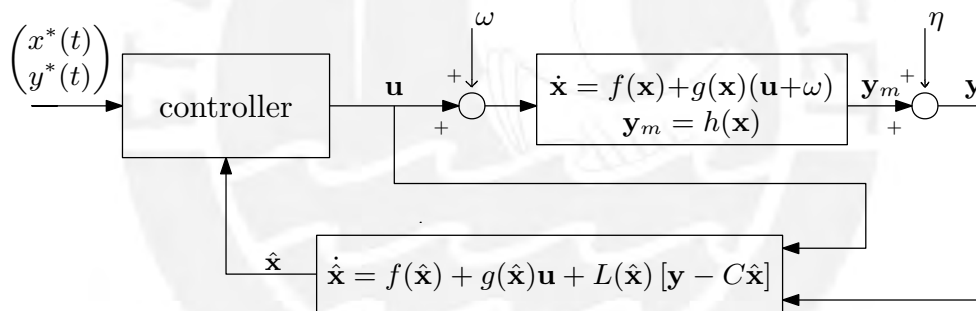

Figure 7.3: Diagram of controller and EKF observer designed for the nonlinear model.

7.3 Delay Compensation in the Measurement

The system has delay in the measurement of the ball's position, because the touch screen not has fast response.

The representation of the system with delay in the measurement of the ball's position and neglecting the delay in the measurement of the plate's angles is presented in Figure 7.4.

Also, since the ball's position is considered with the same measurement delay, the states vectors $\mathbf{X}_1 = [x, y]^{\mathsf{T}}$ and $\mathbf{X}_2 = [\phi, \theta]^{\mathsf{T}}$ are used to simplify the output representation in Figure 7.4, as is shown in **??**.

$$\mathbf{u}(t) \rightarrow \boxed{\begin{array}{c}\text{ball and plate} \\ \text{system}\end{array}} \xrightarrow{\mathbf{y}(t)} \begin{array}{l} x \boxed{e^{-s\tau}} \; x(t-\tau) \\ \varphi \qquad\quad \varphi(t) \\ y \boxed{e^{-s\tau}} \; y(t-\tau) \\ \vartheta \qquad\quad \vartheta(t) \end{array}$$
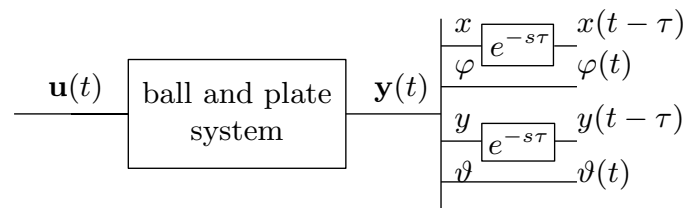
Figure 7.4: Representation of the system with delay in the sensor of ball's position.

In order to compensate the delay it is necessary to use a predictor. In the presented work the Smith predictor is used, explained in 2.6.1.

7.3.1 Delay in the measurement identification

In order to obtain the delay in the ball's position measurement an experiment is provided. In the setup of the experiment (cf. Figure 7.5) the sensor delay of the screen in the x-direction is measured. The used elements are:

- The screen, the ball and the mechanical setup.

- An array of six laser diodes/photoreceptors along the x-axis.

- A circuit of signal conditioning.

- A Desktop PC and dSPACE DS1104 Real Time system for data acquisition, saving and processing (in Matlab).
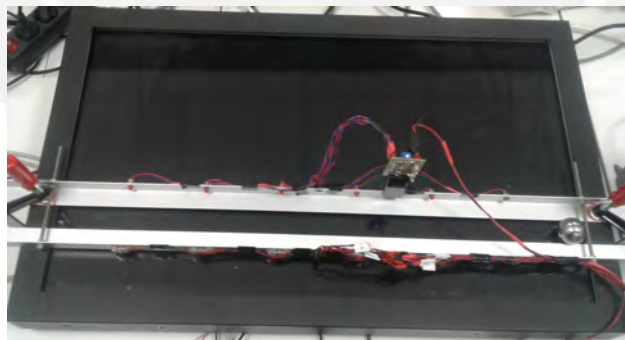
Figure 7.5: Experiment setup.

The representation scheme with the main details is presented in Figure 7.6.

The profile is used as a guidance for the movement of the ball, so that the movement is restricted only on the x-axis. Furthermore the following considerations are used:

- The laser/photoreceptor detection is faster than the screen and it is considered to be instantaneous.
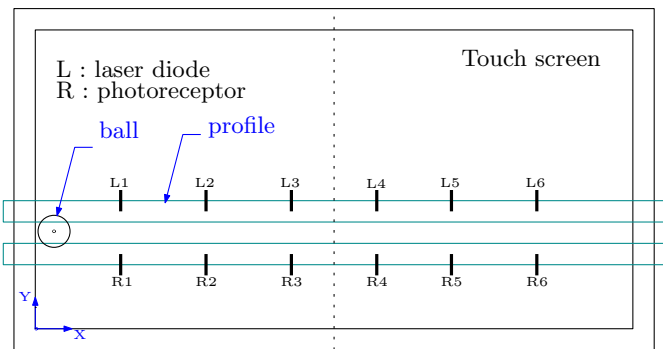
Figure 7.6: Scheme of the test setup.

- The screen has uniform properties in the surface, therefore the delay is the same in any direction of the screen.

- The delay generated for the data transmission from the circuit to the dSPACE real time system and also the error for truncation time are considered negligible.

The sampling time for data acquisition is set to 1 ms and the detection time of the ball using the laser/photoreceptor is obtained using external interrupt in the dSPACE Real Time System. The idea of this experiment is to compare the time in which a designated position is detected by the screen sensor with the time in which it is measured using laser/photoreceptor sensors.

The algorithm for calculating the delay of the touch screen is as follows:

Dynamic and Static Measurement. First, the position-time data is acquired and the corresponding position of the ball triggering the laser is evaluated with a static measurement.

The experiments were performed with movements of the ball on the screen's *x*-axis in forward and backward direction, with different ball's velocities. The experimental test in forward direction is represented in Figure 7.7.
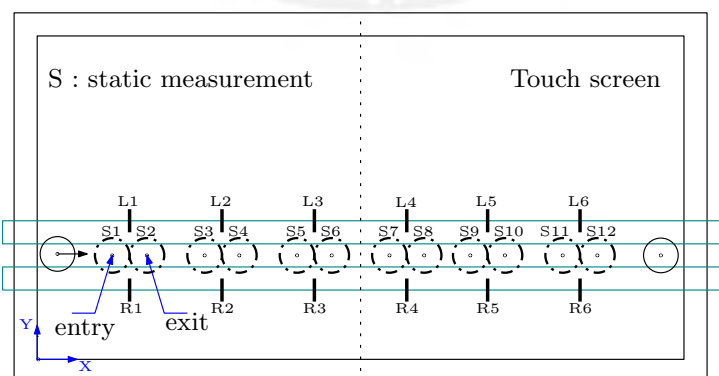

Figure 7.7: Scheme of forward movement test.

There are two static measurements of the ball's positions, for each laser/photoreceptor, that correspond to the entry and exit of the ball. The static measurement is performed manually, moving the ball until it is detected by the laser/photoreceptor entering and leaving, obtaining the corresponding position values S1-S12 on the screen. The static measurements and the ball's x-position measured by the screen are presented in Figure 7.8.
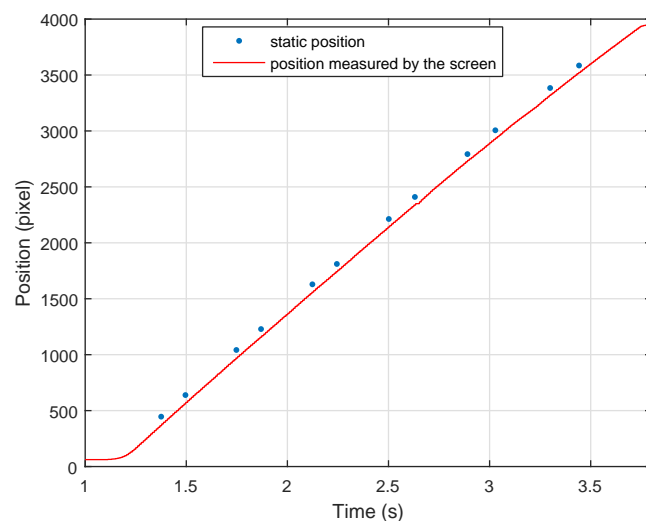

Figure 7.8: x-position of the ball in the forward movement.

The ball's x-position measurement in backward direction, which is useful to have a more precise estimation of the sensor delay, and the static measurement are presented in Figure 7.9.
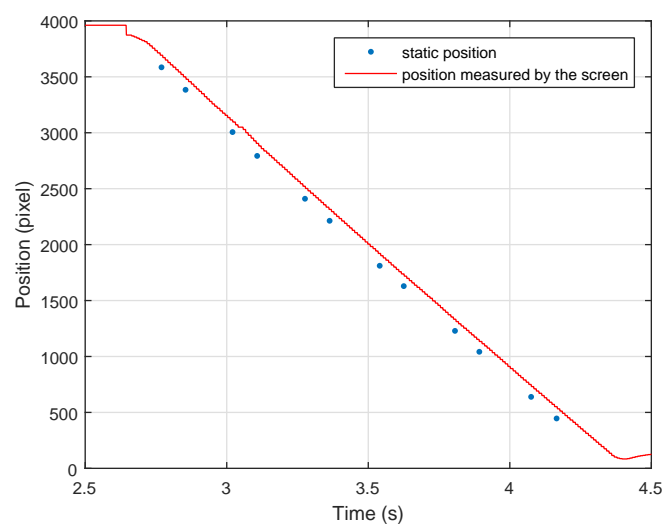

Figure 7.9: x-position of the ball in the backward movement.

Detection Time of the Lasers. From the acquired data, the detection times of the ball by the laser/photoreceptor are obtained and presented in Figure 7.10 as a vertical segment.
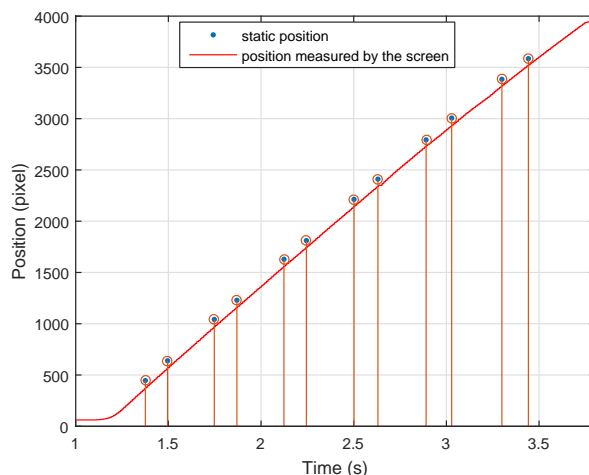
Figure 7.10: Detection times of the ball by the laser/photoreceptor.

Detection Time of the Screen Linear interpolation is used to reduce the sampling time error of the measurement data of the screen sensor. In addition, for obtaining a more accurate measurement linear interpolation between the closest discrete points is performed as shown in Figure 7.11.
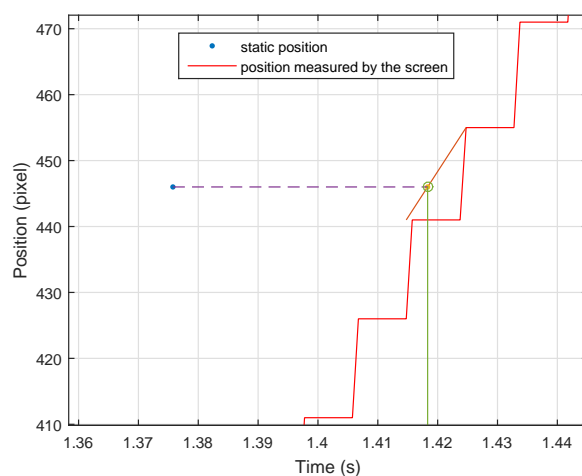

Figure 7.11: Calculation of the time to reach the static position by the screen measurement.

Calculation of the Delay. The delay of the screen is calculated by considering the difference between the trigger time of the laser and the detection time of the screen sensor. The time delay is represented graphically by the length of the dashed segment in Figure 7.11. The calculated values are listed in Table 7.1. The computation of the time difference mean between the twelve discrete points is reasonable to find an average time delay. The experiment is conducted in forward and backward direction to exclude systematic errors and increase the number of data points.

The mean of the delay value in each experiment is presented in Table 7.2. Finally, the overall estimated mean of the delay in the screen's measurement is calculated. It turns out to be $42{,}56\,\mathrm{m\,sec} \pm 1{,}87\,\mathrm{m\,sec}$.

Table 7.1: Delay estimation in the fixed positions.

Forward direction, delay in ms											
	S1	S2	S3	S4	S5	S6	S7	S8	S9	S10	S11	S12
EX1	43.66	41.66	41.99	42.36	43.66	40.49	42.66	42.99	39.49	48.74	42.99	42.99
EX2	43.18	41.99	42.61	41.99	41.78	41.49	42.09	42.26	40.58	46.78	42.52	42.44
EX3	42.56	41.33	43.33	40.71	43.28	40.56	42.42	47.49	40.07	46.76	42.53	43.45
Backward direction, delay in ms											
	S12	S11	S10	S9	S8	S7	S6	S5	S4	S3	S2	S1
EX4	40.99	42.99	42.18	41.90	41.20	43.68	42.08	42.28	43.49	45.21	41.33	40.49
EX5	41.82	42.70	42.40	42.82	41.36	46.88	42.99	42.73	43.21	37.78	41.52	41.15

Table 7.2: Mean and standard deviation of the delay estimation.

Experiment	μ_x (ms)	σ (ms)
EX1	42.80	2.24
EX2	42.47	1.50
EX3	42.87	2.29
EX4	42.31	1.33
EX5	42.28	2.05
Total	42.56	1.87

7.3.2 Smith Predictor for the Ball and Plate System

In order to compensate the delay τ , previously calculated, we proceed to design the Smith predictor using the basic conceptual framework about Smith predictor explained in 2.6.1.

Adding the Smith predictor to the diagram of the ball and plate system with delayed outputs **??** the delay compensation scheme results in Figure 7.12.

The exact model of the ball and plate system (5.9a) is used. For the Smith predictor is given by

$$\dot{\mathbf{x}}_m = f\left(\mathbf{x}_m\right) + g\left(\mathbf{x}_m\right)\mathbf{u}$$
$$\mathbf{y}_m = \mathbf{X}_{1m},$$

(7.18a)

and predicts the current output of the system $\mathbf{X}_{1m}(t)$. However, to compensate small modeling errors and noises in the output, is needed to add the correction term $\mathbf{e}_{sp}$ generated at $t - \tau$ time
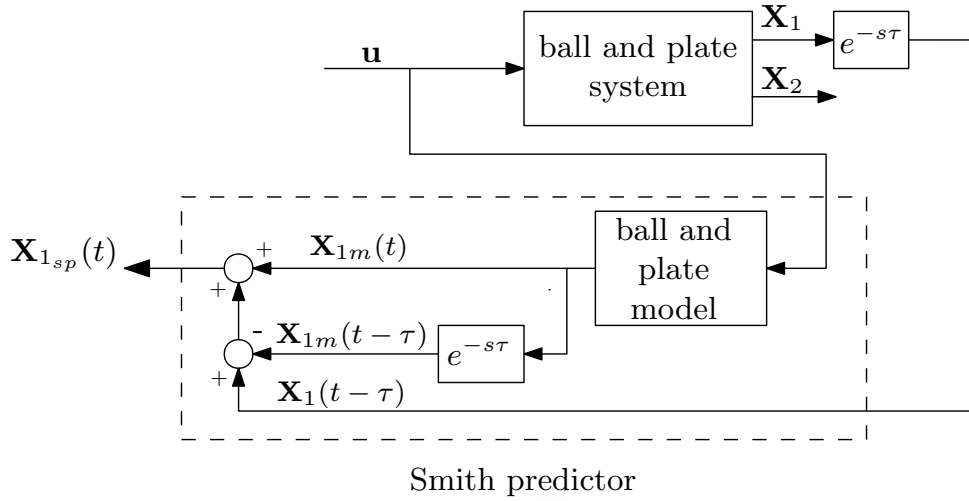
Smith predictor

Figure 7.12: Diagram of the Smith predictor in the ball and plate system with delayed output.

as follows

$$\mathbf{e}_{sp} = \mathbf{X}_1(t - \tau) - \mathbf{X}_{1m}(t - \tau) \tag{7.18b}$$

$$\mathbf{X}_{1sp}(t) = \mathbf{X}_{1m}(t) + \mathbf{e}_{sp}. \tag{7.18c}$$

It can be seen that a good model of the system and the exact value of the delay τ are required to obtain good prediction results.

However, through tests it was observed that when there are non-measurable disturbances in the entrance of the real system, as noise, the output of the real system and the model deviate, which means that correction term $\mathbf{e}_{sp}$ diverges and even more the estimated current output $\mathbf{X}_{1sp}(t)$ be not equal to the real output $\mathbf{X}_1(t)$. Therefore the solution proposed is to use the observer, previously designed, with the Smith predictor (cf. Figure 7.13), in such a way that the states of the predictor $\mathbf{x}_m$ are updated with the estimated states of the observer $\hat{\mathbf{x}}$ as follows

$$\text{Observer} \left\{ \dot{\hat{\mathbf{x}}}(t) = f(\hat{\mathbf{x}}(t)) + g(\hat{\mathbf{x}}(t))\mathbf{u}(t) + L\left(\begin{pmatrix} \mathbf{X}_{1sp}(t) \\ \mathbf{X}_2(t) \end{pmatrix} - h(\hat{\mathbf{x}}(t)) \right), \right. \tag{7.19a}$$

$$\text{Smith predictor} \begin{cases} \mathbf{x}_m(t) &= \hat{\mathbf{x}}(t) \\ \dot{\mathbf{x}}_m(t) &= f\left(\mathbf{x}_m(t)\right) + g\left(\mathbf{x}_m(t)\right)\mathbf{u}(t) \\ \mathbf{y}_m(t) &= C_m\mathbf{x}_m(t) = \mathbf{X}_{1m}(t) \\ \mathbf{X}_{1sp}(t) &= \mathbf{X}_{1m}(t) + \mathbf{X}_1(t - \tau) - \mathbf{X}_{1m}(t - \tau). \end{cases} \tag{7.19b}$$

This means that the dynamics of the Smith predictor will have a feedback component to reduce the effect of the disturbances.
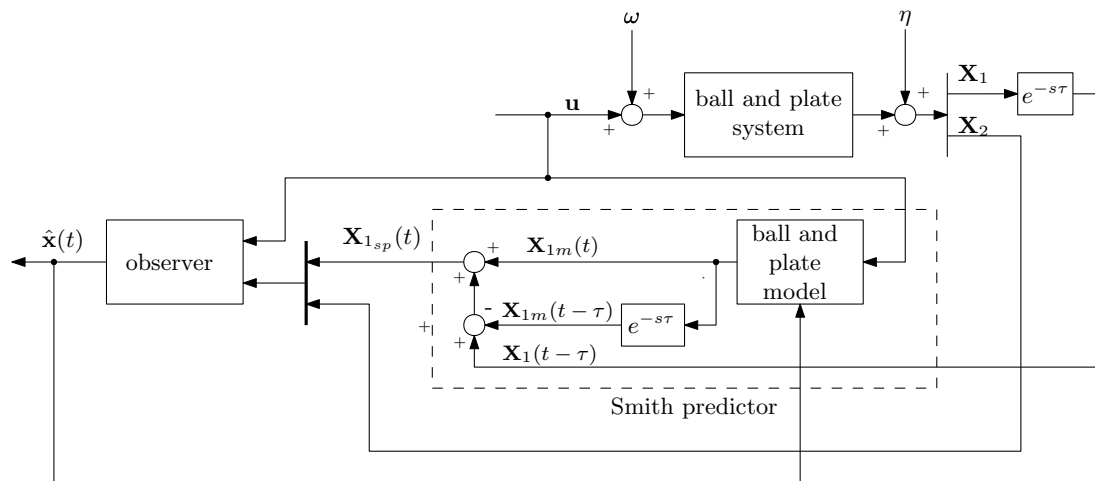
Figure 7.13: Smith predictor diagram with the observer to reduce the effect of disturbance on input of the system.

7.4 Controlled System Scheme

In order to perform simulation tests of the controlled system, the integration of the controller, observer and predictor is performed. The observer and predictor are used as a single block called observer-predictor since together they fulfill the states-feedback function in the current time to the controller. In addition, real conditions are added, such as noise and delay in the measurements, and disturbances in the input as shown in the general scheme Figure 7.14.
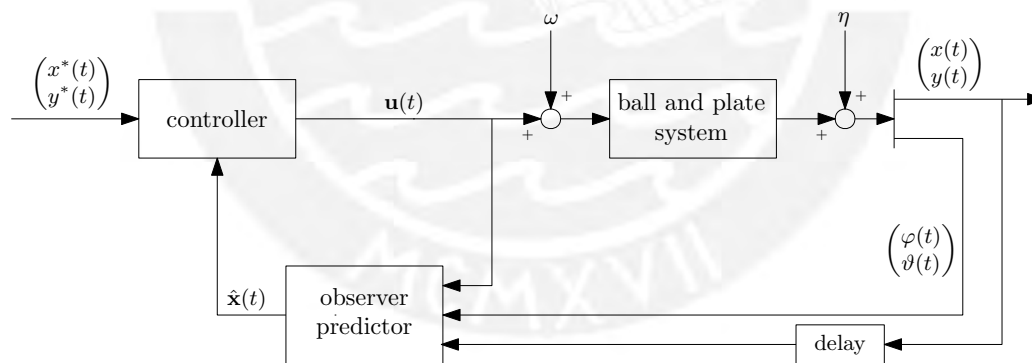

Figure 7.14: Scheme of the controlled system.

The real ball and plate system, it was explained in 4.1, consists of an inner loop of angular velocity of the motors that directly control the dynamics of the plate by means of the cams (actuation unit). On the other hand, because the reference signal to the inner loop is angular velocity, an integrator is used at the input to convert the angular acceleration signal as shown in Figure 7.15. Also, as explained in [3], the conversion between the angles or angular velocities of the plate and the motor are done by means of look up tables. All of the above is part of the extended system and is presented in Figure 7.15.
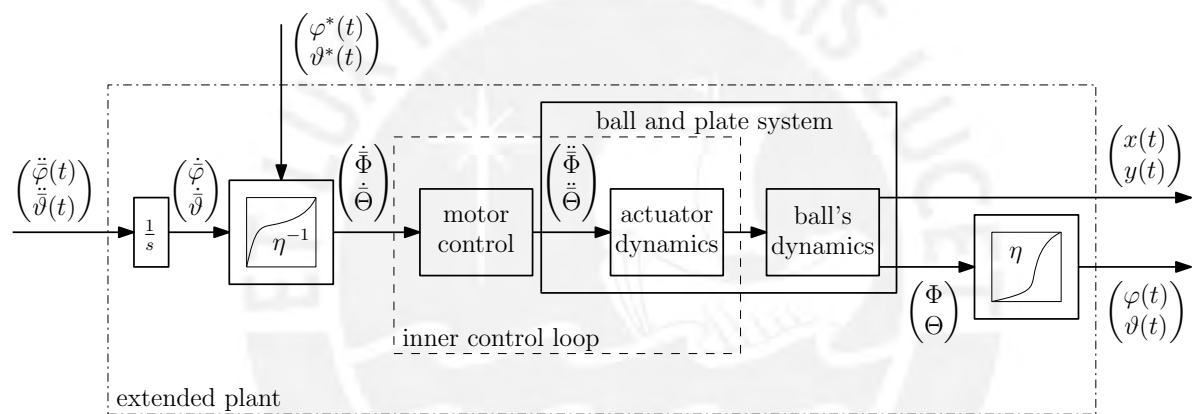
Figure 7.15: Scheme of extended plant [3].

8 Simulation Tests

The simulation tests are performed using a hollow ball with the model parameters given in Table A.2 and the physical constraints as well as the operating range presented in section 3.

First, the results will be presented for the linear controllers, see section 6.1, that only use feedback action, then the nonlinear controllers, designed 6.2, that have feedforward components in the control action will be presented. In addition, it is verified that the terms neglected to obtain the approximate model do not affect the control of the exact model. Then the comparative results of the closed-loop observer and the generation of the control action from the estimated states are presented.

Using the most suitable observer of section 7 incorporated in the closed-loop with the nonlinear controllers designed and are tested with the sensor delay. Then is compared the control results without and with compensation of the delay using the Smith predictor 7.3.2 for different frequencies of the reference trajectories.

8.1 Full State Feedback Controllers

The simulation of the designed controllers is performed assuming that all the states are measurable. Linear controllers are tested for stabilization and also a sinusoidal signal tracking test is performed to demonstrate that the feedback alone is not sufficient to track medium and high frequency trajectories. On the other hand, the nonlinear controllers are tested for the case of sinusoidal reference trajectories in both axis, using the feedforward component in their control action.

8.1.1 Stabilization Controllers

The stabilization control is performed using the control scheme presented in Figure 6.1 with references $x^* = 0.15$ m and $y^* = 0.15$ m. We consider the following performance indicators in order to be able to compare the controllers in the stabilization case: overshooting, the settling time t_{ss}, the approximate settling error during the simulation time e_{ss}, the maximum value of the control action u_{max} and the maximum value of the plate's angle φ_{max}, ϑ_{max}. It takes into account the control action and the plate's angle as performance indicators since they are

variables that represent the physical limits and determine a greater margin of safety in the operation of the system avoiding the influence of vibration.

We only compare the results regarding the $x-$axis since the behavior on the $y-$axis is very similar, however the graphs of all states of the ball and plate system are shown during the simulations.

8.1.1.1 Pole Placement

As mentioned in the design process of the pole placement controller 6.1.1, the desired poles of the closed-loop system are chosen pure real in LHP, so that it is stable and there is no overshoot; however, in order to obtain suitable poles there are infinite options. Therefore, the comparison is made in 3 cases of desired poles presented in Table 8.1 and the performance characteristics are compared. The results of the controller simulation in the presented cases are shown in Figure 8.1.

Table 8.1: Performance and results using pole placement approach.

cases	desired poles	$e_{x_{ss}}$[m]	overshoot%	t_{ss}[s]	φ_{max}[degrees]	$u_{1_{max}}$[rad/s^2]
case 1	$\{-1, -1.5, -2, -2.5\}$	$8.4e-3$	0	5.0	0.482	0.191
case 2	$\{-2, -2.5, -3.5, -4\}$	$1.29e-4$	0	3.0	1.517	1.7839
case 3	$\{-1, -2, -5, -6\}$	$3.0e-3$	0	4	1.0602	1.5291

According to the summary performance indicators Table 8.1, it can be seen that while the poles are more negative, the settling time is reduced but the control action and the plate's angles increase. However, it is proceeded to select the desired poles of case 2 since a fast response is obtained with a reasonable control action.

8.1.1.2 LQR

To determine the suitable weights for the calculation of the control action, we proceed to compare three cases presented in Table 8.2, obtaining the simulation results in the Figure 8.2. The main idea is to obtain the weights for a response with minimum overshoot, fast response and that does not require high control effort.
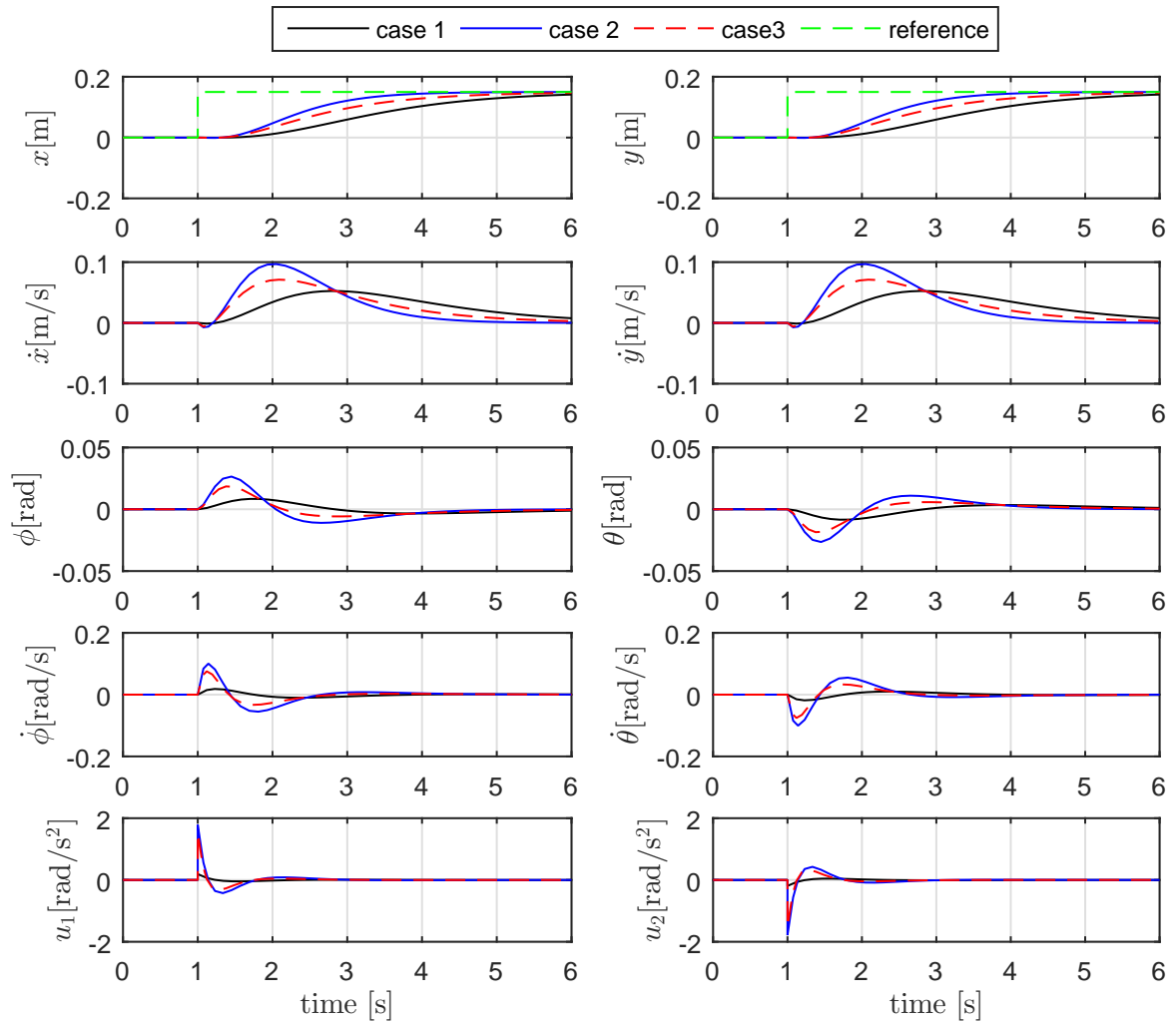
Figure 8.1: Control result using the pole placement approach.

Table 8.2: Performance summary using LQR approach for stabilization.

cases	weights	$e_{x_{ss}}$[m]	overshoot%	t_{ss}[s]	φ_{max}[degrees]	$u_{1_{max}}$[rad/s^2]
case 1	$\rho = 100$, $\kappa = 0.1$	$5.29e - 05$	2.72	3.60	1.94	1.50
case 2	$\rho = 300$, $\kappa = 0.1$	$5.16e - 05$	2.25	3.50	2.21	2.59
case 3	$\rho = 1000$, $\kappa = 0.1$	$4.87e - 05$	2.07	3.40	2.46	4.74

According to the summary of performance indicators in Table 8.2, it can be seen that while increasing the weight ρ of the state error variable, the control action increases and when the weight κ of the error in angle is increased, the required maximum plate's angle value is reduced but the response becomes slower. Therefore we choose the weights of case 2 for the design of the LQR controller as an intermediate solution.
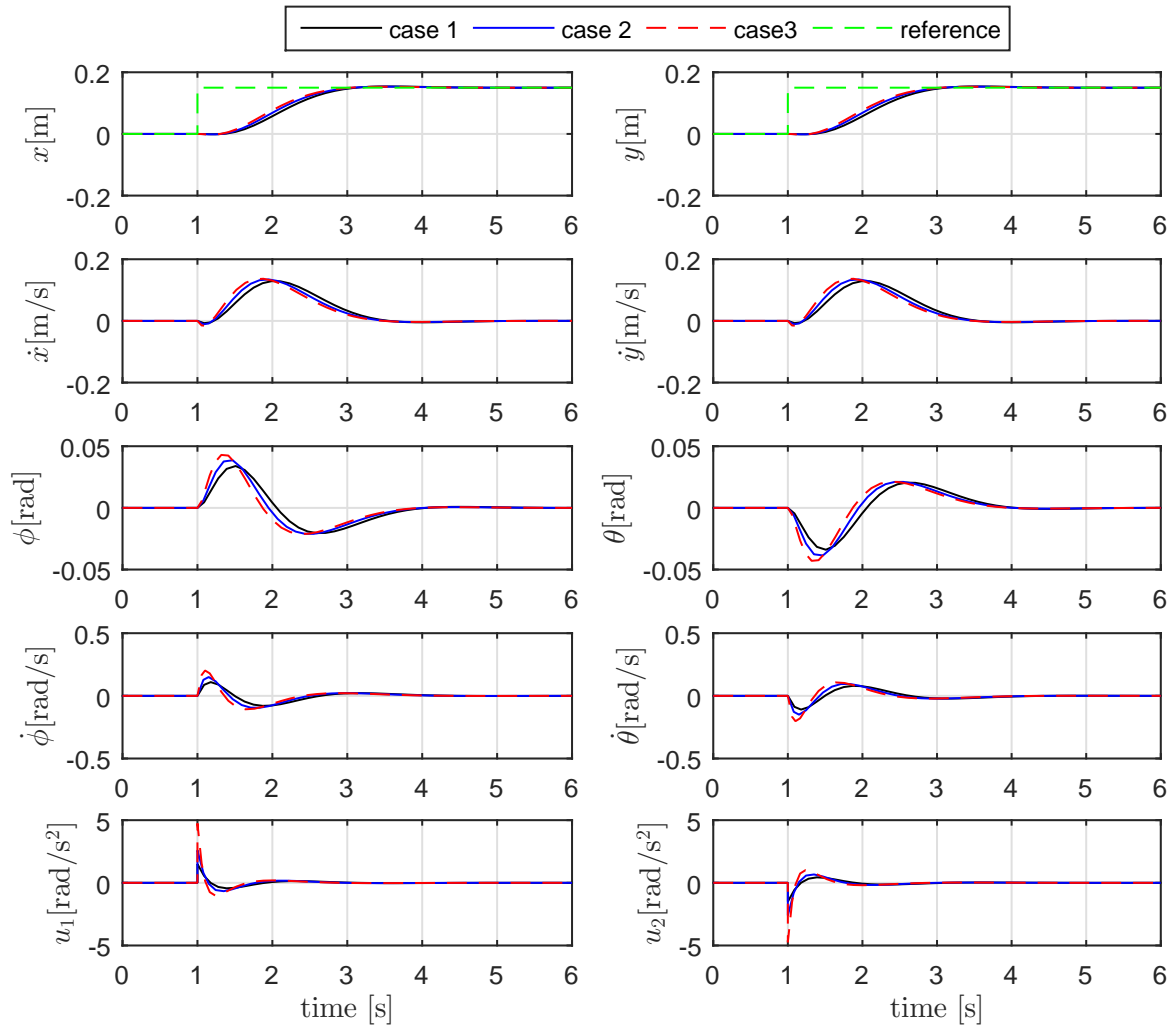
Figure 8.2: Control result using the LQR approach.

The controllers designed for stabilization can not operate well for trajectory tracking since their response is not based on the error dynamics. To verify it is proceeded to test using the LQR controller with a sinusoidal trajectory reference $\mathcal{A}\sin(\omega t)$ of three different frequencies presented in Table 8.3. In addition, this table presents the performance indicators referred to the maximum tracking error, the maximum angle and control effort required.

Table 8.3: Performance summary using LQR for tracking sinusoidal references.

frequency [rad/s]	max. steady track. error [m]	φ_{max}[degrees]	$u_{1_{max}}$[rad/s^2]
$\omega = 0.5$	0.0238	1.3382	1.4405
$\omega = 0.75$	0.0511	1.9855	2.4303
$\omega = 1$	0.0852	2.5955	3.2431

The results of the tracking errors, plate's angles and control efforts are presented in Figure 8.3.
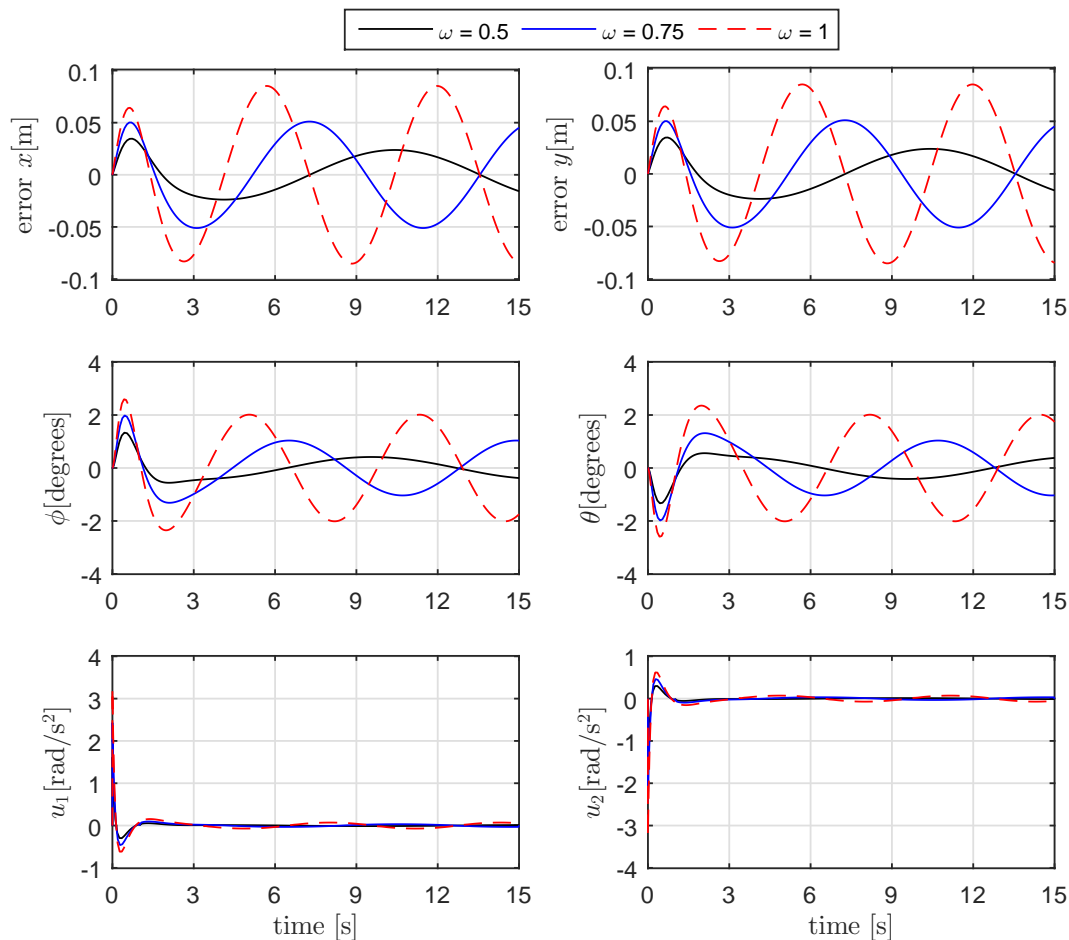

Figure 8.3: Tracking errors and control results for sinusoidal references using LQR.

As shown in Figure 8.3, the tracking error and plate angles increases when the frequency of the reference signal ω increases, in addition to also increasing the plate's angles.

8.1.2 Nonlinear Controllers

8.1.2.1 Tracking Control based on Approximate Feedback Linearization

As detailed in the controller design using feedback linearization for tracking 6.2.2, it is required to select four desired poles, the same poles per each subsystem, to stabilize the tracking error. There are three representative cases of desired pole selection in Table 8.4. In addition, the performance indicators referred to the average tracking error during the simulation time (see appendix C), the maximum angle and control effort required are presented in this table.

Table 8.4: Performance results for sinusoidal reference with $\mathcal{A} = 0.15$ m, $w = 0.5$ rad/s using tracking control based on AFL.

cases	desired poles	average error [m]	φ_{max} [degrees]	$u_{1_{max}}$ [rad/s^2]
case 1	$\{-1, -1.5, -2, -2.5\}$	0.0176	0.6064	0.2230
case 2	$\{-2, -2.5, -3.5, -4\}$	0.0076	1.2667	1.2424
case 3	$\{-3, -4, -5, -6\}$	0.0040	2.2477	4.3005

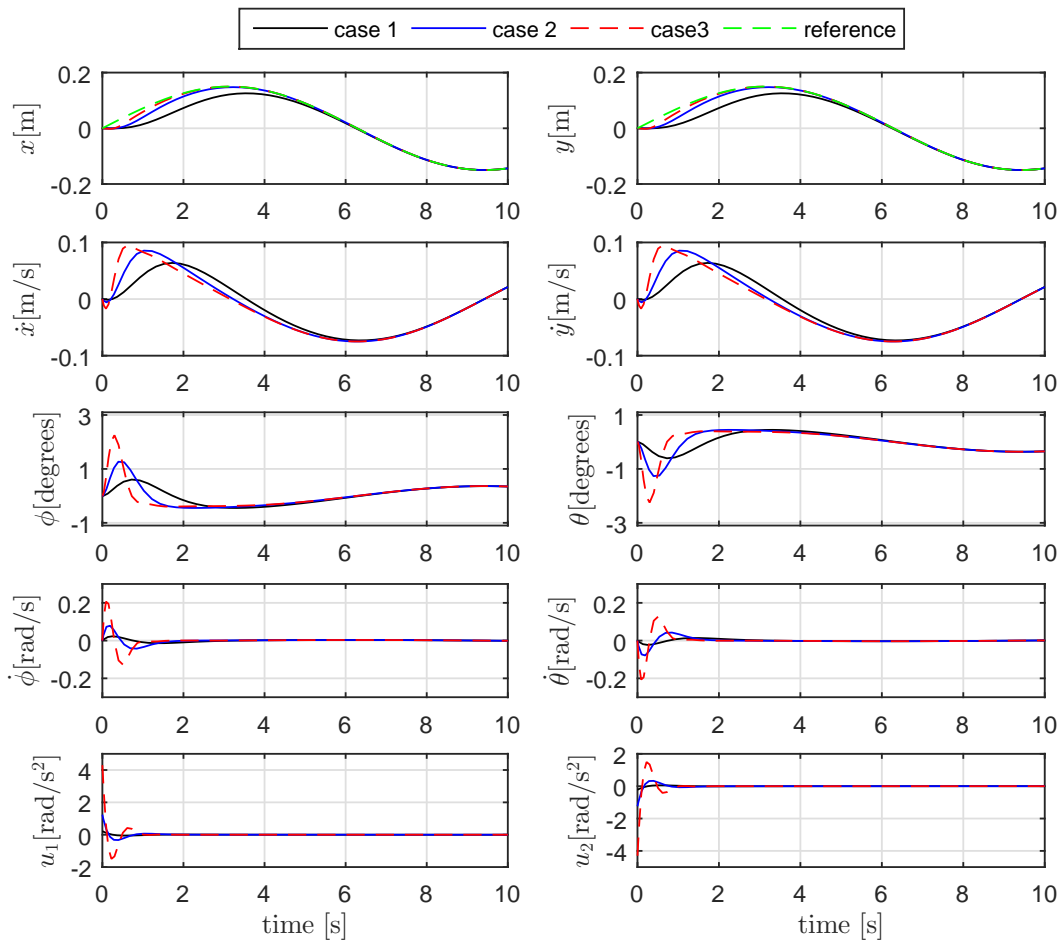The resulting states values and the control efforts are presented in Figure 8.4.

Figure 8.4: Control results using tracking control based on AFL.

It is observed that the initial control action is much greater than the control action when the reference trajectory is reached. When the reference is reached the control action is oscillating of very small value and therefore due to the scale of the graph is not appreciated.

From the results in Table 8.4, it is concluded that while the poles are more negative, the required maximum angle and control action increase considerably. Therefore, the desired poles of case 2 are chosen as an intermediate solution. Then, using these desired poles, proceed to perform tests of tracking sinusoidal signals of different frequencies presented in Table 8.5, obtaining the control results in Figure 8.5.
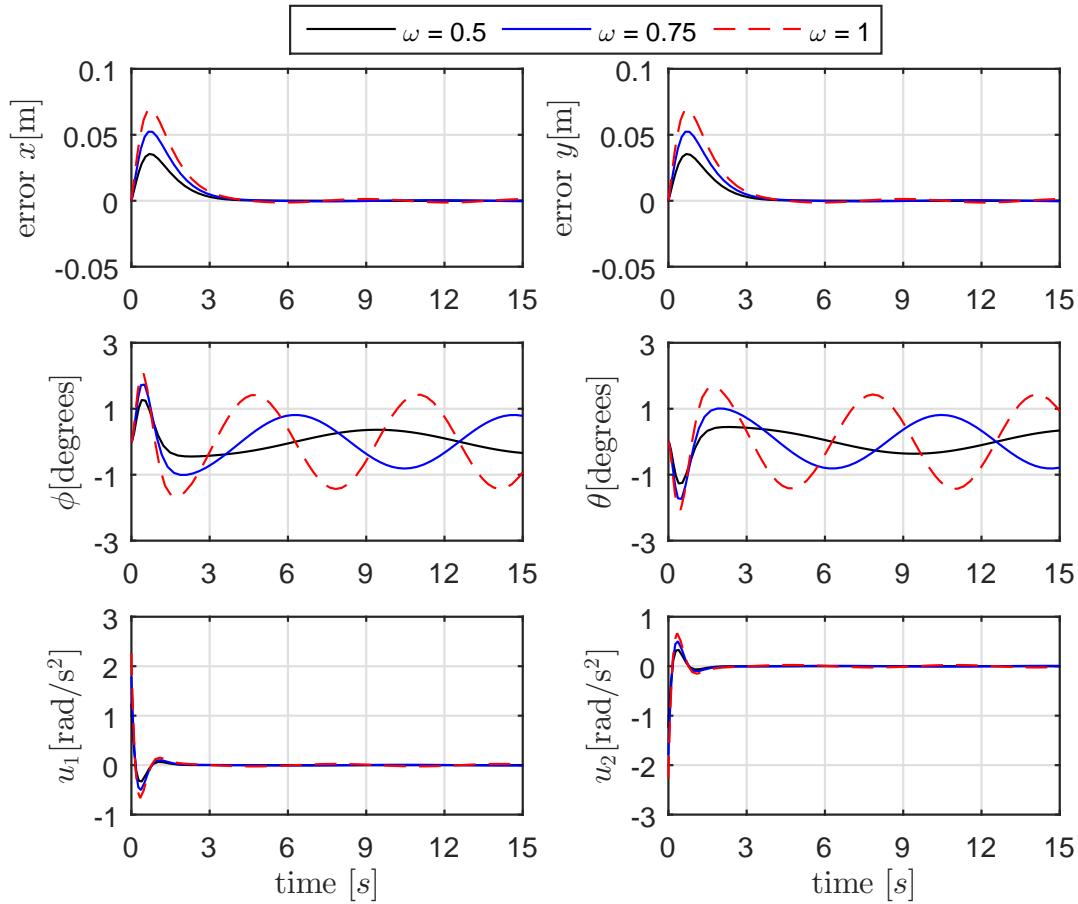

Figure 8.5: Tracking errors and control results for sinusoidal references using tracking control based on AFL.

Table 8.5: Performance summary using tracking control based on AFL for sinusoidal references of different frequencies.

frequency [rad/s]	max. steady track. error [m]	φ_{max}[degrees]	$u_{1_{max}}$[rad/s^2]
$\omega = 0.5$	$1.03e - 04$	1.2667	1.2424
$\omega = 0.75$	$4.75e - 04$	1.7337	1.7919
$\omega = 1$	$1.30e - 03$	2.0609	2.2554

In the result summary Table 8.5, it is shown that as long as the frequency of the reference signal increases, the maximum steady tracking error is increased and also requires a higher plate's angles and control efforts.

On the other hand, using the results Figure 8.5 we proceed to validate the use of the approximate model (6.44) to design the controller for the exact model (5.9a). As explained in 6.2.2, the neglected term must be much less than the main term, which according to the result in Figure 8.6 can be validated.
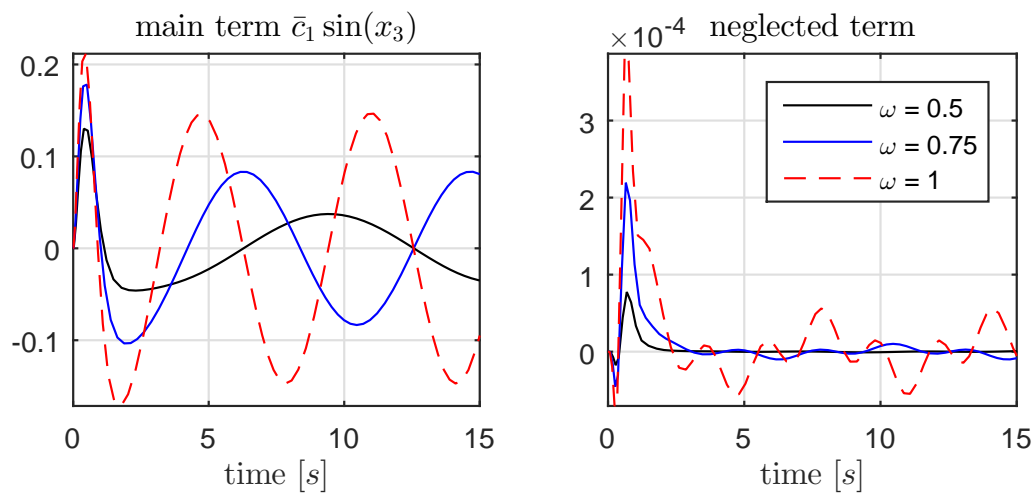

Figure 8.6: Comparison between main and neglected term to apply feedback linearization using the approximate model.

In addition it can be seen in Figure 8.6 that the maximum value of neglected terms depends on the frequency of the reference signal to track, and also on the amplitude that has not been studied because the workspace limits the amplitude. The higher the frequency and amplitude, the greater the neglected term and can make the approach of using the approximate model is not valid; however, according to the results for the considered operation range the approximation is valid.

8.1.2.2 Tracking control with Integral Action

The integral action is added with the intention of obtaining zero tracking error, so the integral of the tracking error is added in the control action. The test process is very similar to the previous tracking control case but now five poles are used as shown in the Table 8.6.

Table 8.6: Performance results for sinusoidal reference with $\mathcal{A} = 0.15\,\text{m}$, $w = 0.5\,\text{rad/s}$ using tracking control based on AFL with integral action.

cases	desired poles	average error [m]	φ_{max}[degrees]	$u_{1_{max}}$[rad/s^2]
case 1	$\{-0.5, -1, -1.5, -2, -2.5\}$	0.0136	0.8290	0.3345
case 2	$\{-1, -1.5, -2, -2.5, -3\}$	0.0082	1.3124	0.8919
case 3	$\{-2, -2.5, -3.5, -4, -5\}$	0.0035	2.8502	4.5872

The resulting states values and the control efforts are presented in Figure 8.7.
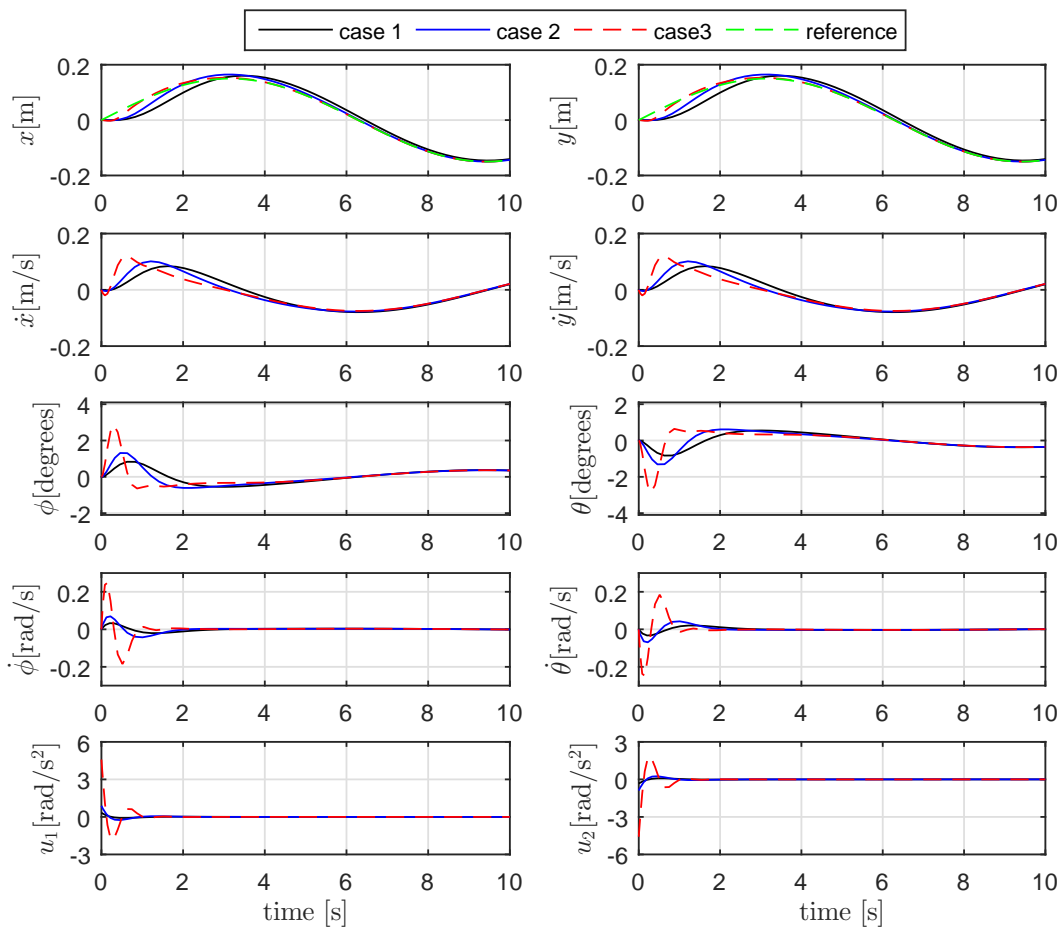

Figure 8.7: Control results using tracking control with integral action based on AFL.

From the results in Table 8.6, it is concluded that while the poles are more negative, the required maximum angle and control action is increased considerably. Therefore, the desired poles of case 2 are chosen as an intermediate solution. Then, using these desired poles, we proceed to perform tests of tracking sinusoidal signals of different frequencies presented in Table 8.7, obtaining the control results shown in Figure 8.8.
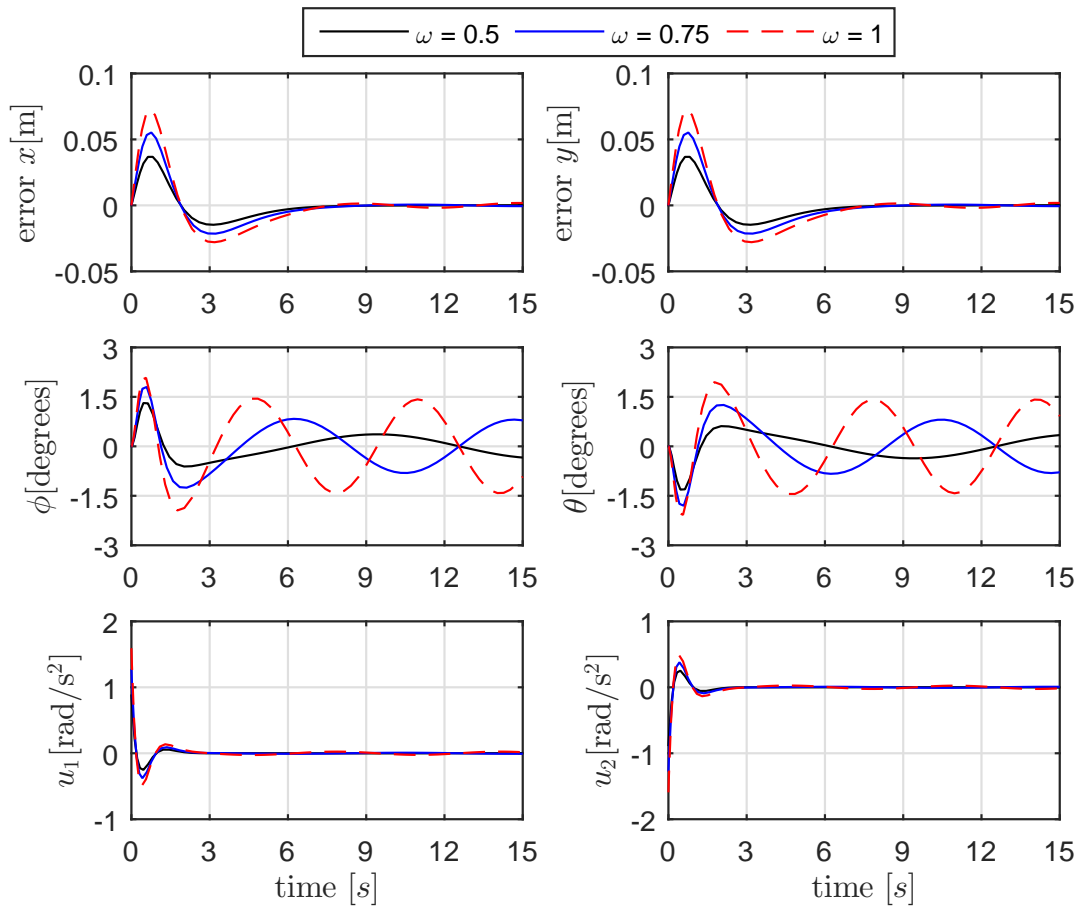
Figure 8.8: Tracking errors and control results for sinusoidal references using tracking control with integral action based on AFL.

Table 8.7: Performance summary using tracking control based on approximate feedback linearization with integral action for sinusoidal references with different frequencies.

frequency [rad/s]	max. steady track. error [m]	φ_{max}[degrees]	$u_{1_{max}}$[rad/s^2]
$\omega = 0.5$	$1.01e - 04$	1.3124	0.8919
$\omega = 0.75$	$5.88e - 04$	1.8011	1.2782
$\omega = 1$	$1.80e - 03$	2.0781	1.5928

It can be seen in the result summary Table 8.7, that as long as the frequency of the reference signal increases, the maximum steady tracking error is increased and also requires a higher plate's angles and control efforts. In addition, the results of the steady error are very similar to the case of tracking without integral action but requires less maximum value of the control efforts and plate's angles; however, a greater initial overshoot in the ball's position is required due to the integral term.

8.1.2.3 Backstepping

As was explained in 6.2.3, the backstepping control has the gains $\{c_1, c_2, c_3, c_4\}$ real positive. These gains are varied to obtain the desired performance and also stability. Because it was designed based on the approximate model (6.44), the global stability for the exact system (5.9a) is not satisfied, but only local stability. There are three representative cases of controller gain selection in Table 8.8.

Table 8.8: Performance results for sinusoidal reference with $\mathcal{A} = 0.15\,\mathrm{m}$, $w = 0.5\,\mathrm{rad/s}$ using backstepping control.

cases	controller gains	average error [m]	φ_{max}[degrees]	$u_{1_{max}}$[rad/s^2]
case 1	$\{0.1, 1, 1.5, 2\}$	0.0109	1.1104	0.5888
case 2	$\{1, 2, 2.5, 3\}$	0.0052	2.0174	1.8452
case 3	$\{1, 4, 5, 6\}$	0.0040	2.5533	4.8576

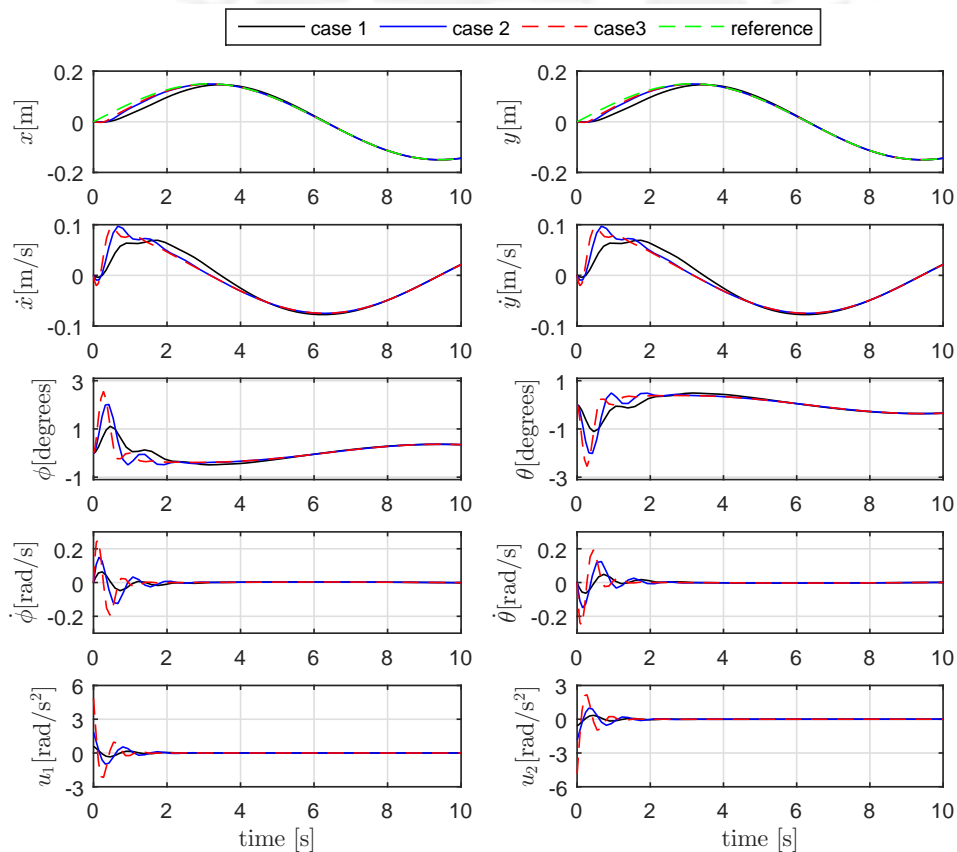The resulting states values and the control efforts are presented in Figure 8.9.

Figure 8.9: Control result using backstepping control.

From the results in Table 8.8, it is concluded that while increasing the value of the controller gains, the average tracking error is reduced but the required maximum plate's angle and control effort increase considerably. Therefore, the controller gains of the case 2 are chosen as an intermediate solution. Then, using these controller gains, proceed to perform tests of tracking sinusoidal signals of different frequencies presented in Table 8.9, obtaining the control results in Figure 8.10.

Table 8.9: Performance summary using backstepping for tracking sinusoidal references.

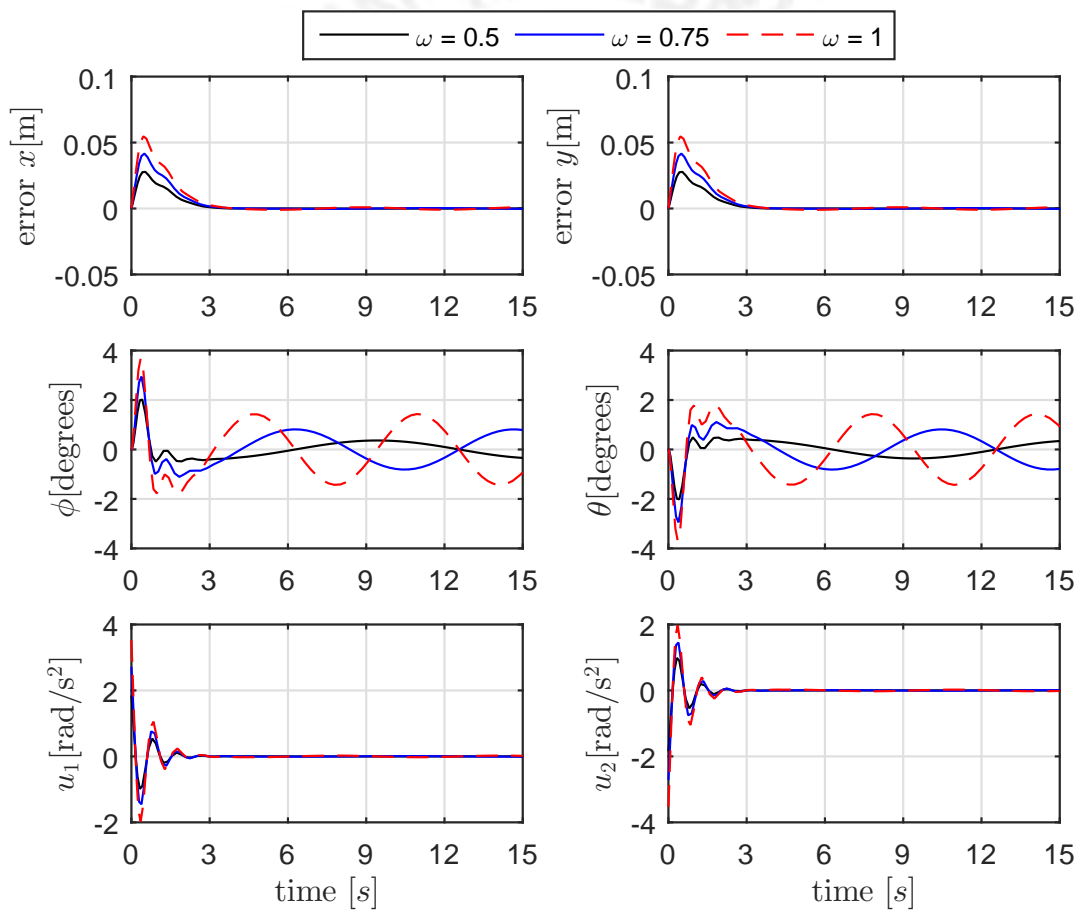| **frequency** [rad/s]	**max. steady track. error** [m]	φ_{max}[degrees]	$u_{1_{max}}$[rad/s^2]
$\omega = 0.5$	$6.6967e - 05$	2.0174	1.8452
$\omega = 0.75$	$3.1891e - 04$	2.9485	2.7170
$\omega = 1$	$9.1574e - 04$	3.6874	3.5279

Figure 8.10: Tracking errors and control results for sinusoidal references using backstepping control.

The results in Table 8.7, show that for higher frequency of the reference signal, the maximum value of the steady tracking errors increases and also requires a higher plate's angles and control efforts. In addition, the results of the steady tracking errors are slightly better than in the methods based on feedback linearization but at the cost of the highest value of the control efforts and plate's angles.

8.1.2.4 Sliding Mode Control

As explained in 6.2.4, the sliding mode controller has the gains α, $\beta_1, \beta_2, \beta_3$ with these last three of positive value. These gains are varied to obtain the desired performance and also stability. Only local stability can be expected, because the controller was designed using the approximate model. A sigmoidal function with $\varepsilon = 0.1$ is used to reduce the chattering since through tests it delivers better trade-off between performance and smoothness of the control action.

In this approach varying the gains α and β_1 does not significantly alter the performance, varying β_2 and β_3 changes the performance but when they are far away from β_1 the stability is lost. Therefore, according to the above, three representative cases of controller gains selection are presented in Table 8.10.

Table 8.10: Performance results for reference $\mathcal{A} = 0.15\,\text{m}$, $w = 0.5\,\text{rad/s}$ using sliding mode control.

cases	controller gains	average error [m]	φ_{max}[degrees]	$u_{1_{max}}$[rad/s^2]
case 1	$\{-1.5, 0.5, 1, 3\}$	0.0164	0.6327	1.2613
case 2	$\{-1.5, 0.5, 2, 3\}$	0.01162	1.2258	1.3225
case 3	$\{-1.5, 0.5, 2, 5\}$	0.0106	1.7125	1.3893

The resulting states values and the control efforts are shown in Figure 8.11. It is appreciated that for greater gain β_3 the chattering takes place and a reaching phase is presented.

From the results in Table 8.10, it is concluded that while increasing the value of the controller gains β_2 and β_3, keeping the stability of the system, the maximum required plate's angle increase considerably and control effort just a little. Using the controller gains of the second case further simulations tracking sinusoidal signals of different frequencies presented in Table 8.11 are performed, obtaining the control results in Figure 8.12.
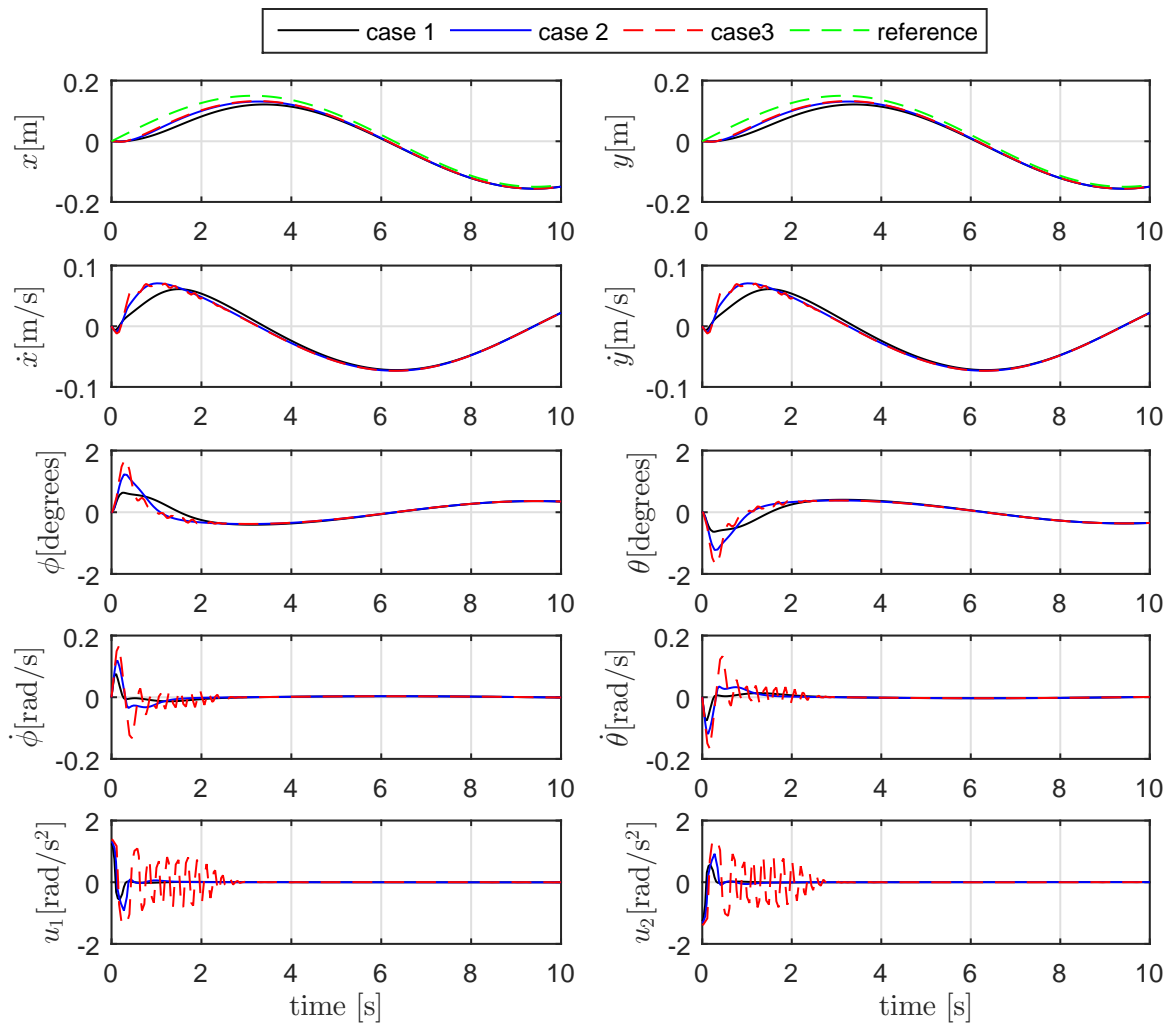
Figure 8.11: Control results using sliding mode control approach.

Table 8.11: Performance summary using sliding mode control for tracking sinusoidal references.

frequency [rad/s]	max. steady track. error [m]	φ_{max}[degrees]	$u_{1_{max}}$[rad/s^2]
$\omega = 0.5$	0.0031	0.6327	1.2613
$\omega = 0.75$	0.0052	0.9508	1.3207
$\omega = 1$	0.0053	1.4631	1.3425

The results in Table 8.11, show that while the frequency of the reference signal increases, the maximum steady tracking errors increases only slightly, but already represents a considerable error and not comparable with the previous cases; however, less maximum plate's angles are used.
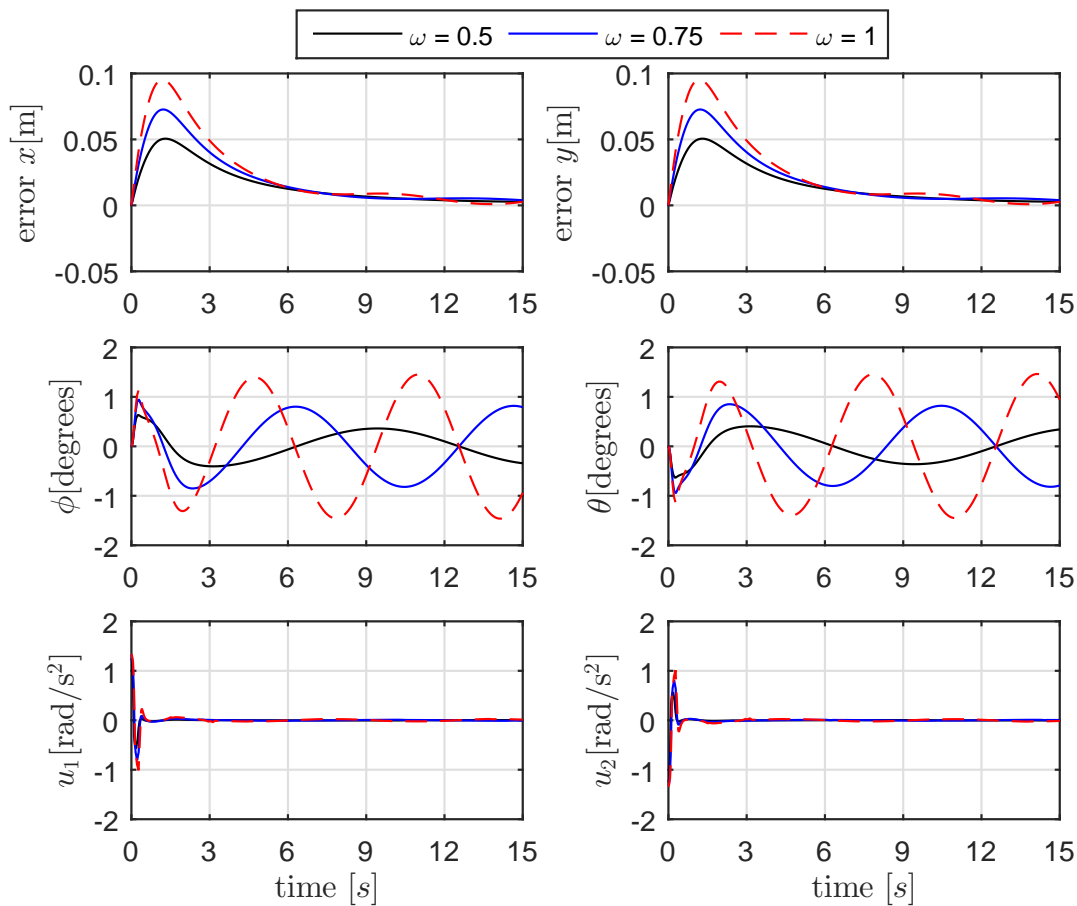
Figure 8.12: Tracking errors and control results for sinusoidal references using sliding mode control.

8.2 Observers

For the real implementation of the full-state feedback controllers presented above, it is necessary to use the state estimator operating correctly. For this, we proceed to the simulation of the linear and nonlinear observers designed in section 7, and to compare characteristics such as the estimation errors and the reduction of the noise that leads to a better generation of the control action.

The observers are applied to the nonlinear model of the system and also the delay in the measurement is not considered in this section.

8.2.1 Linear Observers

The design of the linear observer as was explained in 7.1, consists in calculating the constant gain L of the observer through the pole location method, Luenberger observer, or optimal estimation, Kalman filter, based on Jacobi's linearized model. In addition all the available measurements are used, i.e. the ball's position and plate's angles.

The Luenberger observer is designed considering the poles of the observer in such a way that they give a dynamic four times faster than the controlled system designed in 8.1.1.1, as follows

$$s_o = 4\left(-2, -2.5, -3.5, -4\right), \tag{8.1}$$

then the closed-loop state estimation test is performed, since it is the way it will operate in reality, obtaining the states shown in Figure 8.13.
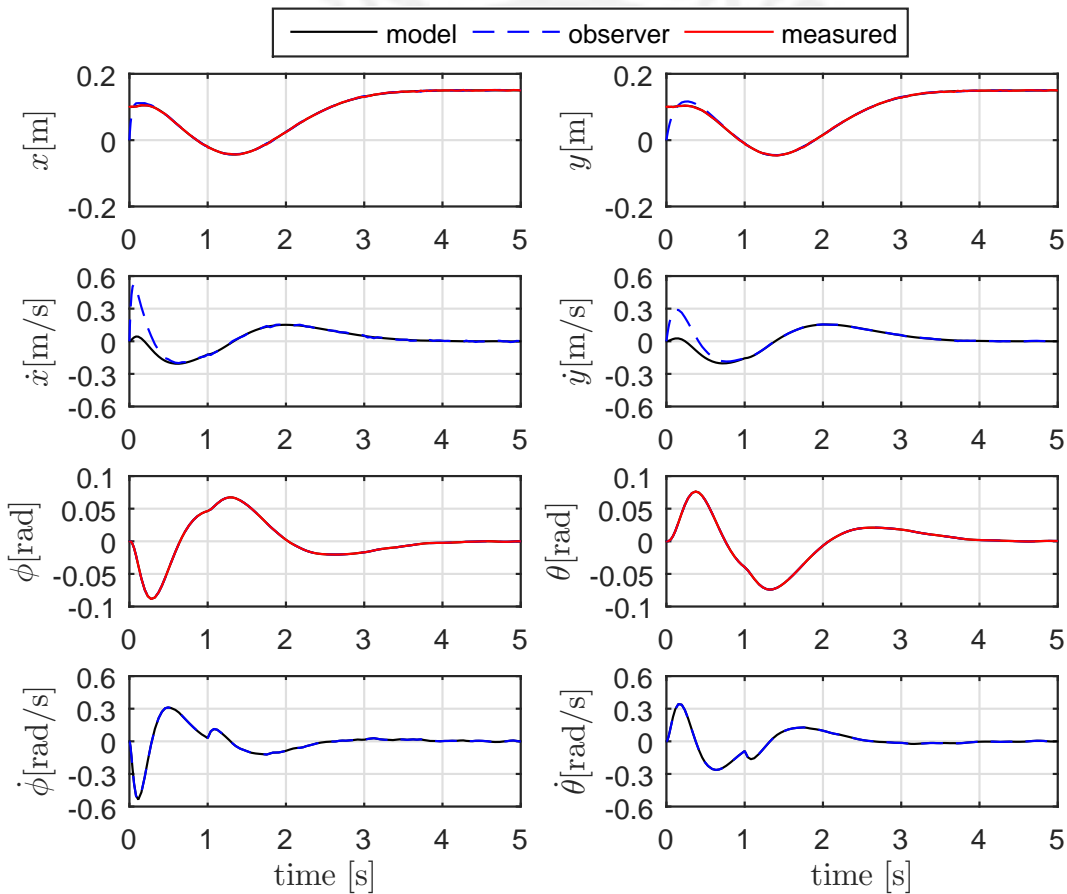
Figure 8.13: Estimates states using Luenberger observer.

Using the estimated states by the Luenberger observer and the pole placement controller 8.1.1.1, the control efforts shown in Figure 8.14 are obtained.
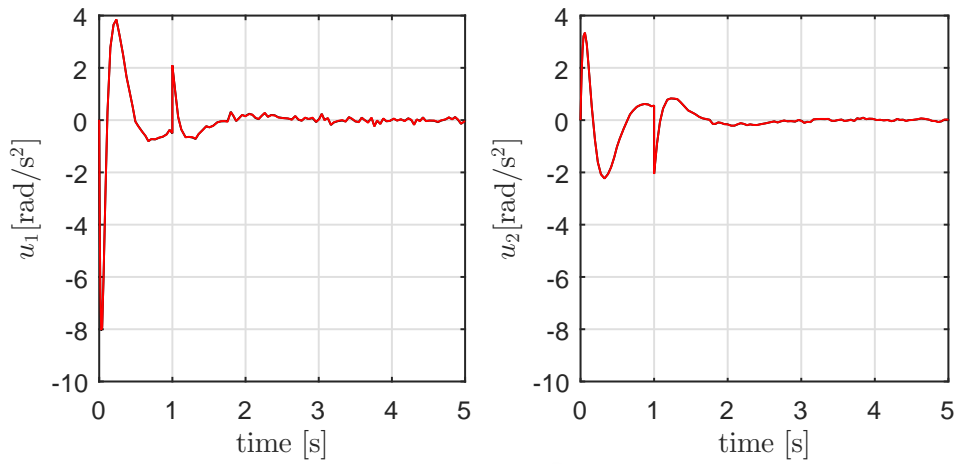
Figure 8.14: Control effort using the Luenberger observer.

The Kalman Bucy filter is designed considering the variance of the measurement noise and the process disturbances, calculated from experimental data shown in appendix B. In this way the covariance matrices Q and R, calculated as explain in 7.1.2, are

$$Q = 10^{-3} \begin{pmatrix} 0.1075 & 0 \\ 0 & 0.0277 \end{pmatrix}, \quad R = 10^{-6} \begin{pmatrix} 0.7254 & 0 & 0 & 0 \\ 0 & 0.1772 & 0 & 0 \\ 0 & 0 & 0.0002 & 0 \\ 0 & 0 & 0 & 0.0001 \end{pmatrix}, \quad (8.2)$$

and are used to obtain the observer gain L. Then applying the closed loop observation gives the states shown in Figure 8.16.
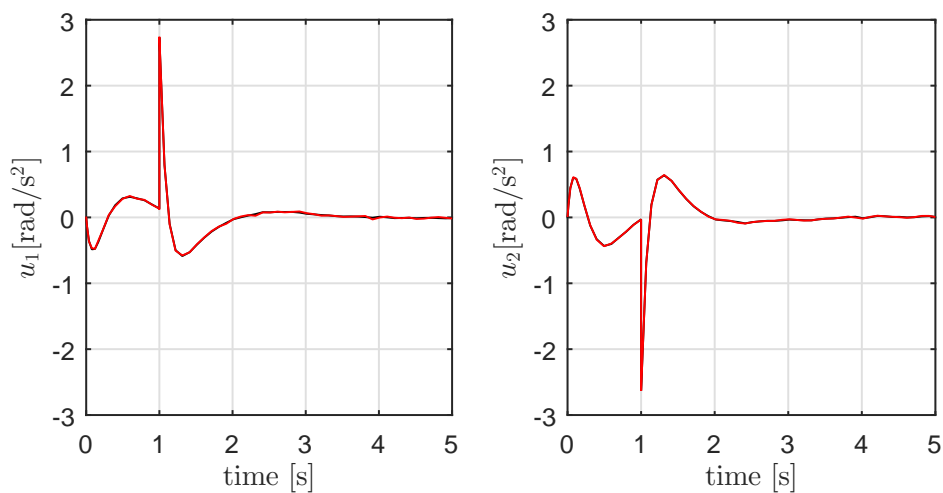

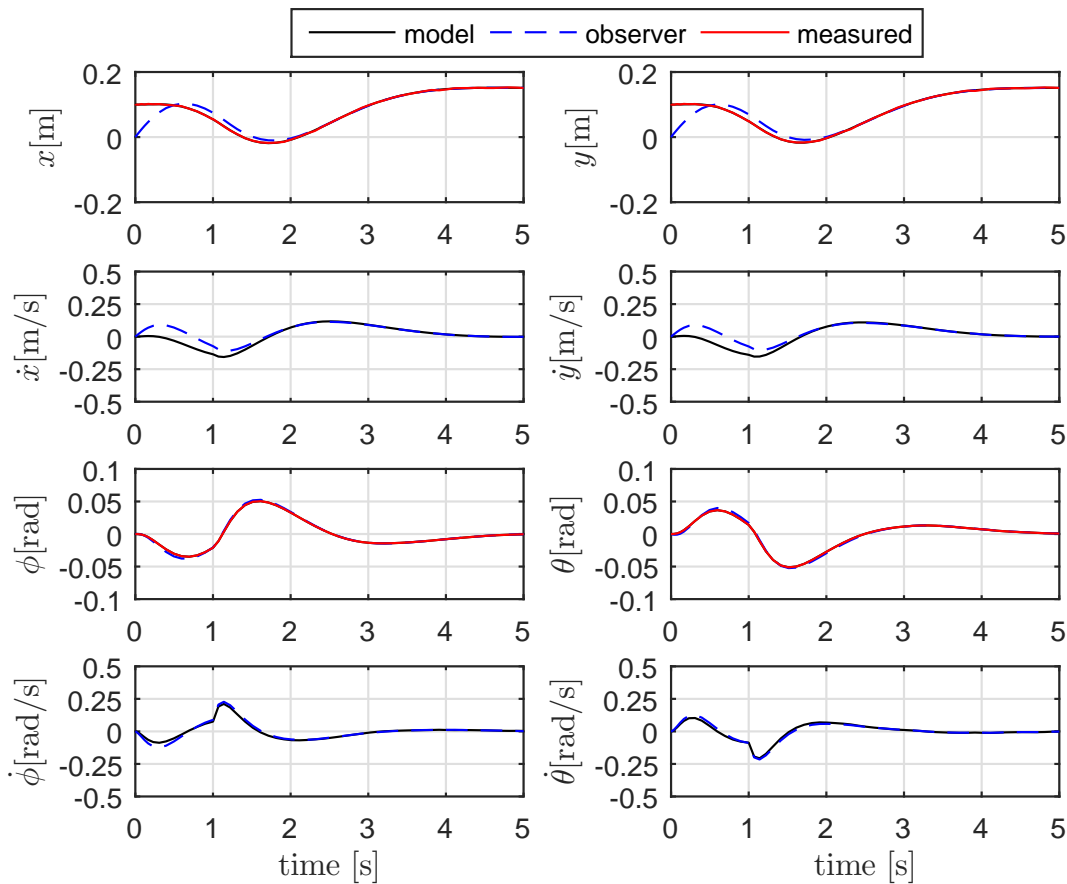Figure 8.15: Control effort using Kalman Bucy filter.

Figure 8.16: Estimates states using Kalman Bucy filter.

Using the estimated states by the Kalman Bucy filter in the calculation of the control action, also the LQR controller 8.1.1.1, the control efforts shown in Figure 8.15 are obtained.

Finally the state estimation errors (see appendix C) and the control effort are compared for both methods in Table 8.12, where it can be seen that the average estimation errors are similar but using Kalman Bucy filter the control effort is smaller and less noisy.

Table 8.12: Comparison performance of Kalman Bucy filter and Luenberger observer.

observer	$\tilde{x}_{1_{average}}$ [m]	$\tilde{x}_{2_{average}}$ [m/s]	$\tilde{x}_{3_{average}}$ [rad]	$\tilde{x}_{4_{average}}$ [rad/s]	$u_{1_{max}}$
Luenberger	$8.32e-04$	$4.60e-03$	$1.35e-05$	$6.20e-04$	8.0471
Kalman filter	$4.38e-04$	$7.34e-04$	$1.96e-04$	$1.80e-03$	2.7291

8.2.2 Nonlinear Observers

The design of the nonlinear observer, as explained in 7.2, consists of calculating the observer gain $L(\hat{x})$ through the nonlinear Luenberger-like observer or extended Kalman filter.

The nonlinear Luenberger-like observer only uses the ball's position to estimate all the states and is based on the approximate model (6.44) for the calculation of the gain $L(\hat{x})$ and structure of the observer. Applying this observer in closed loop, to a stabilization case with the LQR controller 8.1.1.2, the estimated states shown in Figure 8.17 are obtained.
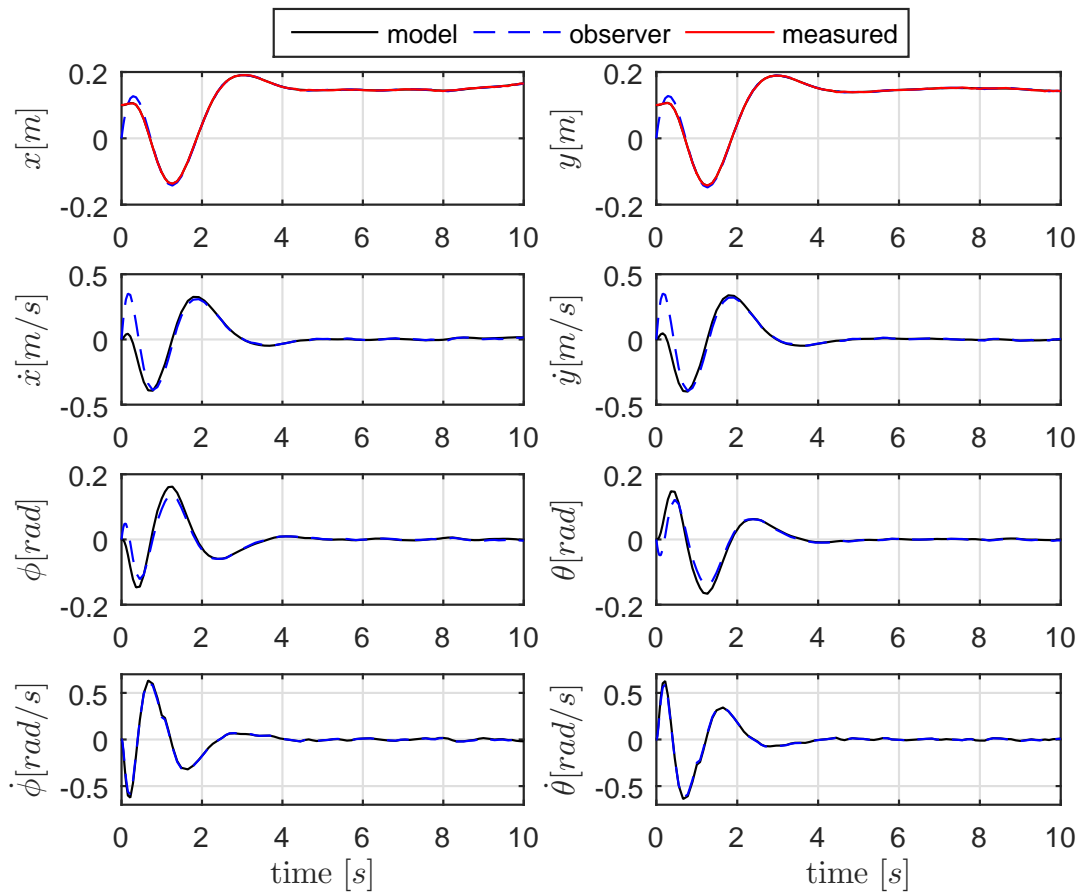

Figure 8.17: Estimated states using nonlinear Luenberger-like observer.

The control efforts calculated from the estimated states by the nonlinear Luenberger-like observer are shown in Figure 8.18.
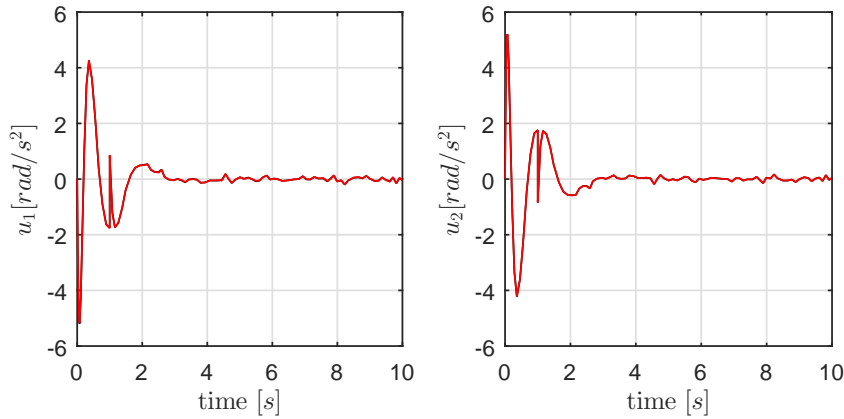
Figure 8.18: Control effort using nonlinear Luenberger-like observer.

The EKF uses all available measurements to estimate all states. The same covariance matrices are used as in the Kalman filter case (8.2) to calculate the observer gain $L(\hat{\mathbf{x}})$. This gain is variant and calculated in each Jacobi linearization of the system around the estimated states.

Applying the EKF in closed-loop, to a stabilization case with the controller LQR 8.1.1.2, the estimated states shown in Figure 8.19 are obtained.
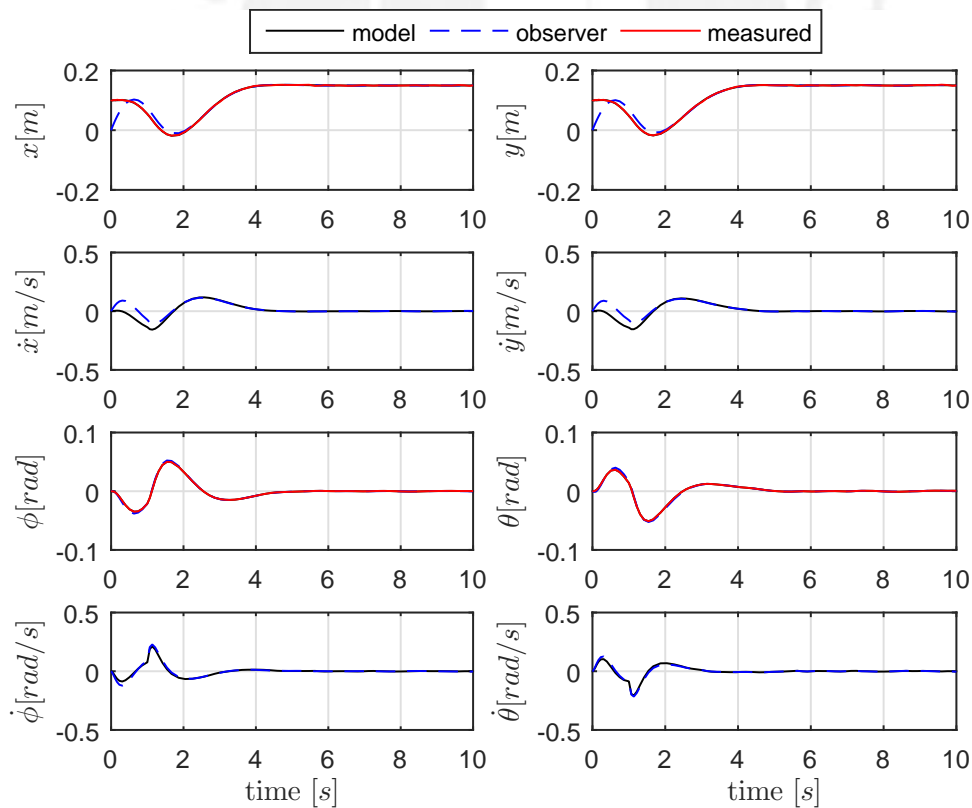

Figure 8.19: Estimates states using the EKF.

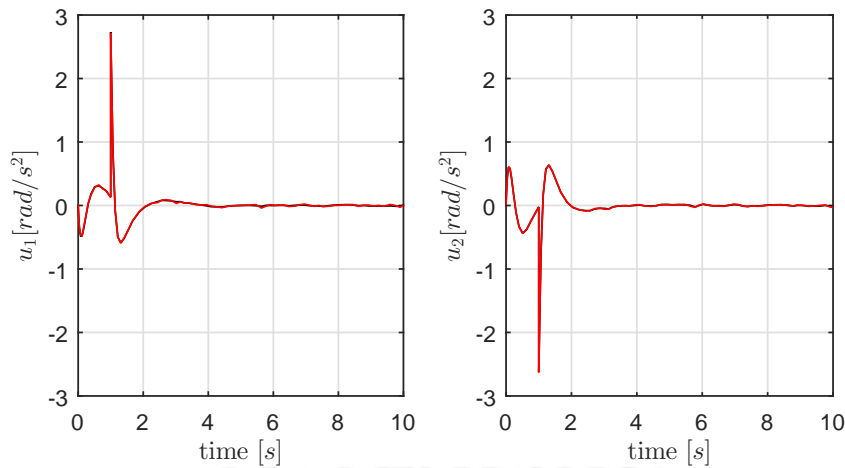The control efforts calculated from the estimated states by the EKF observer are shown in Figure 8.20.

Figure 8.20: Control effort using the EKF.

Finally the state estimation errors (see appendix C) and the generated control action are compared for both methods in Table 8.13, where it can be seen that using the EKF results much lower state estimation errors because it uses all available measurements and the exact structure of the nonlinear observer. Also the required control by the EKF is smaller. However, the nonlinear Luenberger-like observer provides acceptable results respect to the linear Luenberger observer only using the ball's position.

Table 8.13: Comparison performance between nonlinear Luenberger-like observer and EKF.

observer	$\tilde{x}_{1_{average}}$[m]	$\tilde{x}_{2_{average}}$[m/s]	$\tilde{x}_{3_{average}}$[rad]	$\tilde{x}_{4_{average}}$[rad/s]	$u_{1_{max}}$[rad/s^2]
nonlinear Luenberger	$8.06e-04$	$1.10e-02$	$4.30e-03$	0.0066	5.1962
EKF	$4.38e-04$	$7.34e-04$	$1.96e-04$	0.0018	2.7281

8.3 Tracking Control

Simulation of trajectory tracking is performed using the nonlinear controllers with feedforward component in the control action, also using the EKF to estimate the states. EKF was selected since as shown in Table 8.13 it gives better results.

The control scheme Figure 7.14 is used for the simulation, considering two main cases, in the first it is used the measurement of the ball's position with delay towards the observer and the second one considers the compensation of the measurement delay of $\tau = 42$ ms.

Tests are performed using sinusoidal reference trajectories of amplitude $\mathcal{A} = 0.15\,\text{m}$ and frequencies $\omega \in \{0.5, 0.75, 1\}$ rad/s, so that the influence of the delay on medium and high frequencies is observed. The performance indicators used are the trajectory tracking error (see appendix C), the maximum plate angles and control efforts.

8.3.1 Tracking Control based on Approximate Feedback Linearization with Extended Kalman Filter

Tracking control based on approximate feedback linearization is studied with the desired poles used in the case 2 of Table 8.4 and the estimation of states with EKF, also considering the measurement delay.

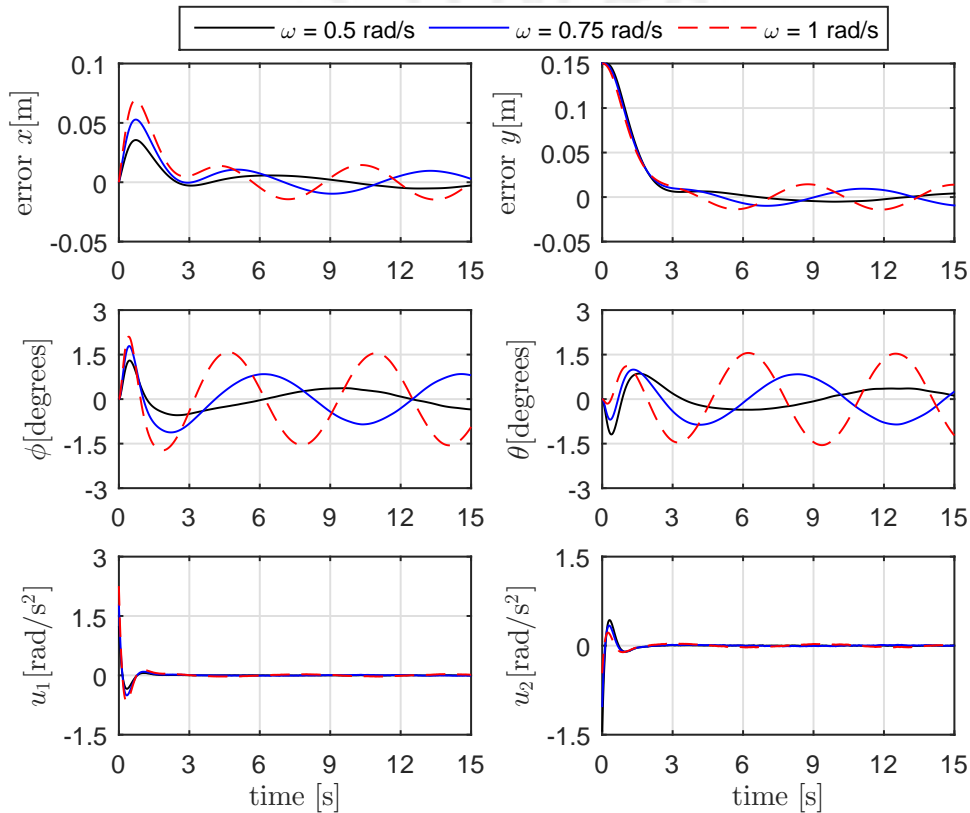The control results are shown in Figure 8.21 and summarized in Table 8.14.

Figure 8.21: Tracking errors and control results for sinusoidal references using tracking control based on AFL and EKF without delay compensation.

It can be seen in Figure 8.21 and the result summary Table 8.7, that as long as the reference signal frequency increases, the maximum steady tracking error increases more than in the case without delay in the measurement presented in 8.1.2.1.

Table 8.14: Performance summary using tracking control based on AFL with EKF for sinusoidal references.

ω [rad/s]	tracking error[%]	φ_{max}[degrees]	$u_{1_{max}}$[rad/s^2]	ϑ_{max}[degrees]	$u_{2_{max}}$[rad/s^2]
0.5	3.5381	1.3002	1.2424	1.1893	1.4494
0.75	6.4775	1.7880	1.7919	0.9945	1.0358
1	9.5683	2.1024	2.2554	1.5558	0.4651

To verify the compensation of the delay in the measurement by the Smith predictor, tracking tests are performed, obtaining the control results shown in Figure 8.22.
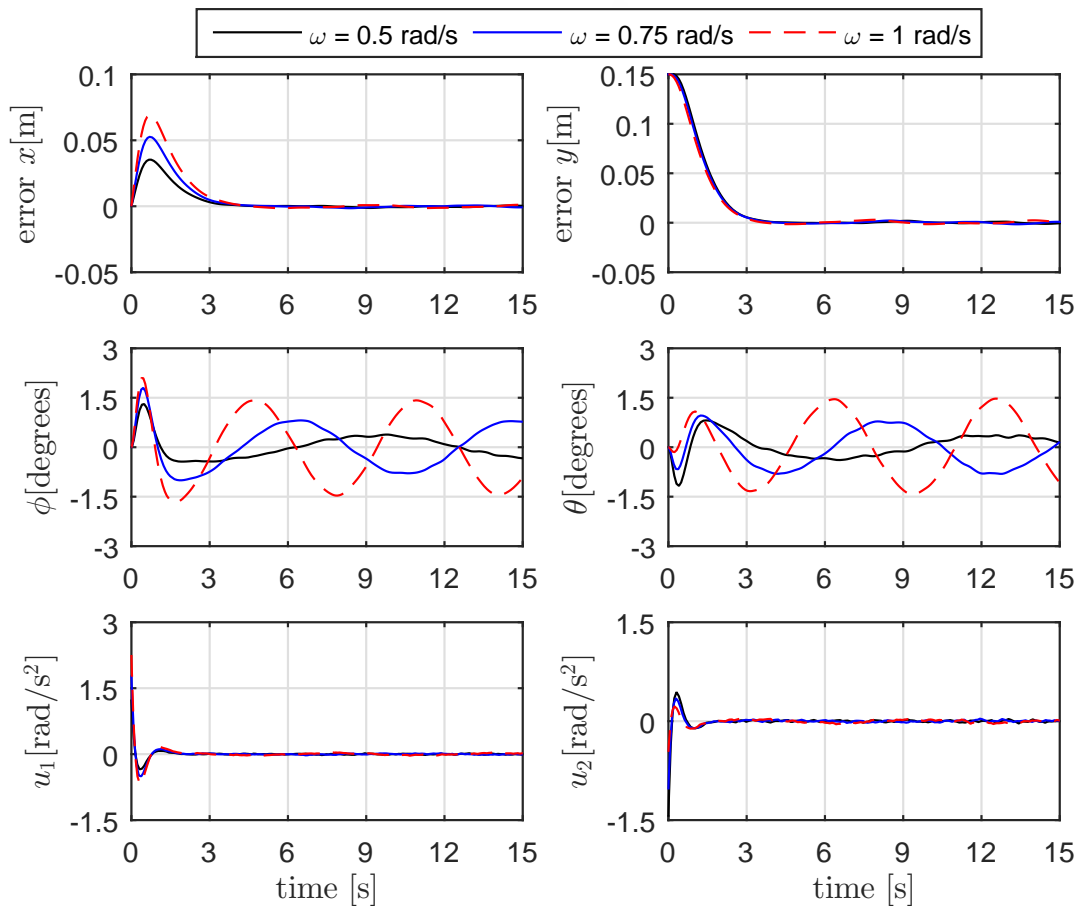

Figure 8.22: Tracking errors and control results for sinusoidal references using tracking control based on AFL, EKF and Smith predictor.

Finally, as shown in Figure 8.22 and referring to Table 8.15, the compensation of the delay in the measurement eliminates its influence even for trajectories of higher frequencies.

Table 8.15: Performance summary using tracking control base on AFL, EKF and Smith predictor for sinusoidal references.

ω [rad/s]	tracking error[%]	φ_{max}[degrees]	$u_{1_{max}}$[rad/s^2]	ϑ_{max}[degrees]	$u_{2_{max}}$[rad/s^2]
0.5	0.7529	1.3013	1.2424	1.1731	1.4494
0.75	0.8893	1.7937	1.7919	0.961	1.0358
1	0.9491	2.0599	2.2554	1.4824	0.4651

8.3.2 Tracking Control with Integral Action with Extended Kalman Filter

Tracking control based on approximate feedback linearization with integral action is studied with the desired poles used in the case 2 of Table 8.6 and the estimation of states with EKF, also considering the measurement delay.

The tests are carried out for sinusoidal reference trajectories of different frequencies presented in Table 8.16 obtaining the control results shown in Figure 8.23.
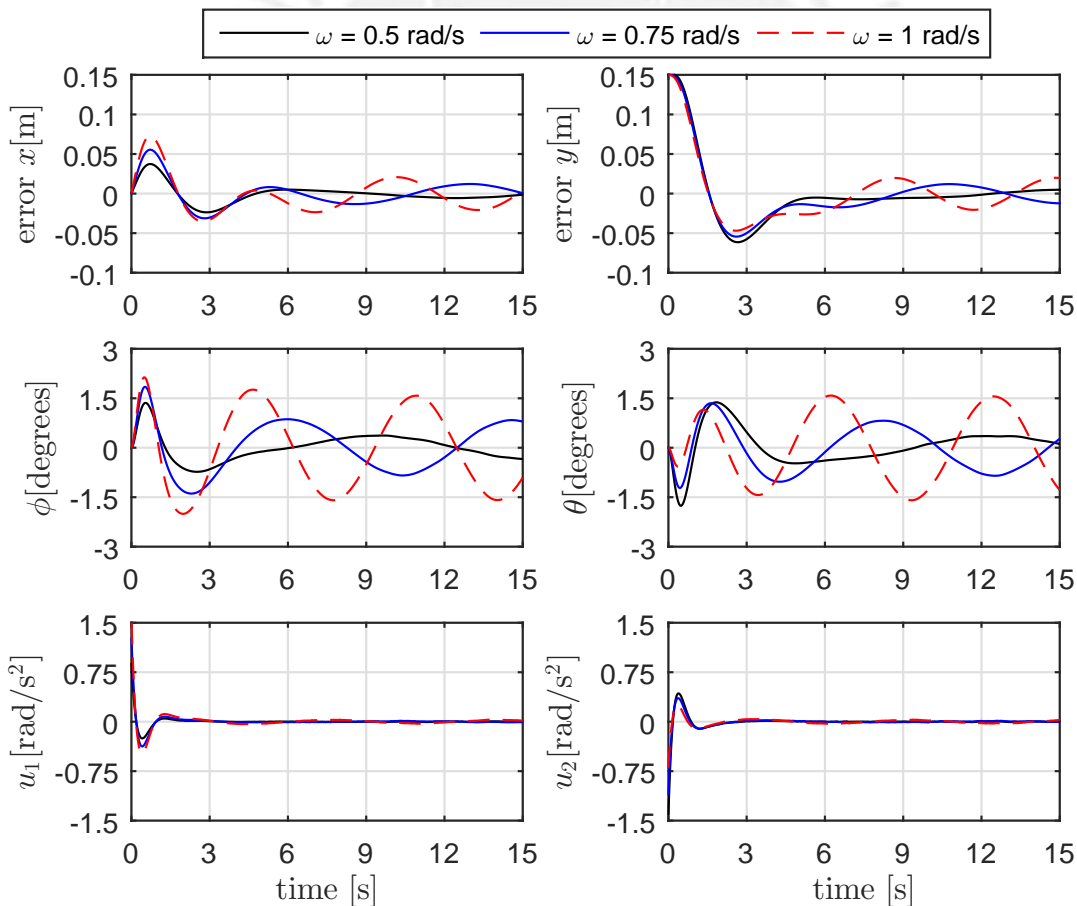

Figure 8.23: Tracking errors and control results for sinusoidal references using tracking control with integral action based on AFL and EKF without delay compensation.

It can be seen in Figure 8.23 and the result summary Table 8.16, that as long as the reference signal frequency increases, the maximum steady tracking error increases more than in the case without delay in the measurement presented in 8.1.2.2.

Table 8.16: Performance summary using tracking control with integral action based on AFL action and EKF for sinusoidal references.

ω [rad/s]	**tracking error**[%]	φ_{max}[degrees]	$u_{1_{max}}$[rad/s^2]	ϑ_{max}[degrees]	$u_{2_{max}}$[rad/s^2]
0.5	3.7548	1.3595	0.8919	1.7592	1.4176
0.75	8.1605	1.8474	1.2782	1.3499	1.1154
1	13.5785	2.1344	1.5928	1.592	0.7008

To verify the compensation of the delay in the measurement by the Smith predictor, tracking tests are performed with the same sinusoidal reference trajectories, obtaining the control results shown in Figure 8.24.
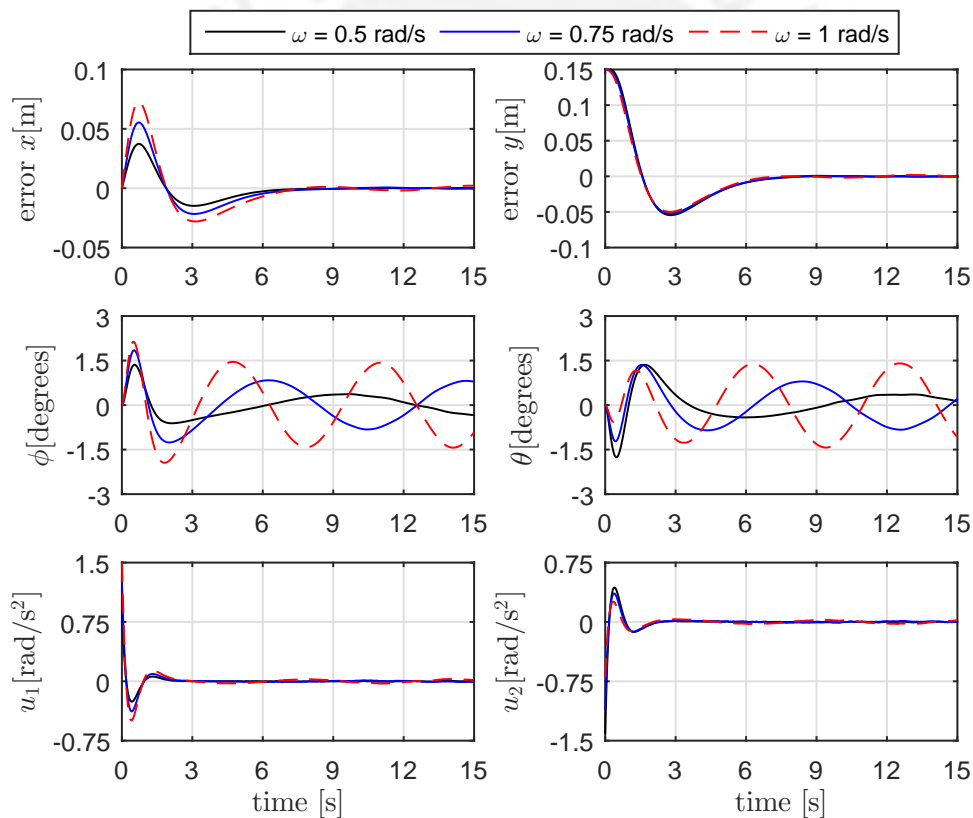

Figure 8.24: Tracking errors and control results for sinusoidal references using tracking control with integral action based on AFL, EKF and Smith predictor.

Finally, as shown in Figure 8.24 and referring to Table 8.17, the compensation of the delay in the measurement eliminates its influence even for trajectories of higher frequencies.

Table 8.17: Performance summary using tracking control with integral action based on AFL, EKF and Smith predictor for sinusoidal references.

ω [rad/s]	tracking error[%]	φ_{max}[degrees]	$u_{1_{max}}$[rad/s^2]	ϑ_{max}[degrees]	$u_{2_{max}}$[rad/s^2]
0.5	0.2722	1.3595	0.8919	1.7592	1.4176
0.75	0.548	1.8474	1.2782	1.3529	1.1154
1	1.4149	2.1346	1.5928	1.4318	0.7008

8.3.3 Backstepping Controller with Extended Kalman Filter

In the same way as in previous approaches, using the backstepping control with the controller gains used in the case 2 of Table 8.8 and the estimation of states with EKF, also considering the delay in the measurement proceed to perform tests for sinusoidal trajectories of different frequencies presented in Table 8.18 obtaining the control results in Figure 8.25.
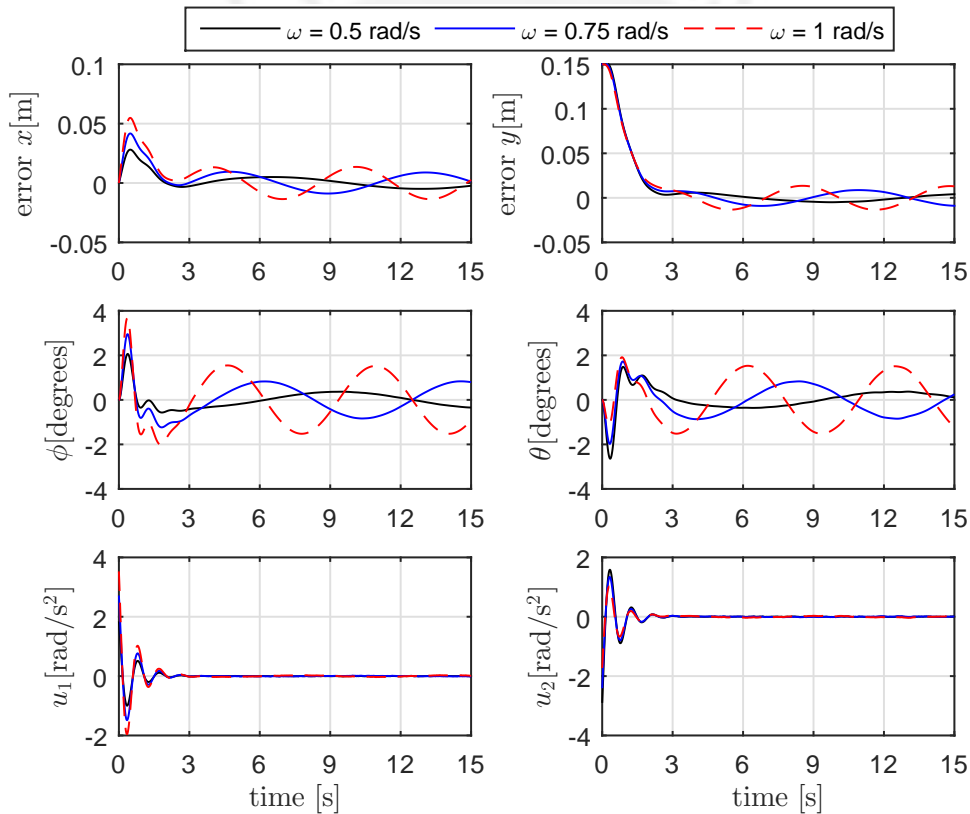

Figure 8.25: Tracking errors and control results for sinusoidal references using backstepping and EKF without delay compensation.

It can be seen in Figure 8.25 and the result summary Table 8.18, that as long as the reference signal frequency increases, the maximum steady tracking error increases more than in the case without delay in the measurement presented in 8.1.2.3.

Table 8.18: Performance summary using backstepping control and EKF for sinusoidal references.

ω [rad/s]	**tracking error**[%]	φ_{max}[degrees]	$u_{1_{max}}$[rad/s^2]	ϑ_{max}[degrees]	$u_{2_{max}}$[rad/s^2]
0.5	3.3052	2.0635	1.8452	2.6421	2.901
0.75	5.9395	2.9514	2.7170	1.9761	2.4086
1	8.9694	3.6775	3.5279	1.9139	1.7276

To verify the compensation of the delay in the measurement by the Smith predictor, tracking tests are performed with the same sinusoidal reference trajectories, obtaining the control results shown in Figure 8.26.
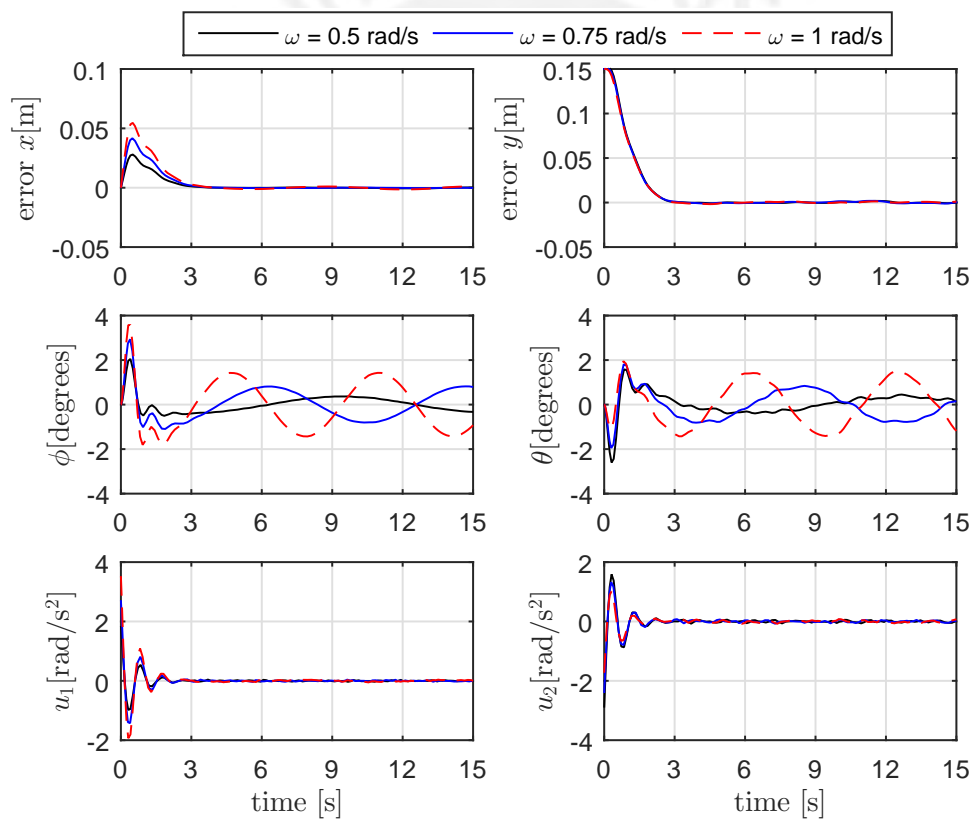

Figure 8.26: Tracking sinusoidal references with delayed output measurement using approximate backstepping controller, EKF and Smith predictor.

Finally, as shown in Figure 8.26 and referring to Table 8.19, the compensation of the delay in the measurement eliminates its influence even for trajectories of higher frequencies.

Table 8.19: Performance summary using backstepping control, EKF and Smith predictor for sinusoidal references.

ω [rad/s]	tracking error[%]	φ_{max}[degrees]	$u_{1_{max}}$[rad/s^2]	ϑ_{max}[degrees]	$u_{2_{max}}$[rad/s^2]
0.5	0.464	2.0507	1.8452	2.6023	2.901
0.75	0.4779	2.9374	2.7170	1.9495	2.4086
1	0.7934	3.5752	3.5279	1.9485	1.7276

8.3.4 Sliding Mode Control with Extended Kalman Filter

In the same way as in previous approaches, the sliding mode control is studied with the controller gains used in the case 2 of Table 8.10 and the estimation of states with EKF, also considering the delay in the measurement.

The control results are shown in Figure 8.27 and summarized in Table 8.20.
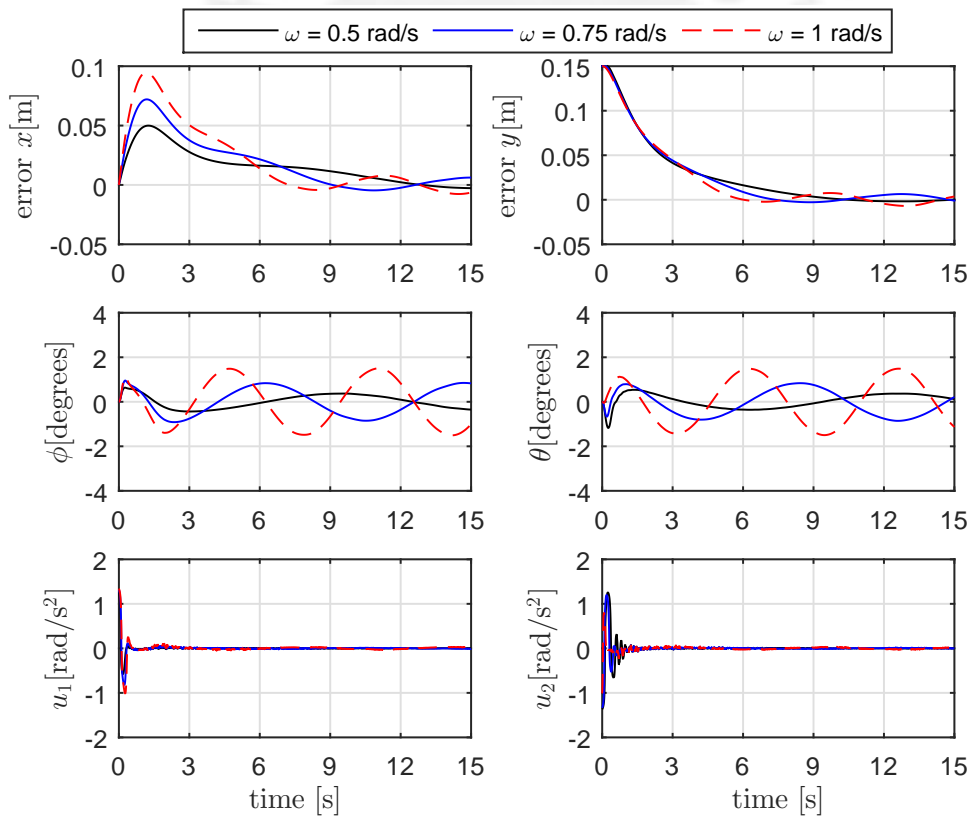

Figure 8.27: Tracking sinusoidal references with delayed output measurement using sliding mode control and EKF

It can be seen in Figure 8.27 and the result summary Table 8.20, that as long as the reference signal frequency increases, the tracking error increases more than in the case without delay in the measurement presented in 8.1.2.4, but not significantly as in the other approaches.

Table 8.20: Performance summary using sliding mode control and EKF for sinusoidal references.

ω [rad/s]	tracking error[%]	φ_{max}[degrees]	$u_{1_{max}}$[rad/s^2]	ϑ_{max}[degrees]	$u_{2_{max}}$[rad/s^2]
0.5	2.8149	0.6348	1.2613	1.1738	1.3681
0.75	4.1877	0.9535	1.3207	0.8558	1.3368
1	4.7941	1.5100	1.3425	1.4975	1.0129

To verify the compensation of the delay in the measurement by the Smith predictor, tracking tests are performed, obtaining the control results shown in Figure 8.28.
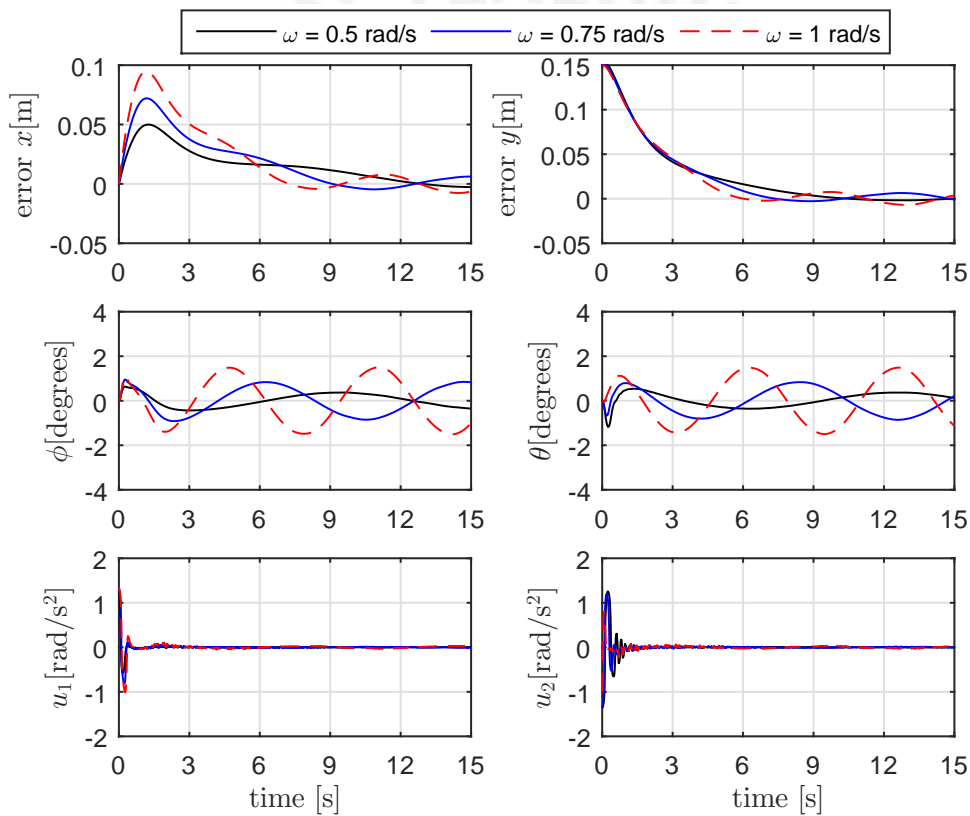

Figure 8.28: Tracking sinusoidal references with delayed output measurement using sliding mode control, EKF and Smith predictor.

Finally, as shown in Figure 8.28 and referring to Table 8.21, the compensation of the delay in the measurement eliminates its influence even for trajectories of higher frequencies.

Table 8.21: Performance summary using sliding mode control, EKF and Smith predictor for tracking references.

ω [rad/s]	tracking error[%]	φ_{max}[degrees]	$u_{1_{max}}$[rad/s^2]	ϑ_{max}[degrees]	$u_{2_{max}}$[rad/s^2]
0.5	3.9101	0.6361	1.2613	1.1687	1.3681
0.75	4.1695	0.9582	1.3207	0.826	1.3368
1	4.5401	1.4720	1.3425	1.4653	1.0129

9 Experimental Tests

Experimental tests are performed using the software ControlDesk v5.1 with the DS1104 RD controller board, presented in 3.1.4, configured with sample time of 2 ms and implementing the control scheme presented in Figure 7.14. In addition, the components presented in the extended plant shown in Figure 7.15 are added.

First, the validation of the mathematical model and the observer is performed. The performance of the Luenberger observer result better, in the experimental tests, than the others studied with respect to their greater speed of convergence and good estimation of the states. This is justified since the variance of the noises of measurement and input disturbance, as seen in appendix B, are quite small in such a way that the Kalman filter does not give a great advantage. The estimated states are compared with the states obtained using offline derivation with filter of the ball's position and plate's angles states. The stabilization and tracking tests presented below were then performed.

9.1 Stabilization

After performing several tests with different weights of the LQR controller for the stabilization case, and also according to the conclusions presented in [7], it was concluded that the friction between the ball and the surface of the screen and the ball deformation considerably affects the performance of the controller. At low ball velocities and small plate angles the friction effect is greater. Therefore, in order to overcome the static friction at the beginning of the movement, it was necessary to increase the initial acceleration and adopt the weights to generate closed-loop poles with an imaginary part.

Using the LQR controller with the weights $\rho = 100$, $\kappa = 0.1$, the ball initially placed at the origin $(0, 0)$ and set points $x^* = y^* = 0.15$ m yields the evolution of the states presented in Figure 9.1 and control efforts in Figure 9.2.

Table 9.1: Performance result using LQR for stabilization.

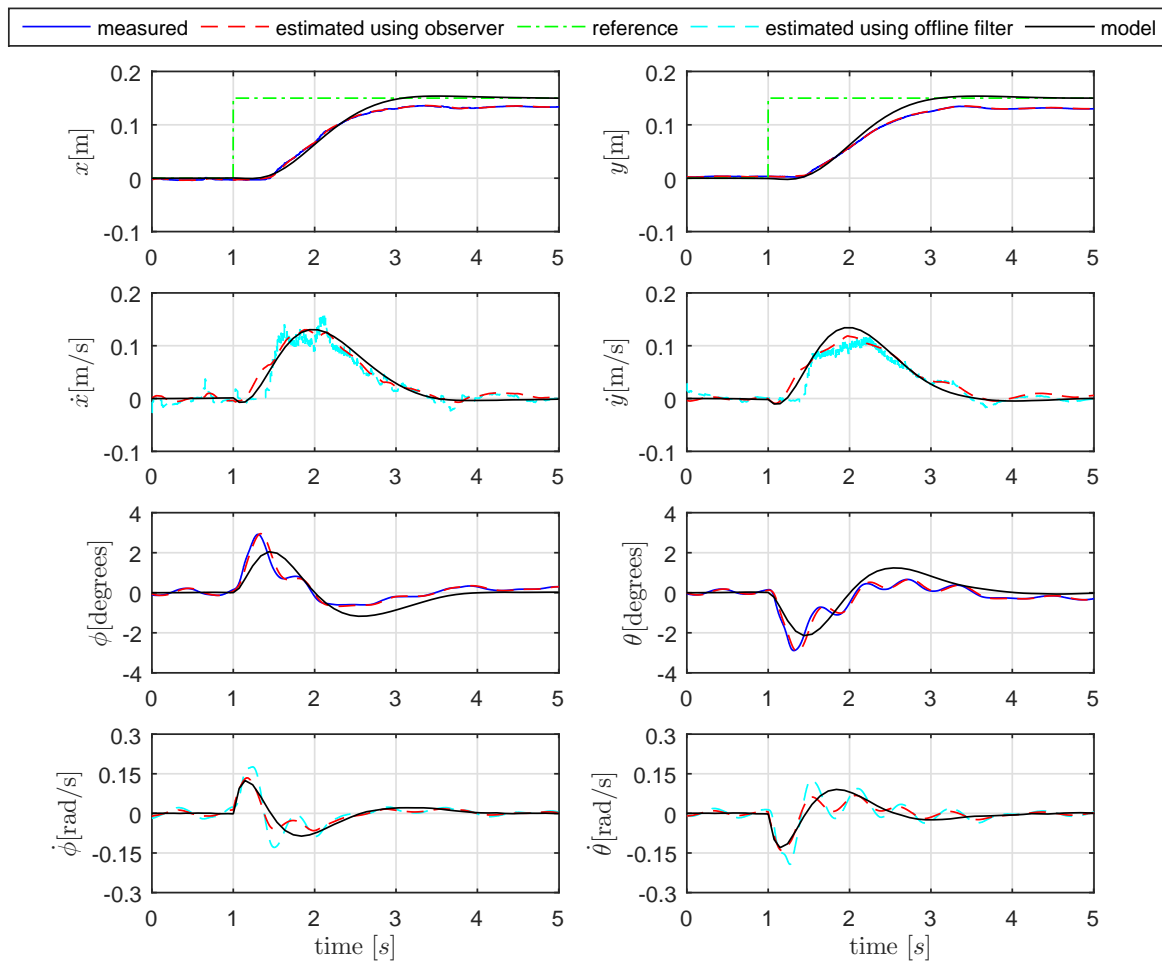| weights	$e_{x_{ss}}$[m]	overshoot%	t_{ss}[s]	φ_{max}[degrees]	$u_{1_{max}}$[rad/s^2]
$\rho = 100$, $\kappa = 0.1$	0.015	0	3	2.95	1.41

Figure 9.1: States in the stabilization test using LQR controller.

As it is shown in Figure 9.1 and Figure 9.2 the stabilization time and the control efforts , respectively, are close to the value obtained in the simulation. However, the steady error is higher due to friction not considered in the model. The results of the control performance for the $x-$axis are presented in Table 9.1.

The experimental results using a solid steel ball are presented in appendix E. The tests was done using the the same closed-loop poles as with the hollow ball. The overshoot was greater and the stationary error less because the friction was less. However, was not possible to use the solid steel ball because it damages the screen surface.
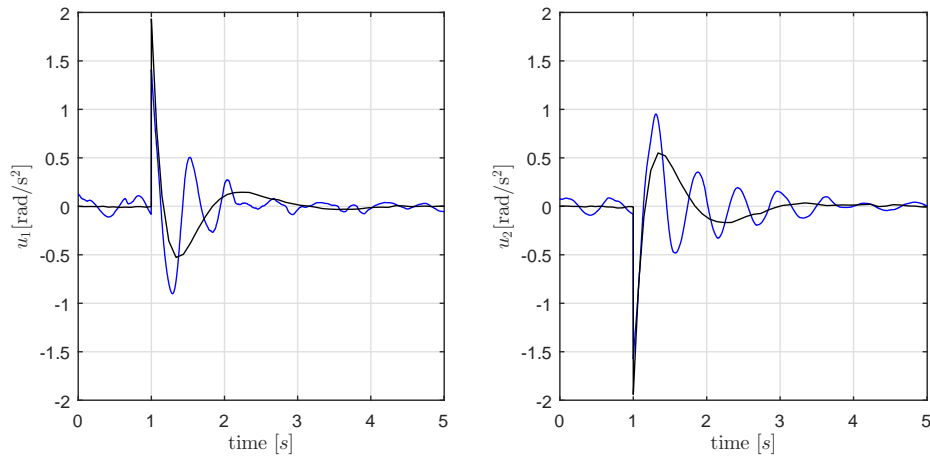
Figure 9.2: Control efforts in the stabilization test using LQR controller.

9.2 Tracking Control

Tracking tests are performed with the ball initially placed at the origin $(0,0)$ and using circular trajectories references with polynomial initialization (see appendix D), i.e. sinusoidal reference signals for the $x-$axis and co-sinusoidal for the $y-$axis, with amplitude $\mathcal{A} = 0.15\,\text{m}$ and frequencies $\omega \in \{0.5, 0.75, 1\}$ rad/s to compare the performance of the controllers.

In addition, the cases are presented without compensation of the delay in the measurement and with compensation of the delay by means of the Smith predictor.

9.2.1 Tracking Control Based on Approximate Feedback Linearization

Without Delay Compensation Better results were obtained using poles with imaginary part of the linearized system in Brunovsky form. With these poles we obtain the controller gain $K_{br} = [180, 162, 66, 13]$. Tests are performed with sinusoidal reference signals of different frequencies obtaining control results presented in Figure 9.3, Figure 9.4 and Figure 9.5. Also, the observer has initial states values equal to zero.

Table 9.2: Performance using tracking control based on AFL for sinusoidal references with $\mathcal{A} = 0.15\,\text{m}$.

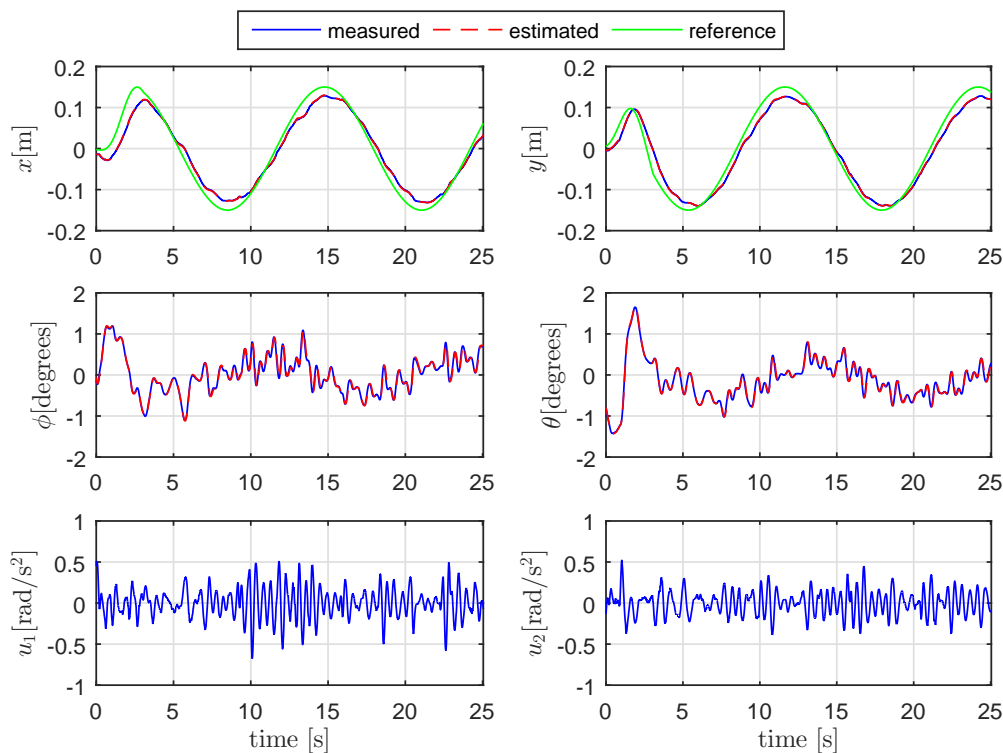| ω [rad/s]	tracking error[%]	φ_{max}[degrees]	$u_{1_{max}}$[rad/s^2]	ϑ_{max}[degrees]	$u_{2_{max}}$[rad/s^2]
0.5	18.01	1.1953	0.6734	1.6494	0.5214
0.75	19.54	2.0874	0.5893	2.2236	0.2862
1	17.44	3.3882	0.5708	4.1060	0.59783

Figure 9.3: Tracking with $\mathcal{A} = 0.15\,\mathrm{m}$, $\omega = 0.5\,\mathrm{rad/s}$ using tracking control based on AFL.
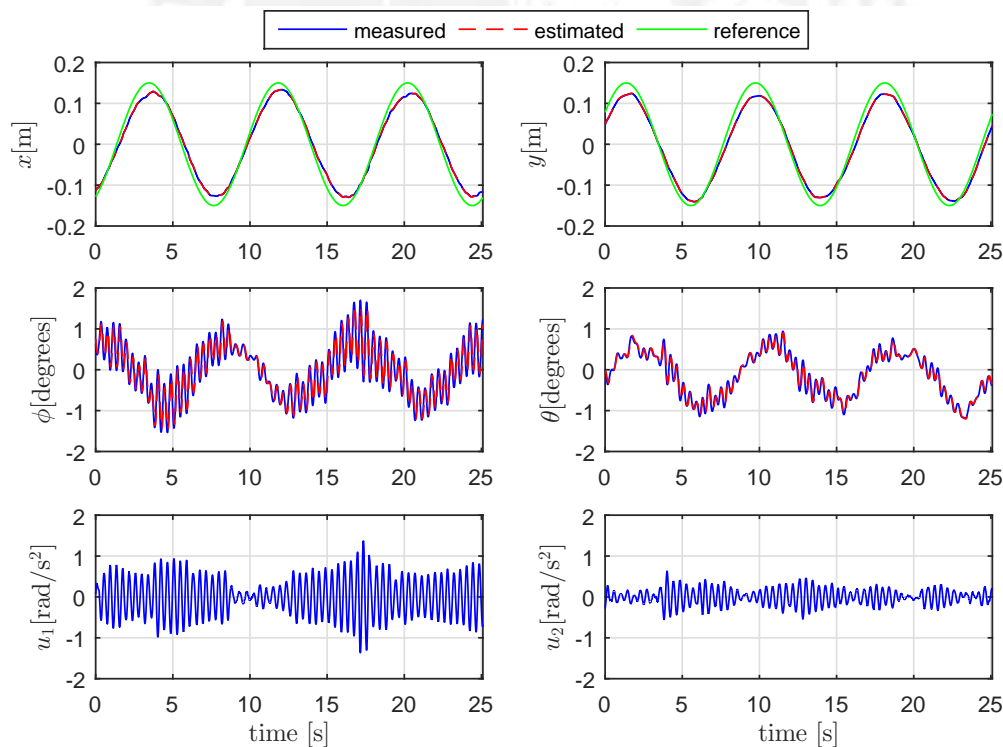

Figure 9.4: Tracking with $\mathcal{A} = 0.15\,\mathrm{m}$, $\omega = 0.75\,\mathrm{rad/s}$ using tracking control based on AFL.
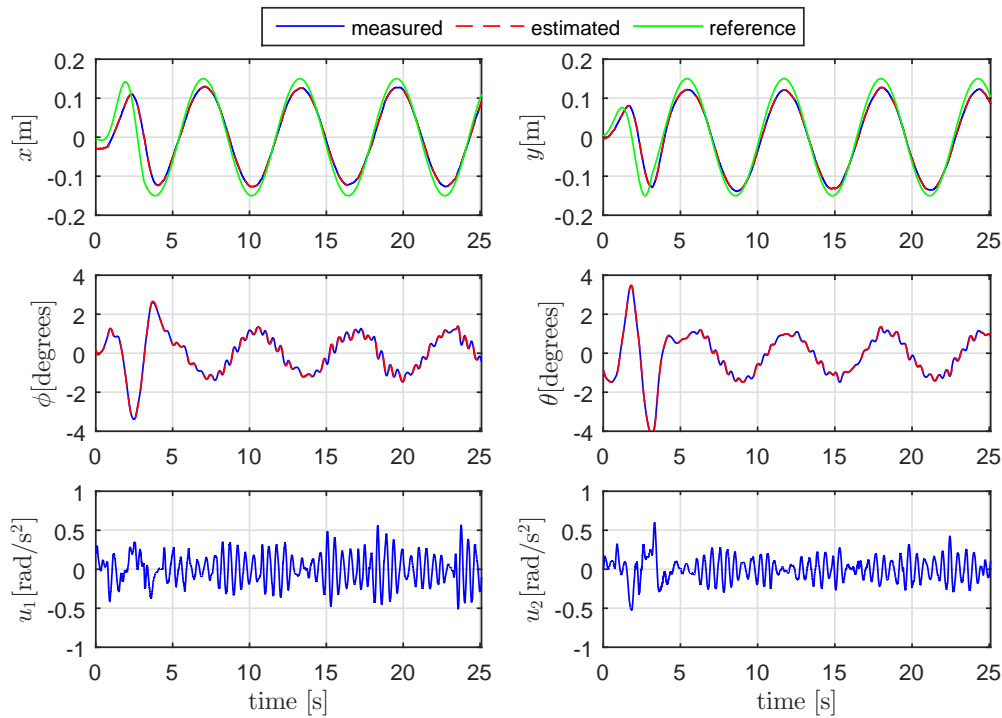
Figure 9.5: Tracking with $\mathcal{A} = 0.15\,\mathrm{m}$, $\omega = 1\,\mathrm{rad/s}$ using tracking control based on AFL.

The controller performance summary presented in Table 9.2 shows that due to the effect of friction the average tracking error does not increase as the frequency of the reference signal increases as it did in the simulation. This effect is because the friction was not considered in the simulations. The friction is reduced when the ball speed is higher, and this occurs when the frequency of the reference signal is greater.

On the other hand, it was observed that the spring generates an oscillatory movement to the plate of greater frequency than the reference trajectory visualized in the plate's angles graphs.

Considering Delay Compensation   Including the Smith predictor to compensate the sensor delay and using the same controller gain as the previous case, the tracking control tests are performed for different frequencies of the reference signals, with the control results presented in Figure 9.6, Figure 9.7 and Figure 9.8.

Table 9.3: Performance using tracking control based on AFL and Smith predictor for sinusoidal references with $\mathcal{A} = 0.15\,\mathrm{m}$.

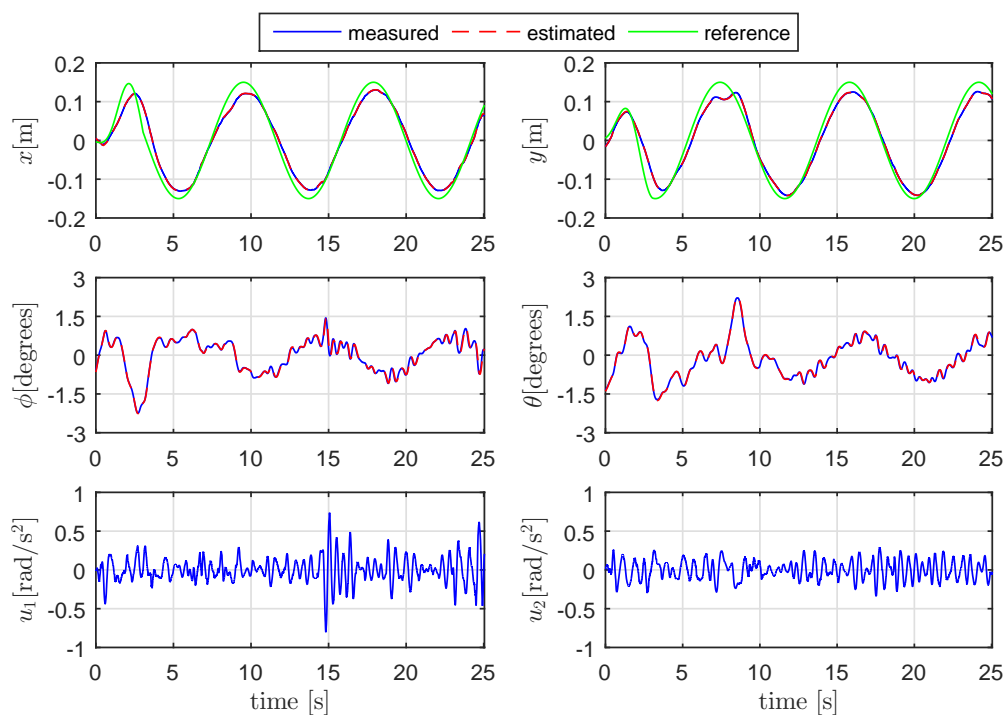| ω [rad/s]	tracking error[%]	φ_{max}[degrees]	$u_{1_{max}}$[rad/s^2]	ϑ_{max}[degrees]	$u_{2_{max}}$[rad/s^2]
0.5	17.98	2.2397	0.801	2.2134	0.3348
0.75	17.98	1.6992	1.3757	1.1909	0.6399
1	16.67	1.8267	0.8787	1.6099	0.4774

Figure 9.6: Tracking with $\mathcal{A} = 0.15\,\mathrm{m}$, $\omega = 0.5\,\mathrm{rad/s}$ using tracking control based on AFL and SP.
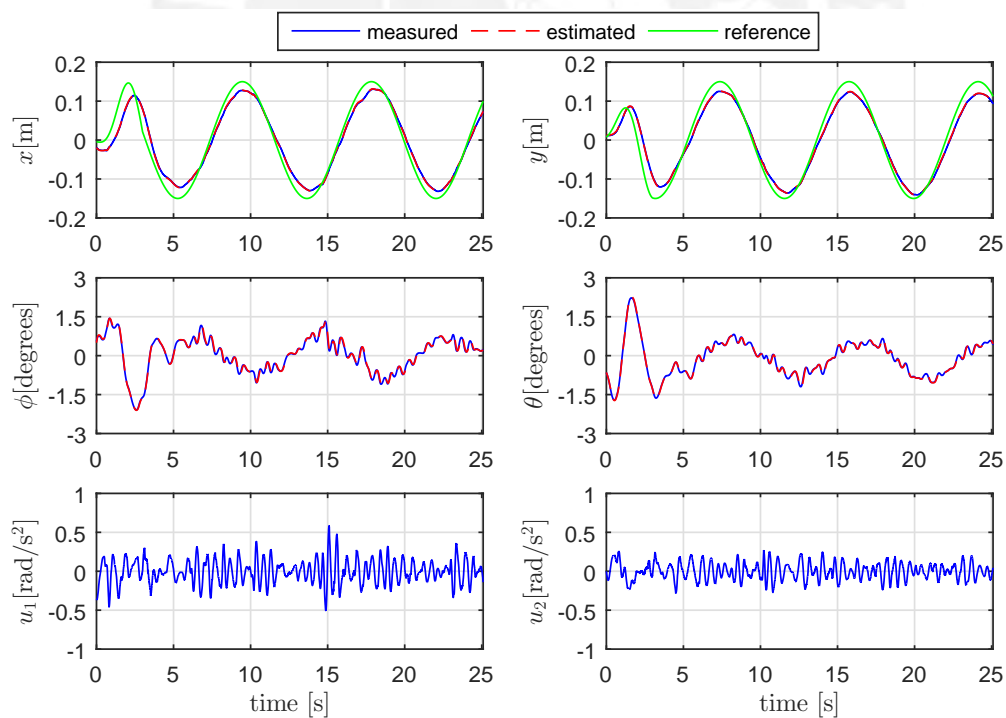

Figure 9.7: Tracking with $\mathcal{A} = 0.15\,\mathrm{m}$, $\omega = 0.75\,\mathrm{rad/s}$ using tracking control based on AFL and SP.
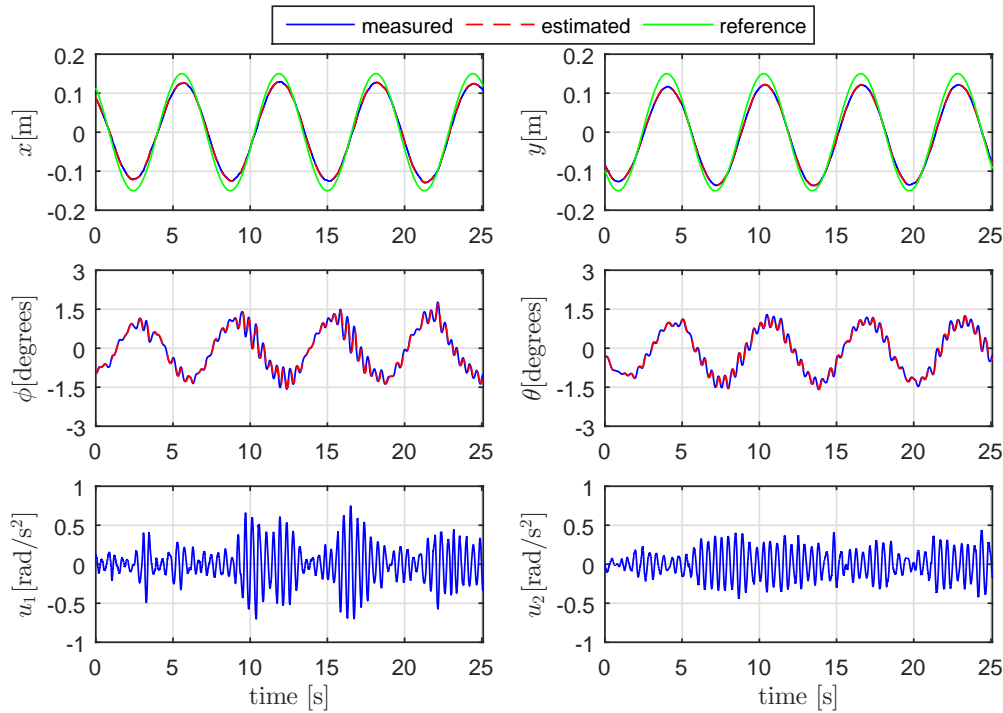
Figure 9.8: Tracking with $\omega = 1\,\text{rad/s}$ using tracking control based on AFL and SP.

The controller performance summary presented in Table 9.3, shows that including the compensation of the delay the average tracking error was reduced, however the benefit is not very appreciable because friction and other characteristics not modeled (e.g. ball deformation, non-uniform distribution of ball mass, rotation of the ball around its vertical axis, etc.) affect in greater proportion.

9.2.2 Tracking Control with Integral Action Based on AFL

Without Delay Compensation   Integral action was added in the control action in order to reduce the tracking error. The controller gain considering desired poles with an imaginary part to overcome static friction is $[K_{br}, K_I] = [200, 132, 51, 12, 4]$. Tests without delay compensation for sinusoidal signals of different frequency are shown in Figure 9.9, Figure 9.10 and Figure 9.11.

Table 9.4: Performance using tracking control with integral action based on AFL for sinusoidal references with $\mathcal{A} = 0.15\,\text{m}$.

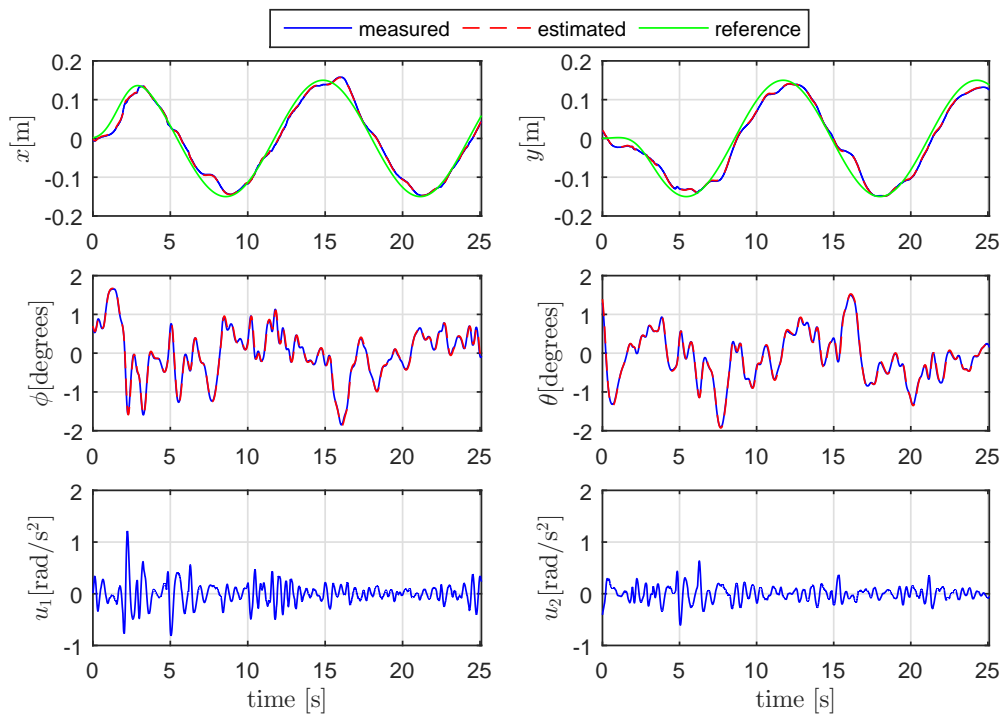| ω [rad/s]	tracking error[%]	φ_{max}[degrees]	$u_{1_{max}}$[rad/s^2]	ϑ_{max}[degrees]	$u_{2_{max}}$[rad/s^2]
0.5	17.09	1.8472	1.2136	1.9058	0.6329
0.75	14.93	1.9204	0.5065	1.7534	0.3582
1	18.03	1.8721	0.442	2.0479	0.3472

Figure 9.9: Tracking with $\mathcal{A} = 0.15\,\text{m}$, $\omega = 0.5\,\text{rad/s}$ using tracking control with integral action.
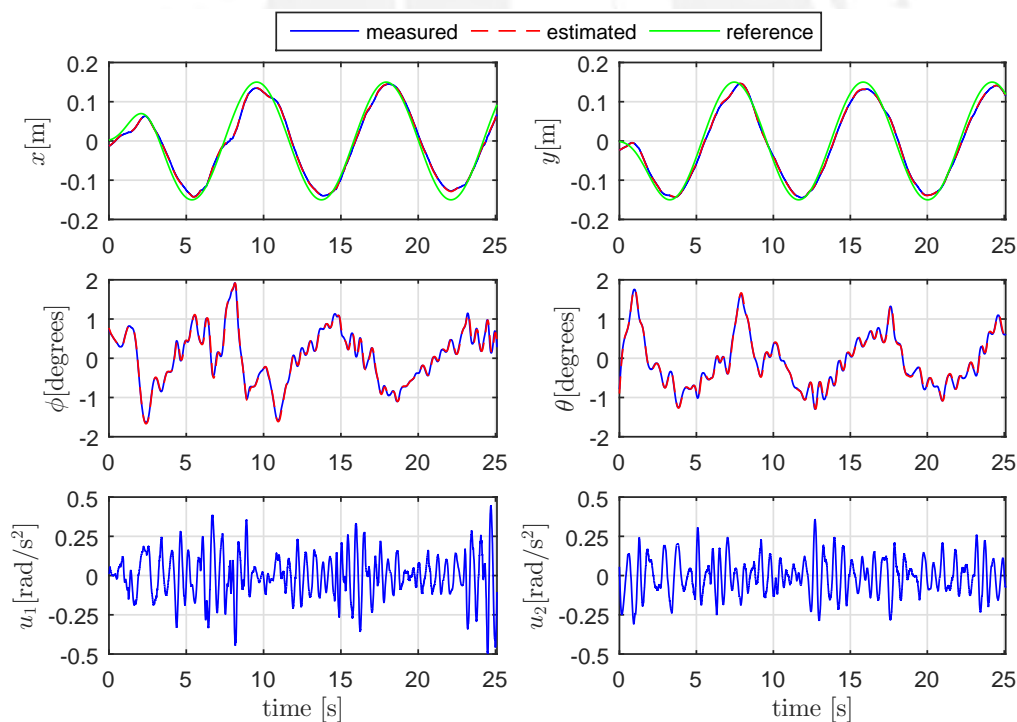

Figure 9.10: Tracking with $\mathcal{A} = 0.15\,\text{m}$, $\omega = 0.75\,\text{rad/s}$ using tracking control with integral action.
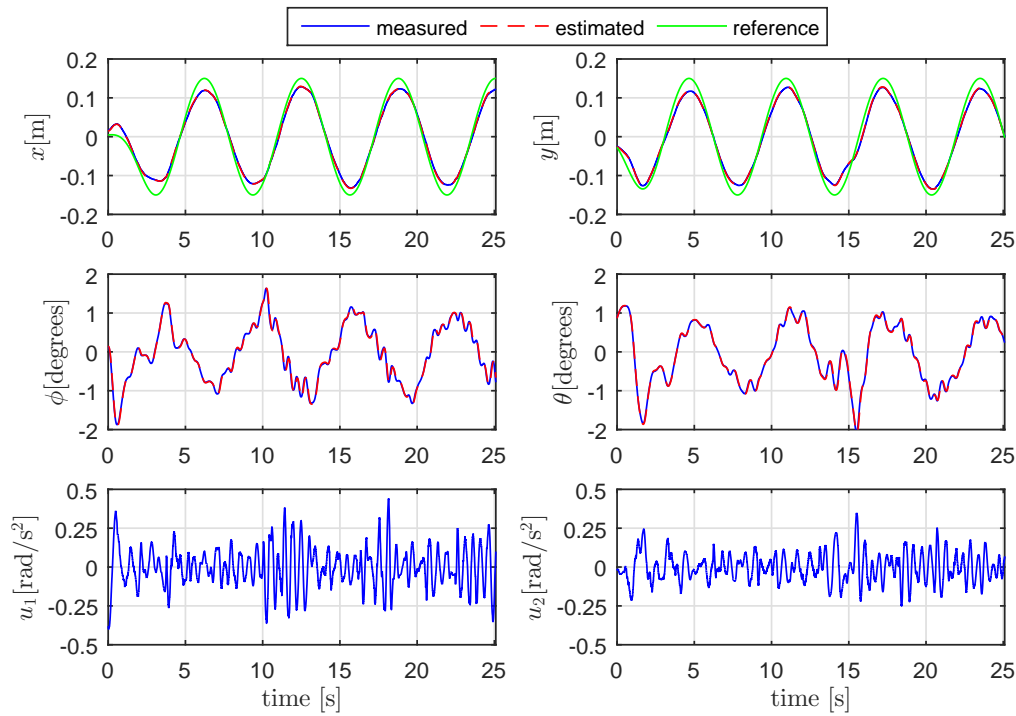
Figure 9.11: Tracking with $\mathcal{A} = 0.15\,\mathrm{m}$, $\omega = 1\,\mathrm{rad/s}$ using tracking control with integral action.

Considering Delay Compensation   Including the Smith predictor to compensate the sensor delay and using the same controller gain as the previous case, tracking control tests are performed for different frequencies of the reference signals, with the control results presented in Figure 9.12, Figure 9.13 and Figure 9.14.

Furthermore the ball trajectories during the tracking control using this approach is presented in appendix F .

Table 9.5: Performance using tracking control with integral action based on AFL and Smith predictor for sinusoidal references with $\mathcal{A} = 0.15\,\mathrm{m}$.

ω [rad/s]	**tracking error**[%]	φ_{max}[degrees]	$u_{1_{max}}$[rad/s^2]	ϑ_{max}[degrees]	$u_{2_{max}}$[rad/s^2]
0.5	12.7737	1.2363	0.5614	1.0928	0.6001
0.75	13.634	2.5283	0.3934	2.335	0.2978
1	16.8383	2.6235	0.8906	1.5425	0.41

During the tests, it was observed that the spring generates an oscillatory movement to the plate of greater frequency than the reference trajectory and that can be easily visualized in the plate's angles graphs. This effect could be considered as an external disturbance that also alters the control effort making it more oscillatory.
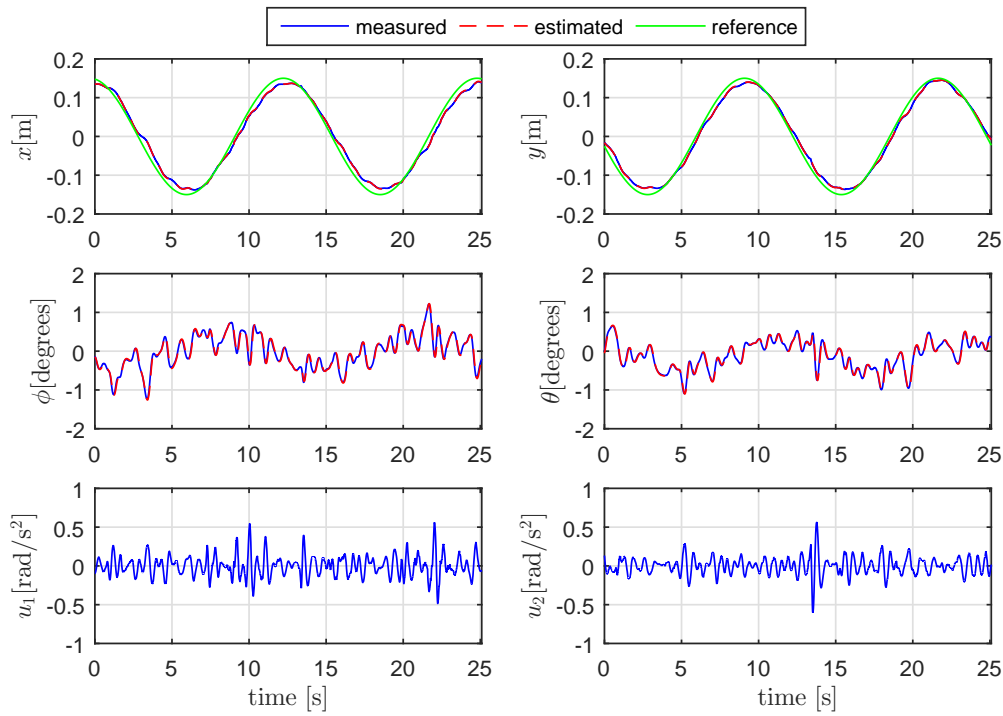
Figure 9.12: Tracking with $\mathcal{A} = 0.15\,\mathrm{m}$, $\omega = 0.5\,\mathrm{rad/s}$ using tracking control with integral action and SP.

Figure 9.13: Tracking with $\mathcal{A} = 0.15\,\mathrm{m}$, $\omega = 0.75\,\mathrm{rad/s}$ using tracking control with integral action and SP.

Figure 9.14: Tracking with $\mathcal{A} = 0.15\,\text{m}$, $\omega = 1\,\text{rad/s}$ using tracking control with integral action and SP.

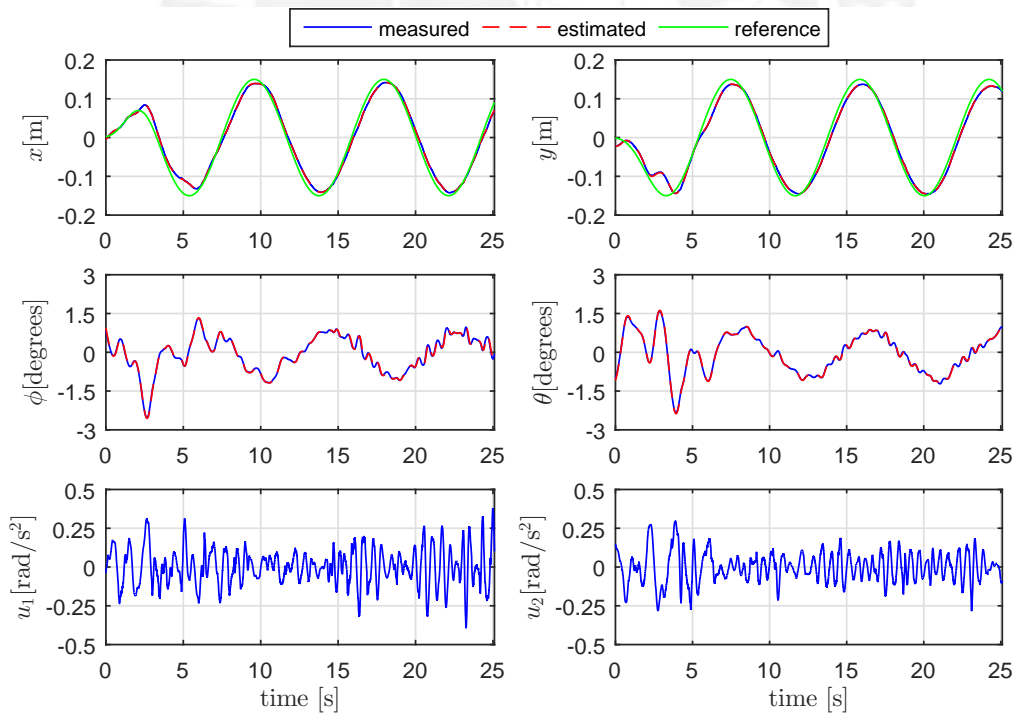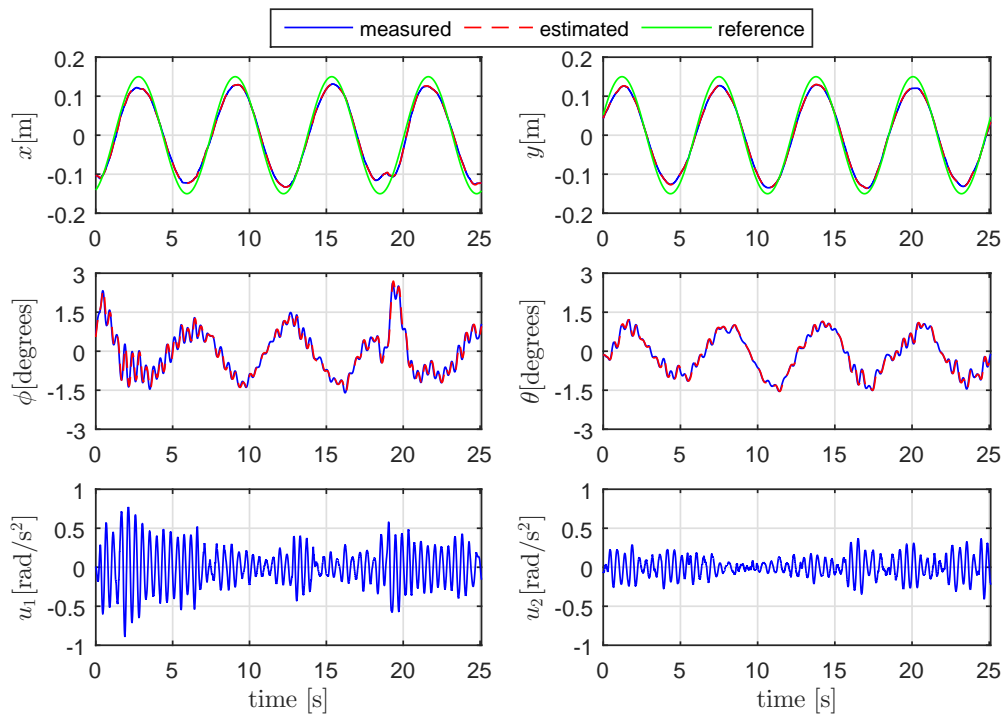The controller performance summary presented in Table 9.5, shows that including the delay compensation the average error of tracking was reduced, however the benefit is not very appreciable because the friction and other characteristics not modeled affect in greater proportion. On the other hand, adding the integral action increases the performance.

9.2.3 Backstepping Control

Without Delay Compensation   Tests are performed using backstepping controller with the controller gains $\{c_1, c_2, c_3, c_4\} = \{2, 3, 4, 5.5\}$. The control results without delay compensation for sinusoidal signals of different frequency are shown in Figure 9.15, Figure 9.16 and Figure 9.17.

Table 9.6: Performance using backstepping controller for sinusoidal references with $\mathcal{A} = 0.15\,\text{m}$.

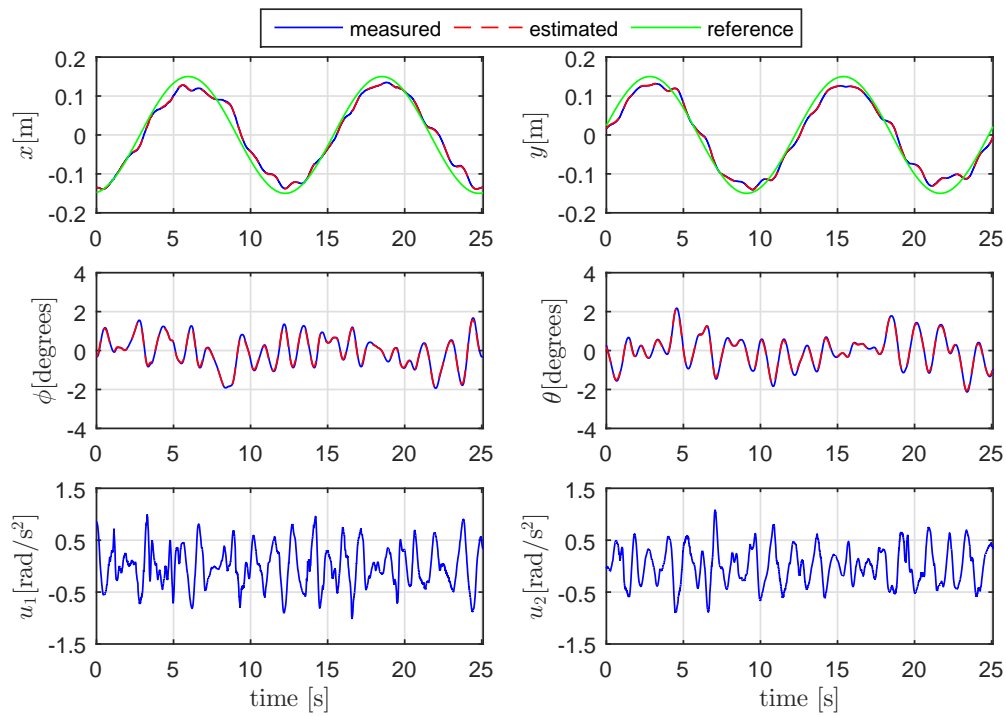| ω [rad/s]	**tracking error**[%]	φ_{max}[degrees]	$u_{1_{max}}$[rad/s²]	ϑ_{max}[degrees]	$u_{2_{max}}$[rad/s²]
0.5	19.5507	1.9307	1.0095	2.1738	1.0871
0.75	17.6480	2.5254	1.5416	2.3701	1.3295
1	15.8435	2.2778	1.1623	3.0791	1.2593

Figure 9.15: Tracking with $\mathcal{A} = 0.15\,\text{m}$, $\omega = 0.5\,\text{rad/s}$ using backstepping controller.
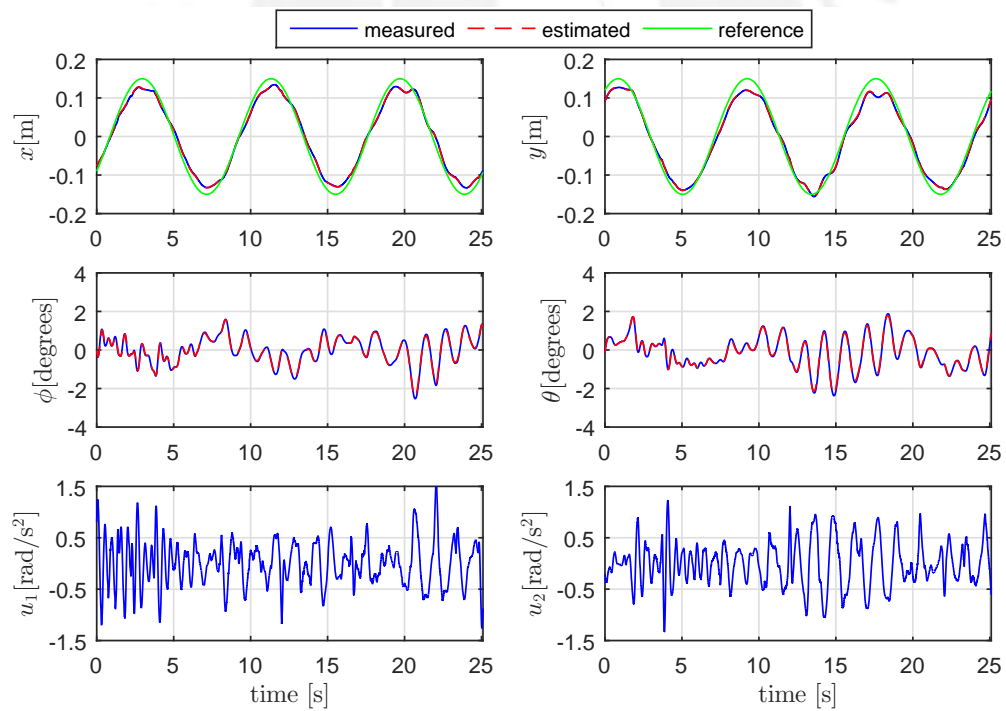

Figure 9.16: Tracking with $\mathcal{A} = 0.15\,\text{m}$, $\omega = 0.75\,\text{rad/s}$ using backstepping controller.
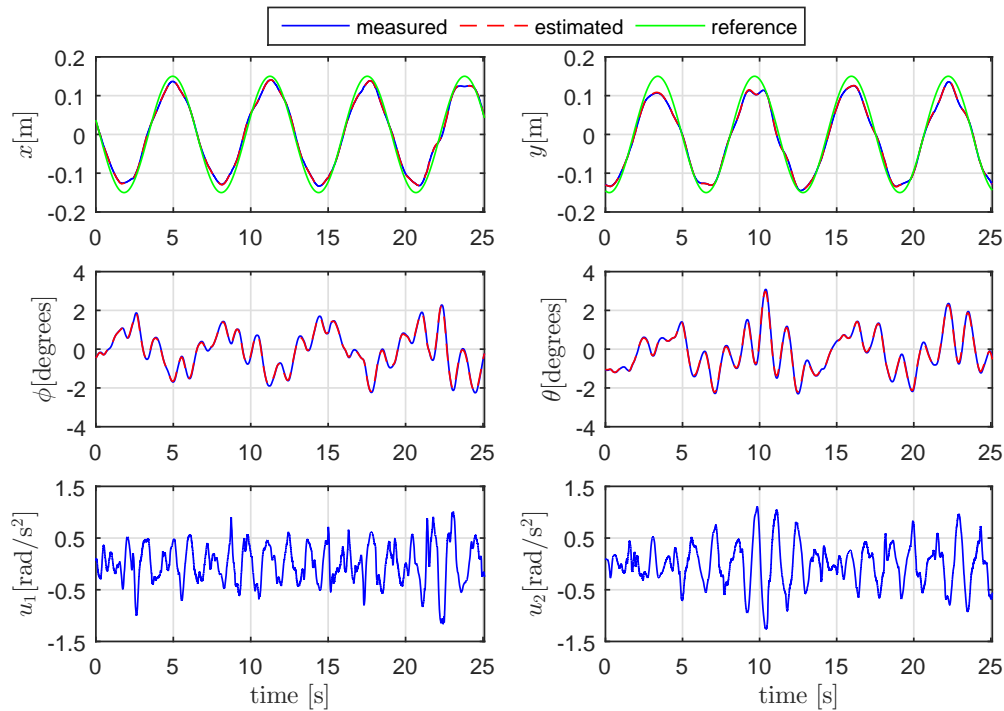
Figure 9.17: Tracking with $\mathcal{A} = 0.15\,\text{m}$, $\omega = 1\,\text{rad/s}$ using backstepping controller.

As in the previous cases, the spring generates an oscillatory movement to the plate of greater frequency than the reference trajectory and alters the control effort making it more oscillatory.

Considering Delay Compensation   Including the Smith predictor to compensate the sensor delay and using the same controller gain as the previous case, tracking control tests are performed for different frequencies of the reference signals, with the control results presented in Figure 9.18, Figure 9.19 and Figure 9.20.

Table 9.7: Performance using backstepping controller and Smith predictor for sinusoidal references with $\mathcal{A} = 0.15\,\text{m}$.

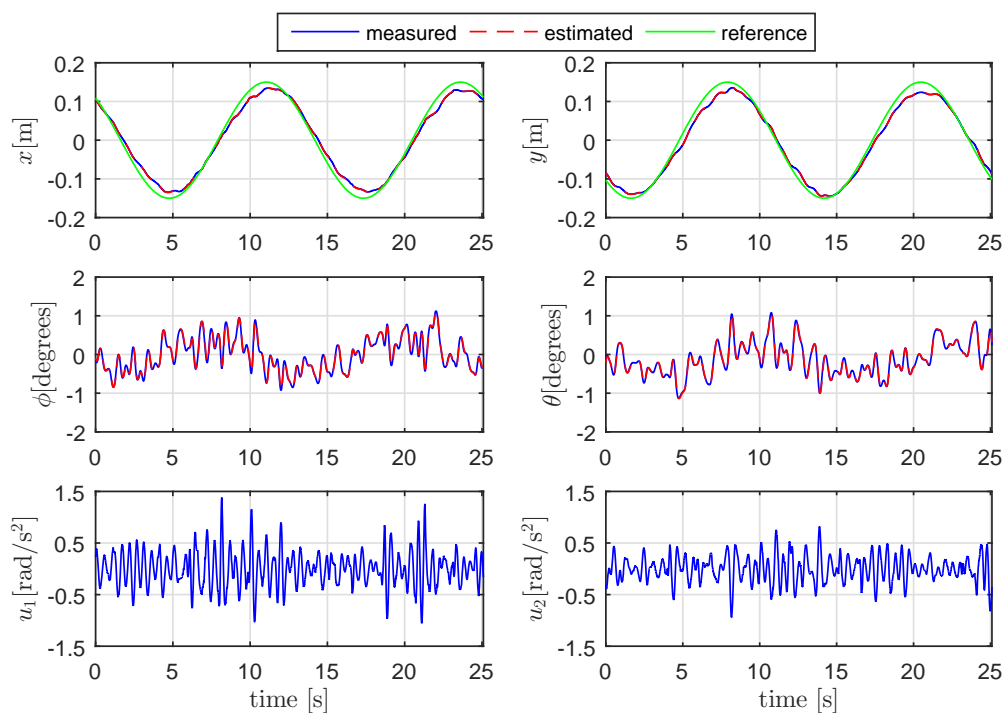| ω [rad/s]	tracking error[%]	φ_{max}[degrees]	$u_{1_{max}}$[rad/s^2]	ϑ_{max}[degrees]	$u_{2_{max}}$[rad/s^2]
0.5	15.6275	1.1279	1.3816	1.1279	0.9421
0.75	13.4502	1.2744	1.0573	1.3989	0.9536
1	13.637	1.4077	0.9119	3.0952	0.6988

Figure 9.18: Tracking with $\mathcal{A} = 0.15\,\text{m}$, $\omega = 0.5\,\text{rad/s}$ using backstepping controller and SP.
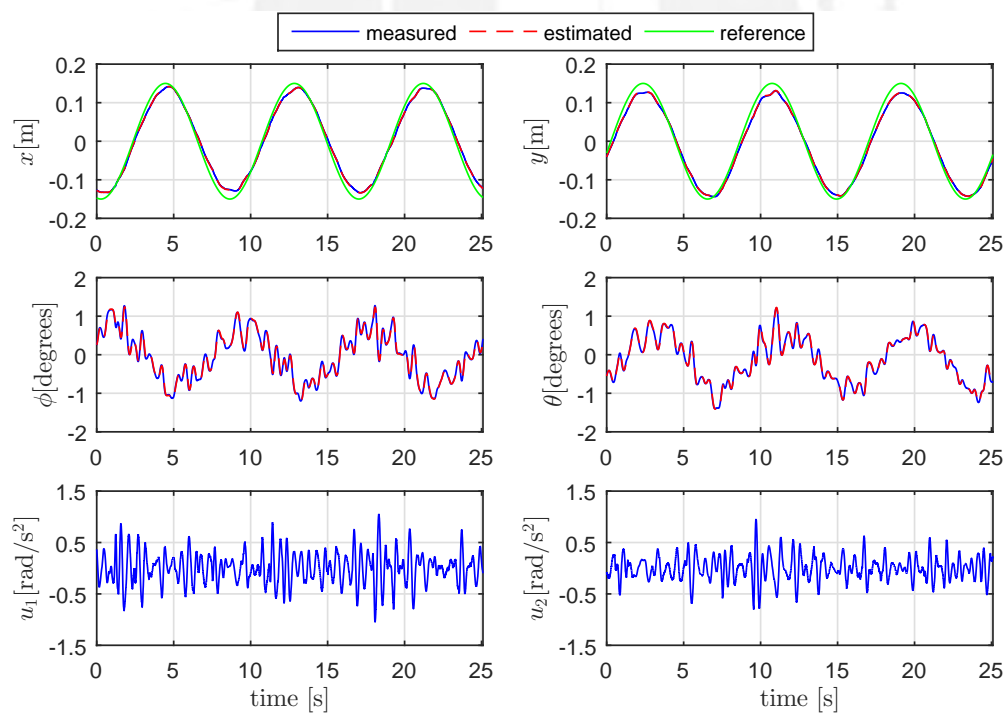

Figure 9.19: Tracking with $\mathcal{A} = 0.15\,\text{m}$, $\omega = 0.75\,\text{rad/s}$ using backstepping controller and SP.
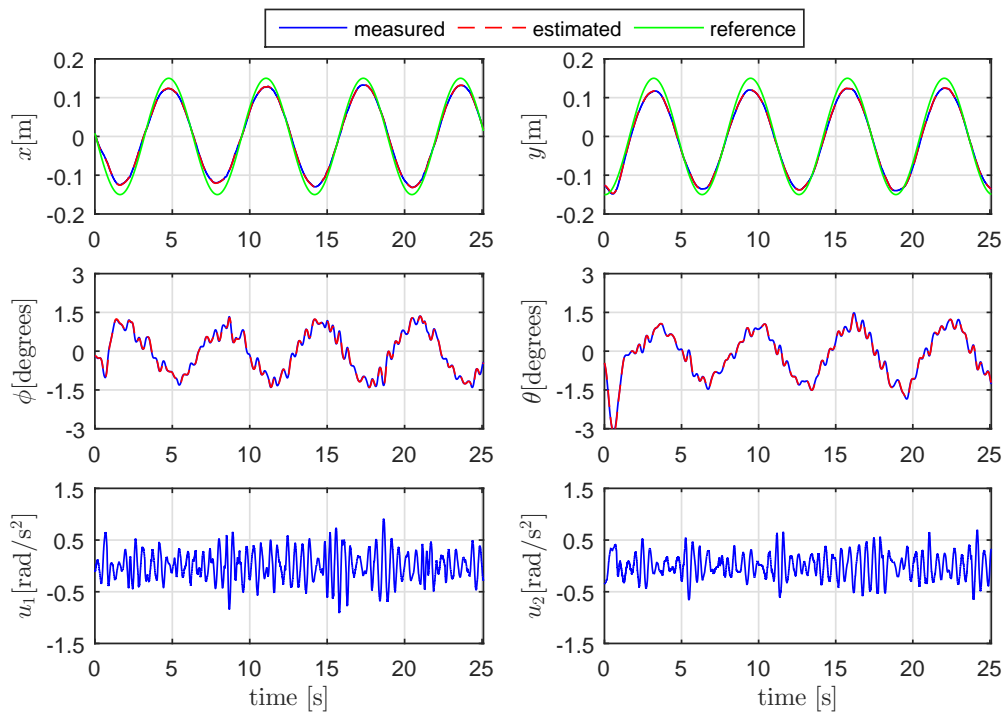
Figure 9.20: Tracking with $\mathcal{A} = 0.15\,\text{m}$, $\omega = 1\,\text{rad/s}$ using backstepping controller and SP.

The controller performance summary presented in Table 9.7, shows that including the delay compensation the average tracking error was reduced; however, the benefit is not very appreciable because the friction and other characteristics not modeled affect in greater proportion. On the other hand, the average tracking error obtained is close to that obtained using tracking control with integral action based on AFL Table 9.5, but uses a greater control effort.

9.2.4 Sliding Mode Control

Without Delay Compensation Tests are performed using sliding mode control with the controller parameters $\{\alpha, \varepsilon, \beta_1, \beta_2, \beta_3\} = \{-1.5, 0.3, 1.5, 3, 5\}$ presented in Table 9.8. The control results without delay compensation for sinusoidal signals of different frequency are shown in Figure 9.21, Figure 9.22 and Figure 9.23.

Table 9.8: Performance using sliding mode control for sinusoidal references with $\mathcal{A} = 0.15\,\text{m}$.

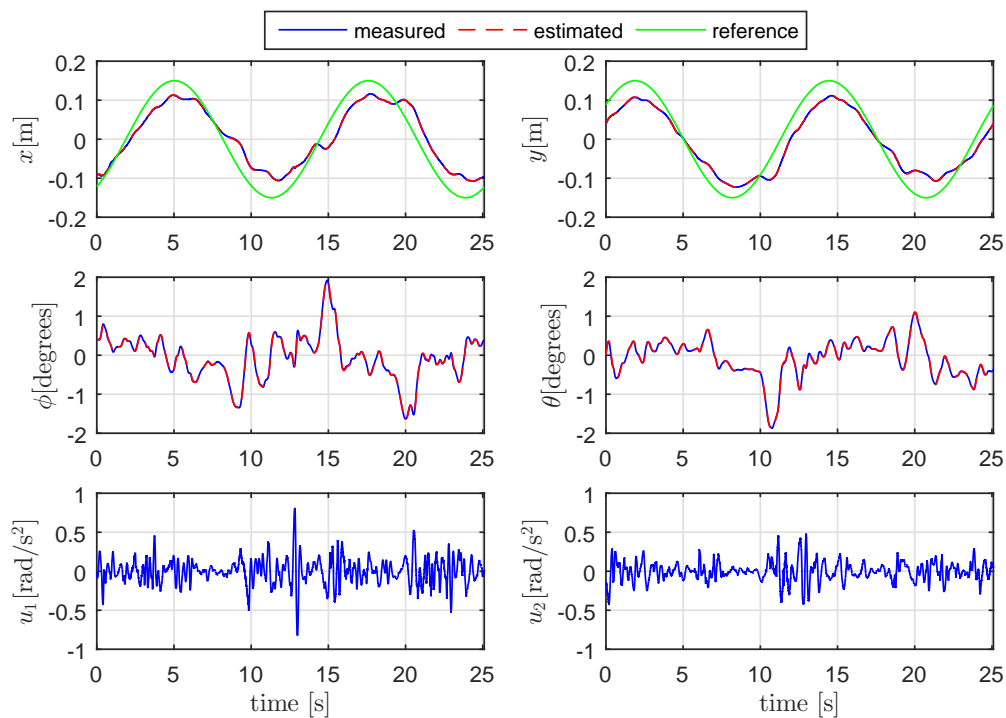| ω [rad/s]	**tracking error**[%]	φ_{max}[degrees]	$u_{1_{max}}$[rad/s^2]	ϑ_{max}[degrees]	$u_{2_{max}}$[rad/s^2]
0.5	38.2362	1.9219	0.8235	1.8706	0.4819
0.75	29.112	1.1016	0.7092	2.6777	0.8503
1	24.6551	1.708	1.5494	1.4517	1.1511

Figure 9.21: Tracking with $\mathcal{A} = 0.15\,\text{m}$, $\omega = 0.5\,\text{rad/s}$ using sliding mode control.
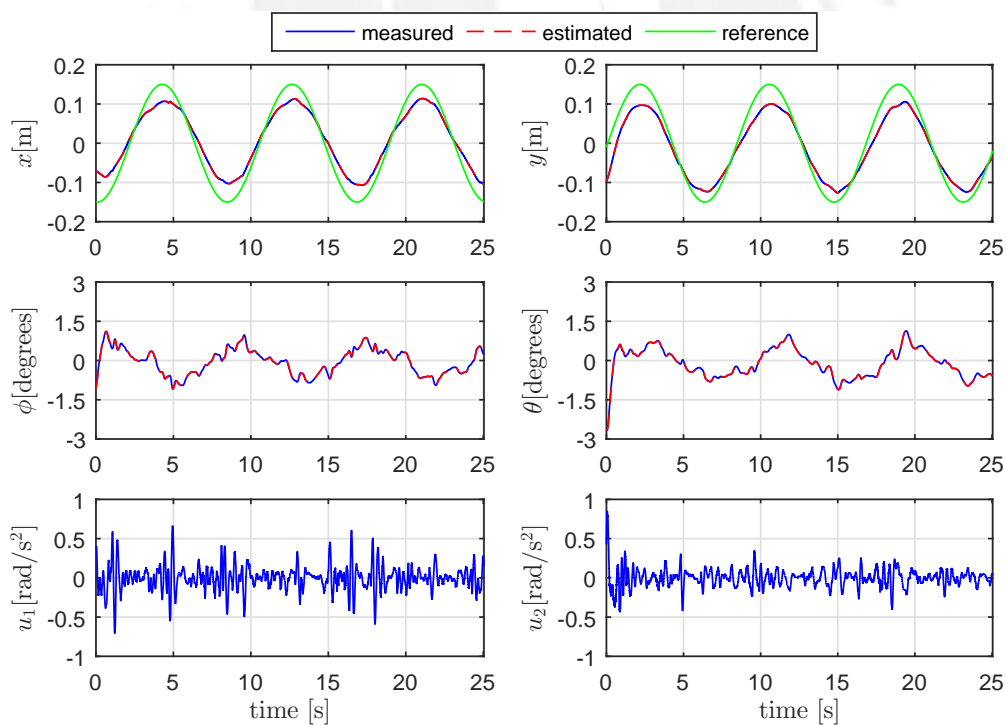

Figure 9.22: Tracking with $\mathcal{A} = 0.15\,\text{m}$, $\omega = 0.75\,\text{rad/s}$ using sliding mode control.
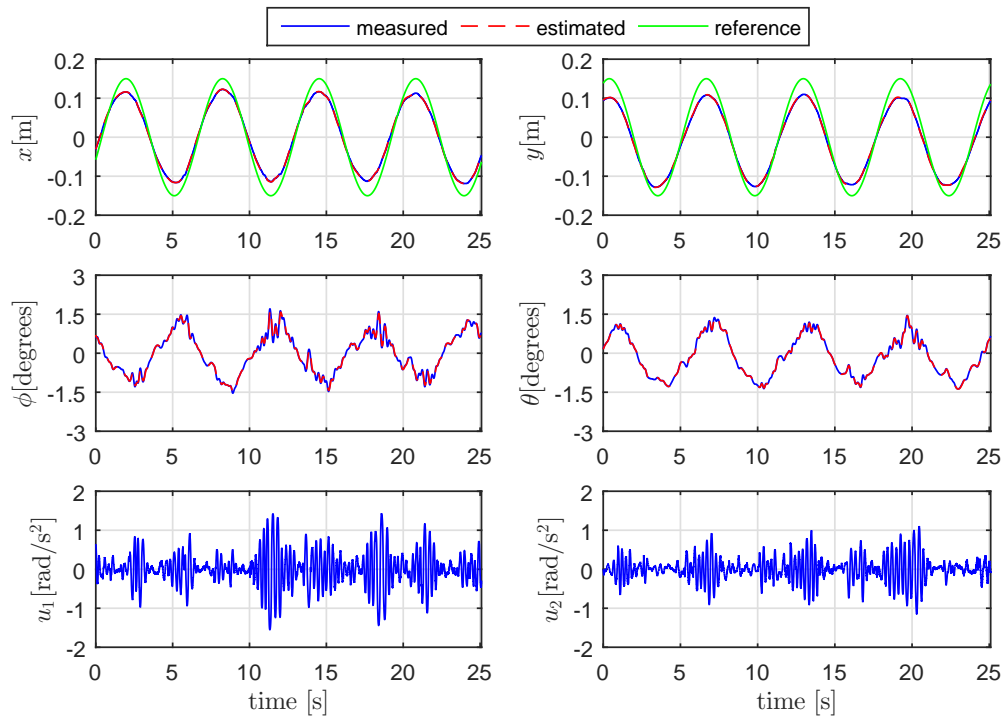
Figure 9.23: Tracking with $\mathcal{A} = 0.15\,\mathrm{m}$, $\omega = 1\,\mathrm{rad/s}$ using sliding mode control.

As in the previous cases, the spring generates an oscillatory movement to the plate of greater frequency than the reference trajectory and alters the control effort making it more oscillatory.

Considering Delay Compensation Including the Smith predictor to compensate the sensor delay and using the same controller gain as the previous case, tracking control tests are performed for different frequencies of the reference signals, with the control results presented in Figure 9.24, Figure 9.25 and Figure 9.26.

Table 9.9: Performance using sliding mode control and Smith predictor for sinusoidal references with $\mathcal{A} = 0.15\,\mathrm{m}$.

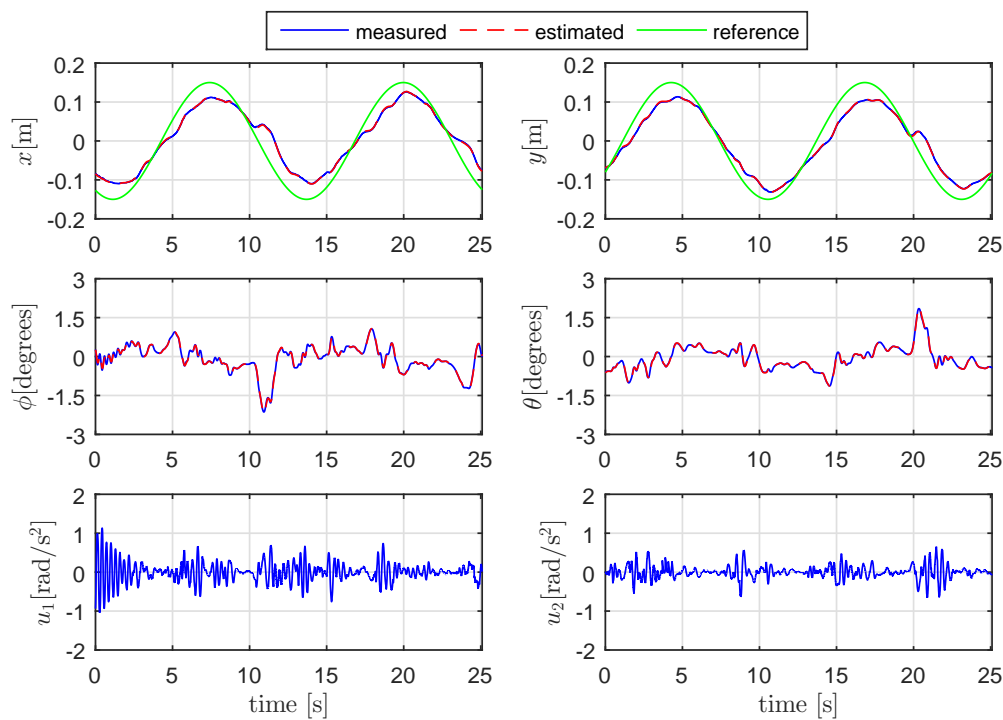| ω [rad/s]	**tracking error**[%]	φ_{max}[degrees]	$u_{1_{max}}$[rad/s^2]	ϑ_{max}[degrees]	$u_{2_{max}}$[rad/s^2]
0.5	35.2914	2.1357	1.1305	1.8457	0.6548
0.75	25.9086	1.2422	1.4972	2.6968	1.3951
1	21.5796	1.7021	1.308	1.4253	0.988

Figure 9.24: Tracking with $\mathcal{A} = 0.15\,\mathrm{m}$, $\omega = 0.5\,\mathrm{rad/s}$ using sliding mode control and SP.
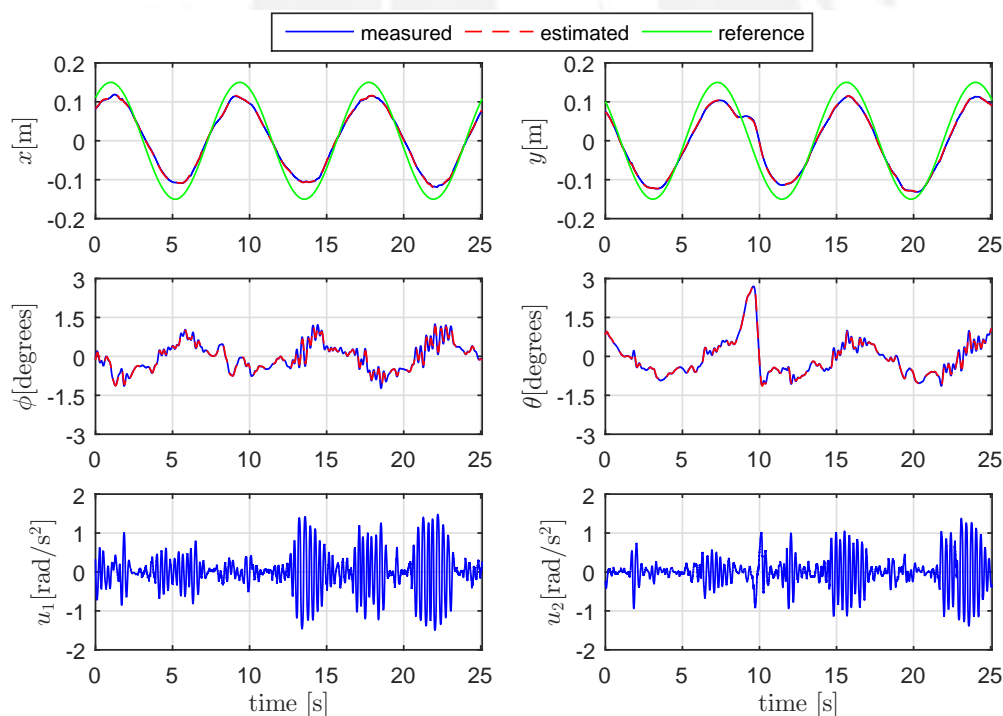

Figure 9.25: Tracking with $\mathcal{A} = 0.15\,\mathrm{m}$, $\omega = 0.75\,\mathrm{rad/s}$ using sliding mode control and SP.
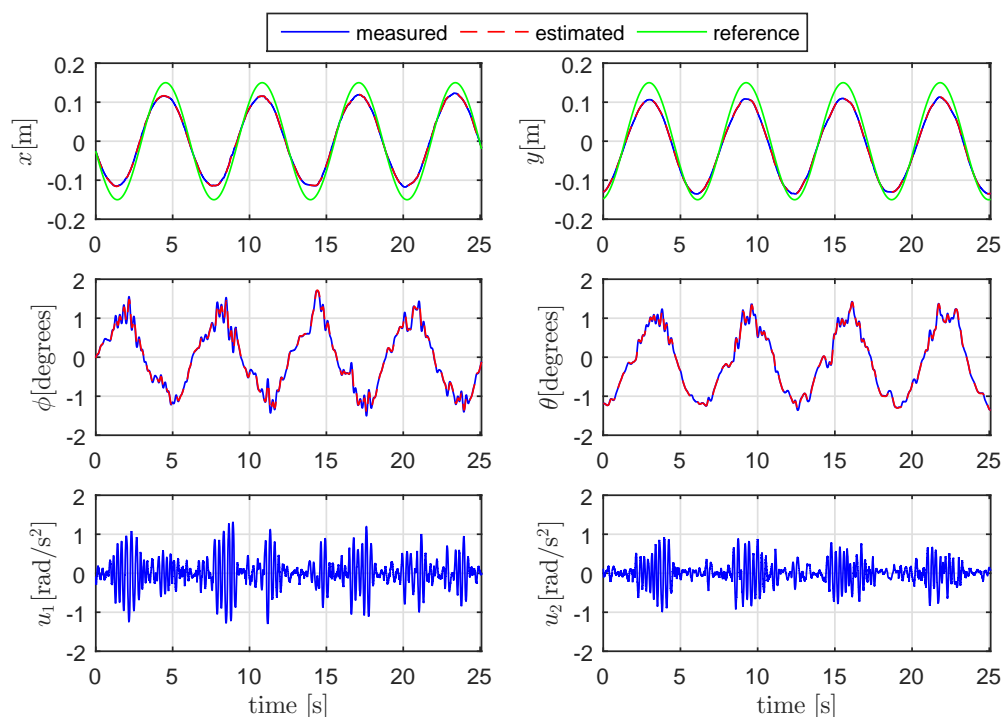
Figure 9.26: Tracking with $\mathcal{A} = 0.15\,\mathrm{m}$, $\omega = 1\,\mathrm{rad/s}$ using sliding mode control and SP.

The controller performance summary presented in Table 9.9, shows that including the compensation of the delay the average tracking error was reduced; however, the benefit is not very appreciable because the friction and other characteristics not modeled affect in greater proportion. On the other hand, the average tracking error obtained is higher than the other methods and therefore does not have a good performance for the ball and plate system under study. The reason for this is because this approach requires high control activity so also requires that the inner loop dynamics be quite fast. However, the maximum angular velocity of the plate was limited, for safety reasons, to avoid vibrations and because the screen has a considerable mass.

To summarize, the Figure 9.27 presents the comparison of the tracking control for $\mathcal{A} = 0.15\,\mathrm{m}$, $\omega = 0.75\,\mathrm{rad/s}$ using the approaches studied. The approaches : tracking control with integral action based on AFL and backstepping provide less tracking error, using the latter greater control action. On the other hand, tracking control based on AFL amplifies the vibratory effect of the spring to the plate angles and control action, and does not achieve good performance either. The sliding mode controller delivers greater tracking error and generates a more oscillatory behavior of the system requiring rapid changes of the control action.
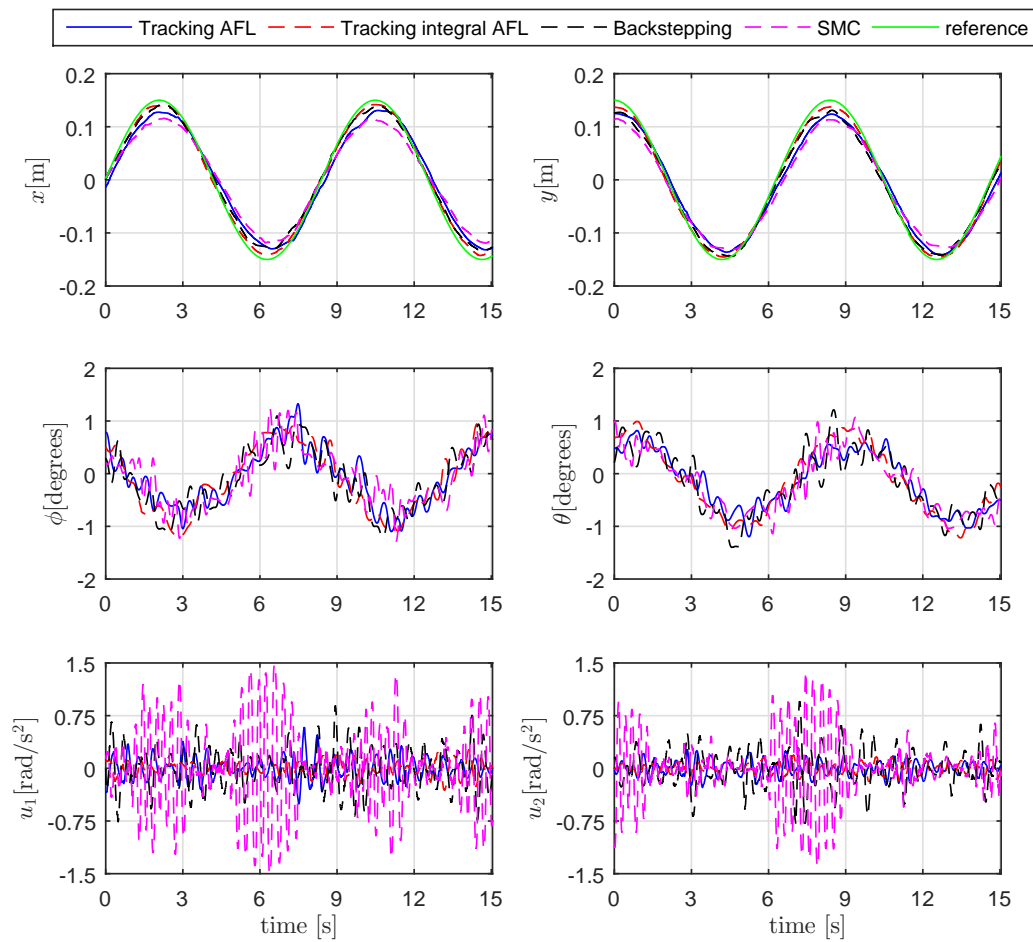
Figure 9.27: Comparing approaches for $\mathcal{A} = 0.15\,\text{m}$, $\omega = 0.75\,\text{rad/s}$, using SP

10 Conclusions and Future Work

10.1 Conclusions

This thesis presents some important contributions regarding the modeling, analysis, and design of the control system for the ball and plate system developed Control Engineering Group of TU Ilmenau. The main objective was to perform the tracking control to the ball; however, this led to the design of the full state observer and the Smith predictor in order to provide the estimated states to the controller. In addition, the comparison of different control approaches was performed.

After modeling the system and analyzing the model, we conclude that the system is globally weak observable and locally controllable for the considered operation range, and therefore the controller and observer can be designed. Also, the Jacobi linearization results in two decoupled linear systems, and this means that near the equilibrium point it is possible to neglect the coupling terms.

On the other hand, when calculating the relative degree of the system with the exact model and analyzing the internal dynamics, we conclude that the system is non-minimum phase, so that the feedback linearization approach can not be applied. Also, perfect tracking can not be done based on the exact model, since the dynamic inversion is unstable. Therefore, an approximate flat model is used to design controllers based on the approaches: feedback linearization, backstepping, and sliding mode. However, by applying these controllers to the ball and plate system, they only guarantee local stability in function to the operating range and its gains, since they are not designed with the exact model.

According to the results in simulation, it was verified that for the considered operation range and frequencies no greater than $\omega = 1$ it is ensured that the neglected terms are very small in comparison to the main terms that belong to the approximate model, then it is a valid approximation. In addition, the delay in the measurement affects more when the reference signal has high frequency. However, using the Smith predictor, the delay is compensated to be able to use the ball position in the estimation of states by the observer. From the studied observers, it was possible to appreciate that the EKF delivers better results since it better filters the noise for the estimation of states but its speed of convergence is slower than that of the Luenberger linear observer.

Furthermore, after performing the simulation tests for each control approach, considering the EKF observer, within the operating range, and verifying that the results satisfy the physical constraints, we conclude that:

- The controllers based only in feedback action has a big error for tracking trajectories, so the controllers with feedforward component in its control action are used.

- The controllers based on AFL provide good performance. Also, for frequencies smaller than $\omega = 1$, adding integral action reduces the tracking error and control action required but at the cost of initial overshoot.

- The backstepping controller provides less tracking error than the previous controllers but uses higher values of the plate angle and control action, however within the physical restrictions.

- The sliding mode control provides a greater tracking error; however, the tracking error varied in smaller proportion according to the frequency of the reference signal respect to the other controllers.

In the experimental tests, the Luenberger observer delivered a faster estimation dynamics than the Kalman Bucy filter, whereby the response of the controlled system was better and therefore was chosen. In addition, because noise measurements and input disturbances were small the effectiveness of the Kalman Bucy filter was not appreciated.

According to the experimental tests, the spring influences as an external disturbance that adds high frequency oscillations to the plate's angles and is amplified in the control action. Also, the friction (between the ball and the surface of the screen) and other characteristics not modeled (e.g. ball deformation, non-uniform distribution of ball mass, rotation of the ball around its vertical axis, etc.) affect in greater proportion the performance of the controllers. At low ball velocities and small plate angles, its effect is greater. Therefore, in order to reduce it, in the case of control approaches based on AFL, poles with an imaginary part were used, while in the backstepping and sliding mode control the controller gains were increased. This generates a greater plate angle and acceleration to overcome the friction. However, by increasing the imaginary part of the closed-loop poles or the controllers gain, a greater vibration is generated in the behavior of the controlled system.

The delay in the measurement causes the system response to be delayed with respect to the reference signal and also that the tracking error increases directly proportional to the frequency of the reference. However, due to friction this effect degenerates because for greater frequencies the speed of the ball is increased reducing the effect of friction.

The inner loop dynamic generates that the system is slower in comparison to the simulations, therefore reduces the bandwidth of the controlled system. Also, this alters the performance of

the controller based on the sliding mode approach, as it requires a fast system response for the switching of the sliding variables.

After performing the experimental tests using each control approach together with the Luenberger observer, we conclude:

- Tracking controllers based on AFL provided good performance and stability.

- The backstepping controller provides a good performance with respect to the tracking error for higher frequencies of the reference signal, however during the tests it was observed that for large position errors the controlled system becomes unstable. This is because the control action has abrupt changes but is saturated in the control scheme implemented.

- The tracking controller with integral action and the backstepping controller offer better results, however the first one uses less control action.

- The controller based on sliding mode has worse performance than the other methods, since the tracking error is greater. In addition, the friction and speed of the inner loop dynamics affect it in greater proportion. On the other hand, to greater amplitudes and frequencies of the reference signal its performance improves.

It was also noticed that the coupling effect was greater than the one of the model since when turning the plate in a single axis, the ball moved in both axes, due to mechanical problems that were compensated by the controller.

10.2 Future Work

The work done is a starting point to experiment with other control approaches in order to obtain better performance and robustness for tracking trajectories in non-minimum phase systems, considering the exact model of the ball and plate system in the design of the control system.

Some proposed approaches are the control based on linearized systems about the trajectory obtaining LTV systems, the method based on stable dynamic inversion and the Byrnes Isidori regulator that uses exosystemas to generate the trajectories in such a way as to guarantee the stability of the internal dynamics. However, it is necessary to clarify that as long as the friction is not considered in the model will not be able to have a good performance of the controller, therefore it is recommended to add the effect of the friction to the obtained model.

Bibliography

[1] R. Seifried, *Dynamics of underactuated multibody systems: modeling, control and optimal design*, vol. 205. Springer Science & Business Media, 2013.

[2] J. E. Normey-Rico, *Control of dead-time processes*. Springer Science & Business Media, 2007.

[3] L. M. G. W. Arturo Contreras Martinez, "Construction, model verification and system analysis of ball and plate system for trajectory tracking controls," 2017.

[4] S. G. Colmenares, M. A. Moreno-Armendáriz, W. Yu, and F. O. Rodriguez, "Modeling and nonlinear pd regulation for ball and plate system," in *World Automation Congress (WAC), 2012*, pp. 1–6, IEEE, 2012.

[5] M.-T. Ho, Y. Rizal, and L.-M. Chu, "Visual servoing tracking control of a ball and plate system: Design, implementation and experimental validation," *International Journal of Advanced Robotic Systems*, vol. 10, no. 7, p. 287, 2013.

[6] H. Liu and Y. Liang, "Trajectory tracking sliding mode control of ball and plate system," in *Informatics in Control, Automation and Robotics (CAR), 2010 2nd International Asia Conference on*, vol. 3, pp. 142–145, IEEE, 2010.

[7] W. Hongrui, T. Yantao, F. Siyan, and S. Zhen, "Nonlinear control for output regulation of ball and plate system," in *Control Conference, 2008. CCC 2008. 27th Chinese*, pp. 382–387, IEEE, 2008.

[8] S. Awtar, C. Bernard, N. Boklund, A. Master, D. Ueda, and K. Craig, "Mechatronic design of a ball-on-plate balancing system," *Mechatronics*, vol. 12, no. 2, pp. 217–228, 2002.

[9] C.-C. Cheng and C.-H. Tsai, "Visual servo control for balancing a ball-plate system," *International Journal of Mechanical Engineering and Robotics Research*, vol. 5, no. 1, p. 28, 2016.

[10] D. Debono and M. Bugeja, "Application of sliding mode control to the ball and plate problem," in *Informatics in Control, Automation and Robotics (ICINCO), 2015 12th International Conference on*, vol. 1, pp. 412–419, IEEE, 2015.

[11] C. C. Ker, C. E. Lin, and R. T. Wang, "Tracking and balance control of ball and plate system," *Journal of the Chinese institute of engineers*, vol. 30, no. 3, pp. 459–470, 2007.

[12] N. Wettstein, *Balancing a ball on a plate using stereo vision*. PhD thesis, 2013.

[13] V. Hagenmeyer, S. Streif, and M. Zeitz, "Flatness-based feedforward and feedback linearisation of the ball & plate lab experiment," in *Proceedings of the 6th IFAC-Symposium on Nonlinear Control Systems (NOLCOS)*, 2004.

[14] G. Torres, E. X. Martín, M. Velasco, P. Martí, and A. Camacho, "Internet-based control of a ball-and-plate system: A case study of modeling and automatic code generation for networked control systems," in *Industrial Electronics Society, IECON 2014-40th Annual Conference of the IEEE*, pp. 4762–4767, IEEE, 2014.

[15] A. KASSEM, H. HADDAD, and C. ALBITAR, "Commparison between different methods of control of ball and plate system with 6dof stewart platform," *IFAC-PapersOnLine*, vol. 48, no. 11, pp. 47–52, 2015.

[16] M. Oravec and A. Jadlovská, "Model predictive control of a ball and plate laboratory model," in *Applied Machine Intelligence and Informatics (SAMI), 2015 IEEE 13th International Symposium on*, pp. 165–170, IEEE, 2015.

[17] Z. Fei, Q. Xiaolong, L. Xiaoli, and W. Shangjun, "Modeling and pid neural network research for the ball and plate system," in *Electronics, Communications and Control (ICECC), 2011 International Conference on*, pp. 331–334, IEEE, 2011.

[18] N. Andinet, *DESIGN OF FUZZY SLIDING MODE CONTROLLER FOR THE BALL AND PLATE SYSTEM*. PhD thesis, aau, 2011.

[19] M. B. Lukas Düker, Maxim Mousto, "Konzipierung, modellierung, simulation und regelung eines - balanciertisches," 2015.

[20] K. J. Aström and R. M. Murray, *Feedback systems: an introduction for scientists and engineers*. Princeton university press, 2010.

[21] J.-J. E. Slotine, W. Li, *et al.*, *Applied nonlinear control*, vol. 199. prentice-Hall Englewood Cliffs, NJ, 1991.

[22] K. Ogata, *Ingenieria de control moderna Ogata Quinta edicion*. Pearson, 2010.

[23] A. Isidori, *Nonlinear control systems*. Springer Science & Business Media, 2013.

[24] J. Zhou and C. Wen, *Adaptive backstepping control of uncertain systems: Nonsmooth nonlinearities, interactions or time-variations*. Springer, 2008.

[25] S. Rudra, R. K. Barai, and M. Maitra, *Block Backstepping Design of Nonlinear State Feedback Control Law for Underactuated Mechanical Systems*. Springer, 2017.

[26] M. Krstic, I. Kanellakopoulos, and P. V. Kokotovic, *Nonlinear and adaptive control design*. Wiley, 1995.

[27] Y. Shtessel, C. Edwards, L. Fridman, and A. Levant, *Sliding mode control and observation*, vol. 10. Springer, 2014.

[28] S. S. Sastry, *Nonlinear systems: analysis, stability, and control*, vol. 10. Springer Science & Business Media, 2013.

[29] B. K. Aliyu, C. A. Osheku, L. M. Adetoro, and A. A. Funmilayo, "Optimal solution to matrix riccati equation–for kalman filter implementation," in *MATLAB-A Fundamental Tool for Scientific Computing and Engineering Applications-Volume 3*, InTech, 2012.

[30] M. Mahmud, H. Pota, and M. Hossain, "Full-order nonlinear observer-based excitation controller design for interconnected power systems via exact linearization approach," *International Journal of Electrical Power & Energy Systems*, vol. 41, no. 1, 2012.

[31] G. Ciccarella, M. Dalla Mora, and A. Germani, "A luenberger like observer for nonlinear systems," *International Journal of Control*, vol. 57, no. 3, 1993.

[32] H. K. Khalil, *Nonlinear control*. Prentice Hall, 2014.

[33] OMRON, *OMRON Servosystem Technical Guide*, 1997. `https://s3.amazonaws.com/Icarus/DOCUMENTS/Omron_Manuals_650.pdf`.

[34] Kollmorgen, *Cartridge DDR*, 2014. `http://www.kollmorgen.com/en-us/products/motors/direct-drive/cartridge-c-and-ch/_literature/cartridge_ddr_catalog_en-us_revb.pdf/`.

[35] L. Inc., *Lumio Crystal Touch*, 2012. `http://www.lumio.com/outgoing/Documentation/Crystal_Touch_Manager/CTM_V6.9.pdf`.

[36] dSPACE Inc., *DS1104 RD Controller Board*, 2001. `http://regpro.mechatronik.uni-linz.ac.at/downloads/pat2/Praktikum/DS1104.pdf`.

[37] A. A. Shabana, *Dynamics of multibody systems*. Cambridge university press, 2013.

[38] B. Cazzolato, "Derivations of the dynamics of the ball and beam system," *School of mechanical engineering, The University of Adelaide*, vol. 11, pp. 2010–05, 2007.

[39] G. Besanon, "Nonlinear observers and applications, volume 363 of lecture notes in control and information sciences," 2007.

[40] J. Birk and M. Zeitz, "Computer-aided analysis of nonlinear observation problems," *IFAC Proceedings Volumes*, vol. 25, no. 13, pp. 257–262, 1992.

[41] V. Manikonda and P. Krishnaprasad, "Controllability of a class of underactuated mechanical systems with symmetry," *Automatica*, vol. 38, no. 11, pp. 1837–1850, 2002.

[42] N. Kheir, *Systems modeling and computer simulation*, vol. 94. CRC Press, 1995.

Appendix

Appendix A − Variables and Parameters of the Ball and Plate System

Table A.1: Variables in the modeling and control system design for the ball and plate system.

Description	Symbol	SI Unit
Ball position respect to the plate in x-coordinate	x	m
Ball position respect to the plate in y-coordinate	y	m
Ball velocity respect to the plate in x-coordinate	$\dot{x}$	m/s
Ball velocity respect to the plate in y-coordinate	$\dot{y}$	m/s
Ball acceleration respect to the plate in x-coordinate	$\ddot{x}$	m/s^2
Ball acceleration respect to the plate in y-coordinate	$\ddot{y}$	m/s^2
Ball position respect to the fixed coordinates in X-coordinate	X	m
Ball position respect to the fixed coordinates in Y-coordinate	Y	m
Ball position respect to the fixed coordinates in Z-coordinate	Z	m
Angle of the plate about x-axis	ϑ	rad
Angle of the plate about y-axis	φ	rad
Angular velocity of the plate about x-axis	$\dot{\vartheta}$	rad/s
Angular velocity of the plate about y-axis	$\dot{\varphi}$	rad/s
Angular acceleration of the plate about x-axis	$\ddot{\vartheta}$	rad/s^2
Angular acceleration of the plate about y-axis	$\ddot{\varphi}$	rad/s^2
Angular velocity of the plate in the X-coordinate	w_{px}	rad/s
Angular velocity of the plate in the Y-coordinate	w_{py}	rad/s
Angular velocity of the plate in the Z-coordinate	w_{pz}	rad/s
Angle of the motor shaft about X-axis	Θ	rad
Angle of the motor shaft Y-axis	Φ	rad
Angular velocity of motor shaft about X-axis	$\dot{\Theta}$	rad/s
Angular velocity of motor shaft about Y-axis	$\dot{\Phi}$	rad/s
Angular acceleration of motor shaft about X-axis	$\ddot{\Theta}$	rad/s^2
Angular acceleration of motor shaft about Y-axis	$\ddot{\Phi}$	rad/s^2

Table A.2: Main parameters of the ball and plate system.

Parameter	Symbol	Value	Unit (SI)
Mass of the ball	m_b	0.024	Kg
Radius of the ball	r_b	0.02	m
Moment of inertia of the ball	J_b	6.4e-06	Kg.m^2
Gravitational acceleration	g	9.81	m.sec^2
Distance beetwen the plate and the cardan	d_{cs}	0.122	m
Dead time of the touch screen sensor	τ	0.042	sec^2
Material of the ball		polypropylen	

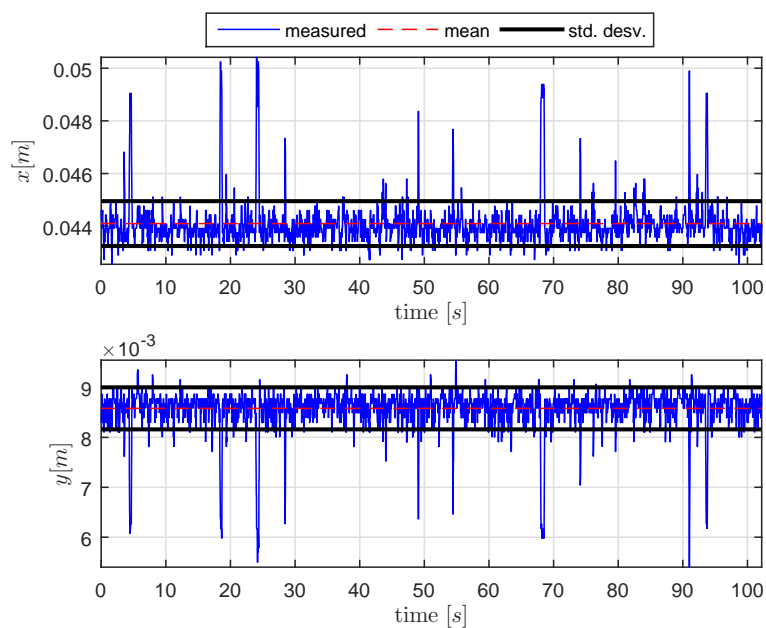# Appendix B – Variance of the Measurement Noises and the Process Disturbances

Figure B.1: Measurement of the ball's position in a static location.
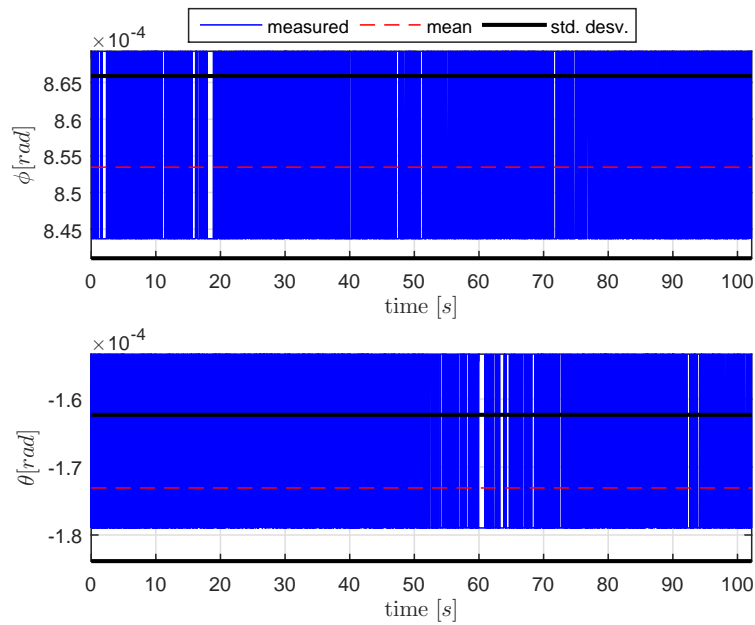
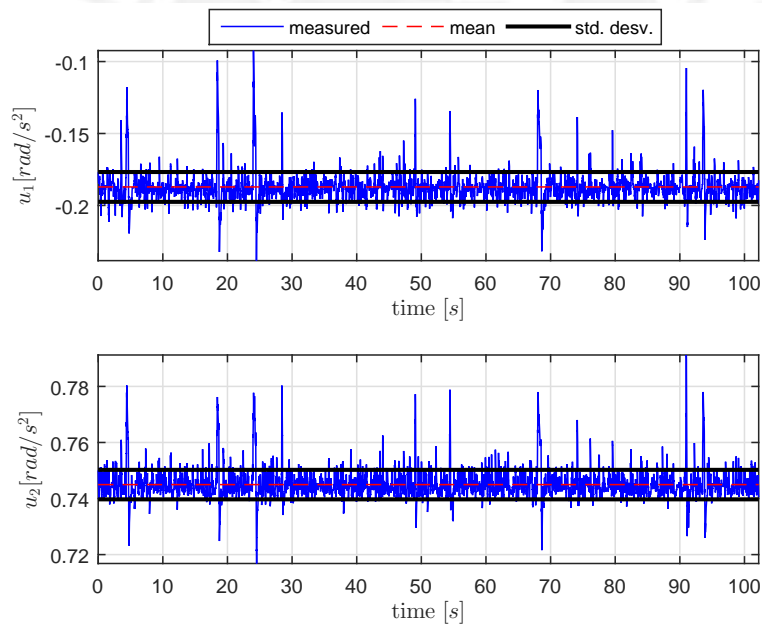Figure B.2: Measurement of the plate's angles in a static location.

Figure B.3: Measurement of the control efforts in a static state.

Table B.1: Variance of the measurement errors and input disturbances.

$\sigma^2_{\eta_x}$	$\sigma^2_{\eta_y}$	$\sigma^2_{\eta_\phi}$	$\sigma^2_{\eta_\theta}$	$\sigma^2_{\omega_1}$	$\sigma^2_{\omega_2}$
7.2538e-07	1.7721e-07	1.5433e-10	1.1580e-10	1.0816e-04	2.8090e-05

Appendix C − Performance Indicators

Average estimation error $(\tilde{x}_{k_{average}})$

$$\tilde{x}_k(t) = x_k(t) - \hat{x}_k(t) \tag{C.1}$$

$$\tilde{x}_{k_{average}} = \frac{\sum_{t=t_i}^{t_f} |\tilde{x}_k(t)|}{t_f - t_i}, \quad k = 1, \ldots, 8 \tag{C.2}$$

Average tracking error $(e_{x_{average}})$

$$e_x(t) = x^*(t) - x(t) \tag{C.3}$$

$$e_{x_{average}} = \frac{\sum_{t=t_i}^{t_f} |e_x(t)|}{t_f - t_i} \tag{C.4}$$

Trajectory tracking error (e_{tt})

$$e_x(t) = x^*(t) - x(t) \tag{C.5}$$

$$e_y(t) = y^*(t) - y(t) \tag{C.6}$$

$$e_{tt}\,(\%) = \sqrt{\frac{\sum_{t=t_i}^{t_f} \left(e_x^2(t) + e_y^2(t) \right)}{\sum_{t=t_i}^{t_f} \left(x^{*2}(t) + y^{*2}(t) \right)}} 100\% \tag{C.7}$$

Appendix D — Circular Trajectory Reference with Polynomial Initialization

The reference trajectory starts with the polynomial function $P(t)$ and at time $t = T$ is changed to the sinusoidal function.

Trajectory reference for $t < T$ Trajectory reference for $t >= T$

$$
\begin{pmatrix}
y_1^*(t) \\
\dot{y}_1^*(t) \\
\ddot{y}_1^*(t) \\
y_1^{*(3)}(t) \\
y_1^{*(4)}(t) \\
y_2^*(t) \\
\dot{y}_2^*(t) \\
\ddot{y}_2^*(t) \\
y_2^{*(3)}(t) \\
y_2^{*(4)}(t)
\end{pmatrix}
=
\begin{pmatrix}
P(t) \\
\dot{P}_x(t) \\
\ddot{P}_x(t) \\
P_x^{(3)}(t) \\
P_x^{(4)}(t) \\
P_y(t) \\
\dot{P}_y(t) \\
\ddot{P}_y(t) \\
P_y^{(3)}(t) \\
P_y^{(4)}(t)
\end{pmatrix}
\quad \text{(D.1a)}
$$

$$
\begin{pmatrix}
y_1^*(t) \\
\dot{y}_1^*(t) \\
\ddot{y}_1^*(t) \\
y_1^{*(3)}(t) \\
y_1^{*(4)}(t) \\
y_2^*(t) \\
\dot{y}_2^*(t) \\
\ddot{y}_2^*(t) \\
y_2^{*(3)}(t) \\
y_2^{*(4)}(t)
\end{pmatrix}
=
\begin{pmatrix}
\mathcal{A}\sin(\omega t) \\
\mathcal{A}\omega\cos(\omega t) \\
-\mathcal{A}\omega^2\sin(\omega t) \\
-\mathcal{A}\omega^3\cos(\omega t) \\
\mathcal{A}\omega^4\sin(\omega t) \\
\mathcal{A}\cos(\omega t) \\
-\mathcal{A}\omega\sin(\omega t) \\
-\mathcal{A}\omega^2\cos(\omega t) \\
\mathcal{A}\omega^3\sin(\omega t) \\
\mathcal{A}\omega^4\cos(\omega t)
\end{pmatrix}
\quad \text{(D.1b)}
$$

For a soft initialization, the trajectory reference and its derivatives at $t = 0$ must satisfy:

$$P_x(0) = \dot{P}_x(0) = \ddot{P}_x(0) = P_x^{(3)}(0) = P_x^{(4)}(0) = 0, \tag{D.2}$$

$$P_y(0) = \dot{P}_y(0) = \ddot{P}_y(0) = P_y^{(3)}(0) = P_y^{(4)}(0) = 0, \tag{D.3}$$

and also by the continuity condition at time $t = T$ the following relations must be satisfied

$$
\begin{pmatrix}
P_x(T) \\
\dot{P}_x(T) \\
\ddot{P}_x(T) \\
P_x^{(3)}(T) \\
P_x^{(4)}(T)
\end{pmatrix}
=
\begin{pmatrix}
\mathcal{A}\sin(\omega T) \\
\mathcal{A}\omega\cos(\omega T) \\
-\mathcal{A}\omega^2\sin(\omega T) \\
-\mathcal{A}\omega^3\cos(\omega T) \\
\mathcal{A}\omega^4\sin(\omega T)
\end{pmatrix}
\quad \text{(D.4a)}
$$

$$
\begin{pmatrix}
P_y(T) \\
\dot{P}_y(T) \\
\ddot{P}_y(T) \\
P_y^{(3)}(T) \\
P_y^{(4)}(T)
\end{pmatrix}
=
\begin{pmatrix}
\mathcal{A}\cos(\omega T) \\
-\mathcal{A}\omega\sin(\omega T) \\
-\mathcal{A}\omega^2\cos(\omega T) \\
\mathcal{A}\omega^3\sin(\omega T) \\
\mathcal{A}\omega^4\cos(\omega T).
\end{pmatrix}
\quad \text{(D.4b)}
$$
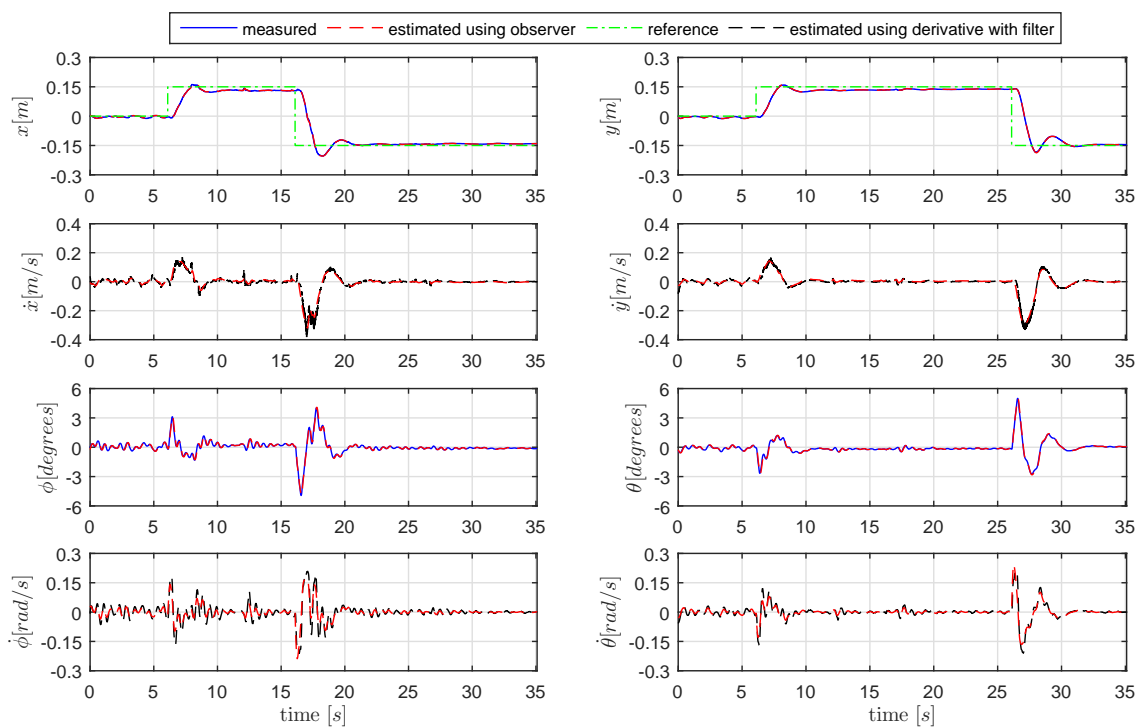
Appendix E – Stabilization Control for the Solid Steel Ball

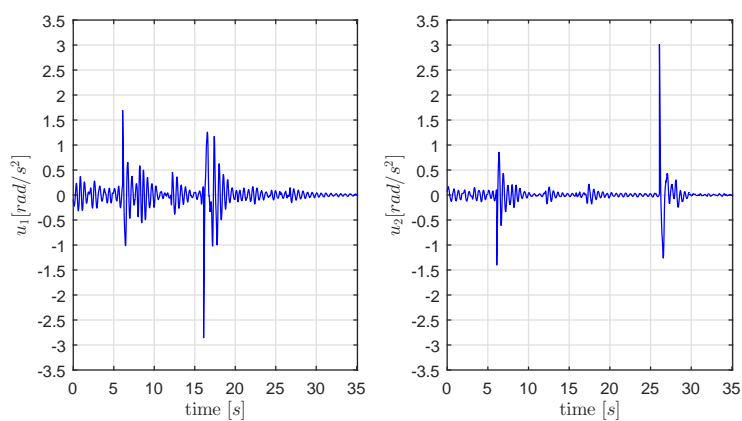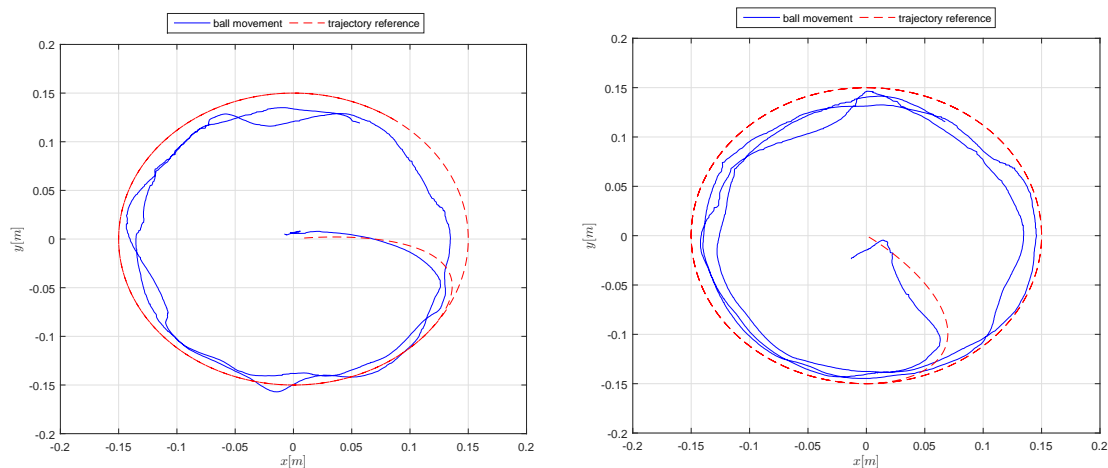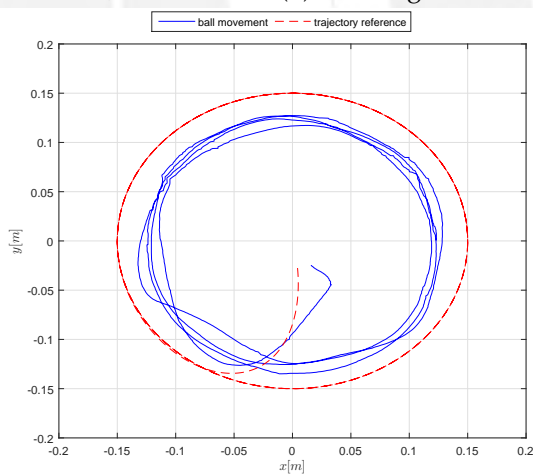Figure E.1: States in the stabilization test using LQR controller.

Figure E.2: Control efforts in the stabilization test using LQR controller.

Appendix F − Ball Trajectory during Tracking Control

(a) Tracking control for $\mathcal{A} = 0.15$, $\omega = 0.5$.

(b) Tracking control for $\mathcal{A} = 0.15$, $\omega = 0.75$.

(c) Tracking control for $\mathcal{A} = 0.15$, $\omega = 1$.

Figure F.1: Trajectory of the ball using tracking control with integral action based on AFL.